

TABLE OF CONTENTS

SYNOPSIS	I
ACKNOWLEDGEMENTS.....	III
PREFACE.....	IV
LIST OF FIGURES	IX
LIST OF TABLES.....	XVI
LIST OF ACRONYMS, ABBREVIATIONS AND DEFINITIONS.....	XVIII
CHAPTER 1	1
1 INTRODUCTION.....	2
1.1 LAYERED DOUBLE HYDROXIDES.....	2
1.2 LDH-BASED POLYMER COMPOSITES	3
1.3 LDH/JOJOBA OIL SUSPENSIONS	6
1.4 RESEARCH OBJECTIVE	6
1.4.1 Methodology	7
1.5 REFERENCES.....	8
CHAPTER 2	11
2 LAYERED DOUBLE HYDROXIDES.....	12
2.1 WHAT IS A LAYERED DOUBLE HYDROXIDE?	12
2.2 LDH PREPARATION ROUTES.....	14
2.2.1 Co-precipitation.....	14
2.2.2 Urea hydrolysis	15
2.2.3 Sol-gel.....	16
2.2.4 Post-preparation techniques.....	17
2.2.5 Texture and morphology.....	18
2.3 INTERCALATION.....	19
2.3.1 Intercalation methods	20
2.3.2 Orientation of intercalated fatty acids	22
2.4 CHARACTERISATION OF LDH AND MODIFIED DERIVATIVES.....	25
2.5 EXPERIMENTAL	25
2.5.1 Materials	25

2.5.2	Preparation of organo-LDH.....	26
2.5.3	Characterisation.....	27
2.6	RESULTS AND DISCUSSION.....	29
2.6.1	Composition and morphology.....	29
2.6.2	X-ray diffraction analysis	33
2.6.3	Fourier transform infrared analysis (FTIR)	34
2.6.4	Thermal analysis	38
2.7	CONCLUSIONS.....	46
2.8	REFERENCES.....	47
CHAPTER 3	55
3	PROPERTIES OF LDH/POLYMER AND NANOCOMPOSITES	56
3.1	POLYMER COMPOSITES.....	56
3.2	POLYMER COMPOSITE STRUCTURES	58
3.2.1	Phase separated composites	58
3.2.2	Intercalated composites	58
3.2.3	Exfoliation/delamination composites	59
3.3	LDH-BASED POLYMER COMPOSITE PREPARATION.....	60
3.3.1	In situ polymerisation	60
3.3.2	Solution intercalation.....	62
3.3.3	Melt processing	63
3.4	PROPERTIES OF LDH-BASED POLYMER NANOCOMPOSITES.....	65
3.4.1	Physical properties	66
3.4.2	Mechanical properties.....	69
3.5	EXPERIMENTAL	75
3.5.1	Materials	75
3.5.2	Preparation of LDH-stearate.....	75
3.5.3	Preparation of polymer/LDH-St.....	75
3.5.4	Characterisation.....	76
3.6	RESULTS AND DISCUSSION.....	77
3.6.1	X-ray diffraction.....	82
3.6.2	Transmission electron microscopy (TEM)	84
3.6.3	Melt viscosity.....	86
3.6.4	Viscoelastic properties.....	89

3.6.5	Mechanical properties.....	91
3.6.6	Thermal analysis	96
3.7	CONCLUSION.....	101
3.8	REFERENCES.....	103
CHAPTER 4		112
4	ORGANO-LDH/OIL SUSPENSIONS	113
4.1	INTRODUCTION.....	113
4.2	RHEOLOGY.....	113
4.3	THICKENING MECHANISM.....	116
4.4	COLLOIDAL DISPERSIONS.....	117
4.4.1	Clay dispersion in aqueous media	118
4.4.2	Clay dispersion in non-aqueous media.....	118
4.4.3	Clay dispersion in emulsions	120
4.5	EXPERIMENTAL	121
4.5.1	Materials	121
4.5.2	Preparation of fatty acid-intercalated hydrotalcite	121
4.5.3	Preparation of 30 wt.% LDH-fatty acid/Jojoba oil formulation	122
4.5.4	Characterisation.....	122
4.6	RESULTS AND DISCUSSION.....	124
4.6.1	Organo-layered double hydroxides (organo-LDHs)	124
4.6.2	Jojoba oil/LDH-derivative formulation	130
4.7	CONCLUSION.....	143
4.8	REFERENCES.....	144
CHAPTER 5		148
5. CONCLUSION AND RECOMMENDATIONS.....		149
APPENDIX A: PUBLICATIONS AND CONFERENCE PROCEEDINGS.....		151
APPENDIX B: FATTY ACID-INTERCALATED LAYERED DOUBLE HYDROXIDES		152
APPENDIX C: LDH-BASED POLYMER COMPOSITES.....		168
APPENDIX D: ORGANO-LDH / JOJOBA OIL SUSPENSION		199

List of Figures

Figure 1.1. Global application market share projections for polymer composites (Adapted from Research and Markets, http://www.researchandmarkets.com)	4
Figure 1.2. Differential scanning calorimetry (DSC) melting endotherm and hot stage microscopy of LDH-stearate (Nhlapo <i>et al.</i> , 2008).....	5
Figure 2.1. Layered structure of LDH-CO ₃	13
Figure 2.2. Common habits of smectite single crystallites (Adapted from Grim & Güven, 1978)	18
Figure 2.3. Intercalation	19
Figure 2.4. Orientation of intercalated fatty acids.....	23
Figure 2.5. Effect of chain length on the close packing of intercalated fatty acids (Adapted from Kanicky & Shah, 2002)	24
Figure 2.6. Effect of pH on the close packing intercalated fatty acid (Adapted from Kanicky & Shah, 2002)	24
Figure 2.7. (a) SEM; (b), (c) and (d) TEM micrographs of neat LDH-CO ₃	30
Figure 2.8. SEM micrographs of the LDH samples: (a) LDH-myristate; (b) LDH-palmitate; (c) LDH-stearate; and (d) LDH-behenate	31
Figure 2.9. EDS data showing different compositions of LDH-palmitate platelets with Mg:Al ratios of (a) 2.09 and (b) 6.95	32
Figure 2.10. WAXS diffractograms of the neat and modified LDH.....	33
Figure 2.11. Increase in basal spacing with increase in alkyl chain lengths (○) obtained experimentally in this study and (◆) obtained from theoretical calculations	34
Figure 2.12. Pristine LDH and its typical FTIR vibrations	35
Figure 2.13. FTIR spectra of pristine and modified LDHs.....	36
Figure 2.14. FTIR zoom of the modified LDH.....	37
Figure 2.16. Temperature scan XRD of LDH-fatty acids	40
Figure 2.17. Effect of temperature on the peak position of the $\nu_{as}(\text{CH}_2)$ band in the FTIR spectra for LDH-stearate, and the corresponding DSC	41
Figure 2.18. TG and DTG of the LDH-CO ₃ indicating the different decomposition stages	42

Figure 2.19. Thermogravimetric analysis: (a) % mass loss and (b) derivative mass loss of pristine and modified LDHs	43
Figure 2.20. Evolved gas analysis for LDH-stearate	43
Figure 2.21. X-ray diffractograms for magnesium stearate, aluminium stearate and magnesium/aluminium stearate prepared by heating an aqueous suspension of the former two reagents in the presence of Tween 60	45
Figure 3.1. Polymer composite structures	59
Figure 3.2. Schematic pathways of in situ polymerisation within the LDH layers in the preparation of polymer/LDH nanocomposites (Adapted from Costa <i>et al.</i> , 2008).....	61
Figure 3.3. Characterisation of LDH-based polymer composites	65
Figure 3.4. Mixing rule conditions for layered composites (Adapted from Verbeek & Focke, 2002).....	70
Figure 3.5. Craze yielding (Adapted from MIT Open Course Ware, 2009).....	71
Figure 3.6. Shear banding (Adapted from MIT Open Course Ware, 2009).....	72
Figure 3.7. Polymer-toughening mechanism with rigid particles (Kim <i>et al.</i> , 1998) (Figure adapted from Zuiderduin <i>et al.</i> , 2003).....	72
Figure 3.8. Freeze-fractured surface of neat EVA, EVA/LDH-St and EVA/LDH-CO ₃ . The latter two samples contained 10 wt.% filler	79
Figure 3.9. Freeze-fractured surface of neat EVAL, EVAL/LDH-St and EVAL/LDH-CO ₃ . The latter two samples contained 10 wt.% filler	80
Figure 3.10. Freeze-fractured surface of neat LLDPE, LLDPE/LDH-St and LLDPE LDH-CO ₃ . The latter two samples contained 10 wt.% filler	81
Figure 3.11. XRD diffractograms (WAXS) of the pristine, modified LDH and the 10 wt.% polymer composites indicating the relevant basal spacing	82
Figure 3.12. TEM images of the 10 wt.% polymer/LDH composites of (a) EVA/ LDH-St; (b) EVAL/LDH-St; (c) LLDPE/LDH-St; (d) EVA/LDH-CO ₃ ; (e) EVAL/LDH-CO ₃ and (f) LLDPE/ LDH-CO ₃	84
Figure 3.13. Agglomeration observed in the different matrices in SEM micrographs	85
Figure 3.14. Schematic of the ‘house-of-cards’ structure: (a) LLDPE/LDH-CO ₃ showing an agglomerate with face-to-edge interactions and (b) with edge-to-edge interactions	86
Figure 3.15. Effect of LDH incorporation on the viscosity of the polymers LLDPE, EVA and EVAL at 190 °C	88

Figure 3.16. DMA data for the storage modulus and $\tan \delta$ of LLDPE and its 10 wt.% derivative composites89

Figure 3.17. DMA data for the storage modulus and $\tan \delta$ of EVA and its 10 wt.% derivative composites90

Figure 3.18. DMA data for the storage modulus and $\tan \delta$ of EVAL and its 10 wt.% derivative composites91

Figure 3.19. Optical light microscope side-views of Charpy impact test specimen of EVAL: (a) neat, (b) LDH-stearate composite and (c) LDH-CO₃ 10 wt.% composite94

Figure 3.20. Top view of the EVAL/LDH-St tensile impact test specimen showing: (a) debonding and (b) fibrillation95

Figure 3.21. TG data for EVAL and derivative composites97

Figure 3.22. DSC cooling traces of each of the 10 wt.% polymer composite systems98

Figure 3.23. POM images of neat LLDPE and derivative composites (scale bar is 40 μm)99

Figure 4.1. The parallel plate depiction of steady state viscous shear flow (Focke, 2012) 114

Figure 4.2. Viscosity curve of (a) Newtonian and (b) non-Newtonian fluids 115

Figure 4.3. Soft microstructure, characterising the system as a “soft-glass” or “gel” (Stokes & Frith, 2008)..... 117

Figure 4.4. SEM micrographs of the LDH-stearates E and S used in the Jojoba oil formulation 124

Figure 4.5. (a) Schematic illustration illustration of silicon dangling bond (Kasap 2001) and (b) euedral and subhedral crystals arrows indicating dangling bonds..... 125

Figure 4.6. XRD diffractograms of: (a) LDH-St (E) and (b) LDH-St (S)..... 126

Figure 4.7. FTIR spectrum of the LDH-St 128

Figure 4.8. Viscosity curves as a function of temperature of: (a) 30 wt.% LDH-St (E) and (b) 30 wt.% LDH-St (S) (The heating run is shown in red and the cooling run in blue)..... 129

Figure 4.9. Arbitrarily scaled X-ray diffractograms for stearic acid, LDH-CO₃, LDH-stearate (S) and a 30 wt.% dispersion of LDH-stearate (S) in Jojoba oil prepared at a temperature of 80 °C130

Figure 4.10. Viscosity-temperature curves of Jojoba oil/stearic acid suspensions heated at 5 °C/min from 10 to 90°C and cooled at the same rate back to 10 °C (The heating runs are shown in red and the cooling run in blue) 131

Figure 4.11. DSC traces for neat Jojoba oil and stearic acid as well as a 60:40 blend of the oil with the acid; samples were heated at 5 °C/min from -40 to 200 °C and cooled at the same rate back to -40 °C.....	131
Figure 4.12. Hot-stage optical microscopy of Jojoba oil suspension containing 20 wt.% stearic acid (magnification bar: 40µm)	132
Figure 4.13. General illustration of a Jojoba oil-stearic acid phase diagram	133
Figure 4.14. The effect of shear rate and LDH-St content on the viscosity of Jojoba oil suspensions (the temperature was kept constant at 30 °C).....	134
Figure 4.15. Comparison of the Jojoba oil thickening efficiency of 30 wt.% Mg-stearate, Al-stearate and LDH-St (the temperature was 30 °C)	134
Figure 4.16. Effect of the presence of small amounts of alcohols (5 wt.% to 25 wt.% LDH-St suspension in Jojoba oil on the suspension viscosity	135
Figure 4.17. The effect of temperature on the viscosity of Jojoba oil and a 30 wt.% LDH-St suspensions subjected to a heating-cooling cycle (The shear rate was 30 s ⁻¹ ; the temperature was scanned at 5 °C/min from 10 to 90 °C and back. The heating run is shown in red and the cooling run in blue)	136
Figure 4.18. Viscosity-temperature heating run subdivided into three stages	137
Figure 4.19. Viscosity-temperature cooling run subdivided into four stages	139
Figure 4.20. Comparison of the Jojoba oil thickening efficiency of Mg-St, Al-St and LDH-St, all at a loading of 30 wt.%. (The shear rate was 5 s ⁻¹ ; temperature was scanned at 5 °C/min from 10 to 90 °C and back. The heating runs are shown in red and the cooling runs in blue coloured symbols).....	140
Figure 4.21. X-ray diffractograms of stearic acid, LDH-St and the LDH-St/Jojoba oil formulation	141
Figure 4.22. FTIR spectra of 30 wt.% LDH-St/Jojoba oil formulation obtained as temperature is increased	142
Figure B-1. Fatty/carboxylic acids used in the study	152
Figure B-2. XRD diffractograms for LDH-myristate	154
Figure B-3. XRD diffractograms for LDH-palmitate	155
Figure B-4. XRD diffractograms for LDH-behenate	156
Figure B-5. XRD diffractogram of co-intercalated organo-LDH	157
Figure B-6. SEM micrographs of co-intercalated LDHs.....	159

Figure B-7. LDH-CO ₃ SEM micrograph, X-ray and composition of platelets.....	160
Figure B-8. LDH-myristate SEM micrograph, X-ray and composition of platelets	161
Figure B-9. LDH-palmitate SEM micrograph, X-ray and composition of platelets	162
Figure B-10. LDH-St SEM micrograph, X-ray and composition of platelets	162
Figure B-11. LDH-behenate SEM micrograph, X-ray and composition of platelets.....	163
Figure B-12. LDH-palmitate and myristate TG profile.....	165
Figure B-13. LDH-behenate TG profile.....	166
Figure C-1. FTIR of the neat and composite derivatives	176
Figure C-2. TEM micrographs of the 5 wt.% LDH-carbonate polymer composites	177
Figure C-3. TEM micrographs of the 5 wt.% LDH-stearate polymer composites	178
Figure C-4. Dynamic mechanical properties of 5% filler formulations.....	179
Figure C-5. Tensile strength and tensile impact test summary of neat EVAL and derivative composites	180
Figure C-6. Tensile strength and tensile impact test summary of neat EVA and derivative composites	181
Figure C-7. Tensile strength and tensile impact test summary of neat LLDPE and derivative composites	182
Figure C-8. Tensile test results	183
Figure C-9. SEM micrographs of fractured surfaces from the Charpy impact test and corresponding data (composites of 10 wt.% LDH).....	184
Figure C-10. DSC scans of EVA and derivative composites	185
Figure C-11. DSC scans of EVAL and derivative composites.....	185
Figure C-12. DSC scans of LLDPE and derivative composites	186
Figure C-13. DSC scans of EVAL and derivative composites.....	186
Figure C-14. DSC scans of EVA and derivative composites	187
Figure C-15. DSC scans of LLDPE and derivative composites	187
Figure C-16. TG data of EVA and derivative composites	188
Figure C-17. TG data of EVA and derivative composites	188
Figure C-18. Evolved gas analysis of neat EVAL by TG-FTIR.....	189

Figure C-19. Evolved gas analysis of EVAL/5% LDH-St by TG-FTIR	190
Figure C-20. Evolved gas analysis of EVAL/10% LDH-St by TG-FTIR.....	191
Figure C-21. Evolved gas analysis of EVAL/5% LDH-CO ₃ by TG-FTIR	192
Figure C-22. Evolved gas analysis of EVAL/10% LDH-CO ₃ by TG-FTIR	193
Figure C-23. Evolved gas analysis of neat EVA by TG-FTIR.....	194
Figure C-24. Evolved gas analysis of EVA/5% LDH-St by TG-FTIR.....	195
Figure C-25. Evolved gas analysis of EVA/10% LDH-St by TG-FTIR.....	196
Figure C-26. Evolved gas analysis of EVA/5% LDH-CO ₃ by TG-FTIR	197
Figure C-27. Evolved gas analysis of EVA/10% LDH-CO ₃ by TG-FTIR.....	198
Figure D-1. Viscosity-temperature curve of different stearic acid compositions in Jojoba oil	200
Figure D-2. 20 wt.% of stearic acid in Jojoba oil heated and cooled to 24 °C (measurement bar is 40 μm)	200
Figure D-3. DSC curves of different stearic acid compositions in Jojoba oil	201
Figure D-4. Viscosity-temperature curve of different palmitic acid compositions in Jojoba oil.....	202
Figure D-5. 20 wt.% palmitic acid in Jojoba oil heated and cooled to 25 °C (measurement bar is 40 μm)	202
Figure D-6. FTIR spectra of neat Jojoba oil, 30 wt.% LDH-stearate/Jojoba oil formulation and stearate.....	203
Figure D-7. The effect of shear rate and temperature on the viscosity of Jojoba oil suspensions (the LDH-stearate content was 30 wt.% and the shear rate was kept constant at 5 s ⁻¹).....	204
Figure D-8. Viscosity as a function of temperature of the neat Jojoba oil	205
Figure D-9. Summary of rhombohedral-shaped LDH-palmitate: A – SEM image of morphology of particles; B – XRD diffractograms with a d-spacing of 4.7 nm; C – TGA data indicating organic content; D – viscosity curve as a function of temperature of the derivative 30 wt.% formulation.....	205
Figure D-10. Summary of subhedral-shaped LDH-palmitate: A – SEM image of morphology of particles; B – XRD diffractograms with a d-spacing of 4.46 nm; C – TGA data indicating organic content; D – viscosity curve as a function of temperature of the derivative 30 wt.% formulation.....	206
Figure D-11. Summary of subhedral-shaped LDH-behenate: A – SEM image of morphology of particles; B – XRD diffractograms with a d-spacing of 6.08 nm; C – TGA data indicating	

organic content; D – viscosity curve as a function of temperature of the derivative 30 wt.% formulation.....	207
Figure D-12. Summary of subhedral-shaped LDH-Pal-St: A – SEM image of morphology of particles; B – XRD diffractograms with a d-spacing of 4.56 nm; C – TGA data indicating organic content; D – viscosity curve as a function of temperature of the derivative 30 wt.% formulation.....	208
Figure D-13. Summary of subhedral-shaped LDH-(Jjoba/stearate): A – SEM image of morphology of particles; B – XRD diffractograms with d-spacings of 5.06 and 4.46 nm; C – TGA data indicating organic content; D – viscosity curve as a function of temperature of the derivative 30 wt.% formulation.....	209

List of Tables

Table 2.1. Summary of layered double hydroxides, year of discovery, polytypes and chemical formulas (Adapted from Zaneva & Stanimirova, 2004).....	14
Table 2.2. Orientation and d-spacing of fatty acid-intercalated LDHs.....	22
Table 2.3. Summary of fatty acids used in the intercalation process	26
Table 2.4. Compositional data and formulae for the LDH-CO ₃ precursor and intercalated products.	29
Table 2.5. Summary of thermogravimetric data and estimates for the degree of intercalation	44
Table 2.6. Summary of XRD and TGA results for the LDH-CO ₃ , LDH-stearates and magnesium stearate and aluminium stearate samples	45
Table 3.1. Layered nanostructured materials for potential use in polymer composites (Adapted from Utracki <i>et al.</i> , 2007).....	57
Table 3.2. Summary of in situ polymerisation in LDH-based nanocomposites.....	62
Table 3.3. Summary of solution intercalation in LDH-based nanocomposites	63
Table 3.4. Summary of melt-processing examples in LDH based nanocomposites	64
Table 3.5. Summary of the mechanical properties of LDH/polymer composites	92
Table 3.6. Thermal stability data at T _{0.1} , T _{0.5} , % residue and change in temperature (ΔT), results pertaining to 10 wt.% composites	96
Table 3.7. DSC data indicating the onset temperature and melting endotherm of the 10 wt.% polymer composites.....	100
Table 4.1. Different types of non-Newtonian fluids (Adapted from Shenoy, 1999).....	116
Table 4.3. Illustration of the different stages associated with the heating run in the viscosity-temperature curve.....	138
Table B-1. Summary of intercalation experiments	153
Table B-2. Observed 2θ reflections of XRD of neat myristic acid and LDH-myristate	155
Table B-3. Observed 2θ reflections of XRD of neat palmitic acid and LDH-palmitate	156
Table B-4. Observed 2θ reflections of XRD of neat behenic acid and LDH-behenate.....	157
Table B-5. Compositional data and formulae of co-intercalated organo-LDHs	158
Table B-6. Summary of thermogravimetric data and estimates for the degree of intercalation	164

Table B-7. Summary of thermogravimetric data, estimates for the degree of intercalation and d-spacing.....	166
Table C-1. Injection moulding comments on EVA and derivative composites.....	168
Table C-2: Injection moulding comments on EVAL and derivative composites	169
Table C-3. Injection moulding comments on LLDPE and derivative composites.....	170
Table D-1. Stearic acid in Jojoba oil formulation (J stands for Jojoba oil and S for stearic acid and their respective compositions).....	199
Table D-2. Palmitic acid in Jojoba oil formulation (J stands for Jojoba oil and P for palmitic acid and their respective compositions)	199
Table D-3. Visual observation of different 30 wt% of intercalated LDHs	204

List of Acronyms, Abbreviations and Definitions

AEC	Anionic exchange capacity – Amount of exchangeable anions available with the crystal structure of an adsorbent material, expressed in meq/100 g
AFM	Atomic force microscopy
DMA	Dynamic mechanical analysis/analyser
DSC	Differential scanning calorimetry
EDS	Energy dispersive X-ray spectroscopy
EVA	Ethylene vinyl acetate
EVAL	Ethylene vinyl alcohol
FTIR	Fourier transform infrared
HT	Hydrotalcite
ICP-OES	Inductively coupled plasma optical emission
LDH	Layered double hydroxides
LDH-Be	LDH-behenate
LDH-My	LDH-myristate
LDH-Pa	LDH-palmitate
LDH-St	LDH-stearate
LDO	Layered double oxide
LLDPE	Linear low-density polyethylene
MFI	Melt flow index
PE	Polyethylene
PLLA	Poly(L-lactide)
PMMA	Polymethyl methacrylate
POM	Polarised optical microscopy
PP	Polypropylene
PS	Polystyrene
SDS	Sodium dodecyl sulphate
SEM	Scanning electron microscopy
TEM	Transmission electron microscopy
TG(A)	Thermogravimetry (Thermogravimetric analysis)
UV	Ultraviolet
XRD	X-ray diffraction

Definitions

Anhedral	Refers to poorly formed crystal with no distinct faces
Delamination	A process in which layers of a multi-layered structure separate
Exfoliation	A process in which layers of a multi-layered structure are separated into single sheets
Fatty acid	Carboxylic acid, is an organic compound with a –COOH functional group
Intercalation	A process in which atoms, ions or molecules are inserted between the layers of a two-dimensional crystal lattice host
Organo-LDH	Surfactant/fatty acid modified layered double hydroxides
Peptisation	To disperse a suspension to form a colloid
Subhedral	Moderately formed crystals
Thermotropic	Changes in structure as temperature changes
Euhedral	Fully-faced crystals, well-formed with sharp, easily recognisable crystal faces.

Chapter 1

Introduction

1 INTRODUCTION

1.1 LAYERED DOUBLE HYDROXIDES

Clays are layered nanostructured materials, widely used as unique additives and fillers in polymeric, cosmetic and pharmaceutical products. For many years they represented the largest and most widely used material. Clay is defined as a hydrous silicate particle less than 2 μm in diameter, composed of silicon, aluminium oxides and hydroxides, as well as structural water. In general, they possess excellent properties, such as low or nil toxicity, biocompatibility and the possibility for use in ‘controlled-release’ pharmaceutical and cosmetic products. A substantial amount of research has been carried out on the application and characterisation of smectite (cationic) clays (Utracki, 2004; Kumar *et al.*, 2009). Smectite or phyllosilicates are predominately natural clays. However, natural clays have drawbacks such as variability in composition, difficulty in purifying, poor reproducibility of the performance of polymer composites, crystallographic defects that prevent total exfoliation and variable colour (Utraki, 2004). Other layered nanostructured materials, such as layered double hydroxides (LDHs), may be considered as potential alternatives. LDHs possess a higher exchange capacity (typically anionic exchange capacity (AEC) = 0.5 to 6) as compared with cationic clays (cation exchange capacity (CEC) = 0.5–2) (Utraki *et al.*, 2007).

LDHs are referred to as ‘hydrotalcite-like’ compounds. They are also described as mixed metal hydroxides that consist of positively charged metal hydroxide sheets with metals in different oxidation states. The crystallography of these materials is similar to that of hydrotalcite, with a formula of $\text{Mg}_6\text{Al}_2(\text{OH})_{16}(\text{CO}_3)\cdot 4\text{H}_2\text{O}$ (Reichle, 1986). LDHs have various advantages, such as low incidence of impurities since they are synthetic, and a wide variety of metal species and mole ratio compositions can be prepared. However, the high charge density within the interlayer renders LDHs unattractive as they do not easily delaminate or exfoliate in polymers or any media of dispersion. This ‘handicap’ may be counteracted by a process called *intercalation*. The intercalation process achieves this through the insertion of exchangeable anions, hence reducing the solid-solid interaction within the clay layers. This is essential as the van der Waals interaction between solid surfaces decreases with the square of the separating distance (Utraki, 2004). The process also improves the compatibility of the clay with the polymer matrices in the preparation of

polymer–nanocomposites (Utraki, 2004). The insertion of anions such as surfactants functionalises the clay by converting the hydrophilic nature of the interlayer into a hydrophobic one. Consequently, non-polar and low-water-soluble organic molecules may be absorbed into the interlayer. Various anions have been exchanged within the interlayer, such as halides (Xu & Zeng, 2001), organic anions, e.g. carboxylates, benzenecarboxylates and alkylsulphates (Meyn *et al.*, 1990; Carlino, 1997; Newman & Jones, 1998), polymeric anions (Oriaki *et al.*, 1996), complex anions (Crespo *et al.*, 1997), macrocyclic ligands and their metal derivatives (Robins & Dutta, 1996), iso- and heteropolyoxometalates (Drezdon, 1998) and biochemical anions (Choy, 2004).

In this study the organo-LDHs were synthesised directly from the LDH-CO₃ through a surfactant-mediated one-pot synthesis. The method is convenient (low reaction temperature and relatively short reaction time), environmentally friendly (no toxic solvent used) and economical. Although the method does not entail procedures to exclude carbon dioxide or carbonate, such as working in inert environments, its products are of good crystallinity and have minimal carbonate contamination.

The surfactants of choice in the study are fatty acids or carboxylic acids. Fatty acids are normally unbranched and have an even number of carbon atoms. The anions were chosen because they are readily available and at low cost. Fatty acids are derived from the hydrolysis of animal fat or vegetable oil in aqueous NaOH to yield glycerol and fatty acids. However, they may be produced synthetically through hydroxycarboxylation of alkenes.

1.2 LDH-BASED POLYMER COMPOSITES

Composite materials make a large contribution to engineering materials in the form of alloys, reinforced concrete and carbon black in vehicle tyres, etc. Biological systems are also good examples that possess a wide variety of composites. The technological world has a constant demand for multifunctional materials. Hence, numerous researchers have embarked on exploring various methods of synthesising and improving materials properties. The main application markets for clay-based polymer nanocomposites are packaging, flame retardants, aerospace and aviation, and the automotive industry. Figure 1.1. shows the

global application market projections for clay-based polymer composites. Growth is predicted in some areas as, well as greater diversity in their application by 2017.

The dispersion of particles with high aspect ratios, such as fibres and platelets in polymeric matrices, together with adequate interfacial adhesion between the filler and polymer, results in improved properties of the polymer matrices. Nanostructured anionic clays such as LDHs impart these properties and are therefore ideal for polymer-clay nanocomposite preparations. The resulting polymeric hybrids exhibit improved gas barrier properties, strength, dimensional stability, flame retardancy and ultraviolet (UV) stability, etc.

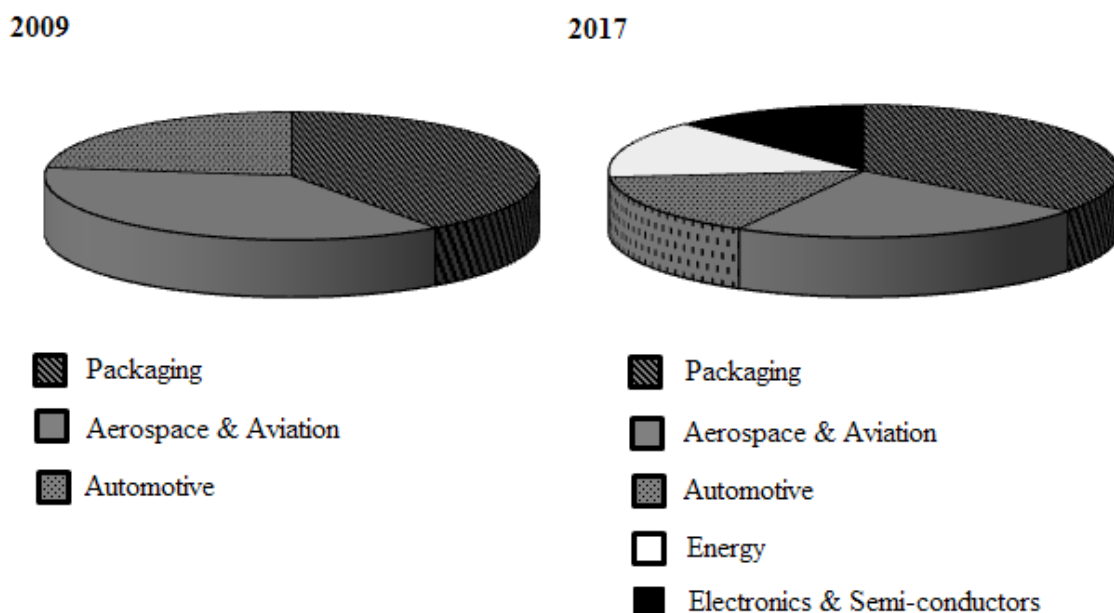


Figure 1.1. Global application market share projections for polymer composites
(Adapted from Research and Markets, <http://www.researchandmarkets.com>)

Surfactant-intercalated LDHs have been reported to exfoliate in polymer matrices and organic solutions (Leroux & Besse, 2001; Khan & O'Hare, 2002; Fischer, 2003). However, the intercalated anions show thermotropic behaviour (Nhlapo *et al.*, 2008; Focke *et al.*, 2010; Moyo *et al.*, 2012). An example of this behaviour is shown in Figure 1.2 where LDH-stearate intercalated above the AEC level melts below typical polymer processing temperatures (120 °C) (Nhlapo *et al.*, 2008). Droplet formation was observed in hot stage optical microscopy, giving a façade of a completely molten LDH-stearate (Nhlapo *et al.*, 2008). This can be attributed to the excess stearate acid exuding and forming a liquid

droplet that surrounds the parent LDH-stearate platelets. However, droplet formation was not observed when the samples were heated in an environmental scanning electron microscope (SEM) because the acid evaporated. This effusion of the excess stearic acid from the bilayer intercalated LDHs proceeds in stages. It starts with the removal of interlayer water and terminates in a monolayer-intercalated clay residue, depending on the temperatures the material is exposed to.

These observations imply that dispersion of LDH-fatty acids in polymer matrices may perhaps not follow the conventional exfoliation or delamination routes (Adachi-Pagano *et al.*, 2000). The exudation of stearic acid may have implications on the processing behaviour and the composite properties (particularly the mechanical properties). Such thermal events are of concern, hence clarity is required as to whether they are advantageous or detrimental to the resultant composite. It was therefore of interest to carry out a comprehensive study on the properties of fatty acid intercalated layered double hydroxides, as well as to follow the micro- and nanopolymer composites obtained therefrom.

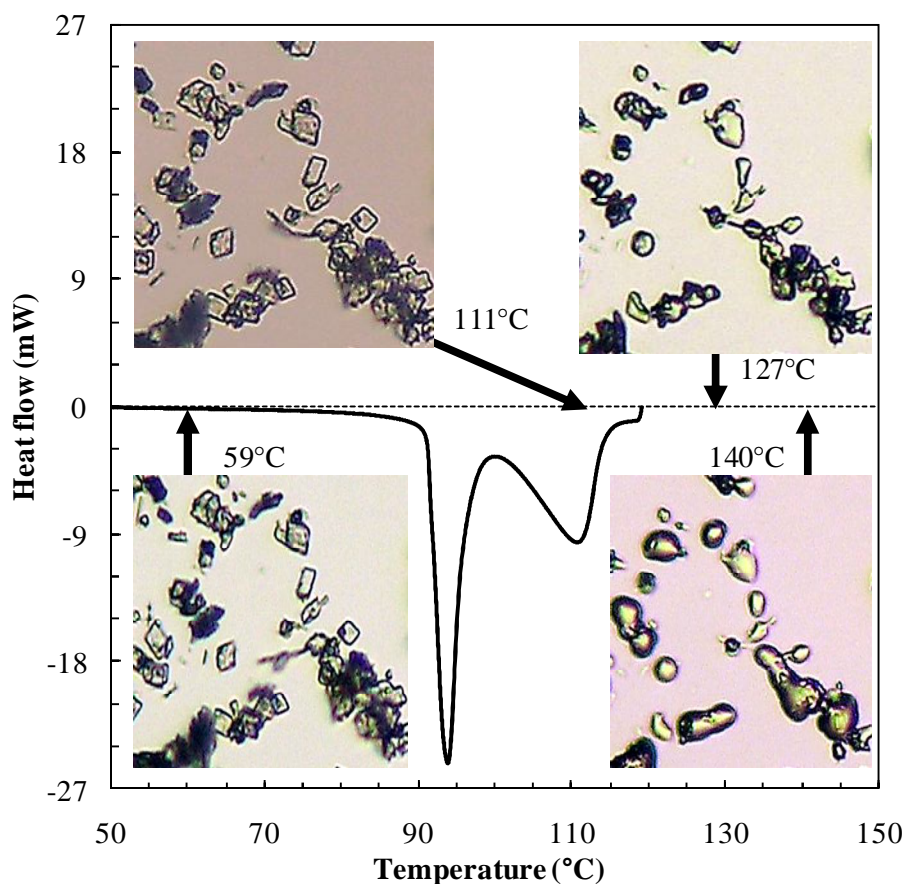


Figure 1.2. Differential scanning calorimetry (DSC) melting endotherm and hot stage microscopy of LDH-stearate (Nhlapo *et al.*, 2008)

1.3 LDH/JOJOBA OIL SUSPENSIONS

Organoclays are rheological modifiers, used as thickeners and for the control of the thixotropic properties of paints, grease and cosmetics (Jones, 1983). They deliver moderate steady-shear viscosity, together with the formation of a strong gel upon cessation of shear (King *et al.*, 2007). The smectite clay minerals are, however, commonly employed. The thickening of organoclay suspensions is thought primarily to be achieved through exfoliation and/or three-dimensional assemblies of particles into a ‘house-of-cards’ structure (Albiston, 1996).

However, the delamination of LDH is difficult compared with that of montmorillonites and laponites which exfoliate into single clay sheets in aqueous suspensions (Wu *et al.*, 2005; King *et al.*, 2007). The extent of exfoliation is proportional to the number of delaminated single crystal layers or their small stacks in the matrix. As mentioned earlier, the pristine LDHs are modified with different anions to increase the interlayer distance, consequently improving their propensity to delaminate or exfoliate.

The focus in this section of the study will be mainly on an investigation into the change of viscosity as a function of temperature of organo-LDH/Jojoba oil formulations. As has already been stated, organo-LDHs demonstrate ‘thermotropic’ behaviour. Therefore the questions are: What effect will the exuded excess acid have on the matrix? Is full exfoliation of organo-LDH in an oil matrix possible? Why Jojoba oil? Jojoba oil (*Simmondsia chinensis*) is a widely used oil phase in cosmetic formulations. The oil has numerous benefits, some of which are improvement of skin tone, excellent oxidative stability and relative stability at high temperatures when compared with other vegetable oils.

1.4 RESEARCH OBJECTIVE

The general objective of the study was to investigate the utility of layered double hydroxides as an additive in polymeric materials and Jojoba oil.

The specific objectives were as follows:

- Extend and optimise the intercalation techniques originally developed for fatty acids and anionic surfactants in hydrotalcite.

- Characterise modified LDH samples by spectroscopic techniques, thermal analysis, X-ray diffraction and microscopy.
- Investigate the properties affected by the incorporation of intercalated clays into candidate polymers, i.e. ethylene vinyl acetate (EVA), ethylene vinyl alcohol (EVAL) and linear low-density polyethylene (LLDPE).
- Prepare and test such nanocomposites, mouldings and oil formulations to confirm suitability for various applications.
- Study the rheological behaviour of organo-LDHs/Jojoba oil suspensions.

1.4.1 Methodology

- Modification of LDHs with long-chain fatty/carboxylic acids which are intended to functionalise the clay and hence improve their compatibility with the matrix
- Comprehensive characterisation of LDHs
- Dispersion of both unmodified and modified LDH through melt compounding, injection moulding of tensile testing dumbbells and mechanical property testing of specimens
- Full characterisation of polymer composites by thermal analysis, and microscopic and spectroscopic studies
- Dispersion of modified LDHs in Jojoba oil, followed by a study of the rheological behaviour of the resultant suspensions.

1.5 REFERENCES

- Albiston, L. (1996). Rheology and microstructure of aqueous layered double hydroxide dispersions. *J. Mater. Chem.*, 6(5): 871.
- Adachi-Pagano, M., Forano, C. & Besse, J-P. (2000). Delamination of layered double hydroxides by use of surfactants. *Chem. Commun.* : 91–92.
- Carlino, S. (1997). The intercalation of carboxylic acids into layered double hydroxides: A critical evaluation and review of the different methods. *Solid State Ionics*, 98, 73–84.
- Choy, J-H. (2004). Intercalative route to heterostructured nanohybrids. *J. Phys. Chem. Solids*, 65: 373–383.
- Crespo, I., Barriga, C., Rives, V. & Ulibarri, M. A. (1997). Intercalation of iron hexacyano complexes in Zn, Al-hydrotalcite. *Solid State Ionics*, 101–103: 729–735.
- Drezdron, M. A. (1988). Synthesis of isopolymetalate-pillared hydrotalcite via organic-anion-pillared precursors. *Inorg. Chem.*, 27: 4628–4632.
- Fischer, H. (2003). Polymer nanocomposites: From fundamental research to specific applications. *Mat. Sci. Eng., C*, 23: 763–772.
- Focke, W. W., Nhlapo, N. S., Moyo, L. & Verryin, S. M. C. (2010). Thermal properties of lauric and stearic acid-intercalated layered double hydroxides. *Mol. Cryst. Liq. Cryst.*, 521(1): 168–178.
- Jones, R. (1983). The properties and uses of clays which swell in organic solvents. *Clay Min.*, 18(4): 399–410.
- Khan, A. & O’Hare, D. (2002). Intercalation chemistry of layered double hydroxides: Recent developments and applications. *J. Mater. Chem.*, 12: 3191–3198.
- King, H., Milner, S., Lin, M., Singh, J. & Mason, T. (2007). Structure and rheology of organoclay suspensions. *Phys. Rev. E.*, 75(2): 1–20.

- Kumar, A. P., Depan, D., Singh Tomer, N., & Singh, R. P. (2009). Nanoscale particles for polymer degradation and stabilization—Trends and future perspectives. *Progress in Polymer Science*, 34(6): 479–515.
- Leroux, F. & Besse, J.-P. (2001). Polymer interleaved layered double hydroxide: A new emerging class of nanocomposites. *Chem. Mater.*, 13(10): 3507–3515.
- Meyn, M., Beneke, K. & Lagaly, G. (1990). Anion-exchange reactions of layered double hydroxides. *Inorg. Chem.*, 29: 5201–5207.
- Moyo, L., Focke, W. W., Labuschagne, F. J. & Verryyn, S. (2012). Layered double hydroxide intercalated with sodium dodecyl sulphate. *Mol. Cryst. Liq. Cryst.*, 555(1): 51–64.
- Newman, S. P. and Jones, W. (1998). Synthesis, characterization and layered double hydroxides containing organic guests. *New J. Chem.*: 105–115.
- Nhlapo, N., Motumi, T., Landman, E., Verryyn, S. M. C. & Focke, W. W. (2008). Hydrotalcite: Surfactant-assisted fatty acid intercalation of layered double hydroxides. *J. Mater. Sci.*, 43(3): 1033–1043.
- Oriakhi, C. O., Farr, I. V. & Lerner, M. M. (1996). Incorporation of poly(acrylic acid), poly(vinylsulphonate) and poly(styrenesulphonate). *J. Mater. Chem.*, 6(1): 103–107.
- Reichle, W. T. (1986). Synthesis of anionic clay minerals (mixed metal hydroxides, hydrotalcite). *Solid State Ionics*, 22: 135–141.
- Research and Markets. Available at: <http://www.researchandmarkets.com> [Accessed 11 January 2011].
- Robins, D. S. & Dutta P. K. (1996). Examination of fatty acid exchanged layered double hydroxides as supports for photochemical assemblies. *Langmuir*, 12: 402–408.
- Utracki, L. A. (2004). *Clay-Containing Polymeric Nanocomposites*, Vol. 1. Shrewsbury, UK: Rapra Technology Ltd, p. 456.
- Wu, Q., Olafsen, A., Vistad, Ø. B., Roots, J. & Norby, P. (2005). Delamination and restacking of a layered double hydroxide with nitrate as counter anion. *J. Mater. Chem.*, 15(44): 4695–4700

Xu, Z. P. & Zeng, H. C. (2001). Decomposition pathways of hydrotalcite-like compounds $\text{MgAl}_x(\text{OH})_2(\text{NO}_3)_x \cdot n\text{H}_2\text{O}$ as a continuous function of nitrate anions. *Chem. Mater.*, 13: 4555–4563.

Chapter 2

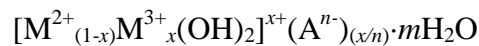
Layered double hydroxides and fatty acid intercalation

Monocarboxylic acids C_{14} - C_{22} were successfully intercalated into Mg-Al-LDH- CO_3 . The one-pot synthesis consistently yields a bilayer intercalated product for the range of acids employed. The intercalated anions have an orientation tilt angle of 55 – 63° depending on the chain length. The thermotropic behaviour of the bilayer fatty acid-intercalated LDHs was studied for each of the fatty acid derivatives within a temperature range of 25 – 200 °C. The stages followed included removal of water and exudation of excess anions, resulting in a monolayer arrangement.

2 LAYERED DOUBLE HYDROXIDES

2.1 WHAT IS A LAYERED DOUBLE HYDROXIDE?

Layered double hydroxides (LDHs) are also known as hydrotalcite-like compounds. Hydrotalcite was first discovered in Sweden in 1842. The mineral is formed from the weathering of basalts or their precipitation in saline water sources (Braterman *et al.*, 2004). Its name derived from its high water content (*hydro*) and talc-like properties, translating to hydrotalcite. The synthetic analogues were first prepared in the laboratory by Feitknecht and Gerber in 1942. They possess a brucite $Mg(OH)_2$ structure in which some of the divalent ions are isomorphously replaced by the trivalent ones. The replacement results in a net positive charge which is counterbalanced by the existence of anions and water molecules in the interlayer. The electrostatic interaction and hydrogen bonding between the layers and the interlayer anions help maintain the overall structure and electro-neutrality of the clay (Cavani *et al.*, 1991; Trifiro & Vaccari, 1996). A schematic presentation of layered double hydroxides is shown in Figure 2.1. LDHs have a generic formula as shown below (Brindley & Kikkawa, 1979; Miyata, 1980; Mascolo & Marino, 1980; Cavani *et al.*, 1991).



where:

M^{2+} is Mg, Zn, Ni, Co, Ca, Mn, etc.

M^{3+} is Al, Cr, Fe, Mn, Co, V, etc.

A^{n-} is CO_3^{2-} , Cl^- , NO_3^- , etc.

The different compositional species derived thereof are referred to as 'hydrotalcite analogues'. In the Mg-Al LDHs, the x -value is the ratio of aluminium to magnesium. It is calculated from the equation below:

$$x = \frac{M(III)}{M(II)+M(III)} \quad [1]$$

where $M(II)$ and $M(III)$ are the divalent and trivalent cations respectively. The x -value is reported to fall within $0.1 \leq x \leq 0.5$, with pure phases existing for $0.2 \leq x \leq 0.3$ (Cavani *et al.*, 1991; Khan & O'Hare, 2002). When the x -value is lower than 0.33, the Al octahedrals

are not neighbouring, leading to a high density of Mg octahedrals in the brucite-like sheet. In the case of higher values of x , the increased number of neighbouring Al octahedrals leads to the formation of $\text{Al}(\text{OH})_3$. The x -value determines the layer charge density and the anion exchange capacity (AEC) (Utracki *et al.*, 2007).

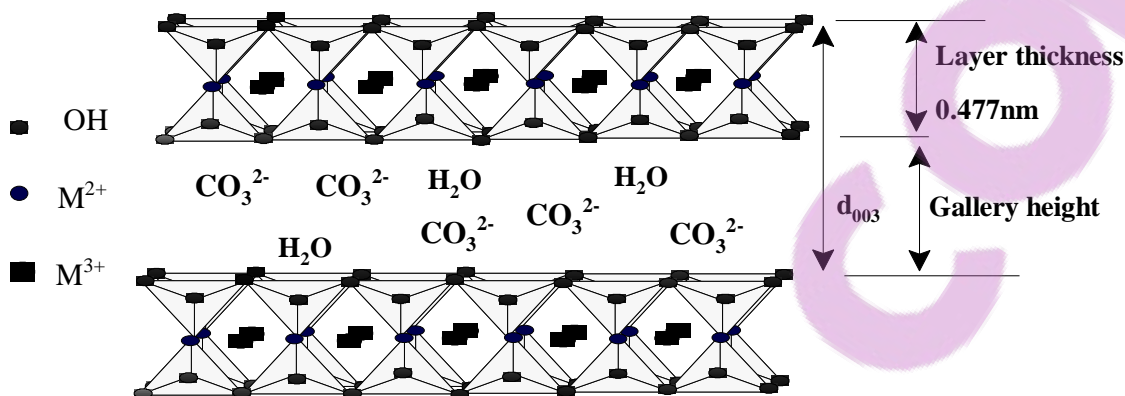


Figure 2.1. Layered structure of LDH- CO_3

The ionic radii of the metal species used in the preparation are usually very close to that of Mg^{2+} . However, when the metal ion radius is above 0.06 nm, the LDH structure becomes unstable, e.g. with cations such as Ca^{2+} the hydrotalcite structure transforms into hydrocalumite (Forano *et al.*, 2006). Several hybrids of LDHs may be synthesised with different stoichiometries and metal compositions. Though most research focuses on the binary metal combinations, ternary and quaternary combinations have also been reported (Kooli *et al.*, 1995; Xiang *et al.*, 2009). Hydrotalcite are attractive compared with other layered compounds due to their versatility, ease of tailoring to suit functionality, simplicity and their low cost in preparation. Synthetic analogues of hydrotalcite can be readily prepared in the laboratory.

Hydrotalcite exists as two polymorphs: the hexagonal (H) and rhombohedral (R). The natural varieties of polymorphs have been described as 1H, 2H₁, 3H₂, 3R₁, 3R₂ and 6R. However, they have been found to occur as a mixture. The most common polytype in synthetic varieties is 3R₁ (Zaneva & Stanimirova, 2004). The polymorphs are given the above-mentioned designations to describe the stacking sequence of the brucite-like sheets. Table 2.1 is a summary of the different species of layered double hydroxides, polytypes and chemical formulas.

Table 2.1. Summary of layered double hydroxides, year of discovery, polytypes and chemical formulas (Adapted from Zaneva & Stanimirova, 2004)

Year of Discovery	Mineral name	Polytype	Chemical formula
1842	Hydrotalcite	3R	$Mg_6Al_2(OH)_{16}CO_3 \cdot 4H_2O$
1865	Pyroaurite	3R	$Mg_6Fe_2(OH)_{16}CO_3 \cdot 4H_2O$
1866	Woodwardite	3R	$Cu_5Al_2(OH)SO_4 \cdot 2 \cdot 4H_2O$
1900	Sjögrenite	2H	$Mg_6Fe_2(OH)_{16}CO_3 \cdot 4H_2O$
1910	Stichtite	3R	$Mg_6Cr_2(OH)_{16}CO_3 \cdot 4H_2O$
1934	Hydrocalumite	2M	$Ca_8Al_4(OH)_{24}(CO_3, Cl, OH)_3 \cdot 11H_2O$
1940	Manasseite	2H	$Mg_6Al_2(OH)_{16}CO_3 \cdot 4H_2O$
1941	Barbertonite	2H	$Mg_6Cr_2(OH)_{16}CO_3 \cdot 4H_2O$
1956	Honessite	3R	$Ni_6Fe_2(OH)_{16}SO_4 \cdot nH_2O$
1957	Takovite	3R	$Ni_6Al_2(OH)_{16}CO_3 \cdot 4H_2O$
1967	Reevesite	3R	$Ni_6Fe_2(OH)_{16}CO_3 \cdot 4H_2O$
1967	Iowaite	3R	$Mg_5Fe(OH)_{12}Cl \cdot 2H_2O$
1975	Meixnerite	3R	$Mg_6Al_2(OH)_{16}(OH)_2 \cdot 4H_2O$
1979	Desautelsite	3R	$Mg_6Mn_2(OH)_{16}CO_3 \cdot 4H_2O$
1980	Comblainite	6R	$Ni_6Co_2(OH)_{16}CO_3 \cdot 4H_2O$
1982	Chlormagaluminite	2H	$Mg_4Al_2(OH)_{12}(Cl, CO_3) \cdot 4H_2O$
1992	Caresite	3R	$Fe_4Al_2(OH)_{12}CO_3 \cdot 4H_2O$
1995	Zincowoodwardite	3R	$Zn_5Al_2(OH)_{12}SO_4 \cdot 2 \cdot 4H_2O$
1996	Kuzelite	6R	$Ca_4Al_2(OH)_{12}SO_4 \cdot 6H_2O$
1997	Quintinite-2H	2H	$Mg_4Al_2(OH)_{12}CO_3 \cdot 4H_2O$
1997	Quintinite-3T	3R	$Mg_4Al_2(OH)_{12}CO_3 \cdot 4H_2O$
1997	Zaccagnaite	2H	$Zn_4Al_2(OH)_{12}CO_3 \cdot 3H_2O$
1998	Charmarite (2H, 3T)	2H, 3R	$Mn_4Al_2(OH)_{12}CO_3 \cdot 4H_2O$
2000	Woodallite	3R	$Mg_6Cr_2(OH)_{16}Cl_2 \cdot 4H_2O$

2.2 LDH PREPARATION ROUTES

2.2.1 Co-precipitation

Co-precipitation is a direct synthesis method that entails nucleation and growth of metal hydroxide layers from two metal species in a basic aqueous solution. The metal salts favoured in this reaction are nitrates and chlorides. This is due to their monovalent charge

which makes them easily exchangeable. Due to the frequent use of the method in the preparation of LDHs, various refinements have been employed. These include:

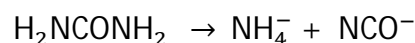
- Co-precipitation in aqueous solution (Bocclair & Braterman, 1999)
- Co-precipitation in non-aqueous solution (He *et al.*, 2005)
- Hydrothermal synthesis by urea hydrolysis (Rao *et al.*, 2005)
- Co-precipitation at low supersaturation (Meyn *et al.*, 1990)
- Co-precipitation at high supersaturation (Constantino & Pinnavaia, 1995)

During synthesis, researchers pay special attention to the nature and mole ratio of the metal species, nature of anions, pH, temperature, precipitation method and the post-preparation treatment of the LDHs. The method allows control of the charge density of the hydroxide layers by regulating the pH of the system. When the pH of the system is too low, not all the mixed metal ions will precipitate, whereas a very high pH leads to the dissolution of one or more of the ion species (Othman *et al.*, 2009). As the precipitate is often in the form of gels, washing tends to be complicated, resulting in very low yields.

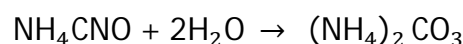
2.2.2 Urea hydrolysis

The methods usually follow the principles of the co-precipitation reaction. However, the base or precipitating agent is generated in situ. The method has been used with much success by many researchers (Adachi-Pagano *et al.*, 2003, Rao *et al.*, 2005, He *et al.*, 2005). Urea is a weak Brønsted base, whose hydrolysis rate is controlled by temperature. Hydrolysis proceeds in a two-step process:

- (i) The rate-determining step, which entails the formation of ammonium cyanate:



- (ii) Fast hydrolysis of the cyanate into ammonium carbonate:



The hydrolysis process of ammonium cyanate to ammonia and carbonate to hydrogen carbonate gives a pH of approximately 9, which is ideal for the precipitation of hydroxides. The resulting LDHs show good crystallinity and large particles. Since the reaction

progresses slowly, this leads to low degrees of supersaturation. Temperature control was observed to be a fundamental parameter for obtaining uniformity and particle sizes (Othman *et al.*, 2009). Iyi *et al.* (2004), used an alternative ammonia releasing/precipitating agent in the form of hexamethylenetetramine (HMT) and they were able to achieve high degrees of crystallinity. However, the production of the carbonate anion is unavoidable in all cases. Microwave synthesis of hydrotalcite by urea hydrolysis was employed by Yang *et al.* (2007), and the hydrotalcite prepared at 600 W power had the highest crystallinity and a homogeneous crystal size.

2.2.3 Sol-gel

The sol-gel technique was pioneered by Lopez *et al.* (1996) in the synthesis of hydrotalcite analogues. The sol is prepared by hydrolysis and condensation of the inorganic salt and organic metal compound (alkoxides) in water and/or organic solvent. Variants of the method include heating and using different types of solvent to achieve dissolution of less-soluble reactants (Othman *et al.*, 2009). Ramos *et al.* (1997) prepared hydrotalcites from magnesium ethoxide using various sources of aluminium, i.e. acetylacetonate, nitrate, sulphate and chloride. The crystallinity of the product and sintering behaviour was found to depend on the aluminium precursor. The observed properties followed this trend: aluminium acetylacetonate > aluminium chloride > aluminium nitrate > aluminium sulphate.

Prinetto *et al.* (2000) also explored sol-gel techniques in the preparation of hydrotalcite and takovite analogues. The starting materials were metal alkoxides and/or acetylacetonate. This preparation method led to pure and well-dispersed nanomaterials. LDH particles derived in this way have a lower particle size and are more reactive compared with those obtained by the co-precipitation reaction (Jitianu *et al.*, 2003). Samples prepared by this method exhibited an increase in specific surface area, which is attributed to an increase in mesopore volume (Forano *et al.*, 2006). These mesoporous structures are ideal for the development of novel catalysts or catalytic systems. Sol-gel LDH properties have been modified by changing the cations used in the sol preparation, the reaction temperature, the ageing time the pH. For example, decreasing the reaction temperature or ageing time increases the specific surface area or particle size of LDHs. The specific surface area of the LDHs was found to be 10–25% greater than that of products achieved from the co-precipitation reaction (Aramendia *et al.*, 2002). Increasing the acid-boehmite molar ratio was

recommended to decrease the porosity of the sintered LDHs (Othman *et al.*, 2009). The areas of concern in this method include the basicity and their $M^{II}:M^{III}$ ratio.

Other methods that have been employed in the preparation of LDHs include electrochemical methods (Sugimoto *et al.*, 1999; Indira *et al.*, 1994), steam activation (Abello *et al.*, 2006), hydrothermal crystallisation of the amorphous acidic precursor (Mascolo *et al.*, 1995) and *chimie douce* (Delmas & Borthomieu, 1993).

2.2.4 Post-preparation techniques

Post-preparation techniques are carried out to improve the quality of crystallites, obtain uniform size distribution and improve the ordering of anions within the interlayer of the LDH. These post-preparation techniques include hydrothermal and solvothermal methods, microwave irradiation and ultra-sound treatments.

Hydrothermal treatment is the most common of the methods used. The sample is subjected to temperatures of up to 200 °C under autogeneous pressure for time periods ranging from hours to days. This treatment has given rise to increases in particle size relative to the ageing time. The LDH platelets obtained thereof are of regular shapes, usually hexagonal morphologies.

Microwave treatments are normally used in combination with hydrothermal methods. However, the advantages of the former over the latter include shorter reaction time. For example, a well-crystallised product was obtained in 12 minutes compared with 1 530 minutes (Kannan *et al.*, 2000). As microwaves interact with liquid or solid materials, they produce a dipole re-orientation in dielectric material and ionic conduction if the ions are mobile. Hence it is possible to achieve a uniform bulk heating of the system, reducing the occurrence of thermal gradients originating from the conventional heating method (Othman *et al.*, 2009).

It is clear from the above preparation methods that hydrotalcites can be tailored to fit their specific requirements and properties. The high charge density on the LDHs renders them unattractive as they do not readily exfoliate or delaminate. LDHs possess an expandable 2-D layer structure which allows the exchange of various anions. Increasing the d-spacing

lowers the van der Waals force between the sheets, hence they can easily be exfoliated or delaminated. Expansion of the interlayer is achieved by a process called *intercalation*.

2.2.5 Texture and morphology

The texture and morphology of platelets are related to the preparation method and crystal growth habits. Like most clay materials, LDHs exhibit a layered structure. Crystal habits similar to those observed in smectite single crystallites are also observed in LDHs, i.e. laths, fibres, and subhedral and euhedral lamellae (see Figure 2.1). The hexagonal shape obtained mainly from the urea hydrolysis method (Yang *et al.*, 2007) has become the archetype of well-synthesised LDHs. The hexagonal and rhombohedral shapes fall into the euhedral lamellae category. They display the presence of well-developed $\{hk0\}$ in addition to a very prominent basal reflection (Grim & Güven, 1978). This is typical of crystals that have had ample space for growth. The majority of researchers observed subhedral forms (Nhlapo *et al.*, 2008, Xu and Braterman 2010, Costa *et al.*, 2006); these have irregular outlines, but with a well-defined basal form. Although the lath and fibre forms are rare, they have been reported (Xu & Braterman, 2010, Moyo et al, 2012). Crystallites of this form originate from the folding of thin lamellae (Grim & Güven, 1978). SEM micrographs of the different LDH crystallites observed in this study are shown in a Section 2.6.1 and Appendix B.

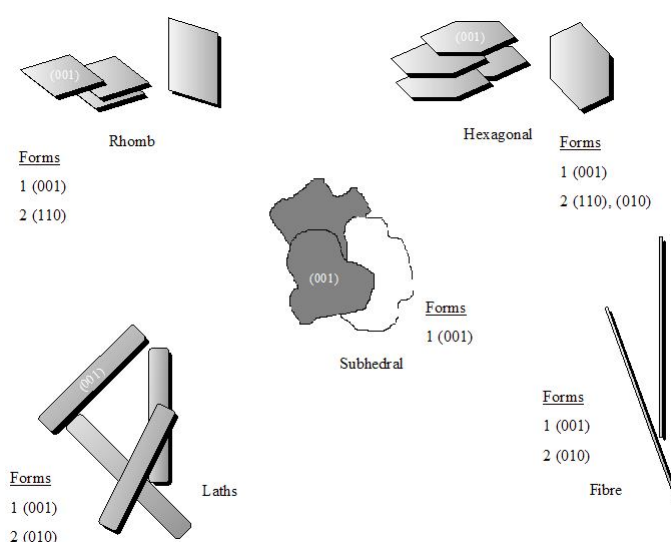


Figure 2.2. Common habits of smectite single crystallites

(Adapted from Grim & Güven, 1978)

2.3 INTERCALATION

Intercalation is a form of clay-surface interaction where the anions or surfactant molecules aggregate within the interlayer, i.e. between pairs of adjacent clay sheets (Crepaldi *et al.*, 2002). O'Hare (1991) defined it as “the reversible insertion of mobile guest species into a crystalline layered host lattice, during which the structural integrity of the latter is formally conserved”. Self-assembly drives intercalation. During this process the anions spontaneously organise themselves into an ordered state (see Figure 2.3). The basic mechanism by which intercalation occurs is either through oxidation-reduction, ion-exchange, acid-base or donor-acceptor reactions (Khan & O'Hare, 2002). LDHs are normally non-selective, although shape and stereo-selectivity have been observed (Ikeda *et al.*, 1984; Lotsch *et al.*, 2001). Most recently, chain length selectivity has been encountered in surfactant-mediated exchange of short chain fatty acids, in which the surfactant chain is intercalated preferentially (Moyo *et al.*, 2008). Intercalation is facilitated by interactions such as electrostatic attractions, hydrogen bonding and hydrophobic associations (Whitesides *et al.*, 1991). The separation of the layers is governed by the dimensions and functional group of the anions to be intercalated. Other factors include the AEC level of the anions intercalated, size, orientation and interaction with the hydroxyl lattice (Cavani *et al.*, 1991). The inclusion of organic anions within the interlayer of LDHs is essential to their physical or chemical functionality. Intercalation has been used to change the chemical, electronic, optical and magnetic properties of the host lattice (Khan & O'Hare, 2002).

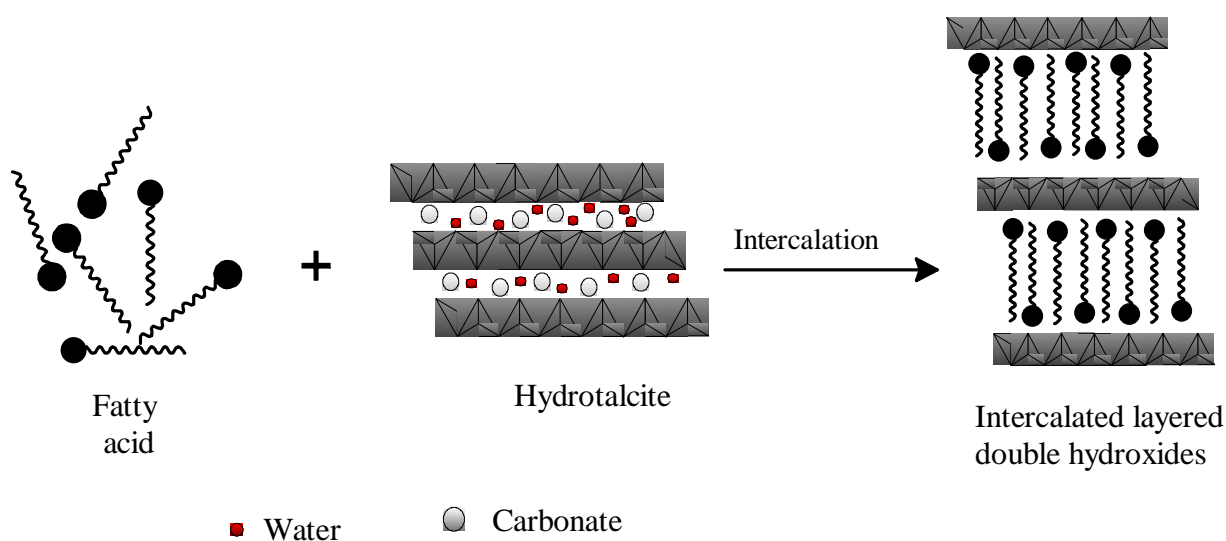


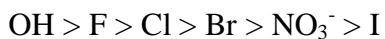
Figure 2.3. Intercalation

2.3.1 Intercalation methods

Crepaldi *et al.* (1999) proposed three main LDH intercalation procedures, i.e. direct synthesis, ion exchange and the regeneration or reconstruction method. Direct synthesis is normally achieved by a co-precipitation reaction (Meyn *et al.*, 1990). The LDH is prepared in situ by adding a mixed metal solution dropwise to an alkaline solution containing the anion to be intercalated. The method has been proved to produce highly crystalline products, especially when followed up by hydrothermal treatments. Moyo *et al.* (2012) employed co-precipitation in the intercalation of dodecyl sulphate, and obtained a pure and highly crystalline bilayer intercalated product.

In the case where the LDH-CO₃ is the precursor, the first step is to eliminate the carbonate anion; this is achieved by either calcination or acid treatment of the LDH-CO₃ (Iyi *et al.*, 2005; Moyo *et al.*, 2008). Hydrotalcite sheets have a high charge density and as a result a higher affinity for multivalent anions such as carbonates. The carbonate anion is therefore tenaciously held within the interlayer. However, the decarbonation process using mineral acids is a challenge due to the strong acidity of HCl and the low acid tolerance of Mg-Al LDH (Iyi *et al.*, 2005).

The LDH precursor in the ion-exchange method is an LDH-A, where A is a monovalent anion that can be easily exchanged, e.g. chloride or nitrate. Miyata and Okada (1977) found that the ease of exchange or affinity of the LDH lattice was found to be in the following order:



The LDH-A is suspended in a solution containing the carboxylic acid or its sodium salt. This method has been employed in the intercalation of α,ω dicarboxylic acids and a range of carboxylic acids (Miyata & Kumura, 1973). Variations of the method have included intercalation of lauric, myristic and palmitic acid carried out in ethanolic solutions (Borja & Dutta, 1992).

The reconstruction method is self-explanatory in that the metal hydroxide is reconstructed from the mixed metal oxides. The carbonate anion is removed from the interlayer by heating the LDH-CO₃ at temperatures between 450–550 °C for 3–4 hours. Calcination yields a decarbonised and dehydroxylated layered double oxide (LDO). The LDO is suspended in an alkaline solution containing the anion to be intercalated. The metal hydroxyl lattice reforms under these conditions, at the same time incorporating the anion into the interlayer. The mechanism has been reported to entail a fast rehydration with the intercalation of OH⁻ anions, which is followed by a slow ion-exchange reaction of the OH⁻ anions with the desired intercalant (Crepaldi *et al.*, 2002). This is attributed to the memory effect of LDOs. Structure recovery is affected by the calcination conditions, such as temperature, heating rate and duration (Rocha *et al.*, 1999). The method has been used with great success in the intercalation of alkyl-sulphates, aryl sulphonates and carboxylic acids (Miyata & Okada, 1977; Sato *et al.*, 1988; Chibwe & Jones, 1989). Latterini *et al.* (2002) also successfully intercalated large organic anions such as phenolphthalein. Although the method is considered effective, it produces a non-homogeneous product, comprising a mixture of modified LDH and a small fraction of unmodified LDH (Costa *et al.*, 2011). The calcination process can cause irreversible changes in the crystalline structure (Hibino & Tsunashima, 1988; Stanimirova *et al.*, 2001). The texture and morphology of the intercalates was also found to be affected by the calcination process (Moyo, 2009).

The preparation method employed in this particular study of carboxylic acid intercalated LDHs is basically an ion-exchange reaction. However, it is unique in that the exchange is direct from the LDH-carbonate precursor. The underlying principle for the success of the method is a basic acid-base reaction. Carbonic acid has pK_a values of 6.35 and 10.33 at 25 °C for the first and second protonation reactions respectively, whereas the pK_a value of fatty acids is approximately 4.8. This implies that the fatty acid would readily protonate the carbonate anion (McMurry, 1999; Landman, 2005). This is similar to the decarbonation method described by Iyi *et al.* (2005). They suggested a two-step mechanism by which intercalation occurs, the first step being the protonation of the carbonate anion to hydrogen carbonate and the second step involving the instantaneous inclusion of the anions in solution. However, the method utilised strong acids such as HCl. Limited success was achieved due to the low acid tolerance of Mg-Al LDH and difficulty in handling the acid in large-scale experiments. The method was later modified by using an acetate buffer (sodium acetate buffer and acetic acid/NaCl mixed solution) (Iyi & Sasaki 2008).

Post-intercalative treatments are necessary to obtain a highly crystalline well-ordered product with large particle sizes. These include hydrothermal, microwave and ultra-sound treatments, which have been discussed in greater detail in Section 2.2.4.

2.3.2 Orientation of intercalated fatty acids

Intercalated anions will always orient themselves in such a manner that they maximise interaction with the hydroxyl layers and adjacent anions. The orientation of intercalated anions is studied by X-ray diffraction (XRD) and the state of anions is investigated through Fourier transform infrared (FTIR) spectroscopy. XRD gives an indication of layer separation and FTIR is used to probe the structure of the interlayer and the phase state of intercalated anions. Changes in the CH₂ stretching and scissoring vibrations are related to interlayer packing density, chain length and temperature (Vaia *et al.*, 1994). These aspects are discussed in Section 2.6 (results) of this chapter. Table 2.2. provides a brief overview of orientation and basal spacing of the fatty acid-intercalated LDHs found in the literature.

Table 2.2. Orientation and d-spacing of fatty acid-intercalated LDHs

Intercalated anion	LDH	M ²⁺ /M ³⁺ ratio	Orientation	d-spacing (nm)	Reference
Myristate	Li-Al; Mg-Al	1:2; 3:1	Monolayer	2.64	Borja & Dutta, 1992
Palmitate	Mg-Al	2:1	Bilayer	4.79	Itoh <i>et al.</i> , 2003
	Mg-Al	2:1	Monolayer	2.82	Nyambo <i>et al.</i> , 2009
	Zn-Al	2:1	Bilayer	4.42	Xu & Braterman, 2010
Stearate	Mg-Al	3:1	Monolayer	3.16	Meyn <i>et al.</i> , 1990
	Mg-Al	2:1	Bilayer	5.37	Itoh <i>et al.</i> , 2003
	Mg-Al	2:1	Bilayer	5.04	Nhlapo <i>et al.</i> , 2008
	Mg-Al	2:1; 3:1	Monolayer	2.95; 2.82	Xu & Braterman, 2010
	Zn-Al	2:1; 3:1	Bilayer	5.00; 4.99	Xu & Braterman, 2010
Arachidate	Mg-Al	2:1	Bilayer	5.72	Itoh <i>et al.</i> , 2003

Generally, two types of orientation have been observed for fatty acid intercalated LDHs, i.e. a monolayer and bilayer, the former being the most common (Figure 2.4). The packing and orientation of carboxylic acids is driven by:

- (i) the advanced hydrophobic interaction of long-chain aliphatic carboxylates that intercalate greater-than-normal AEC levels and pack closely in a bilayer format (Itoh *et al.*, 2003)
- (ii) molecular packing, which is dependent on the use of excess fatty acids and intercalation temperature (Itoh *et al.*, 2003; Nhlapo *et al.*, 2008)
- (iii) the solution pH at which anion-exchange takes place (Kuehn & Poellmann, 2010).

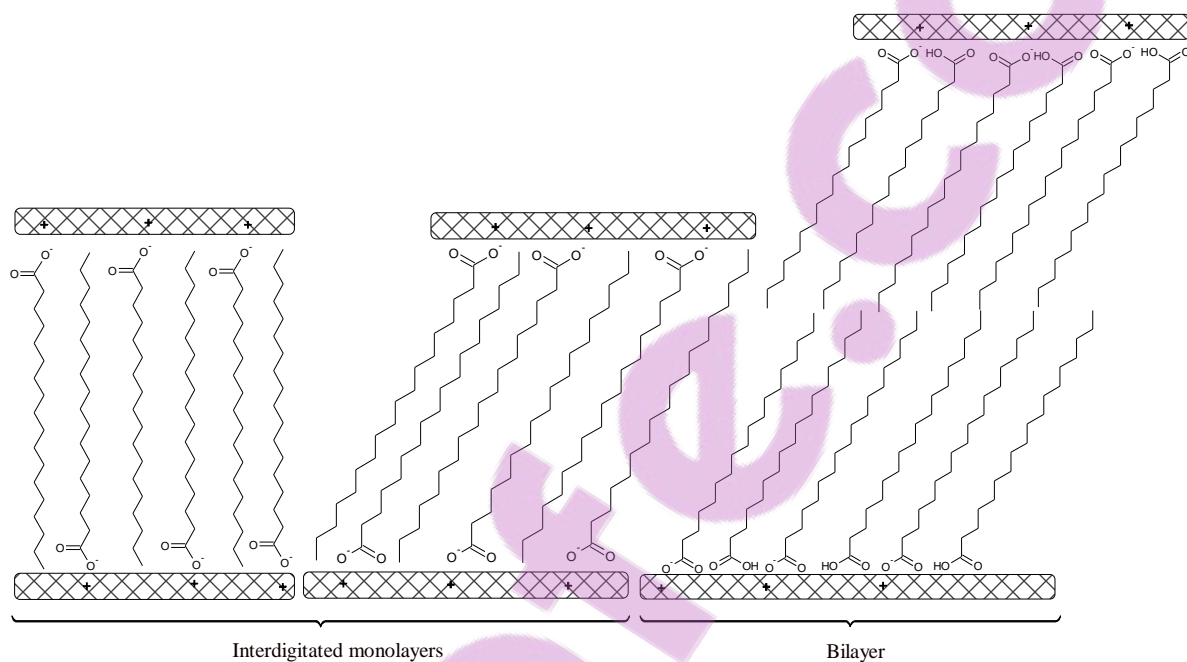


Figure 2.4. Orientation of intercalated fatty acids

Kanoh *et al.* (1991) suggested that LDHs could intercalate fatty acids greater than their normal AEC through the formation of bilayer structures similar to the Langmuir-Blodgett films. The strength, elasticity and stability of an absorbed surfactant film are influenced by surface activity, chain length compatibility and cohesion. Moreover, interactions between polar groups of the molecules in the monolayer have additional influence. The monolayer film of saturated fatty acids compresses to the same limiting area, e.g. stearic acid has a limiting area of 21 Å (Kanicky & Shah 2002; Itoh *et al.*, 2003). Close chain packing is also driven by the length of the surfactant chain (Figure 2.5). The van der Waals interaction between chains increases with increase in the chain length. Hence long-chain surfactants will pack closely and readily as compared with the short-chain carboxylates. This would explain the difficulty encountered by researchers in intercalating chains lengths of C₁ to C₈ (Costa *et al.*, 2011; Nhlapo *et al.*, 2008).

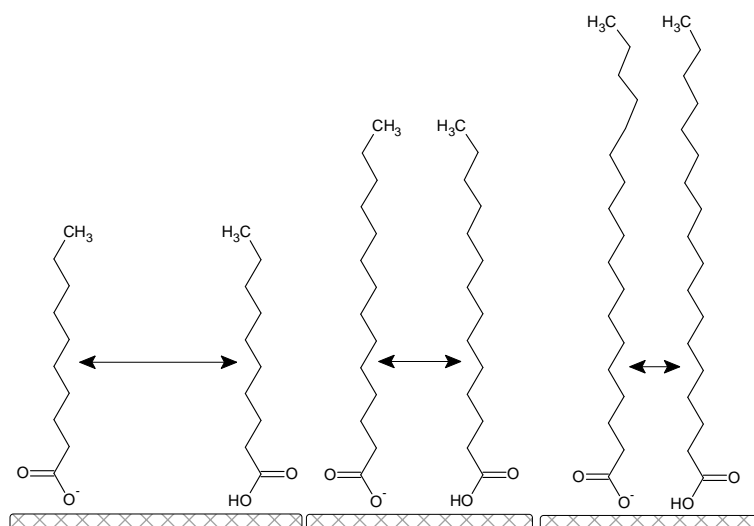


Figure 2.5. Effect of chain length on the close packing of intercalated fatty acids
(Adapted from Kanicky & Shah, 2002)

Intercalation is pH dependent: at high pH the surfactant head groups are completely ionised (Figure 2.6). This results in the repulsion of similarly charged molecules, which ultimately leads to expansion of the monolayer and a weak, unstable film. Close packing is achieved when intercalation is carried out close to its pKa value, as seen from Figure 2.6.

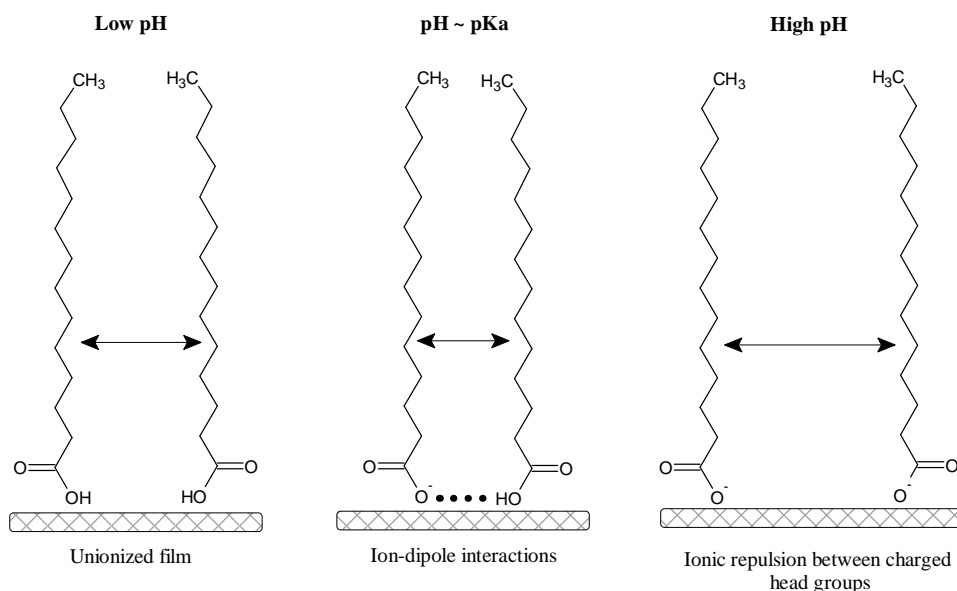


Figure 2.6. Effect of pH on the close packing intercalated fatty acid
(Adapted from Kanicky & Shah, 2002)

2.4 CHARACTERISATION OF LDH AND MODIFIED DERIVATIVES

A combination of characterisation techniques is employed in the structural elucidation of LDH, its composition and the orientation of intercalated anions. The most common techniques are powder XRD, FTIR, thermogravimetry (TG), scanning electron microscopy (SEM) and transmission electron microscopy (TEM).

XRD is the main technique used in determining the extent of intercalation through changes in the d-spacing. It is also used to determine the degree of crystallinity, which is a direct function of the organisation within the hydroxide layer. FTIR provides information on the organic species that has been intercalated and the vibrational spectroscopy of the LDH octahedral lattice and hydroxyl groups. Thermogravimetric methods are essential in studying the thermal stability/behaviour of pristine LDHs and their intercalated derivatives. These methods also allow a comprehensive study of the decomposition pathways of LDHs. SEM and TEM are used to study the different textures and morphologies exhibited by LDHs. In addition, they give an appreciation of the lateral dimensions of the LDH platelets.

The other characterisation techniques used in the study are differential scanning calorimetry (DSC), TG-FTIR, temperature scan XRD and FTIR, and inductively coupled plasma optical emission (ICP-OES) spectrometry.

In this phase of the project the aim was to intercalate straight-chain carboxylic acids from C₁₄–C₂₂ and fully characterise the organo-LDH obtained thereof.

2.5 EXPERIMENTAL

2.5.1 Materials

The layered double hydroxide LDH-CO₃ (hydrotalcite grade HT-5) was supplied by Nkomazi Chemicals, South Africa. The particle size of the LDH was determined in a Malvern Mastersizer 2000 instrument and the particle size distribution was found to be d(0.1): 1.19 μm; d(0.5): 3.94 μm and d(0.9): 23.93 μm. Various fatty acids were used in the intercalation reactions; their properties are summarised in Table 2.3. They were all saturated

fatty acids (C₁₄–C₁₈), with the exception of oleic acid and Jojoba oil. Jojoba oil is composed of unsaturated liquid wax esters ranging from C₃₆–C₄₂.

Table 2.3. Summary of fatty acids used in the intercalation process

Acid	IUPAC name	Formula	Molar mass	Melting point (°C)	Supplier	Purity
Myristic	Tetradecanoic	C ₁₃ H ₂₇ COOH	228.37	54	Merck	≥ 98%
Palmitic	Hexadecanoic	C ₁₅ H ₃₁ COOH	256.42	63	Sigma	≈ 95%
Stearic	Octadecanoic	C ₁₇ H ₃₅ COOH	284.48	70	Biozone Chemicals	-
Behenic	Docosanoic	C ₂₁ H ₄₃ COOH	340.58	80	Fluka	≥ 80%
Oleic	(9z)-Octadec-9-enoic	C ₁₇ H ₃₂ COOH	282.46	14	Merck	

2.5.2 Preparation of organo-LDH

The Mg-Al-LDH-stearate was prepared as reported by Nhlapo *et al.* (2008). A typical intercalation procedure was carried out as follows: 40 g of surfactant (Tween 60) was dissolved in 1.5 litres of preheated distilled water and the temperature was kept at 80 °C. The addition of excess stearic acid (0.384 mol which is an equivalent of four times the AEC) was added in a three-part series. The total amount of 109g was added. The mixture was heated at 80 °C for 8 h and cooled overnight at room temperature. The process was repeated over four days with continuous stirring. On the fourth the day there was no acid addition. The pH of the mixture was maintained by adding ammonia solution, with each correction carried out once each day and corrected to a pH of approximately 9–10. The mixture was allowed to cool and the solids were separated by centrifugation, washing the mixture four times with water and once each with ethanol and acetone respectively. The LDH-stearate solids were dried at room temperature. The other fatty acids, namely myristic, palmitic and behenic acids, were intercalated in a similar manner. Detailed experimental parameters are documented in Appendix B.

The above procedure was repeated using the exact AEC and twice the AEC. The products were labelled LDH-stearate 1AEC and 2AEC respectively. Another experiment was carried out without stearic acid; this was done to determine whether the Tween 60 could intercalate into the LDH-CO₃ on its own. In addition, the neat magnesium stearate and aluminium stearate were subjected to a similar procedure, but in the absence of the LDH-CO₃.

Re-crystallisation of the magnesium stearate (20 g Mg stearate + 40 g surfactant (Tween 60)) was carried out by suspending it in distilled water. The reaction temperature was adjusted to 80 °C with pH \approx 9-10 and it was left to run for 24 h. The samples were recovered by centrifugation, washed once with water, three times with ethanol and once with acetone.

A 2:1 molar mixture of magnesium stearate and aluminium stearate was reacted using a very similar process. A mixture of 40 g of Tween 60, 28.38 g (0.048 mol) of magnesium distearate and 21.06 g (0.024 mol) of aluminium tristearate was suspended in 1 000 ml of distilled water and heated to 70 °C. As before, NH₄OH was added to control the pH (pH = 10). The product was recovered as described above. This product was named magnesium/aluminium stearate.

Finally, LDH-oleate was synthesised by the co-precipitation method. Solutions (0.5 and 0.25 mol respectively) of Mg(NO₃)₂·6H₂O and Al(NO₃)₃·9H₂O were prepared. The mixture of the metal salts solution was added dropwise to an alkaline solution containing 0.35 mol of oleate anions. The pH was adjusted using 2M NaOH to a pH of 10. The temperature was controlled at 80 °C and the solution left to stir for three days. Solids were again recovered by centrifugation and washed with distilled water – four times with ethanol and once with acetone. The solids were oven dried at 60 °C.

2.5.3 Characterisation

ICP-OES was used to determine the elemental composition of the fatty acid-intercalated LDH. Five milligrams of LDH and fatty acid-intercalated LDH samples were leached in an *aqua regia* solution. The aliquots were left to cool; 1 ml of aliquot was diluted with 9 ml of de-ionised water. These were then analysed on a Perkin Elmer SPECTRO ARCOS ICP-OES spectrometer to quantify the amount of Mg and Al present. Calibration was carried out using a multi-element standard (ICP grade). Each sample was measured three times and the average ICP value was recorded.

Powder samples were viewed on a JEOL 5400 SEM and a JEOL JSM-6010LA analytical SEM. They were prepared as follows: a small quantity of the LDH-fatty acid and the LDH-CO₃ precursor was placed onto carbon tape on a metal sample holder. Excess powder was

removed using a single blast of compressed air. The samples were then coated three times with gold under argon gas using the SEM autocoating unit E5200 (Polaron Equipment Ltd). Elemental analysis of the LDHs was done on the JEOL 5400SEM with Energy-dispersive X-ray spectroscopy (EDS). Transmission electron microscopy (TEM) was carried out on a JEOL 2100 TEM. A small quantity of LDH-CO₃ was added to 5 ml of methanol. A homogeneous dispersion was obtained through sonication for 5 to 10 s. Drops of the colloidal liquid were placed on an Agar scientific 300 µm holey carbon film coated copper grid. The solution was allowed to dry out prior analysis.

Phase identification was carried out by XRD analysis on a PANalytical X-pert Pro powder diffractometer with variable divergence and receiving slits and an X'celerator detector using Fe-filtered Co K-alpha radiation (0.17901 nm). X'Pert High Score Plus software was used for phase identification. Temperature-resolved XRD traces were obtained using an Anton Paar HTK 16 heating chamber with a Pt heating strip. Scans were measured between $2\theta = 1^\circ$ to 40° in a temperature range of 25 to 200 °C in intervals of 10 °C with a waiting time of 1 min and measurement time of 6 min per scan. Si (Aldrich 99% pure) was added to the samples so that the data could be corrected for sample displacement using X'Pert High Score plus software.

Differential scanning calorimetry (DSC) data were collected on a Perkin Elmer DSC instrument. Samples of 5–10 mg were placed in a 40 µl alumina pan and heated from -40 to 200 °C and then cooled back to -40 °C at a scan rate of 5 °C/min and a N₂ flow rate of 50 ml/min.

Thermogravimetric analysis was carried out on the neat LDH-CO₃ and the fatty acid-intercalated LDH. A powder sample of 15 mg was analysed on a Mettler Toledo TGA A851 TGA/SDTA machine. The sample was placed in 70 µl alumina open pans. The temperature was scanned at 10 °C/min in air, ranging from 25 to 1 200 °C.

Standard FTIR was carried out on a Perkin Elmer 100 Spectrophotometer with a MIRacle ATR attachment with diamond Zn/Se plate; spectra were recorded between 4000 and 650 cm⁻¹ at a resolution of 2 cm⁻¹, and the data collected over 32 scans.

2.6 RESULTS AND DISCUSSION

2.6.1 Composition and morphology

The ICP data are reported as mol ratio relative to aluminium (Table 2.4). The LDH-CO₃ precursor used in the study is represented by the formula [Mg_{1-x}Al_x(OH)₂](CO₃)_{x/2}·nH₂O, where x quantifies the fractional replacement of Mg by Al ions in the hydroxide sheets. Several studies have cited the tendency of fatty acids to co-intercalate with their sodium salts (Kanoh *et al.*, 1999; Itoh *et al.*, 2003; Nhlapo *et al.*, 2008). To cater for this scenario the general formula for the intercalated LDH was [Mg_{1-x}Al_x(OH)₂]{(CHO)_x(NaCHO)_y}·nH₂O.

Table 2.4. Compositional data and formulae for the LDH-CO₃ precursor and intercalated products

LDH	Aluminium mol ratio to		
	Mg	Na	x
Carbonate	2.33	0.14	0.30
Myristate	1.92	0.04	0.34
Palmitate	2.39	0.02	0.30
Stearate	1.98	0.03	0.34
Behenate	1.95	0.02	0.34

Pristine LDH-CO₃ has a sand-rose morphology when viewed under the SEM. Several researchers have described the morphology of pristine LDH particles as having a plate-like hexagonal shape (Yang *et al.*, 2007). However, their form is not well defined as viewed in the micrographs below. It is composed of very small subhedral platelets with a lateral average size of 1–5 μm. The particle size distribution will differ from one synthesis method to another (Costa *et al.*, 2008). The same morphology can be observed from both SEM (Figure 2.7a) and TEM Figure 2.7b, c & d. In the case of an LDH-platelet placed on edge, the different stratification of the layers can be observed (Figure 2.7d).

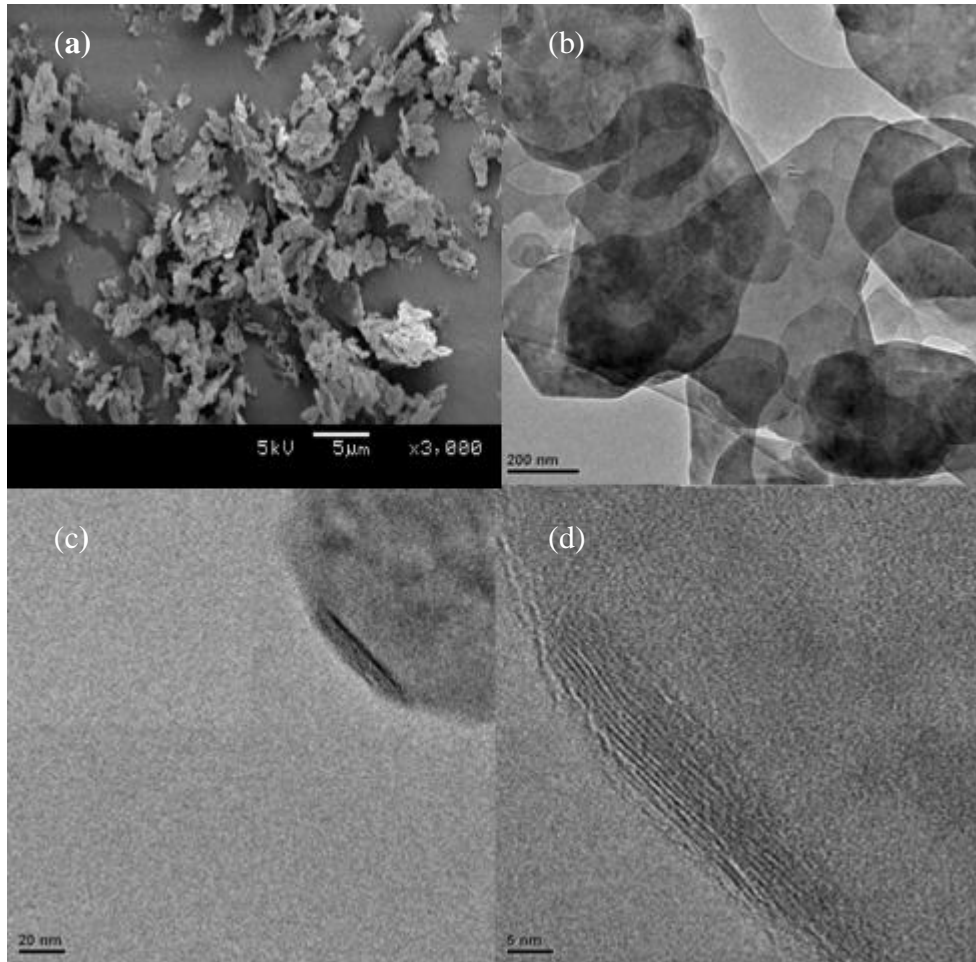


Figure 2.7. (a) SEM; (b), (c) and (d) TEM micrographs of neat LDH-CO₃

The modified LDH appears to have larger platelets (Figure 2.8). This suggests that the modification process involves dissolution and recrystallisation of the parent LDH to the organo-LDH (Cavani *et al.*, 1991). The organo-LDHs generally exhibited irregular subhedral shapes, with the exception of the LDH-palmitate which showed distinct euhedral platelets with a rhombohedral shape.

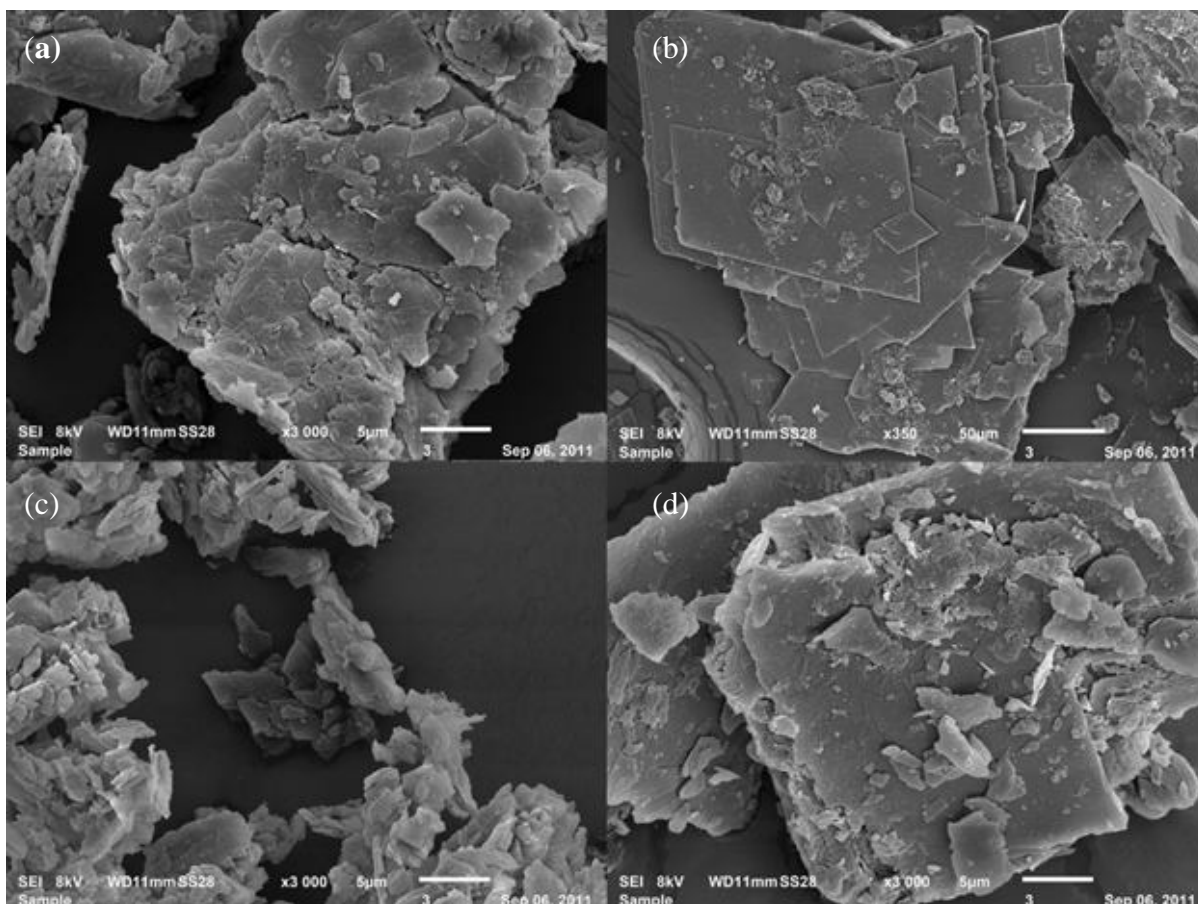


Figure 2.8. SEM micrographs of the LDH samples: (a) LDH-myristate; (b) LDH-palmitate; (c) LDH-stearate; and (d) LDH-behenate

The composition of the platelets was probed by energy dispersive X-ray spectroscopy (EDS). The ratio of Mg to Al is similar or very close to those reported in ICP results. However, it is interesting to note that the well-defined rhombohedral-shaped platelets showed varying Mg:Al ratios. Figures 2.9(a) & (b) shows a typical example with a variety of compositions obtained in LDH-palmitate platelets. The EDS data of the other fatty acid-LDH derivatives are given in Appendix B. This could be an indication that the intercalation process used in the study is followed by dissolution and recrystallisation of the LDH lattice. This is similar to the findings of Grover *et al.* (2010), who explained the changes in the morphology of arsenic-intercalated LDH and hydrocalumite in terms of the anion-exchange mechanism which occurs via a dissolution–precipitation reaction.

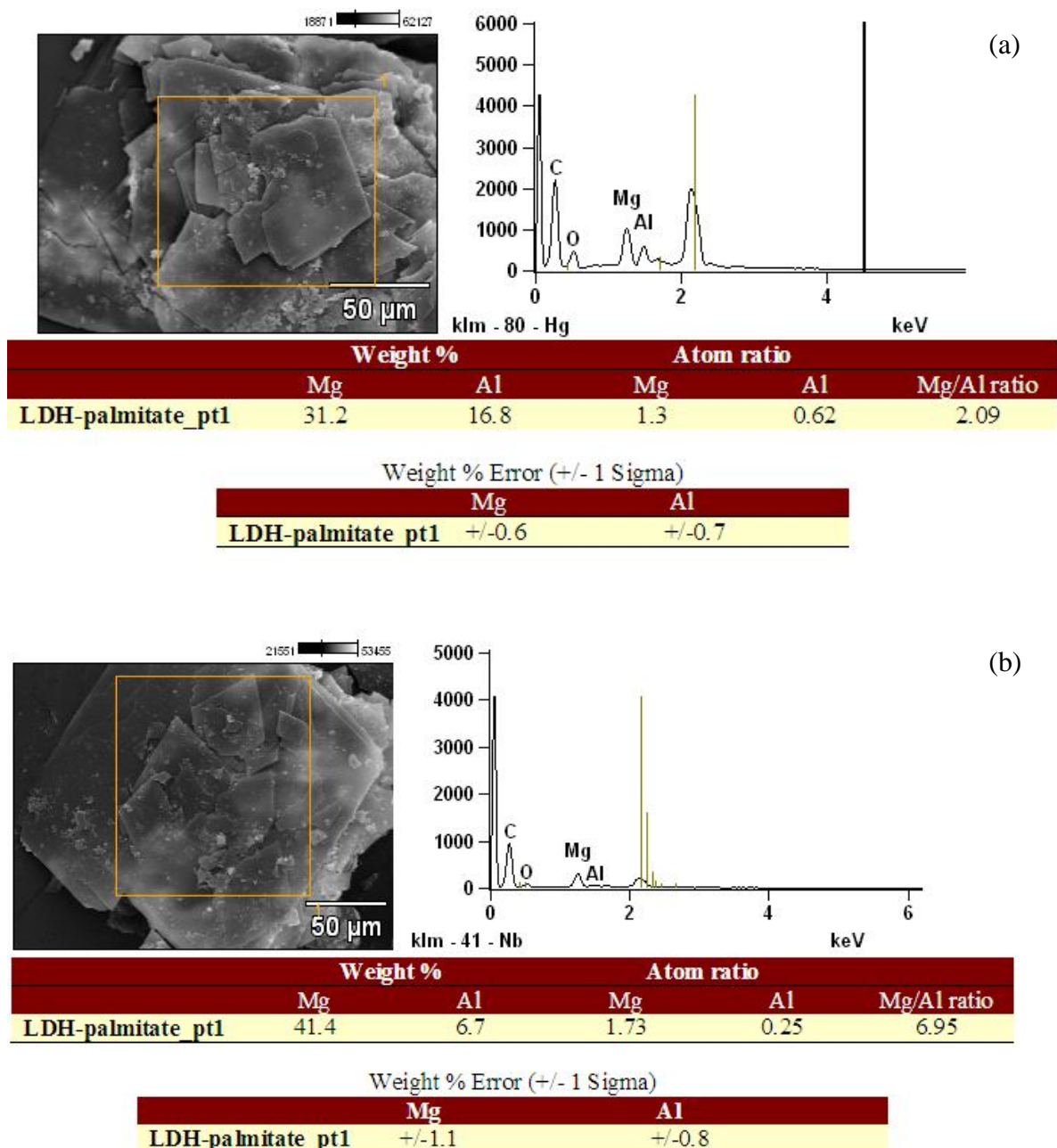


Figure 2.9. EDS data showing different compositions of LDH-palmitate platelets with Mg:Al ratios of (a) 2.09 and (b) 6.95

The elemental analysis by EDS indicates the existence of Mg and Al, with their atomic composition ranging from 1.65 to 6. However, some of the platelets were composed of only Mg; the data on this sample is shown in Appendix B. Zhang *et al.* (2012) also found that increasing concentrations of sodium dodecyl sulphate (SDS) during intercalation resulted in

the product changing from CaAl-SDS to Ca-SDS. The interlayer spacing increased from 2.72 to 3.25 nm.

2.6.2 X-ray diffraction analysis

The morphology, particle size and crystallinity of LDHs are directly related to the organisation of the metal hydroxide lattice. Reaction parameters such as preparation time, temperature, concentrations of reactants, post-preparation treatments and reaction solvents all contribute to these properties (Braterman *et al.*, 2004). Broad powder XRD peaks are normally assigned to phases that lack order, while the narrow sharp peaks are indicative of well-ordered and crystalline phases. A high degree of crystallinity is indicated by the presence of well-resolved XRD patterns (Forano *et al.*, 2006). XRD may also be used as an indicator of phase purity.

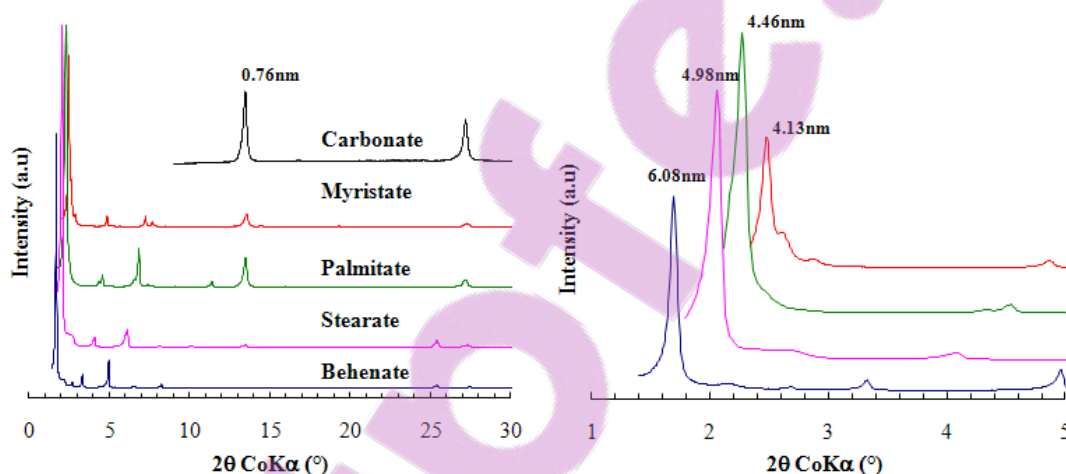


Figure 2.10. WAXS diffractograms of the neat and modified LDH

Assuming the LDH has a rhombohedral stacking order, the basal reflections may be indexed as 003, 006, etc. (Braterman *et al.*, 2004). The characteristic peaks of LDH- CO_3 are observed at 2θ values of 13.5 and 27.2° . These 2θ values are typical for LDH- CO_3 , with a d-spacing (d_L) of 0.76 nm. A shift to lower 2θ values is an indication of layer separation or an increase in d-spacing. All the fatty acid-intercalated LDHs showed an increase in the d-spacing; these were observed to be 4.13, 4.46, 4.98 and 6.08 nm for the myristate, palmitate, stearate and behenate respectively (see Figure 2.10). The peak positions are consistent with a bilayer orientation of fatty acid ions. The d-spacing increases linearly with the increase in the number of carbon atoms of the carboxylic acids, as shown in Figure 2.11.

The intercalated fatty acid anions are envisaged to have a tilt angle of 56–59°, basing the calculation on the equation given below (Carlino, 1997; Xu & Braterman, 2010).

$$d = 1.48 + 0.26(n - 2)\sin\theta \quad [2]$$

where

d is the d-spacing

n is the carbon number in the stearate chain

θ is the slant angle of the intercalated fatty acid anions.

The data obtained experimentally fit well with the theoretical calculation and those obtained from other studies, as seen in Table 2.2. Trace LDH-carbonate phases were present, particularly in the myristate and palmitate. The peaks are sharp and symmetric, which is an indication of good ordering in the synthesised intercalates.

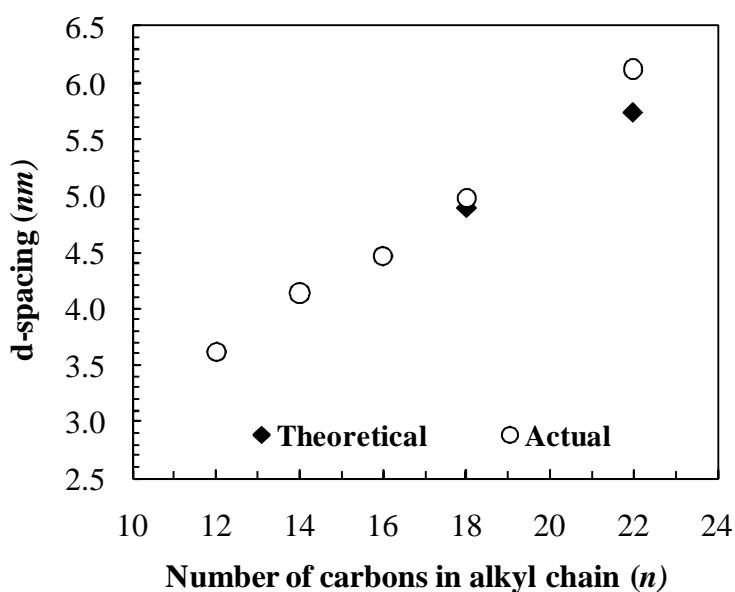


Figure 2.11. Increase in basal spacing with increase in alkyl chain lengths (○) obtained experimentally in this study and (◆) obtained from theoretical calculations

2.6.3 Fourier transform infrared analysis (FTIR)

This technique helps to identify the type of intercalated species and their state within the interlayer.

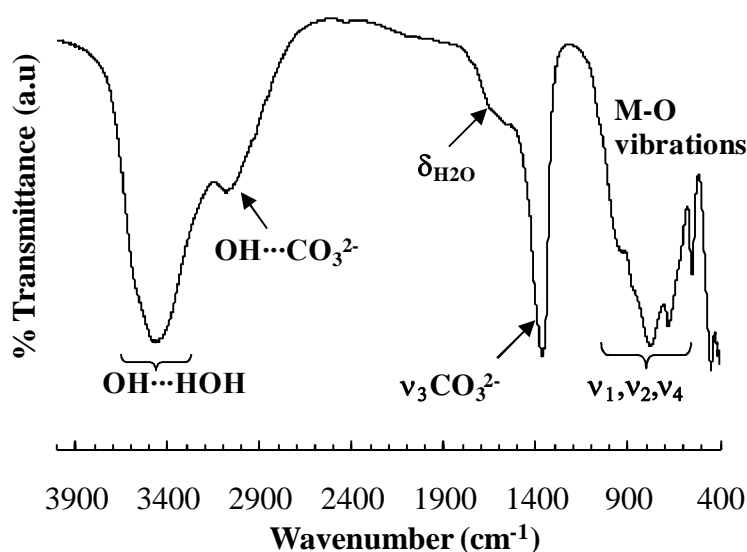


Figure 2.12. Pristine LDH and its typical FTIR vibrations

Figure 2.12 shows FTIR peaks that are typical for the pristine LDH- CO_3 used in the study. The broad band in the range of $3400\text{--}3500\text{ cm}^{-1}$ was assigned to ν_{OH} OH \cdots HOH vibrations. The shoulder at $3000\text{--}3100\text{ cm}^{-1}$ was attributed to the OH vibrations of hydroxyl groups co-ordinated to the interlayer carbonate OH \cdots CO $_3^{2-}$ through hydrogen bonding. A bending vibration ($\delta_{\text{H}_2\text{O}}$) from the interlayer water is observed at $1600\text{--}1650\text{ cm}^{-1}$. Carbonate anions peaks are observed at $850\text{--}880\text{ cm}^{-1}$ (ν_2), $1350\text{--}1380\text{ cm}^{-1}$ (ν_3) and $670\text{--}690\text{ cm}^{-1}$ (ν_4). These were assigned to non-planar bending, asymmetric stretching mode and bending angular mode respectively (Braterman *et al.*, 2004). However, these have been observed to split or shift to lower values if the symmetry of the carbonate anions is compromised. This is due to ionic and/or hydrogen bonding interaction of the CO $_3^{2-}$ with the metal hydroxide lattice, hence interfering with the normal vibrations of the bonds. The position of the ν_3 peak ($1370\text{--}1355\text{ cm}^{-1}$) is sensitive to the $\text{M}^{\text{II}}/\text{M}^{\text{III}}$ ratio. Costa *et al.* (2007) suggested that a strong electrostatic attraction between the interlayer anions is indicated by a decrease in the metal ratio (increase in the x -value). Hernendaz-Moreno *et al.* (1985) found that the ν_3 peak position shifted to lower wavenumbers with a decrease in the metal ratio, i.e. the $\text{M}^{\text{II}}/\text{M}^{\text{III}}$ ratios equal to 3:1 and 2:1 had peaks positioned at 1370 and 1355 cm^{-1} respectively. The ν_3 peak was observed at 1358 cm^{-1} in this current study, which is in good agreement with the literature for an Mg $^{2+}/\text{Al}^{3+}$ ratio that is close to 2:1.

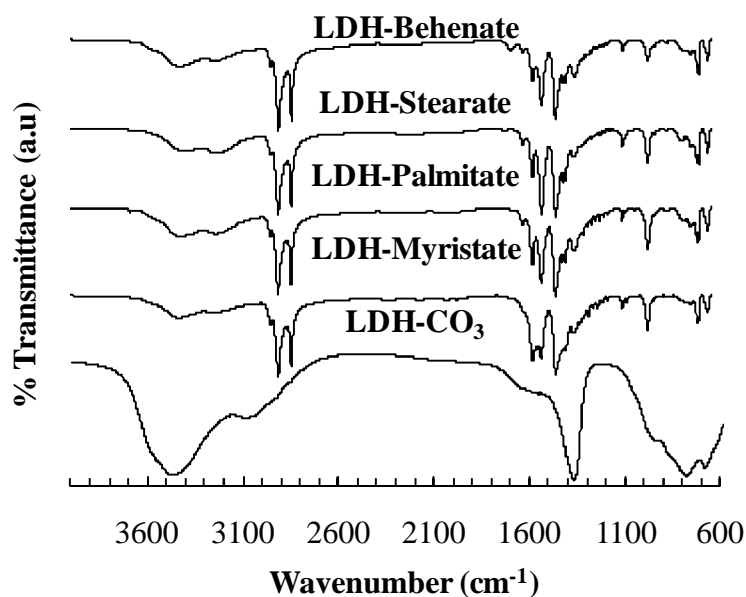


Figure 2.13. FTIR spectra of pristine and modified LDHs

The FTIR spectra were observed to vary for the different orientations of anions within the interlayer, i.e. monolayer or bilayer (Braterman *et al.*, 2004). A monolayer stearate-intercalated LDH was found to have two distinct peaks at 1549 cm^{-1} , attributed to the COO^- asymmetric stretching, and at 1412 cm^{-1} for the COO^- symmetric stretching. In the bilayer stearate-intercalated $\text{Zn}_3\text{Al-LDH}$, peaks were observed at 1597 cm^{-1} with shoulders at 1620 and 1398 cm^{-1} ; these were assigned to H-bonded COOH vibration (Braterman *et al.*, 2004). Figure 2.13 shows the spectra of the fatty acid-modified LDHs. The observed spectra are typical for a bilayer fatty acid-intercalated LDH. The different fatty acid:LDH derivatives had similar spectra. The broad band between 3447 and 3391 cm^{-1} was assigned to hydroxyl groups on the LDH lattice and the presence of the intercalated water molecules. However, it is clear to see this particular peak becomes very broad and somewhat weak in the fatty acid-intercalated LDH as compared with the pristine LDH. This may be explained by the exclusion of a sizable quantity of intercalated water molecules due to the hydrophobisation of the interlayer by the fatty acids. A more detailed view of the peaks present and their exact positions is given in Figure 2.14.

The peaks in the fatty acid intercalated product in the regions 2956 , 2915 and 2848 cm^{-1} are attributed to CH_2 symmetric and asymmetric stretching modes. The $\nu_{\text{as}}\text{CH}_2$ band was observed at a substantially low wavenumber (2915 cm^{-1}), which is an indication of a highly ordered all-trans conformation. The bending vibration of the intercalated water, $\delta(\nu\text{H}_2\text{O})$, was observed at 1636 cm^{-1} . Peaks at 1583 cm^{-1} were attributed to the carboxylic acids being intercalated in the $-\text{RCOOH}$ form (Borja & Dutta, 1992). Carlino & Hudson (1994) assigned the 1535 cm^{-1} peak to the asymmetric stretching mode of ionised $-\text{RCOO}^-$. However, they found that this particular mode may be positioned anywhere within the range of $1558\text{--}1536\text{ cm}^{-1}$. The asymmetric mode was observed by Perez-Ramirez *et al.* (2001) in the range of $1425\text{--}1411\text{ cm}^{-1}$. In the current study these are detected as weak peaks at 1428 and 1411 cm^{-1} . A medium peak around 1466 cm^{-1} was attributed by Borja & Dutta (1992) to CH_2 bending of the carboxylic acid chain. This band was also found to be sensitive to interchain interactions and the packing arrangement (Vaia *et al.*, 1994). The LDH-myristate exhibits a much broader peak and a slightly lower wavenumber. This is an indication of an increase in the chain motion or liquid-like character of the fatty acid chains. The peak at 1368 cm^{-1} shows a broad and very weak band, which is an indication of a slight carbonate impurity.

The summation of the peaks observed is evidence of the presence of carboxylate within the interlayer. It also substantiates the fact that for a bilayer to form, the fatty acid should be intercalated in both an ionised and unionised fatty acid form (Kuehn & Poellman, 2010).

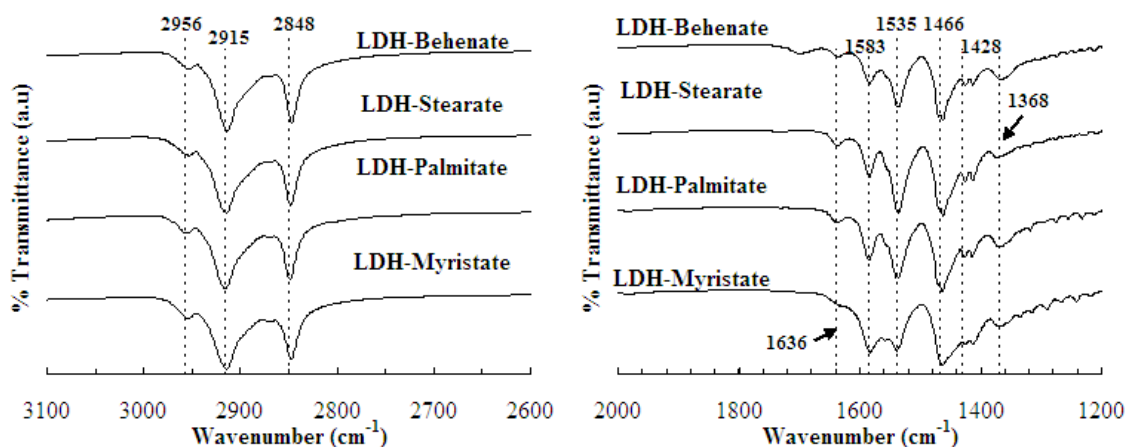


Figure 2.14. FTIR zoom of the modified LDH

2.6.4 Thermal analysis

The thermal behaviour, stability and decomposition pathways of the organo-LDH hybrids were studied by means of DSC, temperature scan FTIR and XRD, TG and TG-FTIR.

2.6.4.1 Differential scanning calorimetry (DSC)

In Figure 2.15 the red dotted and solid black lines denote the neat fatty acid and intercalated LDHs respectively. The DSC scans of the organo-LDH show that the intercalation of the fatty acids results in a shift of the melting temperature to a higher temperature. The confinement of the fatty acids within the LDH layers prevents their premature melting. All the intercalated samples exhibit two or three endotherms, which may be attributed to the different phase transitions undergone by the bilayer intercalated LDH as the temperature increased. The multiple peaks could be an indication of mixed layers as already indicated in the EDS results, where the ratios of Mg to Al vary from platelet to platelet. Another contributing factor to the peaks observed is the water of hydration of the organo-LDH.

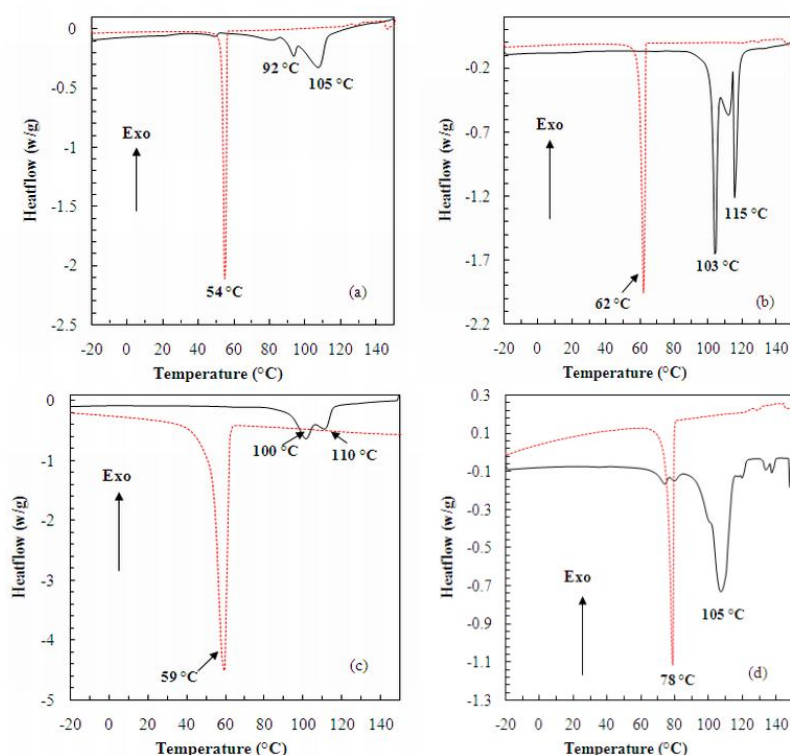


Figure 2.15. DSC traces of neat fatty acids in red and LDH-fatty acids as a solid line:

(a) myristate, (b) palmitate, (c) stearate and (d) behenate

The dominant peaks have been assigned to the melting of the interlayer anions. It is clear from the traces that there is a slight fatty acid impurity for the LDH-stearate and -behenate samples.

2.6.4.2 Temperature scan XRD and FTIR

Figure 2.16 shows the effect of temperature on the crystal structure. Generally, the fatty acid-intercalated LDH has the primary basal reflection shifting to higher 2θ values, indicating a reduction in the d-spacing. The first shift to lower 2θ values is due to the removal of interlayer water, accompanied by a reduction in the d-spacing of 0.3 nm (Pestic *et al.*, 1994). At temperatures higher than 120 °C, another transition occurs, which is accompanied by the disappearance of the 2nd and 3rd reflections. The primary reflection either broadens progressively or disappears completely with increase in temperature; this is attributed to the organo-LDH becoming amorphous. The LDH-stearate exhibits reductions in the basal spacing from 4.98 to 4.26 to 2.92 nm at 25, 90 and 150 °C respectively. The last spacing is consistent with a monolayer arrangement. Similar transitions were observed in the LDH-palmitate with the changes in d-spacing being 4.46 to 4.05 to 2.76 nm at 25, 120 and 200 °C respectively. These transitions, however, were difficult to follow due to peak broadening and disappearance in the LDH-behenate. The LDH-myristate, however, showed an increase in the d-spacing; this deviation from the normal trend is still not fully understood. Dutta & Borja (1992), however, observed a similar phenomenon in myristate-intercalated Li-Mg LDH.

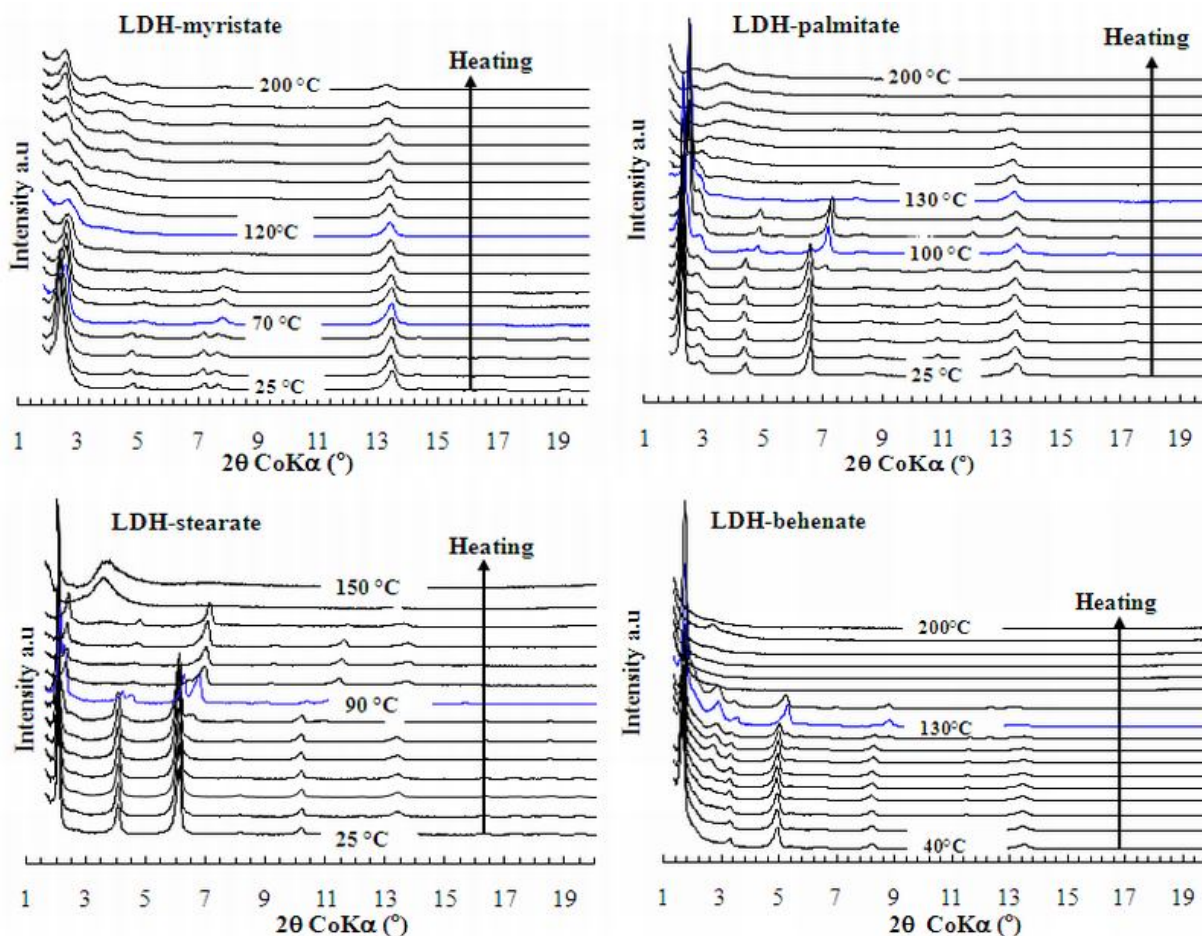


Figure 2.16. Temperature scan XRD of LDH-fatty acids

LDH-stearate was used to further illustrate the thermotropic behaviour of LDH-carboxylate. Figure 2.17 shows the effect of temperature on the peak position of the $\nu_{as}(\text{CH}_2)$ band in the FTIR spectra. Vaia *et al.* (1994) proposed that the wavenumber and width of the above-mentioned band are sensitive to the gauche trans conformer ratio and the packing density of the methylene chains. This band ranges from 2917 to 2929 cm^{-1} for the methylene chains in the all-trans ordered state and when in a liquid-like environment respectively. It showed a shift from values observed for crystalline well-ordered chains (2916.8 cm^{-1}) to higher values of 2925 cm^{-1} . This is consistent with an increase in conformational disorder in the intercalated chains as the temperature increases. The intermediate wavenumber values (2924 cm^{-1}) obtained in our study suggest that the chains still retained a degree of order above the transition temperature, i.e. that they are not completely molten. The investigation also revealed a greater amount of disorder for short-chain fatty acids (laurate) as compared with longer stearate chains (Focke *et al.*, 2010).

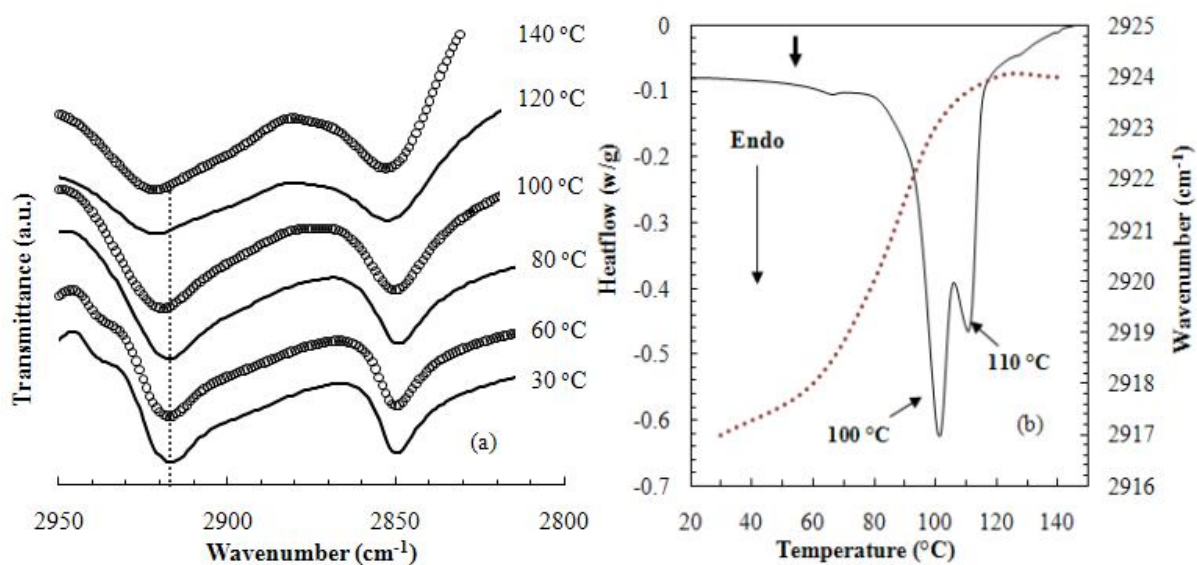


Figure 2.17. Effect of temperature on the peak position of the $\nu_{as}(\text{CH}_2)$ band in the FTIR spectra for LDH-stearate, and the corresponding DSC

From Figure 2.17 it is clear that following the phase changes through temperature scan FTIR is a more sensitive method than following them through XRD. It is evident that the movement of intercalated anions begins at much lower temperatures (≈ 45 °C) as observed in FTIR, whereas in XRD the movement is clearly seen at a much higher temperatures (≈ 90 °C).

2.6.4.3 Decomposition pathway of organo-LDH

The decomposition pathways of LDH and its derivatives were followed by means of TGA (Figure 2.18). The organic content was also derived from these results. The calculation is based on the differences in mass observed at temperatures of 150 and 900 °C relative to the corresponding values for the LDH- CO_3 precursor. A detailed calculation for the degree of intercalation appears in Appendix B, along with the results of the other trials. Pristine LDH- CO_3 follows three distinct steps, i.e. dehydration, dehydroxylation and elimination of interlayer anions. The temperatures at which each of the individual events occur varies with different metal ion species and ratios (Ross & Kodama, 1967), intercalated anions (Xu & Zheng, 2001; Mascolo & Marino, 1982) and post-treatment of the LDH (Hussein *et al.*, 2000). The different stages observed in this study fit well with the decomposition pathway of (Mg-Al)-LDH- CO_3 as proposed by Bera *et al.* (2000):

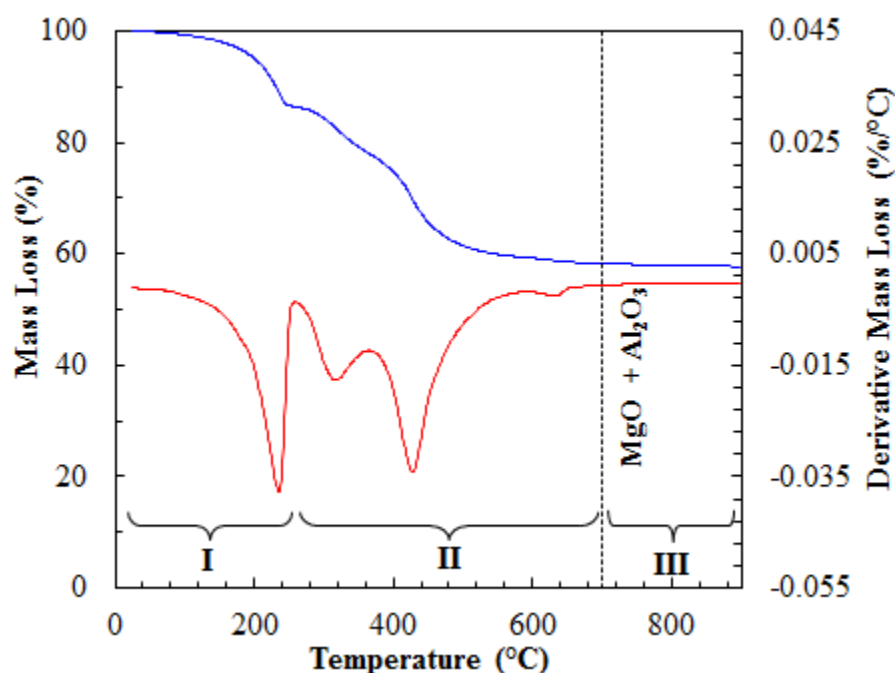
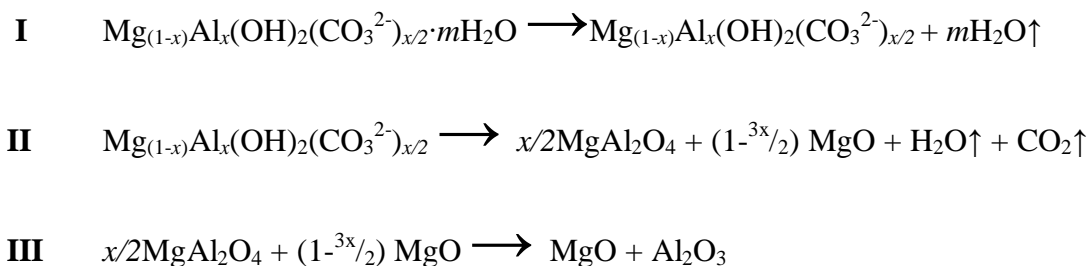


Figure 2.18. TG and DTG of the LDH- CO_3 indicating the different decomposition stages

The first event is usually assigned to the loss of physisorbed interlayer water. The onset of this step begins at about 50 °C and is perceived to be complete at 150 °C (Carlino & Hudson 1994; Kandare and Hossenlopp, 2006; Frost *et al.* 2003). The second step is due to a dehydroxylation process, immediately followed by an oxidative degradation of the carbonate anions within the interlayer, with the former occurring at about 280 °C and the latter above 450 °C.

The difference in mass loss between the LDH- CO_3 and the fatty acid modified LDH was used to calculate the percentage organic and the AEC level (Figure 2.19a). The percentages organic for each respective organo-LDH were as follows: 74, 73, 79 and 81% for LDH-myristate, -palmitate, -stearate and -behenate respectively. The modified LDHs appear to follow the same decomposition pattern as the pristine LDH- CO_3 (Figure 2.19b). It is evident

that the breakdown of the hydroxyl lattice and degradation of anions occurs at temperatures above 280 °C, well above polymer processing temperatures. Mass loss is effectively complete above 700 °C, leaving a residue of MgO and Al₂O₃. The water loss occurs at substantially lower temperatures than with the LDH-CO₃. However, the dehydroxylation process seems to occur simultaneously with the removal of anions (de-anionation). LDH-behenate showed a higher decomposition temperature peak and LDH-myristate the lowest.

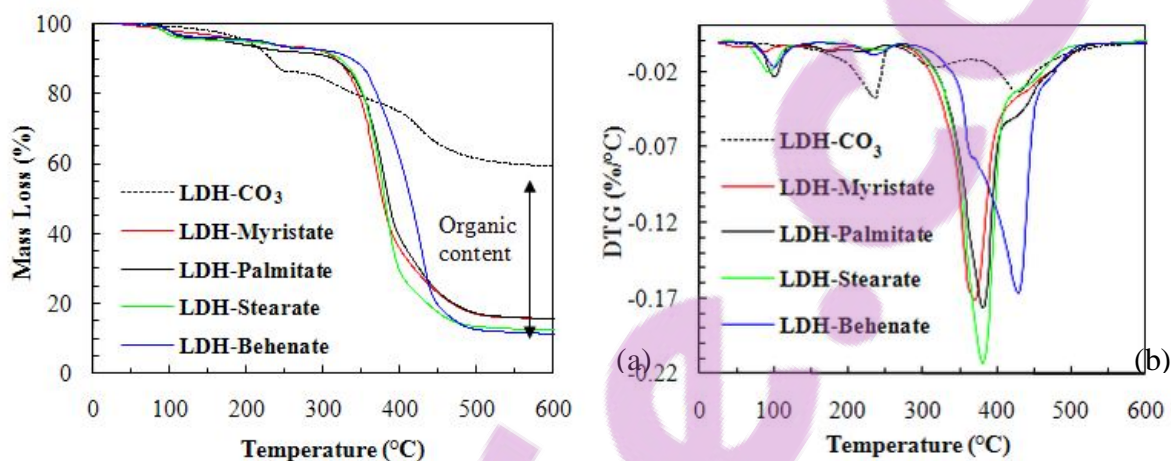


Figure 2.19. Thermogravimetric analysis: (a) % mass loss and (b) derivative mass loss of pristine and modified LDHs

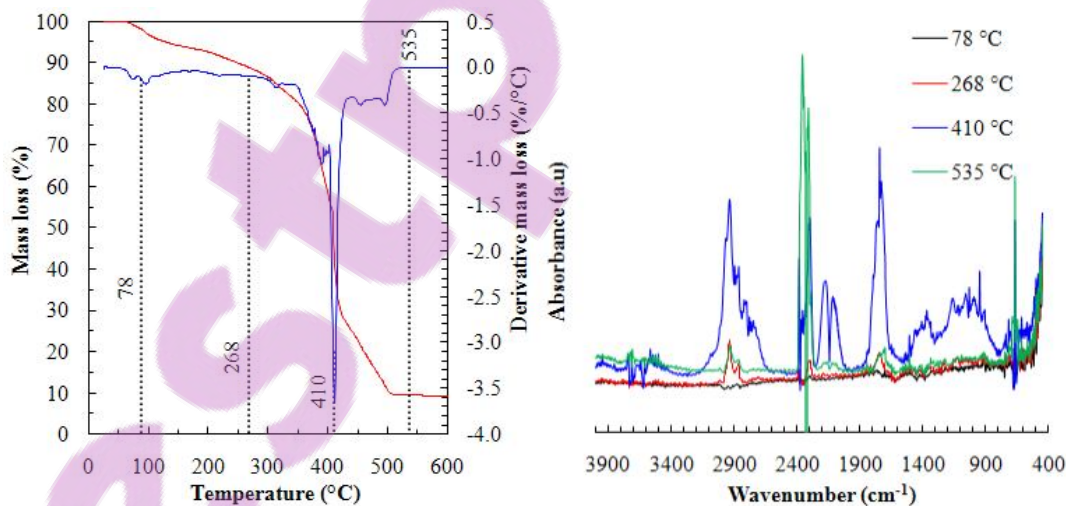


Figure 2.20. Evolved gas analysis for LDH-stearate

To confirm the decomposition pathway, evolved gas analysis was carried out by means of TG-FTIR (Figure 2.20). The water loss is, however, not detected by the FTIR. The regions that would exhibit water peaks (3700–3400 cm⁻¹) are characterised by noise-like signals on the spectra. Decomposition of the LDH-stearate begins at about 268 °C. Methylene groups

(2943 cm^{-1}) and CO_2 asymmetric stretching (2385–2303 cm^{-1}) are detected, but the intensities of the peaks are weak. At 410 °C the peak intensities are relatively larger and were distinguished as follows: alkyl groups CH-symmetric and asymmetric stretching (2943 cm^{-1}), 2385–2303 cm^{-1} ; 2193 and 2162 cm^{-1} peaks are assigned to CO vibrations; 1743 cm^{-1} was attributed to carboxylic acid groups C=O stretching vibration; and CH bending vibrations are picked up at 1412 cm^{-1} . The carbonyl species are identified in the range of 1545–882 cm^{-1} by a very broad peak. At around 535 °C only a CO_2 peak was present.

Table 2.5. Summary of thermogravimetric data and estimates for the degree of intercalation

Sample identity	Residual mass loss (%) at		Carboxylate:Al mol ratio
	150 °C	900 °C	
LDH- CO_3	98.10	57.68	-
LDH-myristate	96.88	14.61	2.64
LDH-palmitate	95.73	14.92	2.24
LDH-stearate	95.40	13.11	2.39
LDH-behenate	96.04	10.72	2.60

The thermogravimetric data and estimates of the degree of carboxylate intercalation are summarised in Table 2.5. Nhlapo *et al.* (2008) calculated the theoretical possible amount to be 2.39 times the AEC for close-packed carboxylate chains. It is evident that intercalation occurs at higher than the AEC expected for LDHs, implying that the excess exists as un-ionised fatty acids. It is worth noting that the TGA data indicates variable levels of intercalation amongst the different batches prepared in this study (compare Tables 2.5, 2.6, B6 and B7). This could be explained by changes in the pH during modification due to the evaporation of ammonia and inadequate/too many washes.

A complete conversion of the LDH- CO_3 precursor to magnesium distearate and aluminium tristearate would result in an apparent degree of intercalation of 6.93. The magnesium/aluminium stearate sample was synthesised in order to explore this possibility. Figure 2.21 compares the XRD diffractograms of this product with those of the two precursors. It clearly shows that heating these two stearates together results in a new product with a larger d-spacing. The TGA data shown in Table 2.6 indicate that there was a net loss of stearic acid. There is also an indication that not all of the aluminium stearate was converted. Furthermore, it is clear that the product is not a simple LDH-stearate but rather a

mixed magnesium/aluminium stearate with a d-spacing that is very similar to that of bilayer-intercalated LDH. This experiment confirms that such a compound can form through partial hydrolysis of the metal stearates. It is therefore conceivable that LDH-stearates that have an exceptionally high AEC and may contain mixed layers of such a product, as well as the conventional LDH-stearate. The EDS analysis (Figure 2.9) of the LDH-palmitate with an AEC of 2.24 shows areas that have the correct Mg:Al ratios, as well as some platelets that are either Mg-rich or Al-rich.

Table 2.6. Summary of XRD and TGA results for the LDH-CO₃, LDH-stearates and magnesium stearate and aluminium stearate samples

Sample	d-spacing (nm)	TG residue* (wt%)	Intercalation** (multiples of AEC)
LDH-CO ₃	0.76	59.7	-
LDH-CO ₃ + Tween 60	0.76	58.4	-
LDH-stearate	4.88	10.23	3.87
Magnesium/aluminium stearate	5.08	8.23	5.16
Magnesium stearate	4.94	7.30	(5.70)
Aluminium stearate	4.01	8.57	(5.11)

*Mass loss at 700 °C relative to the mass loss at 150 °C

**Apparent degree of stearate intercalation expressed as multiples of AEC, assuming that the basis is an LDH clay

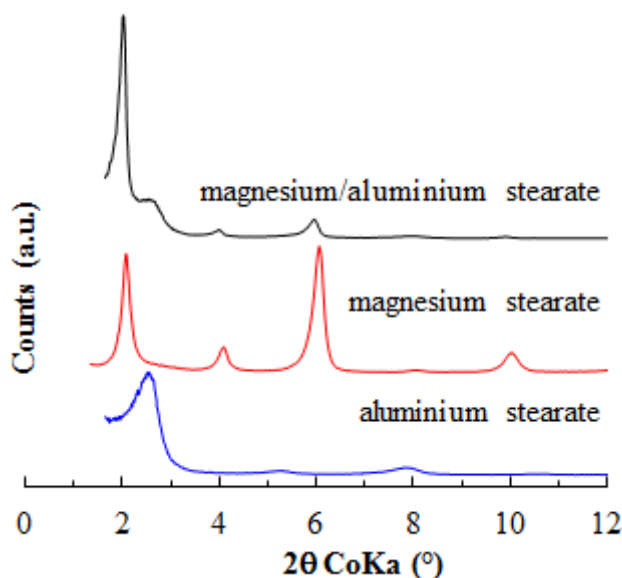


Figure 2.21. X-ray diffractograms for magnesium stearate, aluminium stearate and magnesium/aluminium stearate prepared by heating an aqueous suspension of the former

two reagents in the presence of Tween 60

2.7 CONCLUSIONS

The carboxylate intercalated LDHs were successfully obtained from direct ion exchange of the fatty acid with the interlayer carbonate. The method employed is reproducible with respect to a bilayer intercalated product. It is evident from the FTIR results and the high AEC of intercalated fatty acids that in bilayers orientation will always co-intercalate the carboxylates, as well as the free fatty acid molecules. The incorporation of excess fatty acids is envisaged to be driven by hydrophobic interactions. The presence of the free fatty acids facilitates dense packing, improving the van der Waals interaction between the chains and giving better charge shielding of the same-charge surfactant head group. The high degree of chain order leads to more efficient packing and increased cohesive van der Waals interaction between chains and, ultimately, to a greater interlayer solid-like character as observed in FTIR analysis.

The fatty acid-intercalated LDHs showed structural changes as a function of temperature. They undergo melt-like transitions at elevated temperatures. Above the melting point they assume a liquid-crystalline ‘rotator’ state owing to the localisation of the ionised head group and the two-dimensional confinement imposed by the planar clay sheets. Hence, this event is followed by a reduction in the d-spacing. At higher temperatures the LDH-fatty acid-based materials become XRD-amorphous: basal reflections disappear or become very broad. The LDH-stearate and -palmitate clearly showed a reduction in d-spacing, where the bilayer arrangement collapses to a monolayer.

The study also revealed that various intercalation products can be obtained from the one-pot synthesis as shown by the EDS results. Platelets with different Mg/Al ratios were observed specifically in the well-crystallised LDH-palmitate. This is an indication that the method employed entailed dissolution and recrystallisation of the pristine LDH and organo-LDH respectively. It is further substantiated by changes in the platelet morphology (from subhedral to rhombohedral-shaped platelets) and size. The unusually high AEC values obtained for some of the fatty acid-intercalated LDHs are attributed to the formation of Mg- and Al-rich platelets.

2.8 REFERENCES

- Abelló, S. & Pérez-Ramírez, J. (2006). Steam activation of Mg–Al hydrotalcite. Influence on the properties of the derived mixed oxides. *Microporous Mesoporous Mater.*, 96(1–3): 102–108.
- Adachi-Pagano, M., Forano, C. & Besse J-P. (2003). Synthesis of Al-rich hydrotalcite-like compounds by using the urea hydrolysis reaction – control of size and morphology. *J. Mater. Chem.*, 13: 1988–1993.
- Aramendia, M. A., Borau, V., Jimenez, C., Marinas, J. M., Ruiz, J. R. & Urbano, F. J. (2002). Comparative study of Mg/M(III) (M=Al, Ga, In) layered double hydroxides obtained by coprecipitation and the sol-gel method, *J. Solid State Chem.*, 168: 156–161.
- Bera, P., Rajamathi, M., & Hegde, M. S. (2000). Thermal behaviour of hydroxides, hydroxysalts and hydrotalcites, 23(2): 141–145.
- Bocclair, J. W. & Braterman, P. S. (1999). Layered double hydroxide stability. 1. Relative stabilities of layered double hydroxides and their simple counterparts. *Chem. Mater.*, 11: 298–302.
- Borja, M. & Dutta, P. K. (1992). Fatty acids in layered metal hydroxides: Membrane-like structure and dynamics. *J. Phys. Chem.* 96: 5434–5444.
- Braterman, P. S., Xu, Z.P. & Yarberrry, F. (2004). In: Auerbach, S.M., Carrado, K. A. & Dutta, P. K. (Eds), *Handbook of Layered Materials*, Boca Raton: CSC Press, Taylor & Francis Group, pp 373–449.
- Brindley, G. W. & Kikkawa, S. (1979). A crystal-chemical study of Mg,Al and Ni,Al hydroxy-perchlorates and hydroxy-carbonates. *Am. Mineral.*, 64: 836–843.
- Carlino, S. & Hudson, M. J. (1994). The reaction of molten sebacic acid with a layered (Mg/Al) double hydroxide. *J. Mater. Chem.*, 4: 99–104.
- Carlino, S. (1997). The intercalation of carboxylic acids into layered double hydroxides: A critical evaluation and review of different methods. *Solid State Ionics*, 98: 73–84.
- Cavani, F., Trifirò, F. & Vaccari, A. (1991). Hydrotalcite-type anionic clays: Preparation, properties and applications. *Catal. Today*, 11: 173–301.

- Chibwe, K. & Jones, W. (1989). Intercalation of organic and inorganic anions into layered double hydroxide. *J. Chem. Soc., Chem. Commun.*, 926–927.
- Constantino, V. R. L. & Pinnavaia, T. J. (1995). Basic properties of $Mg^{2+}_{1-x}Al^{3+}_x$ layered double hydroxides intercalated by carbonate, hydroxide, chloride and sulfate anions. *Inorg. Chem.*, 34: 883–892.
- Costa, F. R., Leuteritz, A., Meinel, J., Wagenknecht, U. & Heinrich, G. (2011). LDH as nanofiller: Organic modification and dispersion in polymers. *Macromolecular Symposia*, 301(1): 46–54.
- Costa, F. R., Leuteritz, A., Wagenknecht, U., Jehnichen, D., Häusler, L. & Heinrich, G. (2008). Intercalation of Mg-Al layered double hydroxides by anionic surfactants: Preparation and characterization. *Appl. Clay. Sci.*, 38(3-4): 153–164.
- Costa, F. R., Wagenknecht, U. & Heinrich, G. (2007). LDPE/Mg–Al layered double hydroxide nanocomposite: Thermal and flammability properties. *Polym. Degrad. Stab.*, 92(10), 1813–1823.
- Costa, F. R., Wagenknecht, U., Jehnichen, D., Abdel-Goad, M. & Heinrich, G. (2006). Nanocomposites based on polyethylene and Mg-Al layered double hydroxide. Part II: Rheological characterization. *Polymer*, 47: 1649–1660.
- Crepaldi, E. L., Pavan, P. C. & Valim, J. B. (1999). A new method of intercalation by anion exchange in layered double hydroxides. *Chem. Commun.*, 155–156.
- Crepaldi, E. L., Tronto, J., Cardoso, L. P. & Valim, J. B. (2002). Sorption of terephthalate anions by calcined and uncalcined hydrotalcite-like compounds. *Colloids Surf. A.*, 211: 103–114.
- Delmas, C. & Borthomieu, Y. (1993). Chimie douce reaction: A new route to obtain well crystallized layered double hydroxides. *J. Solid State Chem.*, 104: 345–352.
- Feitknecht, W. & Gerber, M. (1942). Zur Kenntnis der Doppelhydroxide und der basischen Doppelsalze (III). *Helv Chim Acta.*, 25: 131–137.
- Focke, W. W., Nhlapo, N. S., Moyo, L. & Verryn, S. M. C. (2010). Thermal properties of lauric- and stearic acid intercalated layered double hydroxides. *Mol. Cryst. Liq. Cryst.*, 521(1): 168–178.

- Forano, C., Hibino, T., Leroux, F. & Taviot-Gueho, C. (2006). Layered double hydroxides. In: Bergaya, F., Theng, B. K. G. & Lagaly, G. (Eds.), *Handbook of Clay Science*, Amsterdam: Elsevier, pp 1021-1095
- Frost, R. L., Martens, W., Ding, Z. & Klopogge, J. T. (2003). DSC and high-resolution TG of synthesized hydrotalcites of Mg and Zn. *J. Therm. Anal. Calorim.*, 71: 429–438.
- Grim, R.E. & Güven, N. (1978). *Bentonites: Geology, Mineralogy, Properties and Uses*. Amsterdam and New York: Elsevier, p 256.
- Grover, K., Komarneni, S. & Katsuki, H. (2010). Synthetic hydrotalcite-type and hydrocalumite-type layered double hydroxides for arsenate uptake. *Appl. Clay. Sci.*, 48(4): 631–637.
- He, J., Wei, M., Li, B., Kang, Y., Evans, D. G. & Duan, X. (2005). Preparation of layered double hydroxides. In: Evans, D. G. & Duan, X. (Eds). *Layered Double Hydroxides*, Heidelberg, Germany: Springer, pp 89–119.
- Hernandez-Moreno, M. J., Ulibarri, M. A., Rendon, J. L. & Serna, C. J. (1985). IR characteristics of hydrotalcite-like compounds. *Phys. Chem. Miner.*, 12: 34–38.
- Hibino, T. & Tsunashima, A. (1998). Characterization of repeatedly reconstructed Mg-Al hydrotalcite-like compounds: Gradual segregation of aluminum from the structure. *Chem. Mater.*, 10: 4055–4061.
- Hussein, M. Z. B., Zainal, Z. & Ming, C. Y. (2000). Microwave-assisted synthesis of Zn-Al-layered double hydroxide-sodium dodecyl sulfate nanocomposites. *J. Mater. Sci. Lett.*, 19: 879–883.
- Ikeda, T., Amoh, H. & Yasunaga, T. (1984). Stereoselective exchange kinetics of L- and D-histidines for Cl⁻ in the interlayer of a hydrotalcite-like compound by the chemical relaxation method. *J. Am. Chem. Soc.*, 106, 5772–5775.
- Indira, L., Dixit, M., & Kamath, P. V. (1994). Electrosynthesis of layered double hydroxides of nickel with trivalent cations. *Journal of Power Sources*, 52(1): 93–97.
- Itoh, T., Ohta, N., Shichi, T., Yui, T. & Takagi, K. (2003). The self-assembling properties of stearate ions in hydrotalcite clay composites. *Langmuir*, 19: 9120–9126.
- Iyi, N. & Sasaki, T. (2008). Decarbonation of MgAl-LDHs (layered double hydroxides) using acetate-buffer/NaCl mixed solution. *J. Colloid Interface Sci.*, 322: 237–245.

- Iyi, N., Matsumoto, T., Kaneko, Y. & Kitamura, K. (2004). Deintercalation of carbonate ions from a hydrotalcite-like compound: Enhanced decarbonation using acid-salt mixed solution. *Chem. Mater.*, 16: 2926–2932.
- Iyi, N., Okamoto, K., Kaneko, Y. & Matsumoto, T. (2005). Effects of anion species on deintercalation of carbonate ions from hydrotalcite-like compounds. *Chem. Lett.*, 34: 932–933.
- Jitianu, M., Zaharescu, M., Balasoiu, M. & Jitianu, A. (2003). The sol-gel route in synthesis of Cr(III)-containing clays. Comparison between Mg-Cr and Ni-Cr anionic clays. *J. Sol-Gel Sci. Technol.*, 26: 217–221.
- Kandare, E. & Hossenlopp, J. M. (2006). Thermal degradation of acetate-intercalated hydroxy double and layered hydroxy salts. *Inorg. Chem.*, 45: 3766–3773.
- Kanicky, J. R. & Shah, D.O. (2002). Effect of degree, type, and position of unsaturation on the pKa of long-chain fatty acids. *J. Colloid Interface Sci.*, 207: 201–207.
- Kannan, S., Jasra, R. V. & Salt, C. (2000). Microwave-assisted rapid crystallization of Mg-M(III) hydrotalcite where M(III) = Al, Fe or Cr. *J. Mater. Chem.*, 10: 2311–2314.
- Kanoh, T., Shichi, T. & Takagi, K. (1999). Mono- and bilayer equilibria of stearate self-assembly formed in hydrotalcite interlayers by changing the intercalation temperature. *Chem. Lett.*: 117–118.
- Khan, A. & O’Hare, D. (2002). Intercalation chemistry of layered double hydroxides: Recent developments and applications. *J. Mater. Chem.*, 12: 3191–3198.
- Kooli, F., Kosuge, K. & Tsunashima, A. (1995). New Ni-Al-Cr and Ni-Al-Fe carbonate hydrotalcite-like compounds: Synthesis and characterization. *J. Solid State Chem.*, 118: 285–291.
- Kuehn, T., Poellmann H. (2010). Synthesis and characterization of Zn-Al layered double hydroxides intercalated with 1- to 19-carbon carboxylic acid anions. *Clays Clay Miner.*, 58(5): 596–605.
- Landman, E. P. (2005) Stearate intercalated layered double hydroxides: Methods and application. PhD thesis, Pretoria: University of Pretoria.

- Latterini, L., Elisei, F., Aloisi, G. G., Costantino, U. & Nocchetti, M. (2002). Space-resolved fluorescence properties of phenolphthalein-hydrotalcite nanocomposites. *Phys. Chem. Chem. Phys.*, 4(12): 2792–2798.
- Lopez, T., Bosch, P., Ramos, E., Gomez, R., Novaro, O. & Acosta, D. (1996). Synthesis and characterization of sol-gel hydrotalcites. Structure and texture. *Langmuir*, 189–192.
- Lotsch, B., Walton, R., O’Hare, D. & Millange, F. (2001). Separation of nucleoside monophosphates using preferential anion exchange intercalation in layered double hydroxides. *Solid State Science*, 3(8): 883–886.
- Mascolo, G. & Marino, O. (1980). A new synthesis and characterization of magnesium-aluminium hydroxides. *Miner. Mag.*, 43: 619–621.
- Mascolo, G. (1995). Synthesis of anionic clays by hydrothermal crystallization of amorphous precursors. *Appl. Clay Sci.*, 10(1-2): 21–30.
- McMurry, J. (2000). *Organic Chemistry*, 5th edition. USA: Thomson Brooks/Cole, p 1284.
- Meyn, M., Beneke, K. & Lagaly, G. (1990). Anion-exchange reactions of layered double hydroxides. *Inorg. Chem.*, 29: 5201–5207.
- Miyata, S & Okada, A. (1977). Synthesis of hydrotalcite-like compounds and their physico-chemical properties – the systems $Mg^{2+}Al^{3+}-SO_4^{2-}$ and $Mg^{2+}Al^{3+}-CrO_4^{2-}$. *Clays Clay Miner.*, 25: 14–18.
- Miyata, S. & Kumura, T. (1973). Synthesis of new hydrotalcite-like compounds and their physico-chemical properties. *Chem. Lett.*, 843–848.
- Miyata, S. (1980). Physico-chemical properties of synthetic hydrotalcites in relation to composition. *Clays Clay Miner.*, 28: 50–56.
- Moyo L. (2009) A critical assessment of the methods for intercalating anionic surfactants in layered double hydroxides. MSc dissertation, Pretoria: University of Pretoria.
- Moyo, L., Focke, W. W., Labuschagne F.J. & Verryn, S. (2012) Layered double hydroxide intercalated with sodium dodecyl sulphate. *Mol. Cryst. Liq. Cryst.*, 555(1): 51–64.
- Moyo, L., Nhlapo, N. S. & Focke, W. W. (2008). A critical assessment of the methods for intercalating anionic surfactants in layered double hydroxides. *J. Mater. Sci.*, 43: 6144–6158.

- Nhlapo, N., Motumi, T., Landman, E., Verryyn, S. M. C. & Focke, W. W. (2008). Hydrotalcite: Surfactant-assisted fatty acid intercalation of layered double hydroxides. *J. Mater. Sci.*, 43(3): 1033–1043.
- Nyambo, C., Chen, D., Su, S. & Wilkie, C. (2009). Does organic modification of layered double hydroxides improve the fire performance of PMMA? *Polym. Degrad. Stab.*, 94(8): 1298–1306.
- O'Hare, D. (1991). Inorganic intercalation compounds. In: Bruce, D. W. & O'Hare, D. (Eds), *Inorganic Materials*, New York: Wiley, pp 166–228.
- Othman, M. R., Helwani, Z. & Fernando, W. J. N. (2009). Synthetic hydrotalcites from different routes and their application as catalysts and gas adsorbents: A review. *Appl. Organomet. Chem.*, 23(9), 335–346.
- Perez-Ramirez, J., Mul, G., Kapteijn, F. & Moulijn, J. A. (2001). A spectroscopic study of the effect of the trivalent cation on the thermal decomposition behaviour of Co-based hydrotalcites. *J. Mater. Chem.*, 11: 2529–2536.
- Pesic, L., Salipurovic, S., Markovic, V., Vucelic, D., Kagunya, W., & Jones, W. (1992). Thermal characteristics of a synthetic hydrotalcite-like material. *J. Mater. Chem.*, 2(10): 1069.
- Prinetto, F., Ghiotti, G., Graffin, P. and Tichit, D. (2000). Synthesis and characterization of sol-gel Mg/Al and Ni/Al layered double hydroxides and comparison with co-precipitated samples. *Microporous Mesoporous Mater.*, 39: 229-247.
- Ramos, E., Lopez, T., Bosch, P., Asomoza, M. & Gomez, R. (1997). Thermal stability of sol-gel hydrotalcites. *J. Sol-Gel Sci. Technol.*, 8: 437–442.
- Rao, M. M., Reddy, B. R., Jayalakshmi, M., Jaya, V. S. & Sridhar, B. (2005). Hydrothermal synthesis of Mg–Al hydrotalcites by urea hydrolysis. *Mater. Res. Bull.*, 40: 347–359.
- Rocha, J., Arco, M. D., Rives, V. & Ulibarri, M. (1999). Reconstruction of layered double hydroxides from calcined precursors: a powder XRD and ²⁷Al MAS NMR study. *J. Mater. Chem.*, 3(1 M): 2499–2503.
- Ross, G.J. & Kodama, H. (1967) Properties of a synthetic magnesium-aluminum carbonate hydroxide and its relationship to magnesium-aluminum double hydroxide, manasseite and hydrotalcite. *Amer. Miner.*, 52: 1036–1047.

- Sato, T., Tezuka, M., Endo, T. & Shimada, M. (1988). Removal of sulfuroxyanions by magnesium aluminium oxides and their thermal decomposition. *J. Chem. Tech. Biotechnol.*, 39: 275–285.
- Stanimirova, T. S., Kirov, G. & Dinolova, E. (2001). Mechanism of hydrotalcite regeneration. *J. Mat. Sci. Lett.*, 20: 453–455.
- Sugimoto, A., Ishida, S., & Hanawa, K. (1999). Preparation and Characterization of Ni/Al-Layered Double Hydroxide. *J. Electrochem. Soc.*, 146(4): 1251–1255.
- Trifiro, F. & Vaccari, A. (1996). Hydrotalcite-like anionic clays (layered double hydroxides). In: Davies, J. E. D., Atwood, J. L., MacNicol, D. D. & Vogtle, F. (Eds), *Comprehensive Supramolecular Chemistry*, Oxford, UK: Pergamon Press, pp 251–291.
- Utracki, L. A., Sepehr, M. & Boccaleri, E. (2007). Synthetic, layered nanoparticles for polymeric nanocomposites (PNCs). *Polym. Adv. Technol.*, 18(1): 1–37.
- Vaia, R. A., Teukolsky, R. K. & Giannelis, E. P. (1994). Interlayer structure and molecular environment of alkylammonium layered silicates. *Chem. Mater.*, 6(16): 1017–1022.
- Whitesides, G. M., Mathias, J. P. & Seto, C. T. (1991). Molecular self-assembly and nanochemistry: A chemical strategy for the synthesis of nanostructures. *Science*, 254: 1312–1319.
- Xiang, X., Zhang, L., Hima, H. I., Li, F. & Evans, D. G. (2009). Co-based catalysts from Co/Fe/Al layered double hydroxides for preparation of carbon nanotubes. *Appl. Clay Sci.*, 42(3–4): 404–409.
- Xu, Z. P & Braterman, P. (2010). Synthesis, structure and morphology of organic layered double hydroxides (LDH) hybrids: Comparison between aliphatic and their oxygenated analogs. *Appl. Clay Sci.*, 48: 235–242.
- Xu, Z. P. & Zeng, H. C. (2001). Decomposition pathways of hydrotalcite-like compounds $MgAl_x(OH)_2(NO_3)_x \cdot nH_2O$ as a continuous function of nitrate anions. *Chem. Mater.*, 13: 4555–4563.
- Yang, Z., Choi, K.-M., Jiang, N. & Park, S.-E. (2007). Microwave synthesis of hydrotalcite by urea hydrolysis. *Bull. Korean Chem. Soc.*, 28(11): 2029–2033.

Zaneva, S. & Staminirova, T. (2004). Crystal chemistry, classification position and nomenclature of layered double hydroxides. Bulgarian Geological Society, Annual Scientific Conference.

Zhang, P., Qian, G., Xu, Z. P., Shi, H., Ruan, X., Yang, J. & Frost, R. L. (2012). Effective adsorption of sodium dodecylsulfate (SDS) by hydrocalumite (CaAl-LDH-Cl) induced by self-dissolution and re-precipitation mechanism. *J. Colloid Interface Sci.*, 367(1): 264–71.

Chapter 3

Properties of LDH/polymer micro- and nanocomposites

Carbonate- and stearate-intercalated layered double hydroxides were used as fillers to prepare polymer micro- and nanocomposites respectively. The stearate-modified LDH starting material was a bilayer intercalated clay. During melt compounding, excess stearates were released and the clay reverted to a monolayer-intercalated form. The exuded stearate acted as a lubricant, lowering the melt viscosity of the poly(ethylene-co-vinyl acetate) and linear low-density polyethylene matrices. Strong hydrogen bond interactions between the chains of poly(ethylene-co-vinyl alcohol) and the clay platelet surfaces overwhelmed the lubrication effect and caused an increase in the melt viscosity of this matrix. The notched Charpy impact strength of this composite was almost double that of the neat polymer. It appears that this can be attributed to the ability of the highly dispersed and randomly oriented nanosized clay platelets to promote extensive internal microcavitation during impact loading. The creation of a large internal surface area provided the requisite energy-dissipation mechanism.

3 PROPERTIES OF LDH/POLYMER AND NANOCOMPOSITES

3.1 POLYMER COMPOSITES

Polymer composites have attracted attention due to their unique structure and enhanced properties. IUPAC defines a composite as “a multicomponent material comprising multiple different (non-gaseous) phase domains in which at least one type of phase is a continuous phase” according to specifications (Work *et al.*, 2004). A nanocomposite refers to every type of composite materials having one of the components in the nanometre size range at least in one dimension. Manias *et al.*, (2007) defined a nanocomposite as a “fundamentally new material (hybrid) in which the nanometre scale component/structure gives rise to intrinsically new properties not present in the respective macroscopic composites or pure components”. New properties are envisaged to originate from the interaction of the polymer and filler at the interface. A polymer composite is made of three constituents, i.e. the matrix, the filler (LDH in this study) and the interfacial region. The interfacial region is a ‘communication bridge’ between the filler and matrix and is conventionally ascribed properties different from those of the bulk matrix because of its proximity to the surface of the filler (Vaia & Wagner, 2004). These authors further expound it in terms of the radius of gyration of the matrix (R_g), which is the key spatial parameter to which the majority of the polymer’s static and dynamic properties can be ultimately related and has a value in a few tens of nanometres. How then do nanocomposites differ from conventional composites? Vaia and Wagner (2004) cited six interrelated distinguishing qualities of polymer nanocomposites:

- Low percolation threshold ($\sim 0.1\text{--}2$ vol %)
- Particle-particle correlation (orientation and position) arising at low volume fraction ($\phi_c < 0.001$)
- Large number density of particles per particle volume ($10^6\text{--}10^8$ particles/ μm^3)
- Extensive interfacial area per volume of particles ($10^3\text{--}10^4$ m²/mL)
- Short distances between particles (10–50 nm at $\phi \sim 1\text{--}8$ vol %)
- Comparable size scales among the rigid nanoparticle inclusions, distance between particles and the relaxation volume of polymer chains.

Due to the small aspect ratio of spherical particles, the first two points do not apply to them.

Additive/filler materials are used to reduce costs or enhance properties such as tensile strength and modulus of polymer matrices (Hancock, 1995). Different types of filler are used to obtain polymer nanocomposites based on dimensionality/geometry. These include zero-dimensional nanoparticles (inorganic nanoparticles), one-dimensional nanoparticles (carbon nanotubes), two-dimensional nanoparticles (clays and LDHs), and three-dimensional nanoparticles (polyhedral oligomeric silsesquioxanes). The filler employed in this study falls under the two-dimensional category. Table 3.1 is a summary of other nanostructured layered materials that can be used as additives in polymer matrices. The two-dimensional platelet fillers lead to a lamellar microstructure. Hence the polymer composites have found application for their barrier properties such as reduced gas and vapour permeability. Depending on the aspect ratio of the platelets, they may be used to improve mechanical properties.

Table 3.1. Layered nanostructured materials for potential use in polymer composites
(Adapted from Utracki *et al.*, 2007)

Clay type	Examples
Phyllosilicates	Montmorillonite (MMT), bentonite (BT), hectorite, talc, vermiculite, micas, illite, attapulgite, etc.
Layered silicic acid	Kanemite, layered organosilicates
Mineral layered hydroxides	Brucite [Mg(OH) ₂], gibbsite [Al(OH) ₃]
Layered double hydroxides (LDHs)	$[M^{2+}_{(1-x)}M^{3+}_x(OH)_2]^{Y+}(A^{n-Y/2})_mH_2O$, e.g. Mg ₆ Al _{3.6} (OH) _{18.8} (CO ₃) _{1.7} H ₂ O
Layered aluminophosphates	Berlinite (AlPO), vantasselite [Al ₄ (PO ₄) ₃ (OH) ₃ ·9H ₂ O]
M ⁴⁺ phosphates and phosphonates	M ⁴⁺ = Ti, Zr, or Sn, e.g. α-form: Zr(HPO ₄) ₂ ·2H ₂ O
Chlorides	FeCl ₃ , FeOCl, CdI ₂ , CdCl ₂
Chalcogenides	TiS ₂ , (PbS) _{1.18} (TiS ₂) ₂ , MoS ₃
Cyanides	Ni(CN) ₂
Oxides	H ₂ Si ₂ O ₅ , graphite oxide, V ₆ O ₁₃ , HTiNbO ₅
<i>Others</i>	Graphite, boron nitride

The pioneering work done by Toyota into clay-based polymer nanocomposites increased interest and research into clay-based polymer composites, dating back to 1986 (Kawasumi,

2004). Research has focused mostly on smectite-based polymer composites. Anionic clays such as layered double hydroxides (LDHs) are a potential alternative for the preparation of polymer composites. This can be achieved since LDHs possess a layered structure similar to that of layered silicates or cationic clays. It is well established that the dispersion of particles with high aspect ratios, e.g. fibres and platelets, in polymeric matrices improves the mechanical properties. However, good interfacial adhesion and a homogeneous dispersion are prerequisites (Pradhan *et al.*, 2008). Nanostructured clays can improve a wide range of polymer properties and are therefore ideal for polymer-clay nanocomposite preparations. The resulting polymeric hybrids exhibit improved gas barrier properties, mechanical properties (Hsuesh & Chen, 2003; Wang *et al.*, 2006), enhanced flame retardancy (Zammarano *et al.*, 2005; Costa *et al.*, 2005; Chen & Qu, 2003 & 2004; Zubitur *et al.*, 2009), UV and photo-stability (Bocchini *et al.*, 2008) or ease of photo-prodegradability (Magagula *et al.*, 2009), etc.

3.2 POLYMER COMPOSITE STRUCTURES

Organoclay dispersion within a polymer matrix gives rise to three possible structures, i.e. phase separated, intercalated and/or delaminated/exfoliated composites, as shown in Figure 3.1. These structures are usually probed by two complementary techniques, namely X-ray diffraction (XRD) and transmission electron microscopy (TEM). The former gives the degree of separation and the latter serves as a visual confirmation of the XRD analysis.

3.2.1 Phase separated composites

Phase separation results from the polymer chains failing to penetrate the interlayer space of the layered material. The composite retains the same properties as conventional microcomposites. Hence the d-spacing remains the same as that of the clay.

3.2.2 Intercalated composites

In these composites the polymer chain(s) is intercalated within the interlayer of the LDH. They normally exhibit a well-ordered morphology with alternating inorganic and polymeric layers or periodically stacked layers. The composite is made of alternating polymer and inorganic layers. The resulting clay-polymer hybrid exhibits increased d-spacing.

3.2.3 Exfoliation/delamination composites

This structure describes a case where the LDH layers are completely and uniformly dispersed in a polymer matrix. It is identified by the absence of diffraction peaks or basal reflection. This observation is thought to be due to a large increase in the layer separation > 8 nm or lack of ordering or registry (Alexandre & Dubois, 2000). In some instances intercalated and exfoliated structures may co-exist; this is illustrated by the broadening of primary diffraction peaks. To eliminate ambiguous conclusions, TEM is normally used to confirm the results obtained from XRD. Some studies report the exfoliation of surfactant-intercalated LDHs (Leroux *et al.*, 2001; Khan and O'Hare, 2002; Fischer, 2003). In general, a higher degree of exfoliation/dispersion of LDHs has been observed in polar rather than in non-polar matrices. The preparation of polymer composites from polyolefins is difficult due to their low polarity. Hence they do not interact effectively with the LDHs. Dispersion of LDHs in non-polar matrices through melt compounding has been explored using maleic anhydride grafted polyethylene (PE-g-MA) as a compatibiliser (Costa *et al.*, 2005). It is important to note that full exfoliation and full intercalation are seldom observed in nanocomposites.

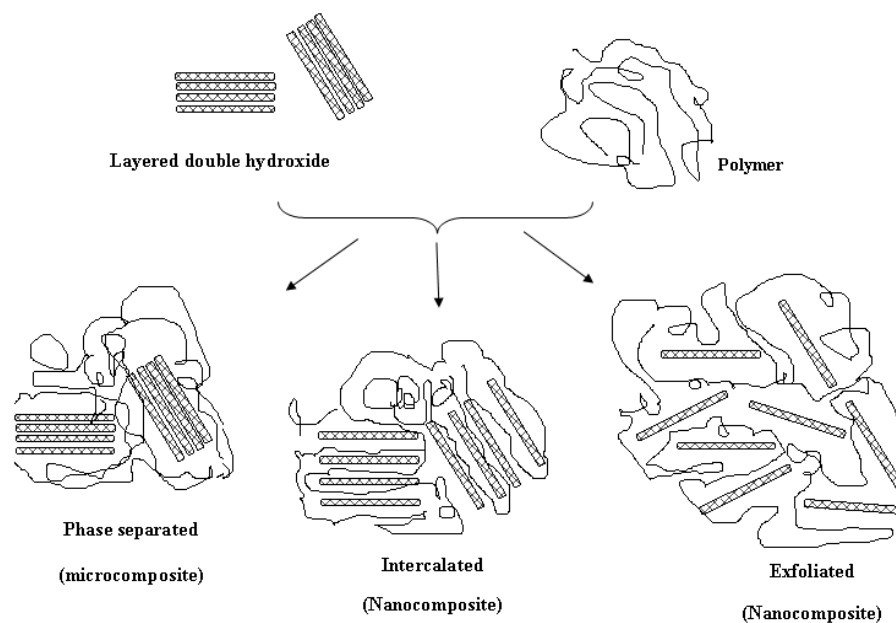


Figure 3.1. Polymer composite structures

The structures that arise are related to the types of interfacial interaction that are favoured between the polymer and the clay. Vaia and Giannelis (1997) proposed three main clay-polymer interactions: polymer-surface, polymer-surfactant and surfactant-surface. They concluded that to achieve complete clay sheet dispersion, a very favourable polymer-surface interaction was necessary (Vaia and Giannelis 1997; Fischer 2003). Therefore the properties displayed by the polymer composite result from these associations.

3.3 LDH-BASED POLYMER COMPOSITE PREPARATION

Polymer-clay composites are mainly prepared in three ways, namely in situ polymerisation (Moujahid *et al.*, 2002; Lee & Im, 2007; Huang *et al.*, 2011), solution-intercalation methods (Ramaraj *et al.*, 2010) and melt-processing (Zammarano *et al.*, 2006).

3.3.1 In situ polymerisation

This is the first and most widely used mode of preparation of clay-based nanocomposites. It has been adopted for the preparation of LDH-based nanocomposites. It combines the basic principles of intercalation of LDHs, namely co-precipitation, regeneration and intercalation via organic/inorganic pillared LDHs (ion exchange), as shown in Figure 3.2. In the case of pillared LDHs, the pillaring agent is chemically active and hence interacts with the polymer chain (Hseuh & Chen, 2003). Usually, the first step entails the intercalation of the monomers/ionomers into the LDH. Polymerisation is initiated by thermal or radiation treatment and is also facilitated by organic initiator and catalyst (Whilton *et al.*, 1997). Recently, polymerisation has been reported to be initiated by microwave irradiation (Herreo *et al.*, 2011). This type of polymerisation makes thermosetting polymer-nanocomposites possible, e.g. epoxy-organoclay nanocomposites.

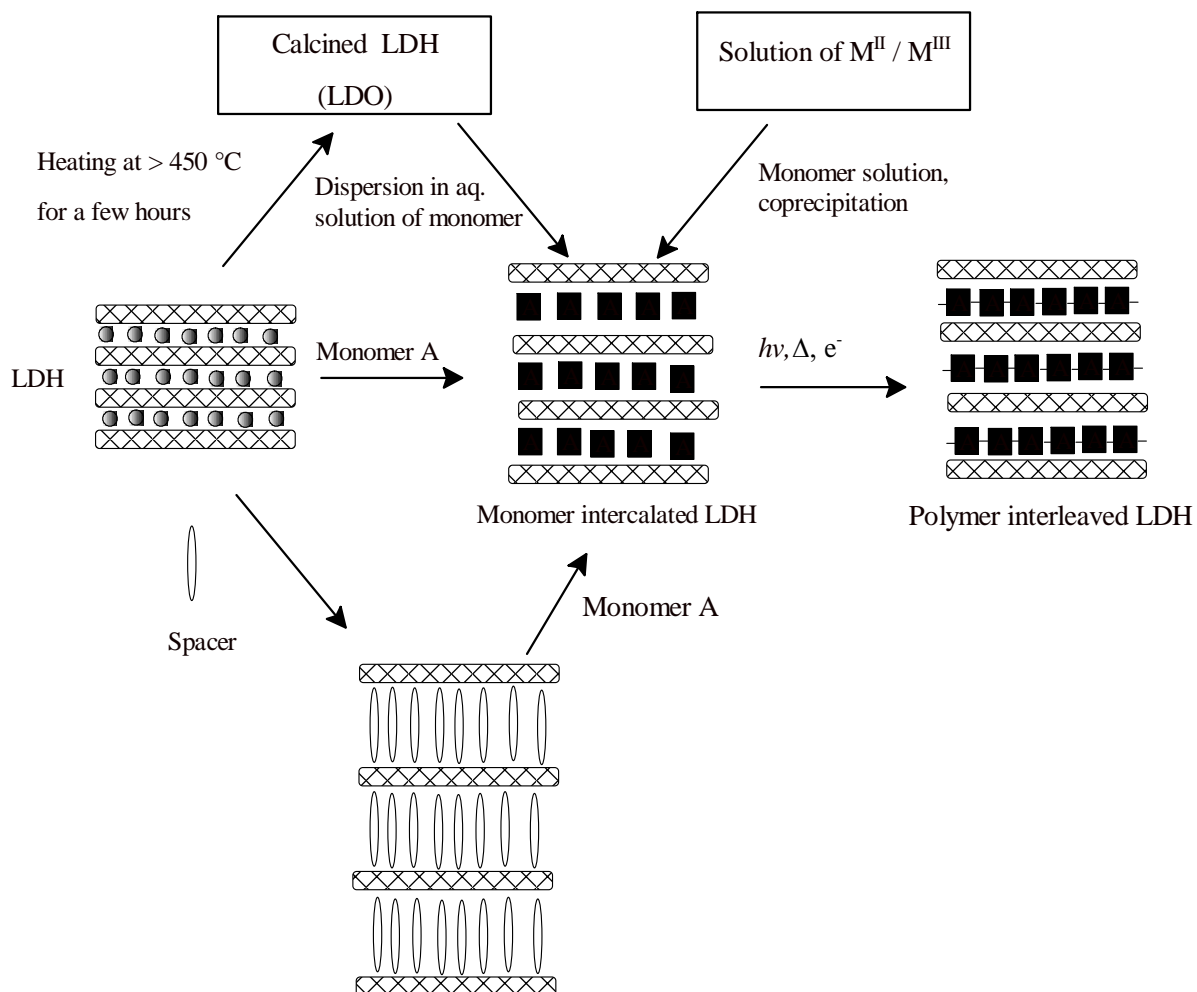


Figure 3.2. Schematic pathways of in situ polymerisation within the LDH layers in the preparation of polymer/LDH nanocomposites (Adapted from Costa *et al.*, 2008)

However, in-situ polymerisation has two limitations. Firstly, there is the distance between the monomers when they are strongly anchored to the host matrix. Secondly, there is the condition that when polymerisation takes place (temperature, pH or redox reaction), it must leave the layered structure intact. This method has been employed with success in the preparation of the LDH-based nanocomposites listed in Table 3.2.

Table 3.2. Summary of in situ polymerisation in LDH-based nanocomposites

LDH	Monomer	Conditions	Reference
Mg-Al	Dimethyl terephthalate	Ethylene glycol catalyst	Cui <i>et al.</i> , 2012
Li-Al	Amino benzoic acid (different isomers)	Ion exchange	Isupov <i>et al.</i> , 2001
Zn-Al	Vinyl benzene sulphonate	Co-precipitation	Moujahid <i>et al.</i> , 2003
Mg-Al	Aspartate	Co-precipitation	Whilton <i>et al.</i> , 1997
Ca-Al	Styrene-4-sulphonate	Co-precipitation	Vieille <i>et al.</i> , 2004
Zn-Al	Styrene sulphonate	Co-precipitation	Vieille <i>et al.</i> , 2004
Mg-Al	Methyl methacrylate (MMA)	Via 10-undecenoate pillared LDH. Catalyst (2,2'- azobisisobutyronitrile) used to prepolymerise MMA	Wang <i>et al.</i> , 2005
Cu-Cr Cu-Al	Aniline	Via terephthalate or hexacyanoferrate pillared LDH	Challier & Slade, 1994
Mg-Al	Acrylate	Via dodecylsulphate pillared LDH	O'Leary <i>et al.</i> , 2002

3.3.2 Solution intercalation

Solution intercalation is also referred to as solution blending and solution casting. This particular method entails the solubilisation of the polymer resin in an organic solvent. The solvents employed include toluene, chloroform, acetonitrile, xylene and dimethylacetamide. The mixed metal aqueous salts may be precipitated into the former solution. In other cases organo-modified LDHs are added to the polymer solution. Chen *et al.* (2003, 2004) synthesised the same polymer composite using the solution intercalation synthesis method. The organo-LDH was added to a solution of PE-g-MA in xylene and the mixture was refluxed in nitrogen for 24 h. The polymers used in this method are normally water soluble, such as PEO, poly(vinyl alcohol) and poly(vinyl pyrrolidone). Table 3.3 provides a summary of a few selected solution intercalation formulations.

Table 3.3. Summary of solution intercalation in LDH-based nanocomposites

LDH	Polymer	Solvent	Reference
Mg-Al	PE-g-MA	Xylene	Chen <i>et al.</i> , 2003
Zn-Al	LLDPE	Xylene	Chen <i>et al.</i> , 2004
Mg-Al	Poly(styrene-co-methylstyrene) grafted polyaniline	Xylene	Abbasian, 2011
Zn-Al	PVA	Water	Marangoni <i>et al.</i> , 2010
Mg-Al	Silicone rubber	Chloroform	Pradhan <i>et al.</i> , 2010
Mg-Al	PVA	Water	Ramaraj <i>et al.</i> , 2010
Mg-Al	Polyurethane	Tetrahydrofuran (THF)	Kotal <i>et al.</i> , 2009
Mg-Al	Poly(propylene carbonate)	Cyclohexanone	Du <i>et al.</i> , 2006
Mg-Al	Poly(vinyl chloride)	THF	Liu <i>et al.</i> , 2008
Mg-Al	Ethylene vinyl acetate	Toluene	Kuila <i>et al.</i> , 2007
Mg-Al	Ethylene propylene diene terpolymer	Toluene	Achyra <i>et al.</i> , 2007

However, the use of organic solvents makes the method environmentally unfriendly and they are not easily removed. In some cases small solvent particles intercalate into the clay gallery rather than the polymer.

3.3.3 Melt processing

This method has been considered to be most challenging, yet it can be easily adopted for industrial product manufacture. It involves the incorporation of the filler into a molten polymer through extrusion, kneading and, to a lesser extent, injection moulding (Manias *et al.*, 2007). In addition to the thermodynamic driving force for filler dispersion, mechanical shear has kinetic contributions. A high degree of dispersion is obtained, depending on the processing conditions and the polarity/affinity of the polymer to the organoclay. Good exfoliated structures have been reported as a result of adequate mean residence time, viscosity of the matrix and shear rate (Cho & Paul, 2001). This method is environmentally friendly and economically advantageous due to the absence of solvents and is a cost-

effective way to prepare samples in large quantities. It has been successfully employed by the researchers cited in Table 3.4.

Table 3.4. Summary of melt-processing examples in LDH based nanocomposites

LDH	Organic modifier	Polymer	Reference
Mg-Al	Dodecylbenzene sulphonate (DBS) 4-hydroxybenzene sulphonate (HBS)	Poly(p-dioxanone)	Zubitur <i>et al.</i> , 2009
Mg-Al	Lauric acid	Poly(L-lactic acid)	Katyar <i>et al.</i> , 2011
Mg-Al	Dodecyl sulphate	LLDPE	Costa <i>et al.</i> , 2007
Mg-Al	Dodecyl sulphate Dodecyl benzene sulphonate Octyl sulphate	PET	Lee <i>et al.</i> , 2006
Zn-Al	Dodecyl sulphate	Polylactic acid	Wang <i>et al.</i> , 2010
Mg/Al	Stearic acid	Poly(vinyl) chloride	Chen, 2007
Mg-Al	Dodecyl benzene sulphonate	Polypropylene	Wang <i>et al.</i> , 2011
Mg-Al	Dodecyl benzene sulphonate	Polypropylene	Coiai <i>et al.</i> , 2010
Mg-Al	2-ethyhexyl sulphate Dodecyl sulphate Eicosyl sulphate	LDPE	Muksing <i>et al.</i> , 2011
Mg-Al	Dodecyl sulphate	Nylon 6 (polycaprolactam)	Du <i>et al.</i> , 2007
Mg-Al	Dodecyl sulphate	Polypropylene	Lonkar <i>et al.</i> , 2009

In the non-polar matrices, such as polyethylene and polypropylene matrices, compatibilisers such as polyethylene grafted maleic anhydride (PE-g-MA) are used to improve the compatibility between the clay and the polymer.

Other methods used in the preparation of polymer nanocomposites, though used to a lesser extent, include co-vulcanisation (Okada & Usuki, 1995), solid state intercalation (Gao *et al.*,

2001) and sol-gel methods (Carrado & Xu, 1999). Vaysse *et al.* (2003) combined chimie douche and redox exchange for the preparation of monomeric intercalated LDH, followed by its in situ polymerisation, resulting in a polyacrylate-intercalated composite.

3.4 PROPERTIES OF LDH-BASED POLYMER NANOCOMPOSITES

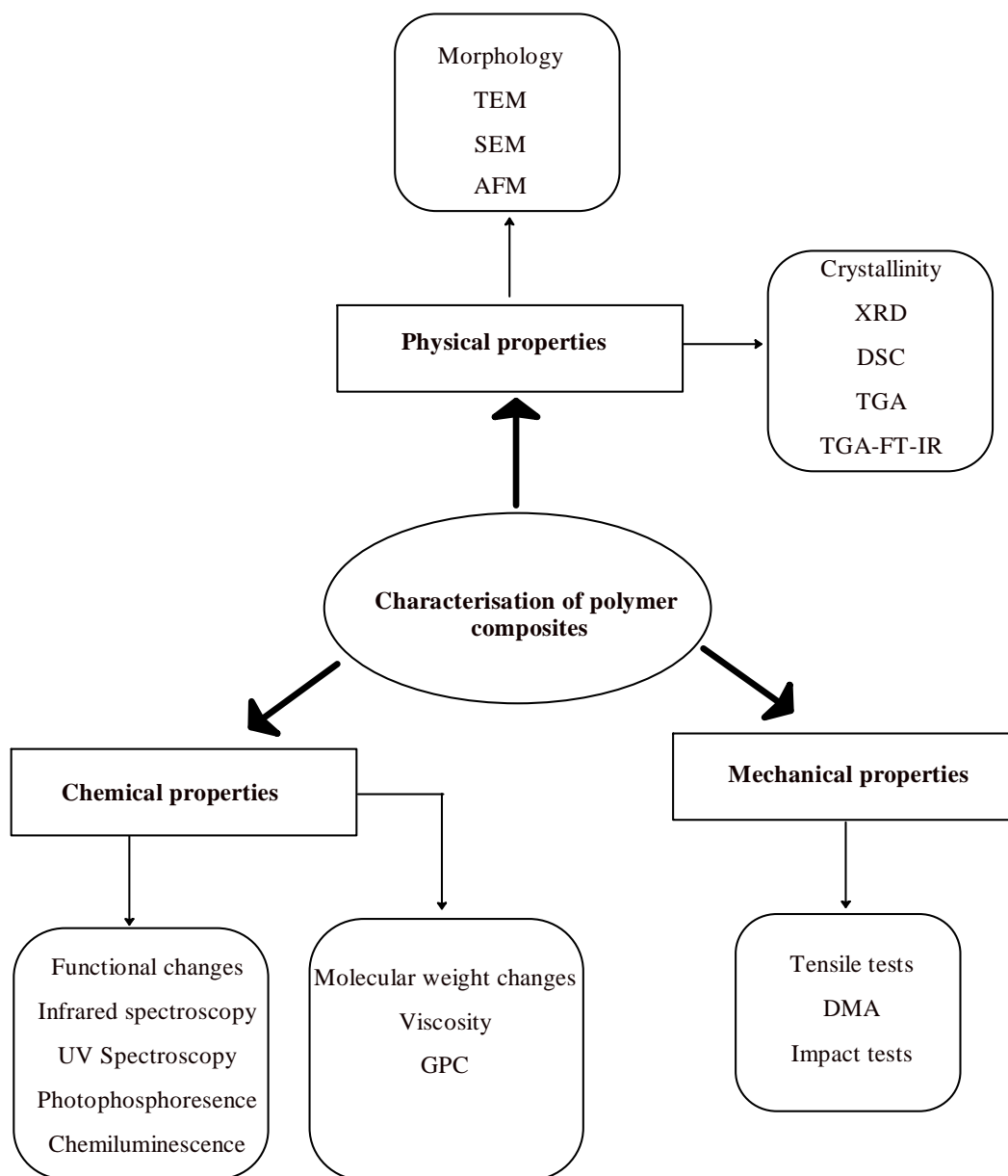


Figure 3.3. Characterisation of LDH-based polymer composites

Figure 3.3 shows a wide variety of characterisation techniques available for the analysis of the properties of polymer nanocomposites. These include X-ray diffraction (XRD), transmission electron microscopy (TEM), scanning electron microscopy (SEM), atomic force microscopy (AFM), thermogravimetric analysis (TGA). Mechanical properties are probed by tensile testing, impact testing and dynamic mechanical analysis (DMA). Chemical changes in the polymer composite matrix are examined through rheology, infrared and UV spectroscopy, gel permeation chromatography, etc. The properties discussed in the following sections are those that were also investigated in this study.

3.4.1 Physical properties

3.4.1.1 Morphology

Among the previously mentioned characterisation techniques, XRD and TEM are the most frequently used for the determination of the composite structure and degree of dispersion. The increase in the d-spacing has been explained as an indication of successful intercalation of the polymer, whereas its loss is evidence of an exfoliated structure. In this context, most researchers publish work on LDH-based nanocomposites as either intercalated or exfoliated. However, the loss of the primary reflection can be easily misinterpreted as exfoliation yet technical errors, such as a low starting angle, misalignment of sample holder, wrong slit setting or orientation, or the resolution limitations of XRD apparatus (i.e. $2\theta < 2$), will give similar results (Chen & Qu, 2004). In other cases, the disappearance of the primary peak could also be a result of a very low filler loading and crystal defects caused by processing. TEM allows a qualitative understanding of the internal structure and the spatial distribution of various phases, and direct visualisation of the defect structure (Ray & Okamoto, 2003).

Compatibility studies of LDHs with polypropylene (PP), polystyrene (PS), polyethylene (PE) and poly(methyl-methacrylate) (PMMA) were carried out by Nyambo *et al.* (2009.) Good dispersion and nanocomposite formation was obtained from the LDH/PMMA composite. Complete exfoliation in polystyrene/ZnAl LDH composite (derived from solution intercalation) was achieved by decreasing the LDH content, extending the reflux time and employing rapid precipitation (Qui *et al.*, 2005). It is clear from the above that the success of preparing a well-dispersed polymer composite depends on the polarity of the polymer and the chemistry of the filler. In the preparation of LDH-based nanocomposites in

non-polar matrices, maleic anhydride grafted polyethylene is normally employed to improve the compatibility of the LDH with the matrix (Costa *et al.*, 2006).

3.4.1.2 Thermal behaviour

LDH-based polymer composites have been studied particularly for improving the thermal stability of the matrix. The mechanism by which LDHs achieve this is in the same manner as traditional metal hydroxide fillers. LDHs contain bound water, interlayer free water and OH-groups on the metal hydroxide lattice. The decomposition of LDHs is endothermic and releases water vapour, which reduces the amount of combustible volatiles at the surface of the polymer (Costa *et al.*, 2007). The incorporation of LDHs improved the thermal stability of the polymer, but the degradation mechanism remained the same (Zubitur *et al.*, 2009; Liu *et al.*, 2009; Nyambo *et al.*, 2008). Low LDH loading also gave improved thermal stability; this is explained by the nanoscale dispersion. Other factors that affect thermal stability include the intrinsic thermal resistance of the polymer matrix, the nanofiller content, the chemical constitution of the organic modifier, the chemical character of the polar compatibiliser, and lastly access of oxygen to composite material during heating. However, the thermal stability of LDH-based nanocomposites was not improved in all cases. Chiang and co-workers (2011) found deterioration of the thermal stability of poly(L-lactide) (PLLA)/layered double hydroxide composites. They attributed this anomaly to the LDH derivative used (P-LDH) which was considered to accelerate thermal decomposition of the polymer. Thermal behaviour is particularly linked with flame retardation studies in LDH-based polymer composites. A number of researchers have embarked on research into the flame-retardant properties of LDHs in their polymer composites (Costache and Wang, 2006; Jaio *et al.*, 2006; Nyambo *et al.*, 2008). This is important since most flame retardants are halogen-based and these tend to be corrosive and toxic. Hence LDHs are more environmentally friendly alternatives.

Thermal behaviour may also be studied by DSC to follow changes in the melting and crystallisation in the composite matrix. The technique measures temperatures and heatflows associated with transitions in the materials as a function of time and temperature in a controlled atmosphere. The fundamental equation for DSC heatflow is give below, under the assumption that work and mass loss are equal to zero:

$$\Delta H = C_p \Delta T \quad [3]$$

In differential form it is represented as:

$$\frac{dH}{dt} = C_p \frac{dT}{dt} \quad [4]$$

where;

C_p = specific heat capacity (J/g°C)

T = temperature (°C)

H = heat (J)

$\frac{dH}{dt}$ = heat flow (J/min)

$\frac{dT}{dt}$ = heating rate (°C/min)

Crystallinity is calculated as:

$$C = \Delta H / \Delta H_{100\%} * 100\% \quad [5]$$

where

C = crystallinity (%)

ΔH = heat of fusion (J/g)

$\Delta H_{100\%}$ = heat of fusion of 100% crystalline polymer

The crystallisation of a polymer is governed by polymer molecules having adequate regular structure and mobility; the temperature should be $T_g < T < T_m$, presence of a nuclei and the rate of crystallisation to be sufficiently high (Utracki 2004). Crystallisation is either homogeneous or heterogeneous; the former occurs when the polymer molecules self-assemble into an ordered state, while in the latter molecules assemble on the surface of a foreign body. In the case of LDH-based composites, LDHs act as heterogeneous nucleation sites. The crystallisation behaviour of LDH-based polymer composites was studied by Ramaraj *et al.* (2010). The LDH particles were found to have a nucleating effect in the polymer matrix.

3.4.2 Mechanical properties

Mechanical properties are investigated by tensile and impact testing, and by dynamic mechanical analysis. The reinforcing property of organoclay in polymer composites depends on the aspect ratio of the fillers, the particle size and distribution, its degree of dispersion and orientation in the matrix, the porosity of the composite and the adhesion at the filler-matrix interface (Cho & Paul 2001; Verbeek & Focke, 2002). The micromechanics of tensile testing of laminated composite materials are represented in a simple mathematical model in which the tensile modulus is described in terms of isostrain and isostress, as illustrated in Figure 3.4. The elastic properties of the composite depend on the orientation of the filler to the applied stress. The effective moduli when the layers are in parallel or in series yield the Voight and Rues moduli respectively (Ward & Hadley, 1993).

An isostrain condition applies when the strain is the same in all composite layers. Hence maximum stiffness is achieved when the stress is applied parallel to the layers. An isostress condition applies when the layers are orientated transverse to the applied stress and each layer is subjected to the same force. This is under the assumption that the area remains constant through the stack and the stress is the same in all the layers. The effective Young's moduli are given by the equations below (Verbeek & Focke, 2002):

$$\text{Isostrain: } E_c = E_m v_f + E_p v_p \quad [6]$$

$$\text{Isostress: } 1/E_c = v_f/E_m + v_p/E_p \quad [7]$$

where

E_c = the tensile modulus of the composite

E_p = the tensile modulus of the polymer

E_m = tensile modulus of the filler

v_p and v_f = volume fraction associated with zero porosity of the polymer and filler respectively.

The particles are assumed to adhere perfectly to the matrix. Several empirical modifications to the model have been made by Nicolais & Narkis; Kerner, Faber & Farris; and Nielson, Haplin-Tsai to mention a few (cited in Utracki, 2004).

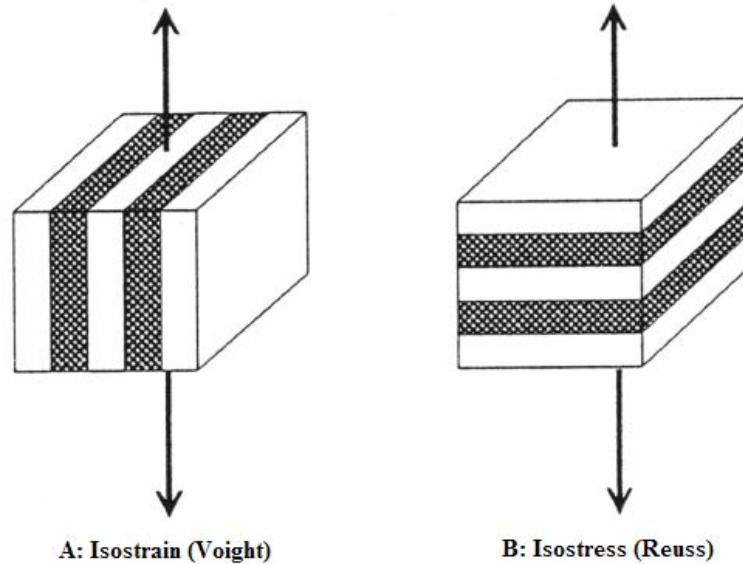


Figure 3.4. Mixing rule conditions for layered composites (Adapted from Verbeek & Focke, 2002)

Camino *et al.* (2001) found that tensile tests indicate that as far as the elongation to break and ultimate strength are concerned, the LDH system behaves similarly to other fillers. Lonkar *et al.* (2012) prepared PP/LDH nanocomposites using PP-g-MAH as a compatibiliser. The specimens showed an increase in modulus and tensile strength parameters, which is an indication of the reinforcing property of LDHs. However, they found that the impact strength and elongation at break steadily decrease with increase of the organo-LDH content.

The incorporation of fillers in the polymer matrix results in a heterogeneous system. When an external load is applied, these particles act as stress concentrators and the magnitude is dependent on the geometry of the particles (Zuiderduin *et al.*, 2003). Rigid fillers to be used as polymer-toughening agents must meet the following prerequisites as given by Zuiderduin *et al.* (2003):

- The particles should be small in size (less than 5 μm). These provide a stable free volume, whereas larger particles act as initiation sites for fracture.
- The aspect ratio must be close to unity to avoid high stress concentrations.

- The particles must debond prior to the yield strain of the polymer matrix in order to allow the stress state of the matrix material to change.
- The particle must be dispersed homogeneously in the polymer matrix; aggregation should be avoided.

Polymer-toughening modifiers alter the stress state in the material around the particles and induce extensive plastic deformation, e.g. multiple crazing (see Figure 3.5), shear banding (see Figure 3.6), crazing with shear yielding, rubber particle stretching or tearing, and debonding at the inorganic filler particles (Kim *et al.*, 1998). These deformations constitute a range of different energy-absorption mechanisms, hence preventing premature fracture.

Crazes are stabilised stress cracks whose separation surfaces are bridged by stretched fibrils and films (see Figure 3.5). A typical fibril diameter is 0.01–0.1 μm . A craze differs from a crack in that it continues to support a load. Craze propagation absorbs fracture energy and effectively increases the toughness of a polymer. It is typically identified by whitening of the crazed region. The white colour is caused by light scattering. Necking of tensile test specimens is not observed in a crazing scenario. However, it is observed in shear banding. The typical size of a craze is approximately 0.5 μm .

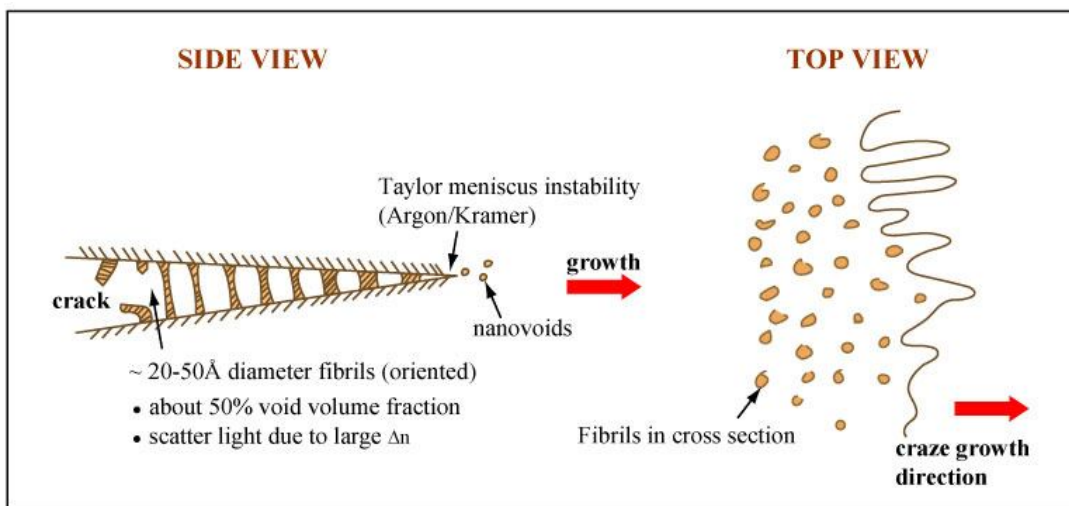


Figure 3.5. Craze yielding (Adapted from MIT Open Course Ware, 2009)

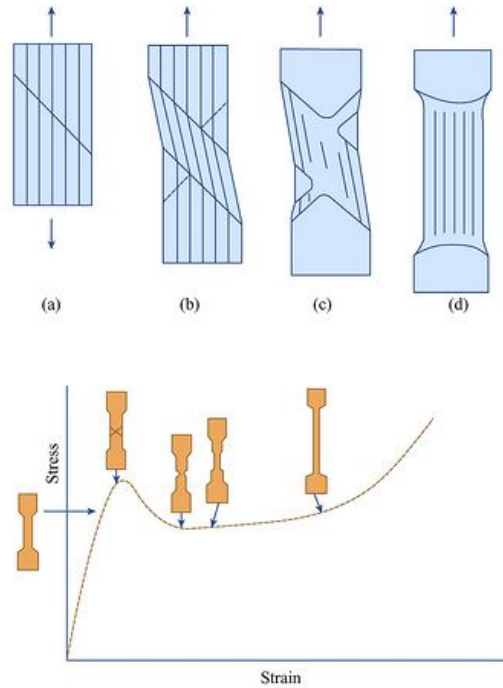


Figure 3.6. Shear banding (Adapted from MIT Open Course Ware, 2009)

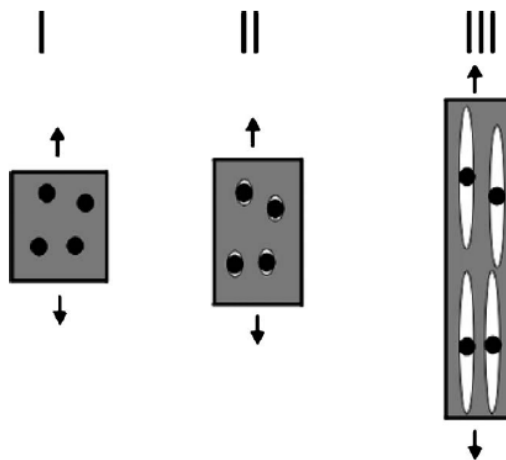


Figure 3.7. Polymer-toughening mechanism with rigid particles (Kim *et al.*, 1998)
(Figure adapted from Zuiderduin *et al.*, 2003)

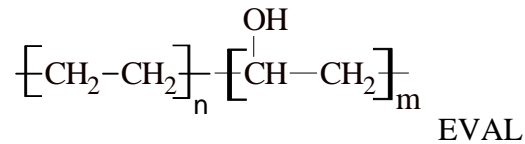
Figure 3.7. shows a polymer-toughening mechanism proposed by Kim *et al.* (1998). The filler is required to debond, hence creating free volume at a sub-micron level, which is a cavitation mechanism similar to that found in rubber-toughened matrices. The figure depicts the following:

- I. *Stress concentration* – The modifier act as stress concentrators, because they have different elastic properties from those of the polymer matrix.
- II. *Debonding* – Stress concentration gives rise to a build up of triaxial stress around the filler particles and leads to debonding at the particle-polymer interface.
- III. *Shear yielding* – The voids caused by debonding alter the stress in the polymer matrix surrounding the voids. This reduces sensitivity towards crazing since volume strain is released. The shear yielding mechanism becomes operative and the material is able to absorb large quantities of energy upon fracture.

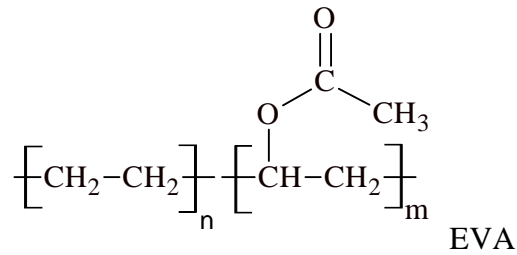
Generally, very few works of literature site mechanical property improvement for LDH-based polymer composites (Lonkar *et al.*, 2012).

Various investigations have demonstrated the thermotropic behaviour of the interlayer anions in surfactant-intercalated LDHs (Nhlapo *et al.*, 2008; Focke *et al.*, 2010). Nhlapo *et al.* (2008) showed that fatty acid-intercalated LDH that was beyond the AEC levels appeared to melt partially without reforming, below polymer processing temperature (120 °C). Globular residues were observed, giving a façade of a completely molten LDH-stearate. However, this was attributed to the exuded stearate anions which formed a droplet on the remaining LDH-stearate platelet. The transudation of the interlayer anions in bilayer intercalated LDHs is envisaged to include stages of removal of interlayer water and excess anions, giving a monolayer orientated residue. The study by Nhlapo *et al.* (2008) suggested that the LDH-fatty acid dispersion in polymer matrices would not result in ordinary exfoliation or delamination. It was therefore of interest to explore this anomaly further with regard to the effect of the exuded anions on the matrix and the utility of LDHs as functional fillers. Hence in the present investigation both the unmodified LDH-carbonate (LDH-CO₃) and the modified LDH-stearate (LDH-St) were compounded into polyethylene copolymers of differing polarities.

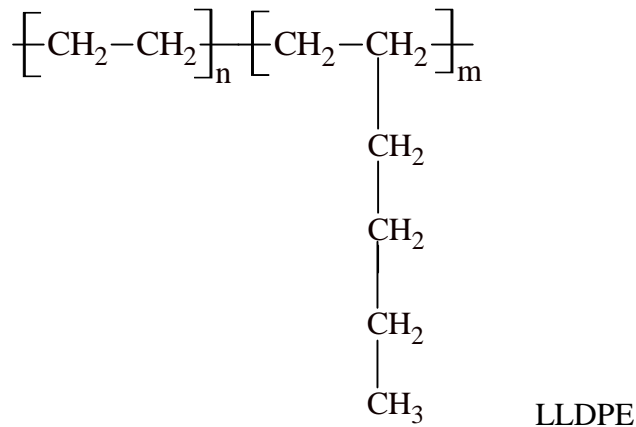
The polymers of choice were poly(ethylene)-co-vinyl alcohol (EVAL), poly(ethylene)-co-vinyl acetate (EVA) and linear low-density polyethylene (LLDPE). EVAL is widely used in the packaging of foods and non-foods because of its excellent gas- and flavour-barrier properties. EVAL is a crystalline random copolymer of ethylene and vinyl alcohol with the molecular formula represented by the structure (EVAL EUROPE Product Sheet):



EVA is a copolymer of ethylene and vinyl acetate. It has applications in packaging (cling wrap), electrical insulation, hot-melt adhesives, foam rubber and biomedical engineering (drug delivery). Its molecular formula is:



LLDPE is a copolymer of ethylene which has a short-branched hydrocarbon chain. Like the other polymers used in the study, it finds application mainly in the packaging industry and flexible tubing. Its formula is:



In this study a combination of complementary techniques was employed to investigate the structure-property relationship of the composites obtained there.

3.5 EXPERIMENTAL

3.5.1 Materials

The 1-hexene random copolymer-based linear low density polyethylene (LLDPE) was supplied by Sasol Polymers (South Africa) rotomolding grade HR411 (density 0.939 g cm^{-3}). Poly(ethylene-co-vinyl acetate) (EVA) grade EV101 (density 0.941 g cm^{-3}) containing 18 mol % vinyl acetate was supplied by Asia Polymer Corporation, Taiwan. Poly(ethylene-co-vinyl alcohol) (EVAL) grade T101B (density 1.17 g cm^{-1}) containing 68 mol % vinyl alcohol was obtained from Kuraray, Belgium. The melt flow index (MFI) values measured at $190 \text{ }^\circ\text{C}/2.16 \text{ kg}$ in units of $\text{g}/10 \text{ min}$ were 3.5, 1.8 and 1.7 for the LLDPE, EVA and EVAL respectively. The materials required for the modification of LDH have been described in Chapter 2.

3.5.2 Preparation of LDH-stearate

A detailed experimental procedure was described in Section 2.5.2 for the intercalation of stearic acid into LDH. The results of the repeat experiments are shown in Appendix B.

3.5.3 Preparation of polymer/LDH-St

The polymer composites in the study were prepared with both pristine and modified LDHs. The constitutive proportions of the LDHs in the composites prepared were 5 and 10 by wt% of organoclay. The polymer/LDH composites were prepared by the melt-compounding process in a TX28P co-rotating twin screw extruder, with a screw diameter of 28 mm with an L/D ratio of 18. The temperature profile from the feed to the die of the extruder was between 100 and $220 \text{ }^\circ\text{C}$. An average screw speed of about 170 rpm was used. The extruded polymer and polymer composite strands were water-cooled as they came out of the die. The extrudents were granulated and left to dry overnight at $60 \text{ }^\circ\text{C}$. A portion of each sample was used to injection mould dumbbells for the tensile tests. Injection moulding was carried out on an Engel injection moulding machine. The set temperature for zones 1/2/3 and nozzle were $200/210/220/220 \text{ }^\circ\text{C}$ for LLDPE and EVAL composites and $140/150/160/170 \text{ }^\circ\text{C}$ for the EVA composites respectively.

3.5.4 Characterisation

Imaging of fractured surfaces was carried out in a JEOL 5400 SEM and in a JEOL 5400 SEM. The polymer composite samples were fractured after they had been placed in liquid nitrogen. The composites were mounted on the sample holder and coated five times with gold under argon gas using the SEM autocoating unit E5200 (Polaron equipment Ltd).

The degree of dispersion was studied by use of transmission electron microscopy (TEM). Analysis was carried out on a JEOL 2100F, at an accelerated voltage of 200 kV. The samples were prepared by means of cryo-ultramicrotomy in a Lecia-Riechert Ultracut R with EMFCS cryo-attachment, with a nominal thickness of 90 ± 10 nm, and sliced at -80 °C using a diamond knife. Each section was then mounted on a 300 mesh copper/palladium grid and viewed.

Thermogravimetric analysis (TGA) was conducted on a Mettler Toledo A851 TGA/SDTA machine. A small piece of sample (ca. 10 mg) was placed in 70 μ l alumina open pans. The temperature was scanned at 10 °C/min in air in the range from 25 to 800 °C.

Differential scanning calorimetry (DSC) data were collected from a Mettler Toledo DSC 1 instrument. Approximately 5–10 mg of sample was placed in an aluminium pan. A pin hole was made in the lid. The sample was heated from 0 to 250 °C at a scan rate of 10 °C/min and at a N₂ flow rate of 50 ml/min.

Viscoelastic behaviour was studied with a Perkin Elmer DMA 8000 dynamic mechanical analyser (DMA) using the single cantilever bending mode. The applied frequency was 1 Hz. The temperature was scanned at 2 °C min⁻¹ from -20 to 180 °C, -80 to 150 °C and -50 to 80 °C for EVAL, LLDPE and EVA respectively.

Melt flow viscosity was determined with a Göttfert High-Pressure Capillary Rheograph 2000 rheometer. The capillary die had a 180 ° entrance angle, a diameter of 1 mm and a length of 30 mm. Measurements were done at 190 °C with shear rates ranging from 1 to 5 000 s⁻¹.

FTIR spectra were recorded on a Perkin Elmer 100 Spectrophotometer with a MIRacle ATR attachment with diamond Zn/Se plate. A piece of solid sample was pressed onto the Zn/Se plate. The reported spectra were obtained over the range 650–4 000 cm^{-1} and represent an average of 32 scans at a resolution of 2 cm^{-1} .

Phase identification was carried out by X-ray diffraction (XRD) analysis on a PANalytical X'pert Pro powder diffractometer. The instrument features variable divergence and receiving slits and an X'celerator detector using Fe-filtered Co K- α radiation (0.17901 nm). X'Pert High Score Plus software was used for data manipulation.

Tensile testing was carried out on a Lloyds Instruments LRX Plus machine according to ASTM D 638 using Type IV dumbbells. Five specimens were tested for each compound. Charpy impact testing was carried out on a Zwick Impact Tester using the 0.5 J hammer. Tensile impact tests were carried out according to ASTM D1822-06 on Type S and L test specimens.

Polarised optical microscopy (POM) was used to study the crystallisation morphology. The samples were sandwiched between two glass slides and heated on a Linkam THMS hot stage (Linkam Scientific Instruments Ltd) from room temperature to 135 °C for LLDPE and its respective composite at a rate of 10 °C/min, and then held at this temperature for 5 min before being cooled at the same rate to 125.5 °C. They were then held isothermally for 10 min, during which time images were taken using a Carl Zeiss POM.

3.6 RESULTS AND DISCUSSION

The two fillers considered in this study are distinguished by the nature of the external planar surface. The LDH-CO₃ featured sheets with exposed hydroxyl groups. They allow strong hydrogen bonding with the alcohol functional groups present in polar matrices such as EVAL. However, these highly polar surfaces would be incompatible with the non-polar LLDPE matrix. In the case of the LDH-stearate, the particles are at least partially covered by stearate anions (Focke *et al.*, 2010). Such surface modification with aliphatic chains should provide improved compatibility with the aliphatic LLDPE chains. The second consideration is the strength of interactions within the clay interlayers. The high charge density and the hydrophilicity of the layers in LDH-CO₃ encumber delamination or

exfoliation of the clay sheets (Adachi-Pagano *et al.*, 2000; Leroux *et al.*, 2001; Hibino & Jones, 2001). In the LDH-stearate, the fatty acid chain ends in the bilayers interact via weak van der Waals forces only. Hence it is much easier to delaminate and disperse this clay in polymer matrices.

The results described below pertain to the 10 wt.% of each respective composite unless stated otherwise. Detailed results of the 5 wt.% composite are presented in Appendix C.

Figures 3.8, 3.9 and 3.10 are SEM images that show the general morphology and texture of freeze-fractured surfaces. In the EVA/LDH-CO₃ and LLDPE/LDH-CO₃ composite (see Figures 3.8 and 3.10), there is clear phase separation of the clay and the polymer. The LDH-CO₃ particles appear to form agglomerates within the polymer matrix. Poor interfacial adhesion is evident in both the LLDPE composites (Figure 3.10). This is shown by the formation of wells around the filler particles. This is also the case for the EVA/LDH-stearate composite. In all the other samples there was relatively good adhesion between the matrix and the filler, shown by the absence of cavities previously occupied by particles. Some spherical cavities were also seen in all the EVAL samples, including the neat polymer. However, they are attributed to volatilisation of residual water during the moulding process.

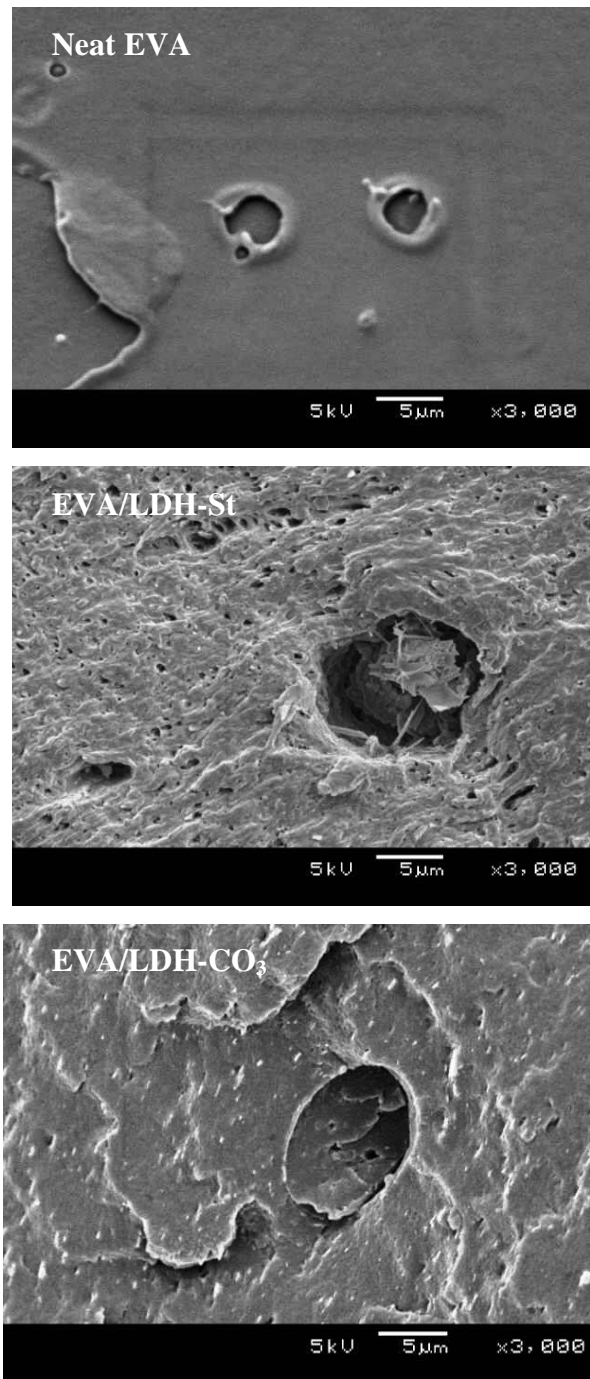


Figure 3.8. Freeze-fractured surface of neat EVA, EVA/LDH-St and EVA/LDH-CO₃. The latter two samples contained 10 wt.% filler.

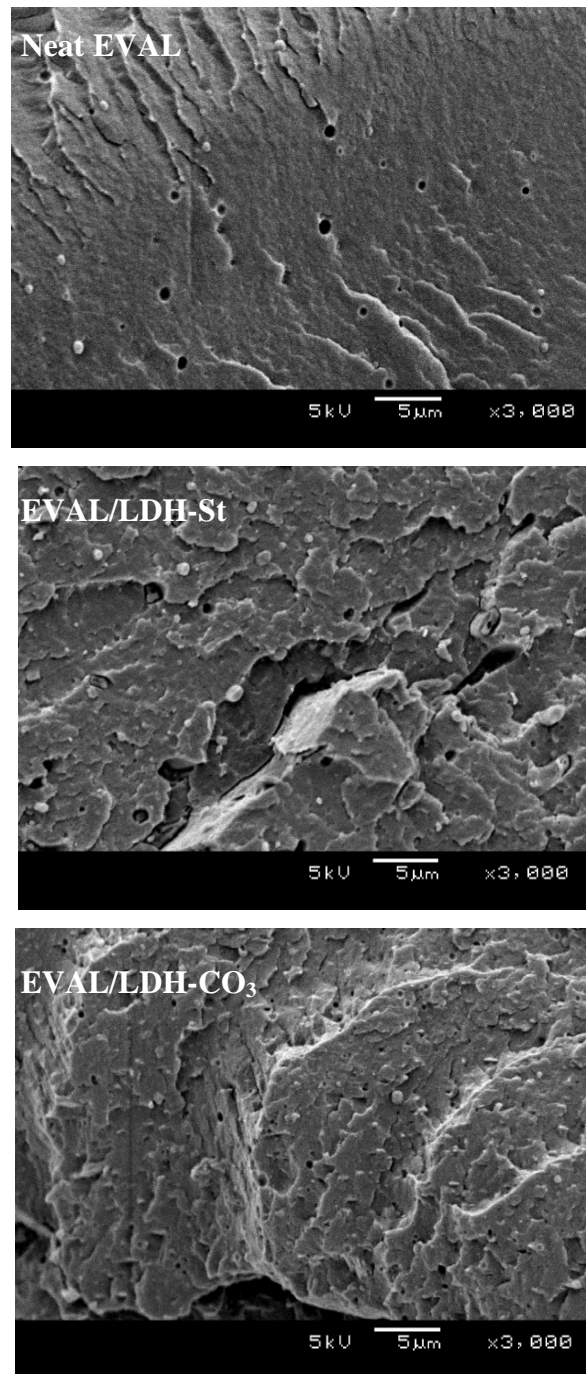


Figure 3.9. Freeze-fractured surface of neat EVAL, EVAL/LDH-St and EVAL/LDH-CO₃. The latter two samples contained 10 wt.% filler.

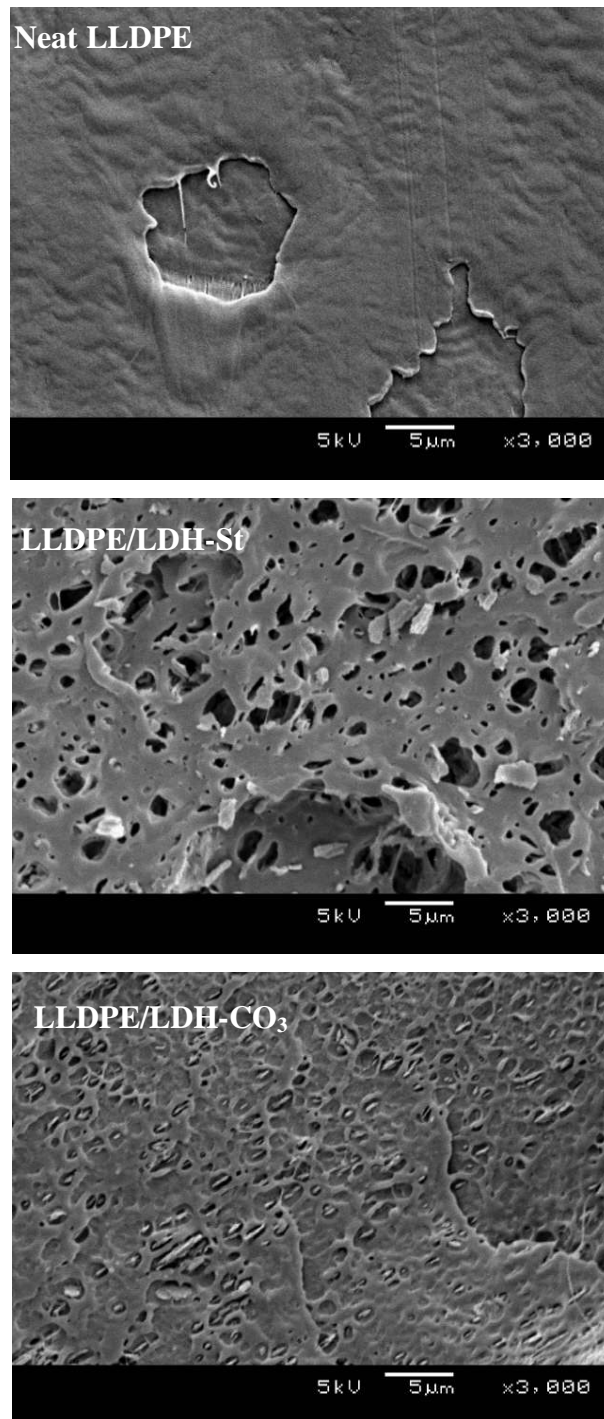


Figure 3.10. Freeze-fractured surface of neat LLDPE, LLDPE/LDH-St and LLDPE LDH-CO₃. The latter two samples contained 10 wt.% filler.

3.6.1 X-ray diffraction

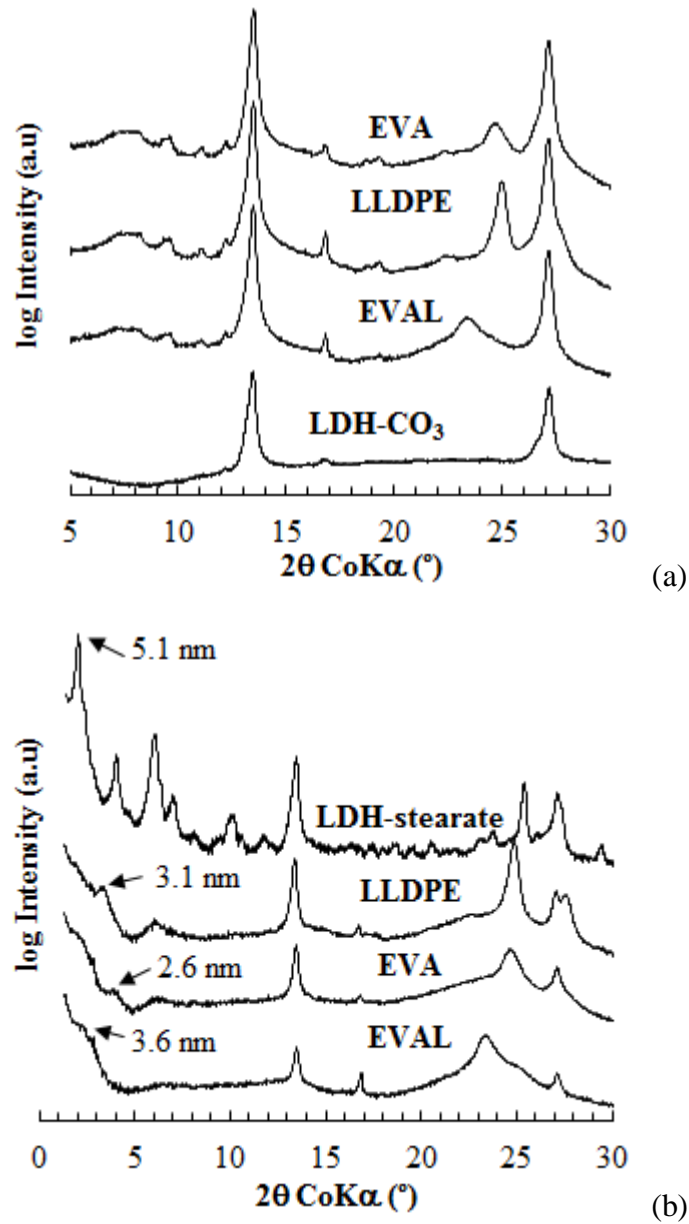


Figure 3.11. XRD diffractograms (WAXS) of the pristine, modified LDH and the 10 wt.% polymer composites indicating the relevant basal spacing

The degree of clay layer separation in the modified LDHs and the clay dispersion in the polymer composite was studied by X-ray diffraction (XRD) (Figure 3.11). The 2θ values of 13.5 and 27.2 °, which are typical for LDH-CO₃, indicate a d-spacing (d_l) of 0.76 nm. These reflections were also observed in the LDH-stearate, indicating LDH-CO₃ as an impurity phase. They were also noted in all the LDH-CO₃ and LDH-stearate polymer

composites, indicating that either this clay phase was retained during melt compounding or more of it was generated by decomposition of the LDH-stearate. The diffractogram for LDH-stearate showed three basal reflections positioned at 2.0° , 4.1° and 6.1° , the 2θ value corresponding to a d-spacing of 5.1 nm. This is consistent with bilayer intercalation of stearate moieties beyond the anion-exchange capacity of the clay (Nhlapo *et al.*, 2008). These diffractions were absent in the diffractograms of the LDH-stearate composites. The first reflection observed at high 2θ values indicated a reduction in the d-spacing of the LDH-stearate in the EVA and LLDPE composites (Figure 3.11b). The interlayer spacing of 3.1 nm determined for the LLDPE composite is consistent with monolayer-intercalated stearic acid (Xu & Braterman, 2010; Braterman *et al.*, 2004). This collapse in the d-spacing implies that the neutral stearic acid molecules, initially present in the interlayer beyond the AEC, were removed during the melt compounding process. As discussed in the Section 3.1, this was expected in view of the results obtained by Nhlapo *et al.* (2008). A collapse was also observed in the d-spacing value for the clay in the EVA composite. However, here the d-spacing was lower and this could be due to a less ordered arrangement of the intercalated chains and/or the loss of the interlayer water. Vestiges of the LDH-stearate reflections were seen in the EVAL composite. Finally, reflections typical for LDH- CO_3 were present in all composite diffractograms. This is attributed to the impurity of the LDH-stearate but it is possible that some could have formed by decomposition of the LDH-stearate during melt processing of the polymer composite. In summary, the XRD data indicated that the LDH-based polymer composites contained two types of filler particle (LDH- CO_3 and monolayer stearate-intercalated LDH) dispersed within the polymer matrices. Furthermore, no evidence for co-intercalation of polymer chains was found.

The neat polymer samples had basal reflections at 2θ values of 23.4° , 24.7° and 25.0° for EVAL, EVA and LLDPE respectively. In the composites these peaks appear to be broader and of reduced intensity. This indicates that the incorporation of LDHs increased the disorder in the packing of polymer chains during crystallisation. Eckel and Blaogh (2004) observed similar behaviour in their clay-based polymer nanocomposites, indicating that there was increased disorder in the polymer matrix.

However, as discussed in the literature review (Section 3.2), XRD analysis alone is insufficient for the assessment of the degree of dispersion in the polymer composite. TEM is used as a visual confirmation of the results obtained from XRD.

3.6.2 Transmission electron microscopy (TEM)

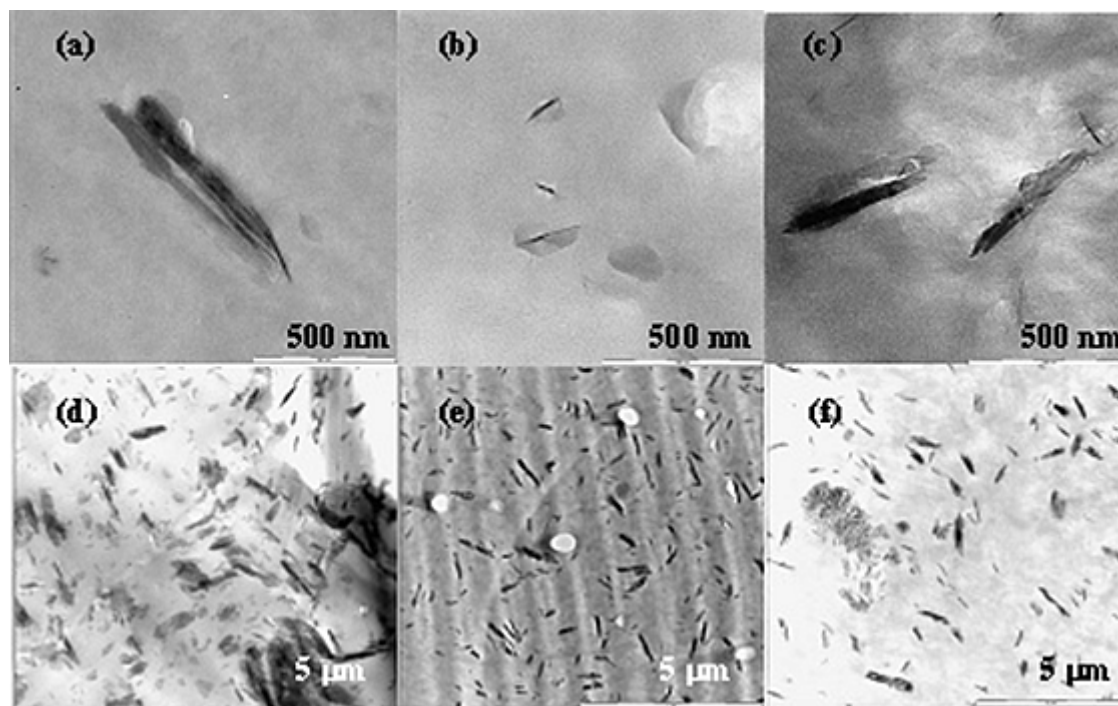


Figure 3.12. TEM images of the 10 wt.% polymer/LDH composites of (a) EVA/ LDH-St; (b) EVAL/LDH-St; (c) LLDPE/LDH-St; (d) EVA/LDH-CO₃; (e) EVAL/LDH-CO₃ and (f) LLDPE/ LDH-CO₃

The LDH-CO₃ composites featured distinct particles in the sub-micrometre range, but also some particle agglomerates (Figure 3.12 and 3.13). In the LDH-stearate composites the filler particles were much smaller, whereas in powder form they featured much larger platelets ranging up to 10 μm. They appeared as planar tactoids with a length up to about 500 nm, but with a thickness of less than 100 nm (Figure 3.12). This considerable reduction in dimensions has two possible origins. LDH platelets are weaker and less rigid than smectite clays and hence more prone to breakage. Each LDH sheet is composed of three atomic layers, whereas layered silicates have 6 to 7 atomic layers; hence LDHs tend to rupture under the shear action during extrusion (Solin *et al.*, 1995). Apart from such breakage, partial delamination may have occurred during the high-shear compounding process. The EVA and LLDPE matrices of the LDH-stearate composites appeared to contain very few tactoids. In summary, the TEM results showed that a combination of microcomposites and nanocomposites were obtained using LDH-CO₃ and LDH-stearate as fillers in the polymer matrices considered.

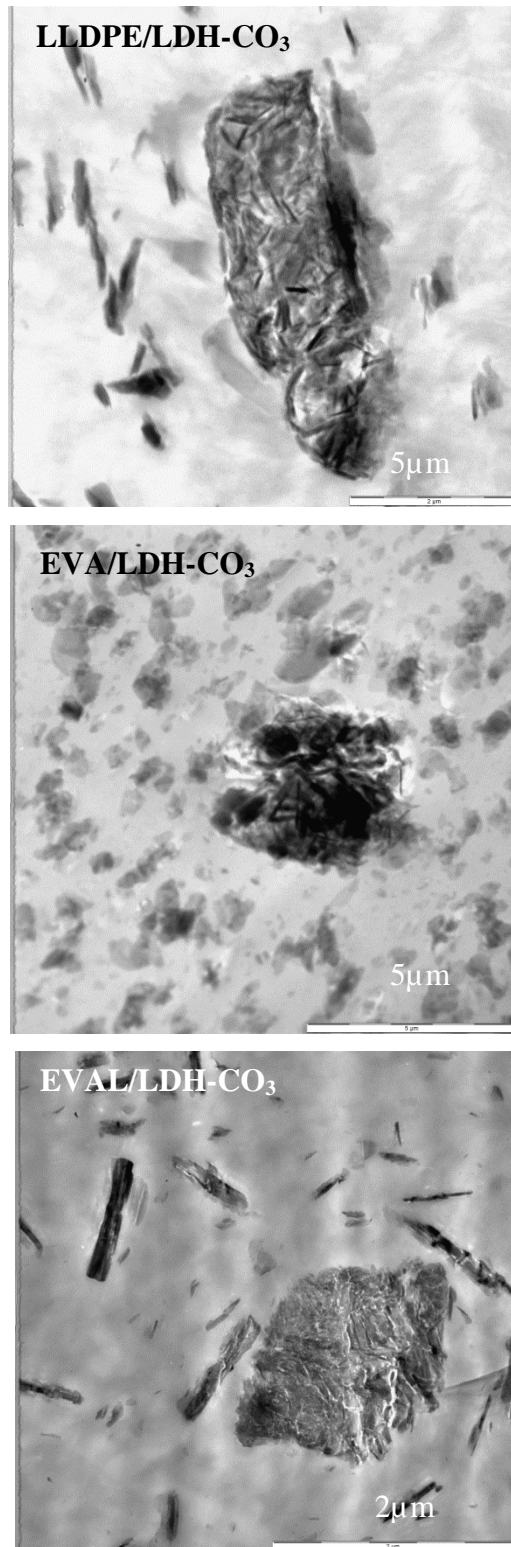


Figure 3.13. Agglomeration observed in the different matrices in SEM micrographs

The matrices of LDH-CO₃ were characterised by the existence of agglomerates/tactoids as those are shown in all the 10wt.% composites (Figure 3.13). One factor in favour of this observation is the differences in polarity between the polymer and the LDH. LDHs contain hydroxyl groups that render them polar and hence they are more compatible with polar polymer matrices, e.g. EVAL. The LDH-CO₃/EVAL composite appears to have agglomerated LDH platelets; this could be due to the high charge density which exists within the layer, hence not permitting effective dispersion/exfoliation (Adachi-Pagano *et al.*, 2000; Leroux *et al.*, 2001; Hibino & Jones, 2001). Another contributing factor is the particle-particle interactions; these are usually strong as a result of the interaction of hydroxyl groups. These interactions can either be face-to-edge ('house-of-cards' structure) or edge-to-edge. Gursky *et al.* (2006) attributed the former arrangement to lack of coordination in microscale LDH particles. A greater effect is experienced at the edges, ultimately influencing edge-to-surface interactions (see Figure 3.14).

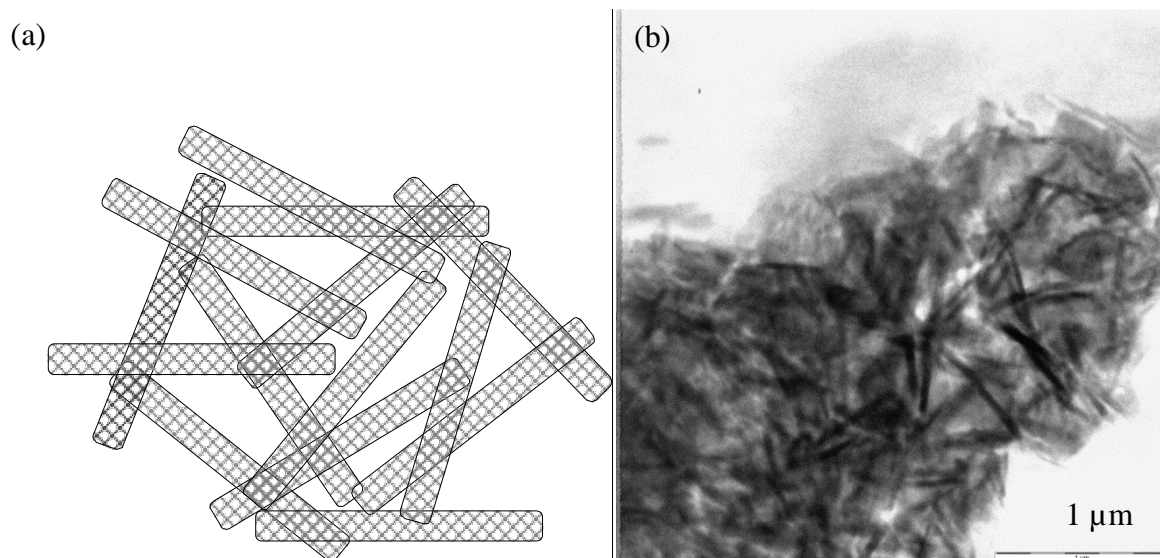


Figure 3.14. Schematic of the 'house-of-cards' structure: (a) LLDPE/LDH-CO₃ showing an agglomerate with face-to-edge interactions and (b) with edge-to-edge interactions

3.6.3 Melt viscosity

It is worth noting that the results obtained are for the polymers and composites prepared without processing aids or other additives.

Figure 3.15 presents the melt viscosity results for the composites obtained at 190 °C. All the samples showed strong shear-thinning behaviour. The EVA and EVAL polymer/LDH-CO₃ composites featured higher apparent viscosity values than the parent polymers. The melt viscosity of the LLDPE/LDH-CO₃ composite was marginally higher than that of the neat polymer. This is attributed to weak interactions between the polar filler surface and the non-polar matrix. The unmodified LDH is hydrophilic owing to the external hydroxyl groups. This results in platelet interactions such as edge-to-face or ‘house of cards’ arrangement, which is clearly demonstrated in Figure 3.14. This microstructure leads to high viscosities at low shear and is possibly responsible for the high viscosities observed in the LDH-CO₃ polymer composites. As the shear rates increase, the platelet aggregation breaks down and the platelets align themselves to the direction of flow, hence recording a low viscosity or one close to that of the neat polymer. The apparent melt viscosities of the EVA and the LLDPE polymer/LDH-stearate composites were lower than that of the neat polymers. This is attributed to the lubricating effect of the exuded stearic acid present in these compounds.

The EVAL/LDH-stearate composite had the highest melt viscosity. This means that the interaction of the filler with the polymer chains must have overwhelmed the lubricating effect of the free stearic acid present. The surfaces of the LDH-stearate filler are partially covered with the chains of the electrostatically attached stearate anions. So it is expected that the interaction of these clay surfaces with the EVAL chains would be weaker than the interactions with the uncoated surfaces of the LDH-CO₃ particles. However, the melt viscosity of the LDH-CO₃ composite was lower, despite its higher surface polarity. Furthermore, according to the TG results, the inorganic content of the LDH-stearate is only 20 wt.%. Taking this into consideration, these observations suggest that the clay surface area available for interaction with the polymer chains must have been much higher for LDH-stearate.

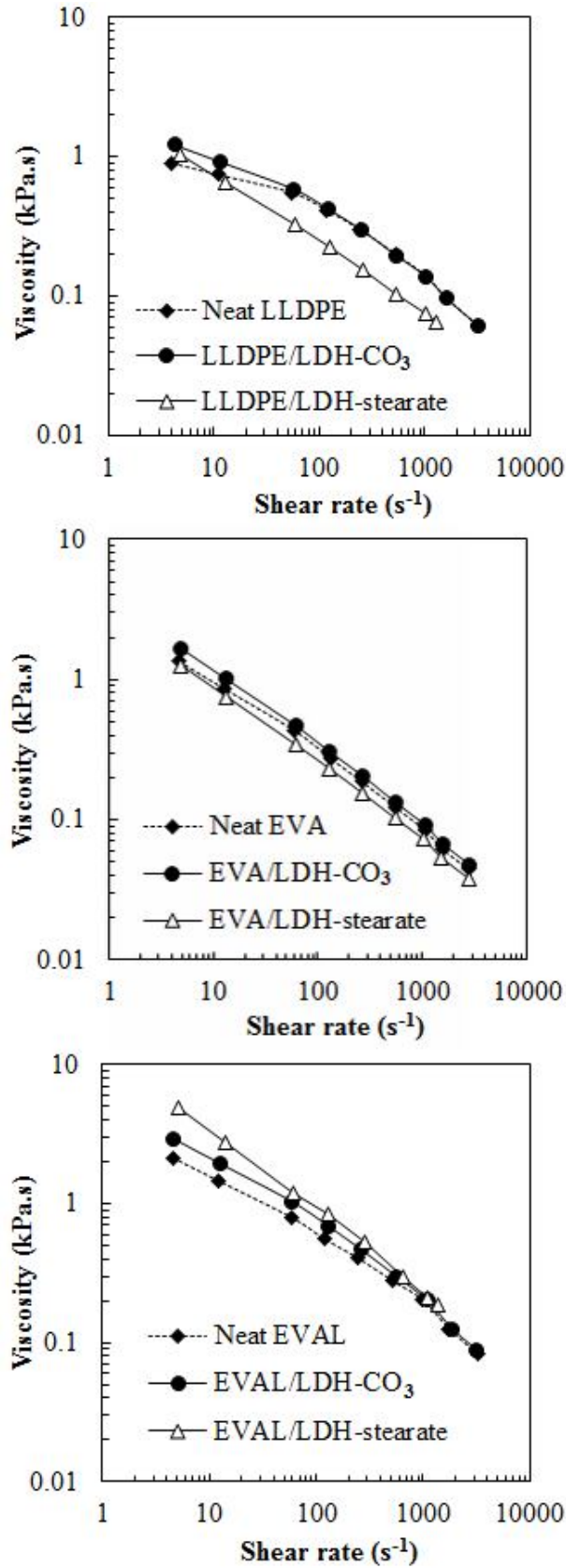


Figure 3.15. Effect of LDH incorporation on the viscosity of the polymers LLDPE, EVA and EVAL at 190 °C

3.6.4 Viscoelastic properties

Figures 3.16 to 3.18 present the DMA viscoelastic properties of the 10 wt.% composites. Results for the 5 wt.% composite may be found in Appendix C. The storage moduli (E') of all the LLDPE (Figure 3.16), EVA (Figure 3.17) and EVAL composites (Figure 3.18) were slightly higher than that those of the neat polymer. This stiffening effect was more pronounced in the rubbery region than in the glassy region for both the EVA and EVAL composites. However, at higher temperatures the LLDPE/LDH-stearate deviated from the LDH- CO_3 composite trend and approached the behaviour of the neat polymer. This could be explained by the melting of the free stearic acid present and it acting like a plasticiser and lubricant, which facilitates the motion of the polymer chains.

The glass transition temperature (T_g) of the EVA composites was the same as that of the neat polymer. However, the T_g of the EVAL composites shifted to higher temperatures. There are two possible explanations for this observation. The exuded stearic acid might have had an anti-plasticisation effect or the mobility of the EVAL polymer chains might have been affected by strong interactions with the surface of the filler particles. Clearly, only the latter explanation can hold for the LDH- CO_3 composite as no stearic acid was present. Based on the viscosity behaviour of the EVAL/LDH-stearate composite, it can be concluded that this explanation also holds for this system.

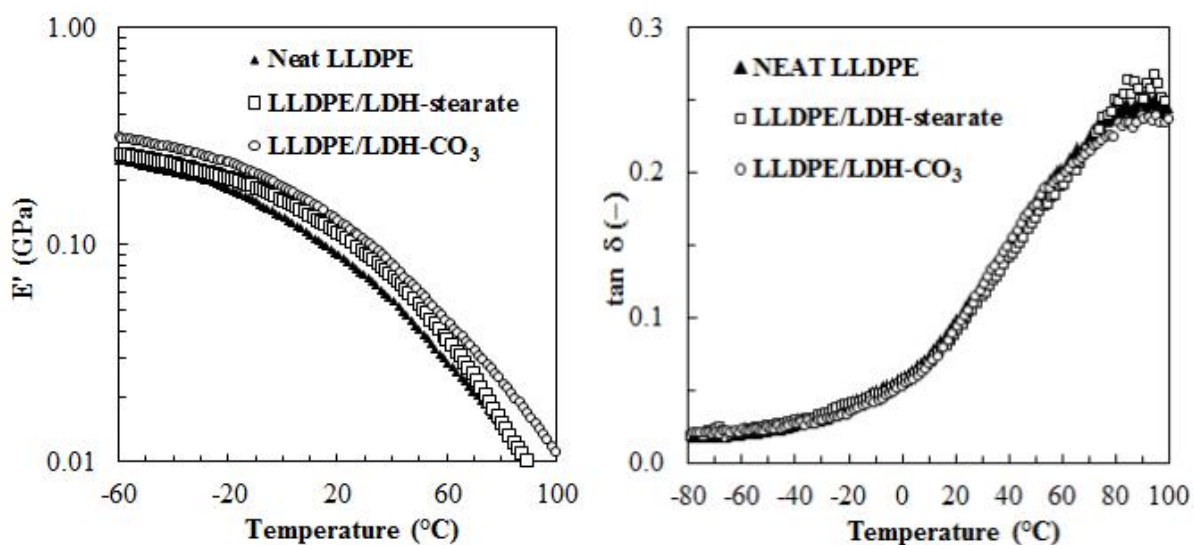


Figure 3.16. DMA data for the storage modulus and $\tan \delta$ of LLDPE and its 10 wt.% derivative composites

The storage modulus for the LLDPE composites (Figure 3.16) was higher than that of the neat polymer within both the glassy and rubbery regions. However, as the temperature increased, the LLDPE/LDH-St deviated from the LDH-CO₃ composite, conforming to a behaviour similar to that of the neat polymer. This could be explained by the probable melting of excess stearic acid, which in turn acts as a plasticiser and lubricant. This facilitates the motion of polymer chains. The damping factor ($\tan \delta$) remained unchanged, signifying poor interfacial adhesion between the fillers and the polymer matrix. A similar trend is observed with the EVA composites, where the storage modulus is higher than that of the neat polymer in both regions.

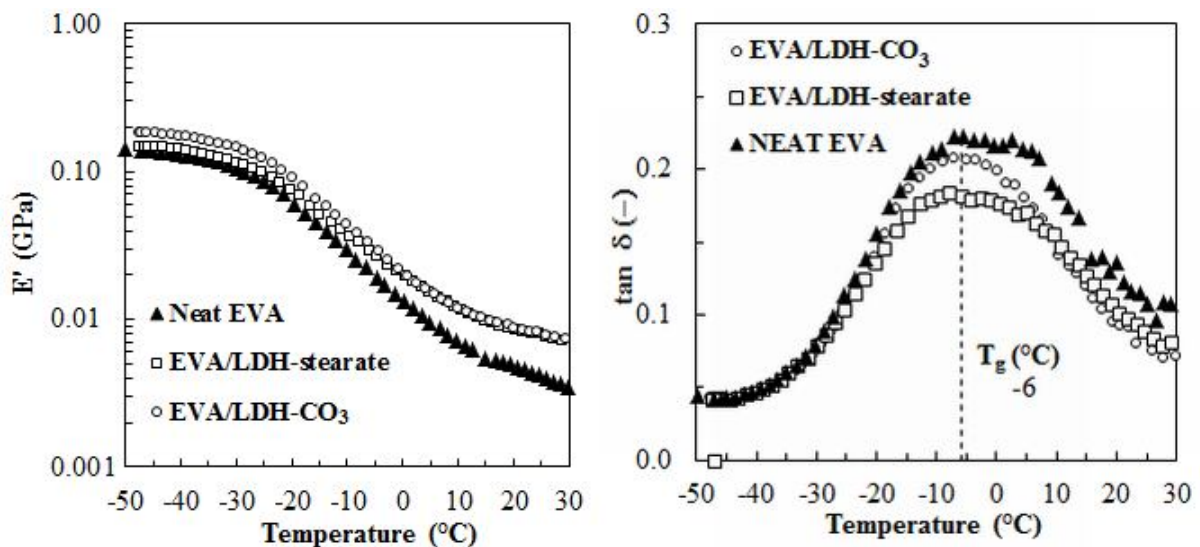


Figure 3.17. DMA data for the storage modulus and $\tan \delta$ of EVA and its 10 wt.% derivative composites

The storage modulus (E') of the EVA composite matrices (Figure 3.17) was slightly higher than that of the neat polymer in the glassy region. However, in the rubbery region the storage modulus is distinctly higher, indicating that the incorporation of the filler yields a stiffer material. The T_g of the composites was the same as for the neat polymer. This implies that the inclusion of LDHs within its matrix did not interfere with the molecular motion of the polymer chains. It also points to minimal interaction between the filler and the polymer. However, the EVA/LDH-St composite showed a reduction in the maximum $\tan \delta$ value, implying that the modification of the LDH with stearate anions improves interaction between the filler and the polymer.

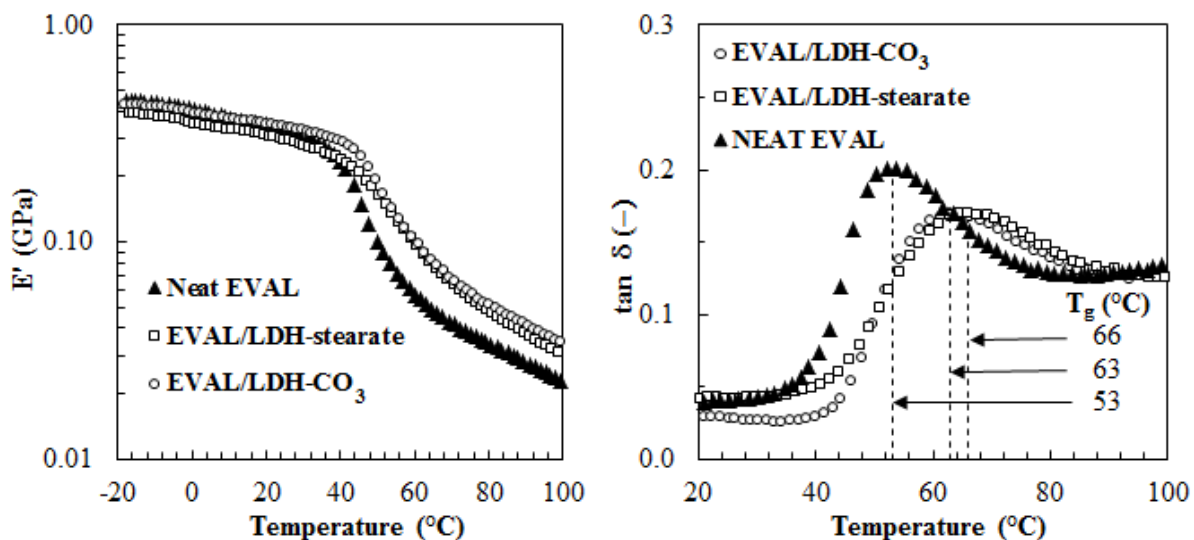


Figure 3.18. DMA data for the storage modulus and $\tan \delta$ of EVAL and its 10 wt.% derivative composites

The storage modulus for the EVAL/LDH-St composite (Figure 3.18) was slightly lower than that of LDH- CO_3 , which is attributed to the plasticising effect of the free stearic acid. The EVAL composites appear to have strong interfacial adhesion between the filler and the polymer, resulting from the probable formation of hydrogen bonds between the EVAL side groups and the LDH hydroxyl. This is demonstrated by restricted segmental motion, which leads to a positive shift and broadening of the $\tan \delta$ peak. It is also accompanied by a decrease in the $\tan \delta_{\max}$ value. The T_g of the LDH-St composite is higher than that of the LDH- CO_3 due to the probable interaction of LDH hydroxyl groups and stearate anions with the polymer matrix.

3.6.5 Mechanical properties

The mechanical properties are listed in Table 3.5 and Appendix C. All the filled samples, except for the EVAL/LDH-St composite, featured higher tensile moduli than the neat polymers. Both LDHs fillers had a reinforcing effect on EVA and LLDPE as both the yield strength and the modulus increased. Enhanced elongations were obtained in the EVA composites, but a decrease was observed for the EVAL and LLDPE composites. The LLDPE/LDH-St 5 wt.% featured an outstanding increase in tenacity.

Table 3.5. Summary of the mechanical properties of LDH/polymer composites

Polymer composite	Young's modulus/ (MPa)	Yield strength (MPa)	Elongation at break (%)	Charpy impact strength/ (kJ/m ²)	Tensile impact strength/ (kJ/m ²)
EVA					
Neat EVA	27 ± 2	10 ± 0.4	277 ± 30	No break	3.8 ± 0.1
EVA / 5% LDH-St	34 ± 3	11 ± 0.1	330 ± 12	-	4.6 ± 0.3
EVA / 10%LDH-St	40 ± 5	12 ± 0.1	422 ± 23	No break	4.3 ± 0.2
EVA / 5% LDH-CO ₃	30 ± 1	10 ± 0.1	305 ± 12	-	3.4 ± 0.1
EVA/10% LDH-CO ₃	37 ± 2	13 ± 1	424 ± 60	No break	5.2 ± 0.1
LLDPE					
Neat LLDPE	171 ± 14	16 ± 0.1	509 ± 29	22 ± 2	1.7 ± 0.1
LLDPE / 5%LDH-St	192 ± 6	24 ± 3	1097 ± 14	-	1.1 ± 0.1
LLDPE / 10%LDH-St	196 ± 7	17 ± 0.4	495 ± 43	12 ± 1	1.2 ± 0.1
LLDPE / 5%LDH-CO ₃	219 ± 43	17 ± 0.2	477 ± 13	-	1
LLDPE/10%LDH-CO ₃	213 ± 12	17 ± 0.2	460 ± 21	11 ± 1	0.8 ± 0.1
EVAL					
Neat EVAL	843 ± 16	64 ± 2	41 ± 21	4.9 ± 1	2 ± 0.3
EVAL / 5%LDH-St	869 ± 23	71 ± 0.2	42 ± 4	-	1.8 ± 0.3
EVAL / 10%LDH-St	718 ± 40	59 ± 6	18 ± 5	9.7 ± 3	0.8 ± 0.3
EVAL / 5% LDH-CO ₃	969 ± 22	77 ± 1	31 ± 1	-	0.8 ± 0.3
EVAL / 10%LDH-CO ₃	1025 ± 18	76 ± 0.4	37 ± 2	4.6 ± 1	0.7 ± 0.3

Polymer toughness is governed by parameters such as the degree of particle dispersion within the polymer matrix, filler mobility, delamination and intrinsic changes to polymer properties promoted by the filler (Chen *et al.*, 2008). The EVA composites did not fracture in the notched Charpy tests because of the rubbery nature of the matrix. The tests were basically carried out at room temperature, so well above the T_g of this polymer matrix; in this case the mobility of the polymer chains is higher. This aspect facilitates the mobility of the LDHs to form temporary bonds which in turn dissipate energy. Hence the clay platelets are able to rotate and align themselves in the direction of the applied stress. During the matrix deformation process, the filler is squeezed tight by the cavity walls as it elongates and narrows. The resulting friction forces generate a region of enhanced strength which

retards the growth of the cavity and thus delays polymer failure (Gersappe, 2002). The tensile impact properties of the filled EVA composites were better than those of the neat polymer. However, the opposite was true for the other polymer matrices. In the tensile strength impact tests the LDH-CO₃ filler gave better results than the LDH-St (see Table 3.5). Considering Figure 3.8, this can be attributed to better interfacial adhesion between the polar filler and the polar EVA matrix.

With the exception of the 10 wt.% EVAL/LDH-St composite, all the other composite samples had poor notched Charpy impact properties compared with the parent polymers. Development of strong energy dissipation mechanisms is a prerequisite for good impact properties. The poor interface adhesion between both the fillers and the polyethylene matrix is evident in Figure 3.10. This means that the incorporation of the fillers led to the creation of internal flaws. These acted as stress concentrators which led to premature mechanical failure. The LLDPE/LDH-St composite had slightly better impact strength properties than the LLDPE/LDH-CO₃. This can be attributed to the slightly better compatibility with the polymer matrix contributed by the exuded stearic acid coating on the LDH particles (Figure 3.10). However, it is clear from the XRD diffractogram (Figure 3.11) that the presence of this filler also affected the morphology of the parent polymer. This is confirmed by the broadening and shift in position of the main reflections attributable to the polymer matrix. This change in the morphology of the polymer matrix could also have affected the impact properties.

Unexpectedly, the notched Charpy impact strength of EVAL increased from 4.9 kJ m⁻² to 9.7 kJ m⁻² when 10 wt.% LDH-stearate was added (Table 3.5). Top-view SEM imaging of the fracture surfaces was inconclusive. The images did not reveal a mechanism that could explain the improved impact behaviour. Figure 3.19 shows side-view images of the fracture surfaces of Charpy impact specimens obtained for the EVAL composites using an optical microscope. The neat EVAL sample and EVAL/LDH-CO₃ composite sample showed clean fractures. In contrast, the EVAL/LDH-St sample showed an extensive stress-whitened damage region which extended deep into the sample. It seems that the clay particles transmitted an incoming crack as multiple crack fronts travelling in different directions. This dissipates mechanical energy by creating numerous internal cracks with a very large total surface area. This ability of the LDH-stearate might derive from its sheet-like nature and random orientation in the glassy matrix. It is noteworthy that the stress-whitened

damage region was located in a narrow region towards the back of the sample. Extensive stress whitening is usually an indication of crazing and/or microfibril formation. The white appearance of the crazed region is due to light scattering.

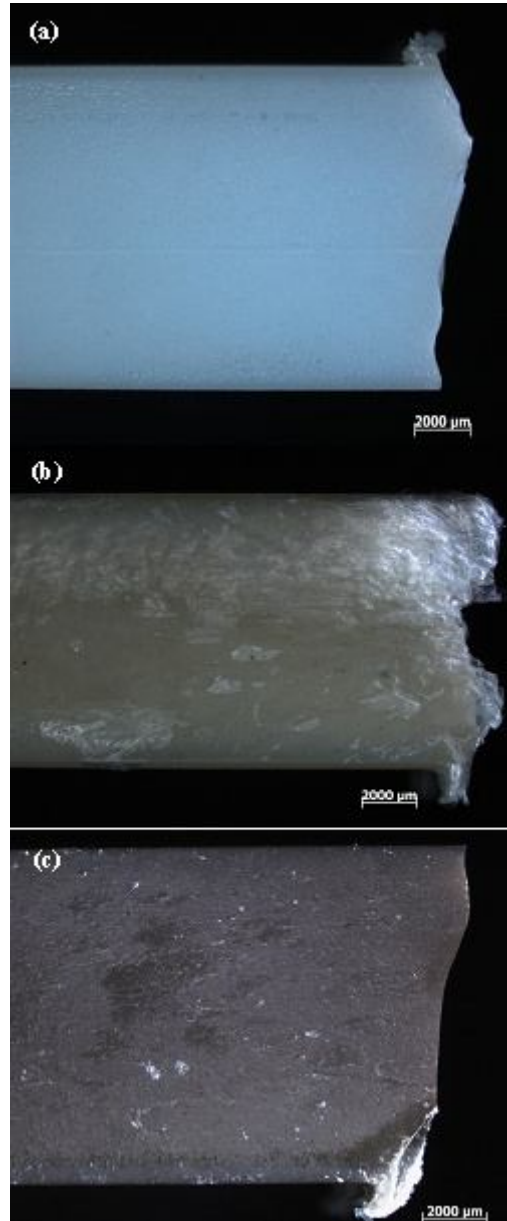


Figure 3.19. Optical light microscope side-views of Charpy impact test specimen of EVAL: (a) neat, (b) LDH-stearate composite and (c) LDH-CO₃ 10 wt.% composite

However, for the tensile impact specimen there is a clear indication of debonding and the matrix has areas of extensive fibrillation (see Figure 3.20). More views are shown in Appendix C.

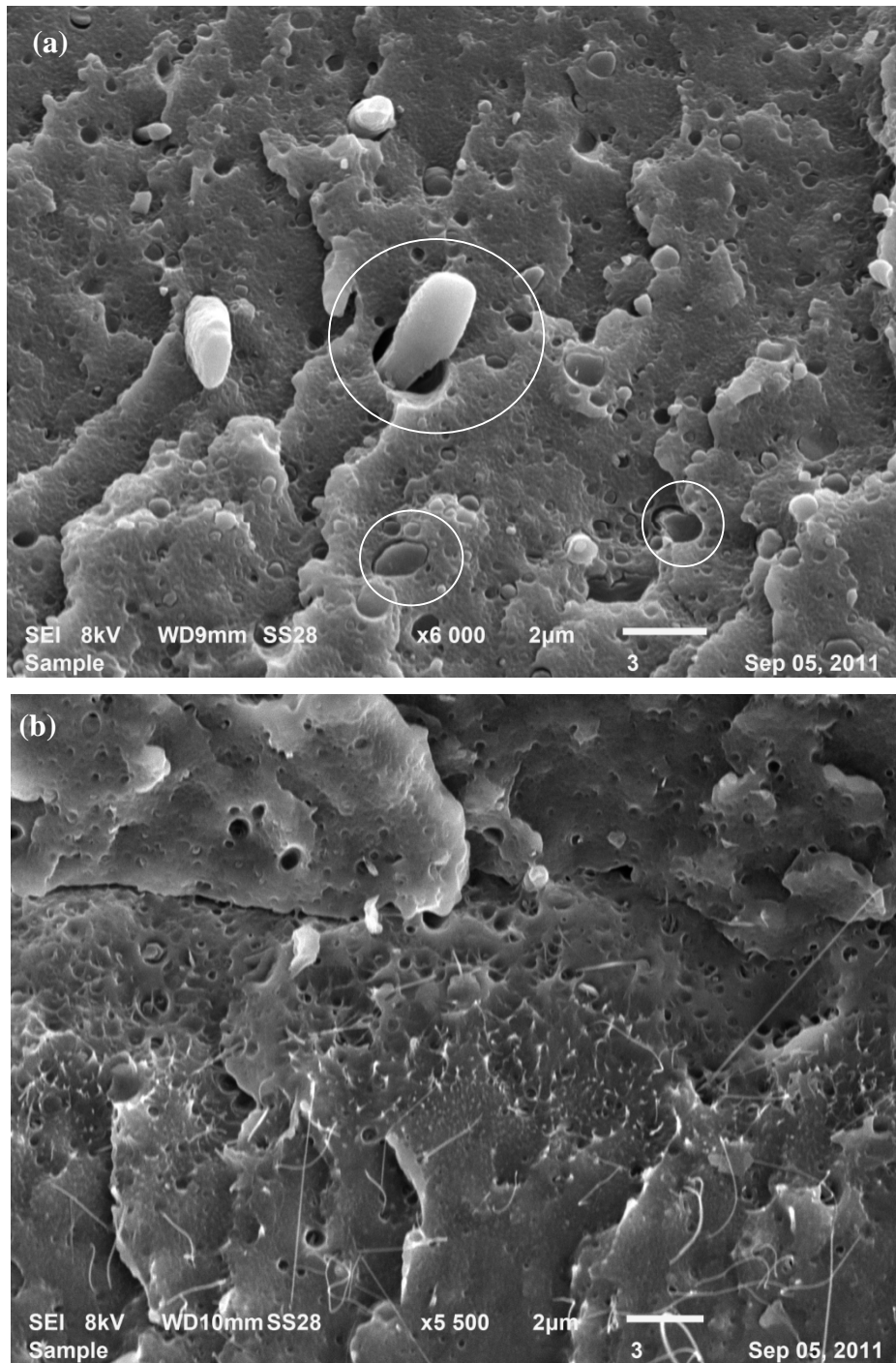


Figure 3.20. Top view of the EVAL/LDH-St tensile impact test specimen showing: (a) debonding and (b) fibrillation

3.6.6 Thermal analysis

The thermal data are summarised in Table 3.6, comparing the temperature changes at 10 and 50% weight loss between the neat polymers and composite samples, i.e. $T_{0.1}$ and $T_{0.5}$ respectively. The addition of LDHs within the different polymer matrices improves the thermal stability at $T_{0.1}$ and $T_{0.5}$, with an increase in the char residue levels in all composite samples. The thermal degradation temperature for the EVA and LLDPE composites was 2-16 °C above that of the neat polymers. However, the improvement was less for the EVA when compared with the LLDPE matrix. EVA and its composites undergo two main thermal events, the first occurring between 220 and 405 °C due to deacetylation with the release of gaseous acetic acid, and the final event as a result of main chain scission (between 410 and 510 °C) associated with polyolefinic groups (Camino *et al.*, 2000; Riva, 2002; Peeterbroeck *et al.*, 2005; Jiao *et al.*, 2006).

Table 3.6. Thermal stability data at $T_{0.1}$, $T_{0.5}$, % residue and change in temperature (ΔT), results pertaining to 10 wt.% composites

Sample	$T_{0.1}$ (°C)	$T_{0.5}$ (°C)	Residue (%)	$\Delta T_{0.1}$ (°C)	$\Delta T_{0.5}$ (°C)
Neat EVA	350	438	0		
EVA/LDH-St	349	447	1.4	-1	9
EVA/LDH-CO ₃	353	440	6.0	3	2
Neat EVAL	370	406	0		
EVAL/LDH-St	291	309	1.5	-79	-97
EVAL/LDH-CO ₃	296	315	5.4	-74	-91
Neat LLDPE	387	426	0		
LLDPE/LDH-St	381	441	2.0	-6	15
LLDPE/LDH-CO ₃	403	442	5.8	16	16

In the EVAL samples the first event occurs at about 358 °C and the same applies for all the composite samples (see Figure C-16 in Appendix C). The second event is shifted to a higher temperature, from 440 °C to 443 and 453 °C for the EVA/LDH-St and LDH-CO₃ composites respectively. The EVA/LDH-CO₃ composite showed greater thermal stability at $T_{0.5}$ than the neat polymer. A marked difference is observed in the EVAL composites where

the temperature difference between the onset decomposition temperatures, $T_{0.1}$ and $T_{0.5}$, is a magnitude of 88–115 °C lower than that of the neat polymer. This could be explained by the formation of metal oxides and/or radical species that catalyse the thermal degradation of the polymer; hence a significant difference is observed. In addition, it may be explained as a result of thermo-oxidative degradation of the polymer. In the thermogram (Figure 3.21), one can clearly observe the shift at which thermal degradation occurs for the EVAL composites.

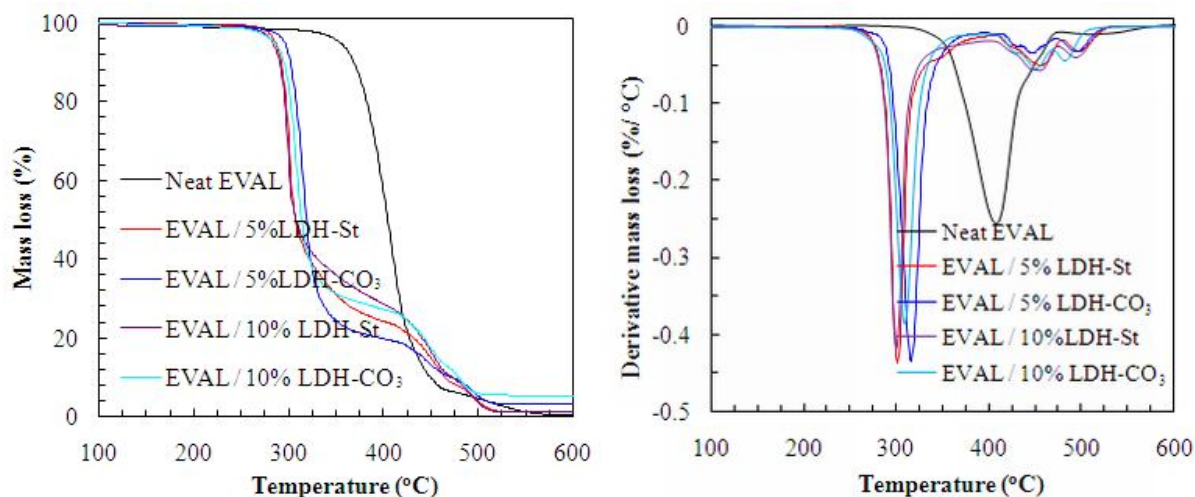


Figure 3.21. TG data for EVAL and derivative composites

3.6.6.1 Differential scanning calorimetry

Differential scanning calorimetry (DSC) was employed to study thermal transitions and follow the changes in enthalpies in the composites (see Table 3.7). The data discussed pertain to those obtained from the second heating and first cooling. There is a general increase in the melting temperature in the filled polymers. The same trend is observed in the crystallisation temperature in Figure 3.22, with the exception of the EVAL composite for which a distinct difference is observed. An increase in the crystallisation temperature of the composites of EVA and LLDPE is an indication of the nucleating effect of the LDH incorporation. However, the enthalpy of the melting endotherms of the polymer composites decreases; this is a result of a decrease in crystallinity or a change in the ordering of the polymer chains induced by the filler materials (Ramaraj & Yoon, 2008). It is established that fillers can affect the crystallinity of some polymers, and consequently affect their mechanical properties. An inverse correlation was obtained between the nucleating ability of fillers and loss of impact strength in the filled systems (Hutley & Darlington, 1985). The

same correlation is observed in the LLDPE composites where the crystallisation temperature increases. However, the impact strength reduces by a magnitude of almost 50%, as seen in Tables 3.5 and 3.7.

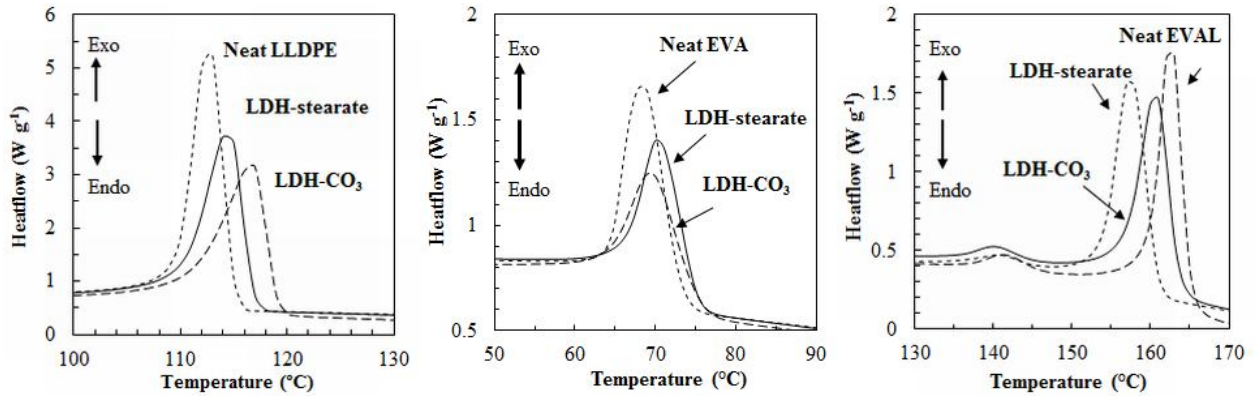


Figure 3.22. DSC cooling traces of each of the 10 wt.% polymer composite systems

To further study the nucleating effect of LDH in the LLDPE matrix, POM analyses were carried out (see Figure 3.23). The samples show a reduction in the grain size of crystallites in the composites. This is attributed to the availability of numerous nuclei (LDH particles) in the composite, resulting in very small crystallites. Though the LLDPE/LDH-CO₃ sample generally exhibits a reduced crystallite size, there are areas with large crystals which are indicated by arrows in Figure 3.23. Such big crystallites may act as stress concentrators, leading to premature fracture.



Figure 3.23. POM images of neat LLDPE and derivative composites (scale bar is 40 μm)

The same fillers retarded the crystallisation of the EVAL (Figure 3.22). This is attributed to a strong interaction of the EVAL polymer chains with well-dispersed clay platelets and the higher melt viscosity which suppresses the diffusion processes required for the chains to orient and pack into crystallites.

Table 3.7. DSC data indicating the onset temperature and melting endotherm of the 10 wt.% polymer composites

	Onset melting temperature (°C)	Melting temperature, T_m (°C)	Melting endotherm (J/g)	Onset of crystallisation (°C)	Crystallisation temperature T_c (°C)	Crystallisation exotherm (J/g)
Neat EVA	60	85	55	75	70	55
EVA/LDH-St	60	85	42	76	71	46
EVA/LDH-CO ₃	64	85	60	74	70	63
Neat EVAL	176	182	55	164	162	47
EVAL /LDH-St	175	183	48	161	157	46
EVAL /LDH-CO ₃	175	181	45	163	161	46
Neat LLDPE	121	126	76	117	115	61
LLDPE/LDH-St	121	127	68	118	116	63
LLDPE /LDH-CO ₃	120	128	67	119	117	61

3.7 CONCLUSION

Anionic clay/polymer composites were prepared by melt compounding two different LDH fillers into polyethylene random copolymers. In order of increasing polarity, the latter were 1-hexene-based LLDPE, EVA and EVAL. A standard carbonate form (LDH-CO₃) and a stearate-modified LDH (LDH-St) were used as fillers. The latter comprised a bilayer-intercalated form containing ca. 50% more stearic acid than expected from the anionic exchange capacity of the parent clay. The composite materials were characterised by XRD, SEM, TEM, TGA, DSC, DMA and capillary rheology. Mechanical testing in tensile mode and Charpy impact tests were also conducted.

During melt compounding of the LDH-stearate composites, the excess stearic acid in the clay was released and the clay reverted to a monolayer-intercalated form. This conclusion is supported by XRD data and the reduction in melt viscosity observed for the LLDPE and EVA polymer/LDH-stearate composites. The latter is caused by the lubrication effect of the free stearic acid present. The EVAL/LDH-stearate nanocomposite featured the highest melt viscosity. This suggests that the clay surface area available for interaction with the EVAL polymer chains must have been very high in the EVAL/LDH-stearate composite in order to overwhelm the lubrication effect. Such strong interaction in this system is supported by the increase in the glass transition temperature (T_g) observed by DMA.

XRD confirmed that the presence of LDH-stearate-based polymer composites contained two types of filler particle (LDH-CO₃ and monolayer stearate-intercalated LDH) dispersed within the polymer matrices. The TEM results showed that microcomposites and nanocomposites were obtained using LDH-CO₃ and LDH-St as fillers in the polymer matrices considered. SEM images of freeze-fractured surfaces indicated good interfacial adhesion between the clay and the matrix, not only in the EVAL composites, but also in the EVA/LDH-CO₃ composite.

DSC showed that the presence of the fillers interfered with the polymer crystallisation processes. Both fillers acted as nucleating agents in LLDPE and EVA. The degree of crystallinity of the EVA even improved, as shown by an increase in the enthalpy of crystallisation. The XRD results confirmed that the crystal morphology of the LLDPE was changed. Both fillers retarded the crystallisation of the EVAL. This is attributed to the strong

interaction of the EVAL polymer chains with the well-dispersed clay platelets and the higher melt viscosity, which suppresses the diffusion processes required for the chains to orient and pack into crystallites.

Both LDHs fillers had a reinforcing effect on EVA and LLDPE as both the yield strength and the modulus improved. Better elongations were obtained in the EVA composites, but a decrease was observed for the EVAL and LLDPE composites. Both fillers improved the tensile impact strength of EVA. Unexpectedly, the notched Charpy impact strength of EVAL increased significantly (from 4.9 to 9.7 kJ m⁻²) when 10 wt.% LDH-stearate was added. This is attributed to the ability of the highly dispersed and randomly oriented nanosized clay platelets to promote extensive internal microcavitation during impact loading. The creation of a large internal surface area provided the requisite energy-dissipation mechanism.

3.8 REFERENCES

- Abbasian, M. (2011). Exfoliated poly(styrene-co-methylstyrene) grafted polyaniline/layered double hydroxide nanocomposite synthesized by solvent blending method. *J. Appl. Polym. Sci.*, 122: 2573–2582.
- Acharya H, Srivastava, S. K, Bhowmick A. K. (2007). A solution blending route to ethylene propylene diene terpolymer / layered double hydroxide nanocomposites. *Nanoscale Res. Lett.*, 2:1-5.
- Adachi-Pagano, M., Forano, C. & Besse, J-P. (2000). Delamination of layered double hydroxides by use of surfactants. *Chem. Commun.*, 13: 91–92.
- Alexandre, M. & Dubois, P. (2000). Polymer-layered silicate nanocomposites: preparation, properties and uses of a new class of materials. *Mater. Sci. Eng., R.*, 28(1–2):1–63.
- Bocchini, S., Morlattherias, S., Gardette, J. & Camino, G. (2008). Influence of nanodispersed hydrotalcite on polypropylene photooxidation. *Eur. Polym. J.*, 44(11): 3473–3481.
- Braterman, P. S., Xu, Z. P. & Yarberry, F. (2004). In: Auerbach, S. M., Carrado, K. A. & Dutta, P. K. (Eds), *Handbook of Layered Materials*, Boca Raton: CSC Press, Taylor & Francis Group, pp 373–449.
- Camino, G., Maffezzoli, A., Braglia, M., De Lazzaro, M. & Zammarano, M. (2001). Effect of hydroxides and hydroxycarbonate structure on fire retardant effectiveness and mechanical properties in ethylene-vinyl acetate copolymer. *Polym. Degrad. Stab.*, 74(3): 457–464.
- Carrado, K.A. & Xu, L. (1999). Materials with controlled mesoporosity derived from synthetic polyvinylpyrrolidone-clay composites. *Microporous & Mesoporous Mater.*, 27: 87–94
- Challier, T. & Slade, R. C. T. (1994). Nanocomposite materials: Polyaniline-intercalated layered double hydroxides. *J. Mater. Chem.*, 4(3): 367–371.
- Chen, B. (2004). Polymer–clay nanocomposites: An overview with emphasis on interaction mechanisms. *Br. Ceram. Trans.*, 103(6): 241–249.
- Chen, B., Evans, J. R. G., Greenwell, H. C., Boulet, P., Coveney, P. V., Bowden, A. A & Whiting, A. (2008). A critical appraisal of polymer-clay nanocomposites. *Chem. Soc. Rev.*, 37(3): 568–94.

- Chen, G. (2007). Preparation of a poly(vinyl chloride)/layered double hydroxide nanocomposite with a reduced heavy-metal thermal stabilizer. *J. Appl. Polym. Sci.*, 106: 817–820.
- Chen, W. & Qu, B. (2003). Structural characteristics and thermal properties of synthesized by solution intercalation. *Chem. Mater.*, 15(14): 3208–3213.
- Chen, W. & Qu, B. (2004). LLDPE/ZnAl LDH-exfoliated nanocomposites: Effects of nanolayers on thermal and mechanical properties. *J. Mater. Chem.*, 1705–1710.
- Chiang, M.-F., Chu, M.-Z. & Wu, T.-M. (2011). Effect of layered double hydroxides on the thermal degradation behavior of biodegradable poly(l-lactide) nanocomposites. *Polym. Degrad. Stab.*, 96(1): 60–66.
- Cho, J. W. & Paul, D. R. (2001). Nylon 6 nanocomposites by melt compounding. *Polymer*, 42: 1083–1094.
- Coiai, S., Passaglia, E., Hermann, A., Augier, S., Pratelli, D. & Streller, R. C. (2010). The influence of the compatibilizer on the morphology and thermal properties of polypropylene-layered double hydroxide composites. *Polym. Compos.*, 1–11.
- Costa F. R., Saphiannikova M., Wagenknecht, U. & Heinrich, G. (2008) Layered double hydroxide based polymer nanocomposites. *Adv. Polym. Sci.*, 210: 101–168.
- Costa, F. R., Abdel-Goad, M., Wagenknecht, U. & Heinrich, G. (2005). Nanocomposites based on polyethylene and Mg-Al layered double hydroxide. Part I: Synthesis and characterization. *Polymer*, 46: 4447–4453.
- Costa, F. R., Wagenknecht, U. & Heinrich, G. (2007). LDPE/Mg–Al layered double hydroxide nanocomposite: Thermal and flammability properties. *Polym. Degrad. Stab.*, 92(10), 1813–1823.
- Costa, F. R., Wagenknecht, U., Jehnichen, D., Abdel-Goad, M. and Heinrich, G. (2006). Nanocomposites based on polyethylene and Mg-Al layered double hydroxide. Part II: rheological characterization. *Polymer*, 47: 1649–1660.
- Costache, M. & Wang, D. (2006). The thermal degradation of poly(methyl methacrylate) nanocomposites with montmorillonite, layered double hydroxides and carbon nanotubes. *Polym. Adv. Technol.*, 17: 272–280.

- Cui, W., Jiao, Q., Zhao, Y., Li, H., Liu, H. & Zhou, M. (2012). Preparation of poly (ethylene terephthalate)/ layered double hydroxide nanocomposites by in-situ polymerization and their thermal property. *Express Polym. Lett.*, 6(6): 485-493
- Du, L. & Qu, B. (2006). Structural characterization and thermal oxidation properties of LLDPE/MgAl-LDH nanocomposites. *J. Mater. Chem.*, 3: 1549–1554.
- Du, L., Qu, B. & Zhang, M. (2007). Thermal properties and combustion characterization of nylon 6/MgAl-LDH nanocomposites via organic modification and melt intercalation. *Polym. Degrad. Stab.*, 92(3): 497-502.
- Eckel, D. & Balogh, M. (2004). Assessing organo-clay dispersion in polymer nanocomposites. *J. Appl. Polym. Sci.*, 93: 1110–1117.
- Fischer, H. (2003). Polymer nanocomposites: From fundamental research to specific applications. *Mat. Sci. Eng. C.*, 23: 763–772.
- Focke, W. W., Nhlapo, N. S., Moyo, L. & Verryn, S. M. C. (2010). Thermal properties of lauric- and stearic acid intercalated layered double hydroxides. *Mol. Cryst. Liq. Cryst.*, 521(1): 168–178.
- Gao, F., Chen, S., Hull, J.B. (2001). Layer expansion of layered silicates in solid polymer matrices by compression. *J. Mater. Sci. Lett.* 20, 1807–1810.
- Gersappe, D. (2002). Molecular mechanisms of failure in polymer nanocomposites. *Phys. Rev. Lett.*, 89(5): 58301–5830.
- Gursky, J. A, Blough, S. D., Luna, C., Gomez, C., Luevano, A. N. & Gardner, E. A. (2006). Particle-particle interactions between layered double hydroxide nanoparticles. *J. Amer. Chem. Soc.*, 128(26): 8376–8377.
- Hancock, M. (1995). Particulate filled polymer composites, Chapter 8. In: Rotheron, R. N. (Ed.), *Particulate Filled Polymer Composites*, Harlow, UK: Longman Scientific and Technical.
- Herrero, M., Martínez-Gallegos, S., Labajos, F. M. & Rives, V. (2011). Layered double hydroxide/polyethylene terephthalate nanocomposites. Influence of the intercalated LDH anion and the type of polymerization heating method. *J. Solid State Chem.*, 184(11): 2862–2869.

- Hibino, T. & Jones, W. (2001). New approach to the delamination of layered double hydroxides. *J. Mater Chem.*, 11(5): 1321–1323.
- Hsueh, H.-B. & Chen, C.-Y. (2003). Preparation and properties of LDHs/epoxy nanocomposites. *Polymer*, 44: 5275–5283.
- Huang, S., Cen, X., Zhu, H., Yang, Z., Yang, Y., Tjiu, W. W. & Liu, T. (2011). Facile preparation of poly(vinyl alcohol) nanocomposites with pristine layered double hydroxides. *Mater. Chem. Phys.*, 130(3): 890–896.
- Hutley, T. J. & Darlington, M. W. (1985). Further observation on impact strength-DSC correlation in mineral filled polypropylene. *Polym. Commun.*, 26: 264–267
- Isupov, V. P., Chupakhina, L. E., Ozerova, M. A., Kostrovsky, V. G. & Poluboyarov, V. A. (2001). Polymerization of m-NH₂C₆H₄COO anions in the intercalation compounds of aluminium hydroxide [LiAl₂(OH)₆][m-NH₂C₆H₄COO]·nH₂O. *Solid State Ionics*, 141–142: 231–236.
- Jiao, C. M., Wang, Z. Z., Ye, Z., Hu, Y. & Fan, W. C. (2006). Flame retardation of ethylene-vinyl acetate copolymer using nano magnesium hydroxide and nano hydrotalcite. *J. Fire Sci.*, 24: 47–64.
- Katiyar, V., Gerds, N., Koch, C. B., Risbo, J., Hansen, H. C. B. & Plackett, D. (2011). Melt processing of poly(L-lactic acid) in the presence of organomodified anionic or cationic clays. *J. Appl. Polym. Sci.*, 122: 112–125.
- Kawasumi, M. (2004). The discovery of polymer-clay hybrids. *J. Polym. Sci. Part A: Polym. Chem.*, 42(4): 819–824.
- Khan, A. & O'Hare, D. (2002). Intercalation chemistry of layered double hydroxides: Recent developments and applications. *J. Mater. Chem.*, 12: 3191–3198.
- Kim, G.M. & Michler, G.H. (1998). Micromechanical deformation process in toughened and particle-filled semicrystalline polymers: Part 1. Characterization of deformation processes in dependence on phase morphology. *Polymer*. 39: 5689–5697.
- Kotal, M., Kuila, T., Srivastava, S. K. & Bhowmick, A. K. (2009). Synthesis and characterization of polyurethane/Mg-Al layered double hydroxide nanocomposites. *J. Appl. Polym. Sci.*, 114: 2691–2699.

- Kuila, T. & Acharya, H. (2007). Synthesis and characterization of ethylene vinyl acetate/Mg–Al layered double hydroxide nanocomposites. *J. Appl. Polym. Sci.*, 1–7.
- Kuila, T., Srivastava, S. K., Bhowmick, A. K. & Saxena, A.K. (2008) . Thermoplastic polyolefin based polymer-blend-layered double hydroxide nanacomposite. *J.Comp. Sci. Tech.*, 68: 3234-3239
- Lee, W.D., Im, S.S., Hyung-Mi, L. & Kwang-Jin, K. (2006). Preparation and properties of layered double hydroxides/poly(ethylene terephthalate) nanocomposites by direct melt compounding. *Polymer*. 47: 1364-1371
- Lee, J. H., Nam, J., Rhee, W. & Jung, D. (2008). Hybrid assembly of layered double hydroxide nanocrystals with inorganic , polymeric and biomaterials from micro- to nanometer scales. *Euro. J. Inorg. Chem*, 5573–5578.
- Lee, W.D. & Im, S.S. (2007). Thermomechanical properties and crystallization behaviour of layered double hydroxides/poly(ethylene terephthalate) nanocomposites prepared by in-situ polymerization. *J. Polym. Sci., Part B: Polym. Phys.* 45, 28–40.
- Leroux, F., Adachi-Pagano, M., Intissar, M., Chauvière, S., Forano, C. and Besse, J-P. (2001). Delamination and restacking of layered double hydroxides. *J. Mater. Chem.*, 11: 105–112.
- Liu, J., Chen, G. & Yang, J. (2008). Preparation and characterization of poly(vinyl chloride)/layered double hydroxide nanocomposites with enhanced thermal stability. *Polymer*, 49(18): 3923–3927.
- Liu, J., Chen, G., Yang, J. & Ding, L. (2009). Improved thermal stability of poly(vinyl chloride) by nanoscale layered double hydroxide particles grafted with toluene-2, 4-di-isocyanate. *Mater. Chem. Phys.*, 118: 405–409.
- Lonkar, S. P., Morlat-Therias, S., Caperaa, N., Leroux, F., Gardette, J. L. & Singh, R. P. (2009). Preparation and nonisothermal crystallization behavior of polypropylene/layered double hydroxide nanocomposites. *Polymer*, 50(6): 1505–1515.
- Lonkar, S. P., Therias, S., Leroux, F., Gardette, J-L. & Singh, R. P. (2012). Thermal, mechanical and rheological characterization of polypropylene/layered double hydroxide nanocomposite. *Polym. Eng. Sci.*, 52(9): 2006–2014.

- Magagula, B., Nhlapo, N. & Focke, W. W. (2009). Mn₂Al-LDH- and Co₂Al-LDH-stearate as photodegradants for LDPE film. *Polym. Degrad. Stab.*, 94(6): 947–954.
- Manias, E., Polizos, G., Nakajima, H. & Heidecker, M. J. (2007) Fundamentals of polymer nanocomposites. In: Morgan, A. B. & Wilkie, C. A. (Eds), *Flame Retardant Polymer Nanocomposites*. New York: Wiley, pp 31–66.
- Marangoni, R., Costa Gardolinski, J. E. F., Mikowski, A. & Wypych, F. (2010). PVA nanocomposites reinforced with Zn₂Al LDHs, intercalated with orange dyes. *J. Solid State Electrochem.*, 15(2): 303–311.
- MIT Open Course Ware (2009). *Polymer Physics*. Boston: MIT School of Engineering.
- Moujahid, E. M., Besse, J.-P. & Leroux, F. (2002). Synthesis and characterization of a polystyrene sulfonate layered double hydroxide nanocomposite. In-situ polymerization vs. polymer incorporation. *J. Mater. Chem.*, 12(11): 3324–3330.
- Moujahid, E. M., Leroux, F., Dubois, M. & Besse, J. (2003). In situ polymerisation of monomers in layered double hydroxides. *C.R. Chimie*, 6: 259–264.
- Muksing, N., Magaraphan, R., Coiai, S. & Passaglia, E. (2011). Effect of surfactant alkyl chain length on the dispersion, and thermal and dynamic mechanical properties of LDPE/organo-LDH composites. *Express Polymer Letters*, 5(5): 428–448.
- Nhlapo, N., Motumi, T., Landman, E., Verryn, S. M. C. & Focke, W. W. (2008). Hydrotalcite: Surfactant-assisted fatty acid intercalation of layered double hydroxides. *J. Mater. Sci.*, 43(3): 1033–1043.
- Nyambo, C., Kandare, E., Wang, D. & Wilkie, C. (2008). Flame-retarded polystyrene: Investigating chemical interactions between ammonium polyphosphate and MgAl layered double hydroxide. *Polym. Degrad. Stab.*, 93: 1656–1663.
- Nyambo, C., Wang, D. & Wilkie, C. (2009). Will layered double hydroxides give nanocomposites with polar or non-polar polymers? *Polym. Adv. Technol.*, 20: 332–340.
- O’Leary, S., O’Hare, D. & Seeley, G. (2002). Delamination of layered double hydroxides in polar monomers: New LDH-acrylate nano composites. *Chem. Comm.*, 14: 1506–1507.

- Okada, A. & Usuki, A. (1995). The chemistry of polymer-clay hybrids. *Mater. Sci. Eng. C.*, 3: 109–115.
- Peeterbroeck, S., Alexandre, M., Jerome, R. & Dubois, P. (2005). Poly(ethylene-co-vinyl acetate) clay nanocomposites: Effect of clay nature and organic modifiers on morphology, mechanical and thermal properties. *Polym. Degrad. Stab.*, 90: 288–294.
- Pradhan, S., Costa, F. R., Wagenknecht, U., Jehnichen, D., Bhowmick, A. K. & Heinrich, G. (2008). Elastomer/LDH nanocomposites: Synthesis and studies on nanoparticle dispersion, mechanical properties and interfacial adhesion. *Eur. Polym. J.*, 44(10): 3122–3132.
- Qiu, L., Chen, W. & Qu, B. (2005). Structural characterisation and thermal properties of exfoliated polystyrene/ZnAl layered double hydroxide nanocomposites prepared via solution intercalation, 87: 433–440.
- Ramaraj, B. & Yoon, K. (2008). Thermal and physicochemical properties of ethylene–vinyl acetate copolymer and layered double hydroxide composites. *J. Appl. Polym. Sci.*, 108: 4090–4095.
- Ramaraj, B., Nayak, S. & Yoon, K. (2010). Poly(vinyl alcohol) and layered double hydroxide composites: Thermal and mechanical properties. *J. Appl. Polym. Sci.*, 116: 1671–1677.
- Ray, S. S. & Okamoto, M. (2003) Polymer/layered silicate nanocomposites: A review from preparation to processing. *Prog. Polym. Sci.*, 28(11):1539–1641.
- Riva, A. (2002). Thermal degradation and rheological behaviour of EVA/montmorillonite nanocomposites. *Polym. Degrad. Stab.*, 77(2): 299–304.
- Solin, S. A., Hines, D., Yun, S. K., Pinnavaia, T. J. & Thorpe, M. F. (1995). Layer rigidity in 2-D disordered Ni-Al layer double hydroxides. *J. Non-Cryst. Solids*, 182: 212–220.
- Utracki, L. A. (2004). *Clay-Containing Polymeric Nanocomposites*, Vol. 1. Shrewsbury, UK: Rapra Technology Ltd, p. 456.
- Utracki, L. A., Sepehr, M. & Boccaleri, E. (2007). Synthetic, layered nanoparticles for polymeric nanocomposites (PNCs). *Polym. Adv. Technol.*, 18(1): 1–37.
- Vaia, R. & Wagner, H. (2004). Framework for nanocomposites. *Materials Today*, 32–37.

- Vaia, R. A. & Giannelis, E. P. (1997). Polymer melt intercalation in organically-modified layered silicates: Model predictions and experiment. *Polymer*, 9297(96): 8000–8009.
- Vaysse, C., Guerlou-Demourgues, L., Duguet, E. & Delmas, C. (2003). Acrylate intercalation and in situ polymerization in iron-, cobalt-, or manganese-substituted nickel hydroxides. *Inorg. Chem.*, 42(15): 4559–67.
- Verbeek, C. R. J. & Focke, W. W. (2002) Modelling the Young's modulus of plate;et reinforced thermoplastic sheet composites. *Composites Part A*. 33: 1697–1704.
- Vieille, L., Moujahid, E. M. &Taviot-gue, C. *et al.* (2004). In situ polymerization of interleaved monomers:a comparative study between hydrotalcite and hydrocalumite host structures. *J. Phys. Chem. Solids*. 65: 385–393.
- Wang, B., Zhang, H., Evans, D.G. & Duan, X. (2005). Surface modification of layered double hydroxides and incorporation of hydrophobic organic compounds. *Mater. Chem. Phys.*, 92: 190–196.
- Wang, D.-Y., Leuteritz, A., Kutlu, B., Landwehr, M. A. D., Jehnichen, D., Wagenknecht, U. & Heinrich, G. (2011). Preparation and investigation of the combustion behavior of polypropylene/organomodified MgAl-LDH micro-nanocomposite. *J. Alloys Compd.*, 509(8): 3497–3501.
- Wang, G., Wang, C. & Chen, C. (2006). The disorderly exfoliated LDHs/PMMA nanocomposites synthesized by in situ bulk polymerization: The effects of LDH-U on thermal and mechanical properties. *J. Phys. Chem. B.*, 91: 2443–2450.
- Wang, L., Li, B., Chen, C. & Jia, L. (2010). Structural characterization and related properties of the stearate anions intercalated Ni–Al hydrotalcite-like compound prepared by the microwave crystallization. *J. Alloys Compd.*, 508(2): 426–432.
- Ward, I. M. & Hadley, D. W. (1993) *An Introduction to Mechanical Properties of Solid Polymers*, 1st ed. New York: Wiley.
- Whilton, N. T., Vickers, P. J. & Mann, S. (1997). Bioinorganic clays: synthesis and characterization of amino- and polyamino acid intercalated layered double hydroxides. *J. Mater. Chem.*, 7(8): 1623–1629.
- Work, W. J., Horie, K., Hess, M. & Stepto, R. F. T. (2004). Definition of terms related to polymer blends, composites, and multiphase polymeric materials (IUPAC Recommendations). *Pure Appl. Chem.*, 11: 1985–2007.

- Xu, Z. P & Braterman, P. (2010). Synthesis, structure and morphology of organic layered double hydroxides (LDH) hybrids: Comparison between aliphatic and their oxygenated analogs. *Appl. Clay Sci.*, 48: 235–242.
- Zammarano, M., Bellayer, S., Gilman, J. W., Franceschi, M., Beyer, F. L., Harris, R. H. & Meriani, S. (2006). Delamination of organo-modified layered double hydroxide in polyamide by melt processing. *Polymer*, 47: 652–662.
- Zammarano, M., Franceschi, M., Gilman, J. W. & Meriani, S. (2005). Preparation and flame resistance properties of revolutionary self-extinguishing epoxy nanocomposites based on layered double hydroxides. *Polymer*, 46: 9314–9328.
- Zubitur, M. A., Gomez, M. & Cortazar, J. (2009). Structural characterisation and thermal decomposition of layered double hydroxide/poly(p-dioxanone) nanocomposites. *Polym. Degrad. Stab.*, 94: 804–809.
- Zuiderduin, W. C. J., Westzaan, C., Huétink, J. & Gaymans, R. J. (2003) Toughening of polypropylene with calcium carbonate particles. *Polymer*, 44: 261–275.

Chapter 4

Organo-LDH/Oil suspensions

The study considers fatty acid-intercalated Mg_2Al -LDH as a rheological additive in Jojoba oil. The 20 wt.% LDH in the Jojoba oil formulation was found to be stable (does not bleed out). In this investigation 30 wt.% LDH-stearate was selected. The viscosity of the neat Jojoba oil is Newtonian, whereas the LDH/oil formulation shows shear thinning, which is a typical non-Newtonian behaviour. The viscosity was observed to increase rapidly with an increase in LDH content. The viscosity, at a constant shear rate, shows complex temperature behaviour for the long-chain fatty acids C_{16} – C_{22} . Although LDH-palmitate and LDH-behenate also showed complex viscosity behaviour, particular attention was paid to LDH-stearate. The viscosity increase is assumed to be caused by a reversible loss of excess fatty acid and/or the insertion of Jojoba oil constituents.

The preliminary investigation of the suitability of LDH-stearate as a rheology modifier for Jojoba oil revealed that:

- The viscosity of the 30% LDH-stearate formulation showed complex temperature behaviour at a constant shear of 30 s^{-1} .
- FT-IR analysis showed changes in the configuration of the surfactant chains of the 30% LDH-stearate formulation, which changes as temperature increases.
- XRD analysis showed that the LDH-stearate in the formulation is no longer intercalated.

4 ORGANO-LDH/OIL SUSPENSIONS

4.1 INTRODUCTION

Organoclay suspensions are of importance in that rheological properties are achieved economically (i.e. at low volume fraction); organoclays exhibit good thermal stability (may be used where polymer thickening agents would fail); and the gels formed are resistant to gel-breaking effects from other chemicals. In addition, the dispersion of organoclay is seen as essential in property enhancement for clay-based polymer composites (King *et al.*, 2007). The dispersion of organoclays, particularly in their delaminated form, is of importance in self-assembling monolayers (SAM), Langmuir Blodgett film preparation, as well as emulsion stabilisation (Adachi-Pagano *et al.*, 2000).

This section discusses the potential use of stearate-intercalated LDS as a rheological modifier in Jojoba oil. It is a liquid wax ester mixture with an average molecular weight of 606 g/mol (MSDS). The ester mixture is composed mostly of eicosenyl eicosenoate, docosenyl docosenoate, eicosenyl docosenoate and docosenyl eicosenoate, as well as wax esters from C₃₆–C₄₆ (Miwa, 1971; Spencer *et al.*, 1976). Its chemical composition is closest to that of human sebum and it can therefore control the natural balance of the skin, while maintaining the flow of sebum. Jojoba oil possesses non-allergenic and non-comedogenic (non-clogging) properties (Sandha & Swami, 2009).

4.2 RHEOLOGY

Rheology was defined as the study of deformation and flow by Professor Bingham. This definition was accepted by the American Society of Rheology in 1929. In 1687 Isaac Newton made the hypothesis, 'The resistance which arises from lack of slipperiness of the parts of the liquid, other things being equal, is proportional to the velocity with which the parts of the liquid are separated from one another' (Barnes *et al.*, 1989). Viscosity can therefore be described as the resistance of a substance to flow. It is best understood by considering the flow between parallel plates (see Figure 4.1). The viscosity law states that the force per unit surface area (shear stress) is proportional to the velocity gradient (shear rate), i.e. for laminar flow in a Newtonian fluid.

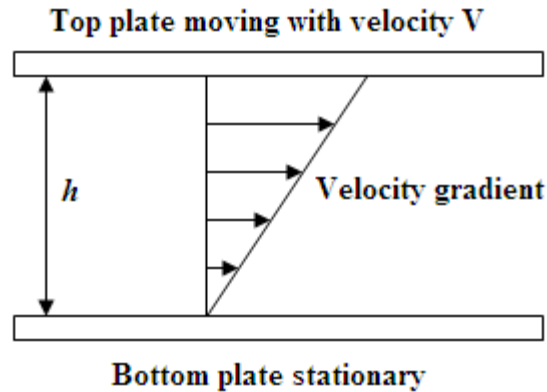


Figure 4.1. The parallel plate depiction of steady state viscous shear flow (Focke, 2012)

Dynamic viscosity or shear viscosity (η) is expressed as a ratio of shear stress (τ) to the corresponding shear rate ($\dot{\gamma}$):

$$\eta = \tau / \dot{\gamma} \quad [8]$$

Shear stress is given by the expression:

$$\tau = F/A \quad [9]$$

where

F = shear force (N)

A = shear area (m²)

The shear rate $\dot{\gamma}$ is given by the equation:

$$\dot{\gamma} = v/h \quad [10]$$

where

v = velocity (m/s)

h = distance between the plates

The flow behaviour of fluids can be described as either Newtonian or non-Newtonian. A Newtonian fluid exhibits a directly proportional relationship between the applied shear stress and the rate of shear. It has no solid-like properties and has a characteristic viscosity. Examples of Newtonian fluids include mineral oil, water, sugar solution, etc. Non-Newtonian fluids have a non-linear relationship between the applied shear stress and the rate of shear, as shown in Figure 4.2. Typical non-Newtonian fluids include pastes, emulsions and cosmetic

formulations. In this particular study we refer to clay particles dispersed in Jojoba oil; this system is more likely to exhibit complex viscosity behaviour. Under non-Newtonian flow behaviour there are further classifications (see Table 4.1 for definitions and examples).

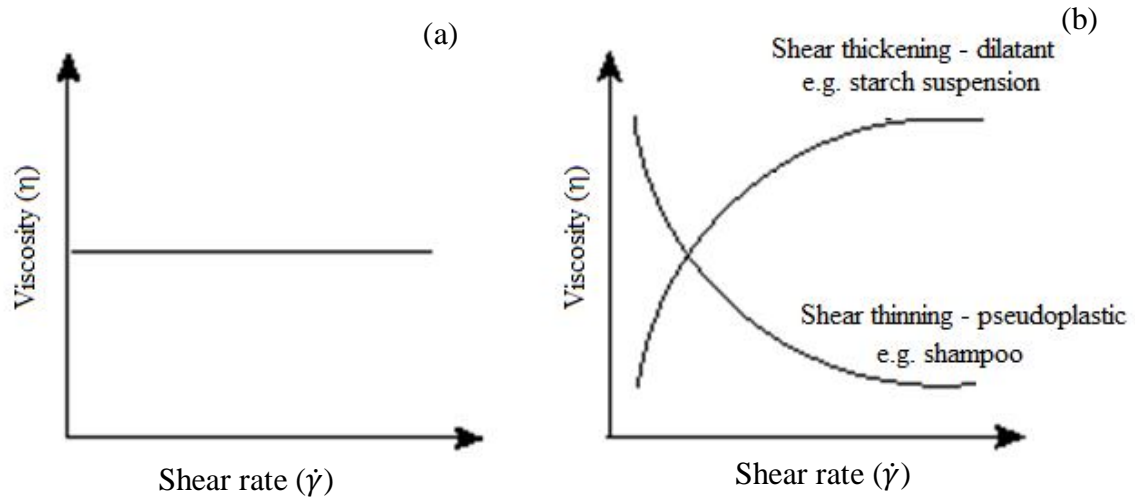


Figure 4.2. Viscosity curve of (a) Newtonian and (b) non-Newtonian fluids

Viscosity is affected by temperature, pressures and additives. It is also affected by the size and shape of the molecules/additives. In addition, intermolecular forces play a role in changes in viscosity, i.e. if the forces of attraction are high, then the viscosity of the liquid will be high.

Table 4.1. Different types of non-Newtonian fluids (Adapted from Shenoy, 1999)

Fluid type	Definition	Typical examples
Pseudoplastic	Exhibit decrease in viscosity with increasing shear rate and hence are often referred to as shear-thinning fluids.	Filled polymer systems Shampoo Lotion
Dilatant	Materials that depict an increase in viscosity with increasing shear rate and hence are often referred to as shear thickening fluids.	Wet sand Starch suspension Gum solutions
Bingham plastics	Fluids that do not flow unless the stress applied exceeds a certain minimum value, referred to as yield stress, and then show a linear shear stress vs shear rate relationship.	Toothpaste Tomato ketchup
Pseudoplastic with a yield stress	Fluids that exhibit a non-linear shear stress vs shear rate relationship in addition to the presence of yield stress.	Heavy crude oils with high wax content Filled polymer systems
Thixotropic	These fluids depict a reversible decrease in shear stress with time at a constant rate of shear and fixed temperature. However, the shear stress approaches a limiting value.	Mayonnaise Brush paint Synovial fluid
Rheopectic	Fluids that show a reversible increase in shear stress with time at a constant rate of shear and fixed temperature. At a given shear rate, the shear stress increases to approach an asymptotic maximum value.	Some clay suspensions, e.g. laponite
Viscoelastic	These fluids have an added feature of elasticity apart from viscosity. They exhibit properties that lie in between those of viscous liquids and elastic solids.	Filled polymer systems Polymer melts Polymer solutions

4.3 THICKENING MECHANISM

Thickening agents may act as gelling agents by dissolving in the liquid phase as a colloid that forms a weakly cohesive internal structure. Pastes are complex fluids with the properties of both solids and liquids. An underlying feature of these materials is the presence of an internal structure that gives a space-filling network capable of supporting its own weight under gravity (see Figure 4.3). They consist of ordered nanostructures and microstructures. Stokes and Frith (2008) describe such materials as “soft matter”, which they further categorise as either “soft-glass” or gel. The elasticity of soft glass arises from caging effects, whereas gels

arise from a percolated network structure that typically occurs due to attractive interactions between at least one of its components (Stokes & Frith, 2008).

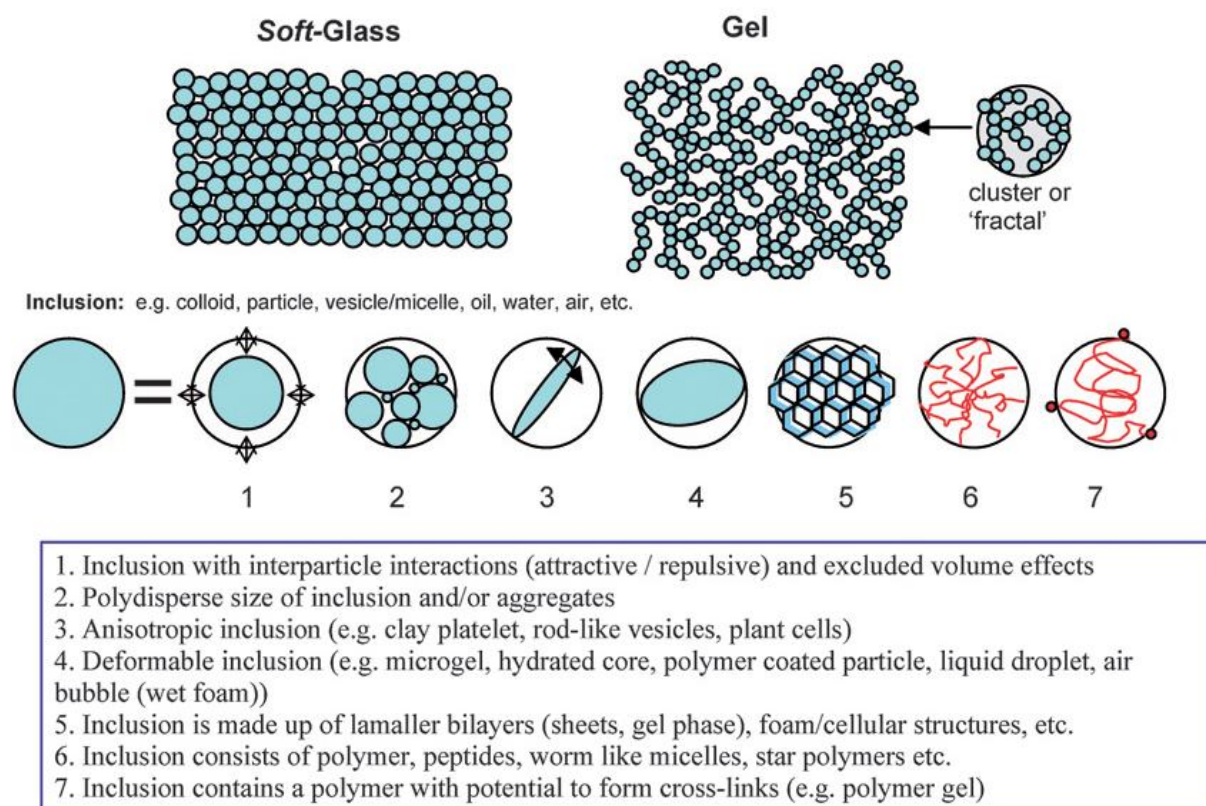


Figure 4.3. Soft microstructure, characterising the system as a “soft-glass” or “gel” (Stokes & Frith, 2008)

4.4 COLLOIDAL DISPERSIONS

IUPAC defines a *colloidal dispersion* as a system in which particles of colloidal size (at least in one direction a dimension roughly between 1 nm and 1 μm) of any nature (e.g. solid, liquid or gas) are dispersed in a *continuous phase* of a different composition (or state). On the other hand, a *suspension* describes solid particles that are dispersed in a liquid. Forano *et al.* (2006) interpreted the colloidal solutions of LDHs in two ways: firstly as a suspension of LDH particles, and secondly as a dispersion of exfoliated single layers of LDH (i.e. delaminated LDH). The delamination of surfactant intercalated LDH was pioneered by Adachi-Pagano and co-workers (2000). The hydrophobisation of clay minerals is a prerequisite for the

preparation of stable dispersion of clays in organic solvents (Lagaly & Malberg, 1990).

Dispersibility is governed by:

- Degree of hydrophobisation
- Polarity and chemical nature of the solvent molecules
- Extent of intercrystalline swelling
- Water content (Yun & Pinnavaia 1995; Adachi-Pagano *et al.*, 2000; Leroux *et al.*, 2001).

4.4.1 Clay dispersion in aqueous media

These types of dispersion are not as common as those in non-aqueous media. The delamination of LDHs in water was pioneered by Hibino and co-worker (Hibino & Jones, 2001; Hibino, 2004; Hibino & Kobayashi, 2005). Hibino (2010) prepared an aqueous colloidal dispersion of delaminated LDH-lactate in a hot aqueous solution of agarose. The mixtures gelled when cooled to room temperature. A uniform dispersion was obtained for the modified LDH; in contrast, the LDH-CO₃ particles agglomerated (Hibino, 2010). Albiston (1996) considered the rheology and microstructure of LDHs in aqueous suspension. Thickening and gelling was controlled by addition of electrolytes; the latter was found to be driven by the interaction of predominately rod-shaped aggregates formed from face-to-face association of the primary LDH particles. Iyi and co-workers (2011) studied the delamination of LDHs intercalated with short chain organic sulphonates. The LDH-isethionate exhibited water-swelling behaviour and formed viscous gels on contact with water (Iyi *et al.*, 2011). In another study, they delaminated LDHs intercalated with short chain carboxylates in water, which yielded a colloidal suspension via a gel state (Iyi & Sasaki, 2008).

4.4.2 Clay dispersion in non-aqueous media

The dispersion of LDH is widely reported in alcohols (Adachi-Pagano *et al.*, 2000; Leroux *et al.*, 2001; Venugopal *et al.*, 2006). Alcohols are composed of non-polar and polar segments that can interact with the alkyl chains and hydroxyl groups of the metal hydroxides respectively, leading to good solvation/delamination (Jones, 1983; Venugopal *et al.*, 2006). The study by Venugopal and co-workers (2006) revealed that the degree of dispersion differs among alcohols. An increase in the chain length of the alcohol led to an increased degree of

dispersion. A typical delamination entails refluxing the organo-LDH in the alcohol at 120 °C (Adachi-Pagano *et al.*, 2000). Peptisation has also been achieved by amino acid intercalation and subsequent treatment with formamide (Hibino & Jones, 2001, 2004). Although delamination of modified LDH was stated to occur readily in organic solvents, poor dispersion was observed in non-polar organic solvents such as hexane (Venugopal *et al.*, 2006). Moreover, dispersions of modified LDHs in more polar solvents are kinetically and thermodynamically unfavourable.

An increase in the dipole moment of the solvent molecules decreases chain solvation, which consequently depresses the rate of solvent incorporation within the interlayer (Jobbágy & Regazzoni, 2004). A higher extent of delamination and stability of colloids was obtained in LDHs containing long surfactant anions and a low $M^{II}:M^{III}$ ratio (Venugopal *et al.*, 2006). Jobbágy and Regazzoni (2004) reported delamination and restacking of LDH-DS in chloroform (CCl_4) and toluene. They rationalised delamination in terms of the miscibility of the organo-LDH and the selected solvent. In their study, dispersion was viewed as a two-component solution. Each dodecyl sulphate-LDH platelet was regarded as a solute molecule, hence the solubility in a given solvent was determined by interplay of the main attractions, i.e. chain-chain, solvent-chain and solvent-solvent. They also attributed it to an entropic contribution due to the loss of the interdigitated dodecyl chain structure, caused by the incorporation of the solvent in the hydrophobic gallery space. These researchers further explained delamination by means of Flory-Huggins theory in which the entropic contribution is modified. This correction was made to account for changes in the interdigitation of aliphatic chains. Hence, above a critical temperature (T_c), the transition from a swollen LDH-DS to delaminated form must be continuous and take place once a critical concentration is surpassed. Below T_c , delamination is only possible at higher dilutions (Jobbágy & Regazzoni, 2004).

Dèkány *et al.* (1997) reported that hydrophobisation of LDHs led to an increase in the adsorption capacity towards organic liquids. Interlamellar swelling of both the LDH-DS and DBS was observed in *n*-heptane. On the other hand, preferential adsorption of propanol by the dodecyl benzene sulphonate derivative was observed, whereas the dodecylsulphate derivatives adsorbed propanol and toluene in almost equal amounts (Dèkány *et al.*, 1997).

Martin *et al.* (1991) explored the potential use of intercalated-LDHs as argillaceous minerals in various oils for gel formulations. The organically modified LDHs were found to demonstrate good swelling properties. The study reported negative aspects of the use of montmorillonite in gel formulations. These included the fact that during gel formulation a high percentage of activators, such as alcohols, acetone and quaternary ammonium salts, could possibly cause skin irritations and allergic reactions. The impurities in the montmorillonite clay and organic additives give it an unpleasant colour and odour. However, LDHs are white in colour and would be advantageous to use as a substitute for montmorillonite.

4.4.3 Clay dispersion in emulsions

Solid particles of colloidal size are employed as stabilisers for Pickering emulsions. These emulsions are encountered in cosmetics, food, pharmaceuticals, oil recovery and waste treatment (Yang *et al.*, 2006). A combination of LDHs and smectite clays was used in the stabilisation of paraffin oil-in-water emulsions, by forming envelopes around the oil droplet (Abend *et al.*, 1998; Lagaly *et al.*, 1999). LDHs have also been employed in the stabilisation of Pickering emulsions (Yang *et al.*, 2006; Yang *et al.*, 2007; Wang *et al.*, 2010). The use of such particulate emulsifiers has the following advantages (Abend *et al.*, 1998):

- The amount of emulsifier may be reduced and/or organic emulsifying agents can be completely replaced.
- The Pickering emulsions obtained therefrom are difficult to break by changing the chemical parameters such as pH, salt concentration, temperature and composition of the oil phase.
- Changes in the solid content or type of solid result in changes in viscosity and type of flow. Hence the emulsifier is easily adjusted to the required practical applications.
- The type of emulsion – oil-in-water (O/W) or water-in-oil (W/O) – changes at different compositions of the solid stabiliser.

Yilmaz *et al.* (1999) studied kaolinite dispersions in water and water-alcohol mixtures. They attributed the increase in viscosity to ‘face-to-edge’ interaction between clay particles at the lower alcohol concentration on the other hand the viscosity decreases again because, the kind of interaction between the particles changes ‘edge-to-edge’ interaction at higher alcohol

concentration. This non-ideal plastic behavior is characteristic of flocculated/aggregated colloidal dispersion, in which every collision between particles results in the formation of a temporary or permanent association.

Yan and co-workers (1991a, 1991b) studied the rheology of oil-in-water emulsions with added solids. The addition of solids appeared to increase viscosity and shear-thinning tendencies (non-Newtonian behaviour). Viscosity was also found to be influenced by other aspects, such as:

- Solids with irregular shapes or surface irregularities gave a much higher viscosity than spherical solids (glass beads), i.e. at the same solids volume fraction.
- Smaller solids gave higher viscosity than larger solids. However, as size ratio of the solids to the oil droplets increases, the size effect decreases.

It is clear that the delamination of organoclays plays a vital role in the formation of stable gels, in either aqueous or non-aqueous media. Limited literature is available on the use of LDHs as rheological modifiers in oils. A preliminary study showed that the viscosity at constant shear of the Jojoba oil /LDH-stearate formulation presented complex temperature behaviour. However, it is important to note that this observation is consistent with a certain morphology and size. This investigation reports anomalous viscosity-temperature behaviour of Jojoba oil LDH-stearate suspensions.

4.5 EXPERIMENTAL

4.5.1 Materials

The materials used in the modification of LDHs are stated in Section 2.5.1. Jojoba oil (100% pure cold pressed) was obtained from Cr  d   Natural Oils.

4.5.2 Preparation of fatty acid-intercalated hydrotalcite

Fatty acid-intercalated LDHs were prepared using the same procedure described in Section 2.5.2 and Appendix B.

4.5.3 Preparation of 30 wt.% LDH-fatty acid/Jojoba oil formulation

Preliminary studies showed that the formulation should contain at least 20 wt.% LDH-stearate, otherwise the oil bleeds out. For this investigation 30 wt.% LDH-stearate was selected. Other formulations using LDH-laurate, -myristate, -palmitate, -oleate and -behenate were also attempted. Three grams of LDH-derivative and 7 g of Jojoba oil were mixed using a pestle and mortar at room temperature. The formulation was then heated up to 80 °C in an oven with occasional stirring to ensure good mixing. The product was allowed to cool down to room temperature overnight. Additional samples were prepared at room temperature, with no heating employed. The samples showed no marked difference as both exhibited complex rheological behaviour.

The 30 wt.% Mg-stearate and 30 wt.% Al-stearate formulations were prepared according to the above procedure, but replacing the LDH-derivatives with Mg-stearate and Al-stearate respectively. In addition, formulations containing stearic acid and Jojoba oil were prepared, having percentage weight ratios of Jojoba oil to fatty acid of 95:5, 90:10, 80:20 and 70:30 respectively.

4.5.4 Characterisation

Phase identification was carried out by XRD analysis on a PANalytical X'pert Pro powder diffractometer with variable divergence and receiving slits and an X'celerator detector using Fe-filtered Co K-alpha radiation (0.17901 nm). X'Pert High Score Plus software was used for phase identification. Temperature-resolved XRD traces were obtained using an Anton Paar HTK 16 heating chamber with a Pt-heating strip. Scans were measured between $2\theta = 1^\circ$ to 40° in a temperature range of 25 to 45 °C at intervals of 5 °C, with a waiting time of 1 min and a measurement time of 6 min per scan. Si (Aldrich 99% pure) was added to the samples so that the data could be corrected for sample displacement using X'Pert High Score Plus software. In the case of the Jojoba/LDH-stearate formulation, the formulation was pocketed in a plastic film and analysed from 25–50 °C.

Differential Scanning Calorimetry (DSC) data were collected on a Mettler Toledo DSC 1 instrument. Samples of 5–10 mg were placed in a 40 μ l alumina pan and heated from -40 °C

to 150 °C and then cooled back to -40 °C at a scan rate of 10 °C/min and an N₂ flow rate of 50 ml/min. A pin hole was made in the lid.

Polarised optical microscopy (POM) was used to study the crystallisation behaviour of the formulations using a Carl Zeiss POM. The samples were sandwiched between two glass slides and heated on a Linkam THMS hot stage (Linkam Scientific Instruments Ltd) from room temperature (\approx 25 °C) to 90 °C at a rate of 10 °C/min, and held at this temperature for 2 min before being cooled back to room temperature.

Standard FTIR was carried out on a Perkin Elmer 100 Spectrophotometer with a MIRacle ATR attachment with diamond Zn/Se plate; spectra were recorded between 4000 and 650 cm⁻¹ at a resolution of 2 cm⁻¹ and the data collected after 32 scans. The temperature scan FTIR spectra were traced between 4000 and 400 cm⁻¹ on a Perkin Elmer Spectrum RX I FTIR. The sample was heated from 25 to 130 °C at a ramp rate of 5 °C/min. Data were obtained from an average of 32 scans, recorded at a resolution of 2 cm⁻¹, background-corrected, using the KBr windows which sandwiched the sample.

Viscosity measurements were carried out on an Anton Paar MCR 301 Rheometer with a Peltier heating system using a 50 mm parallel-plate measuring system. The effect of temperature on the viscosity was measured by placing the sample in the centre of the stationary plate, and the shear rate of the rotating plate was kept constant at 5 s⁻¹. Different shear rates were explored, i.e. 10 and 50 s⁻¹, but no substantial difference was noted. The formulation was heated from 10 to 90 °C and cooled back down to 10 °C. The temperature ramp was 10 °C/min.

The effect of shear rate on the viscosity of the sample was investigated, during which the temperature of the system was maintained at 30 °C. The shear rate of the rotating plate was increased from 1 to 100 s⁻¹.

4.6 RESULTS AND DISCUSSION

4.6.1 Organo-layered double hydroxides (organo-LDHs)

The properties of the organo-LDHs are briefly revisited here as the study showed that intercalation results in different products.

The main difference in the LDH-stearates used is in the platelet size and shape (see Figure 4.4). LDH-stearate (E) had very large rhombohedral-shaped (euhedral) platelets ranging from 10 to 50 μm , and showed very little particle-particle interaction. On the other hand, LDH-stearate (S) had a combination of anhedral- and subhedral-shaped platelets with a size less than 5 μm . Heavy agglomeration was also observed. Euhedral crystals have flat, easily recognisable faces with sharp angles. The well-defined edges are oriented in a specific way relative to the underlying atomic arrangement of the crystal. Crystal faces are defined by indicating their intercepts on the crystallographic axes; this is usually denoted by their Miller indices.

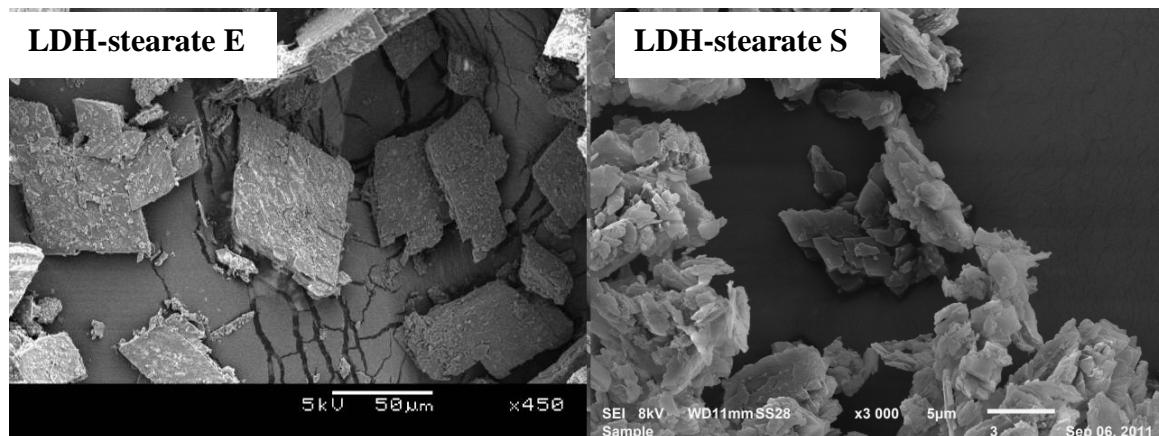


Figure 4.4. SEM micrographs of the LDH-stearates E and S used in the Jojoba oil formulation

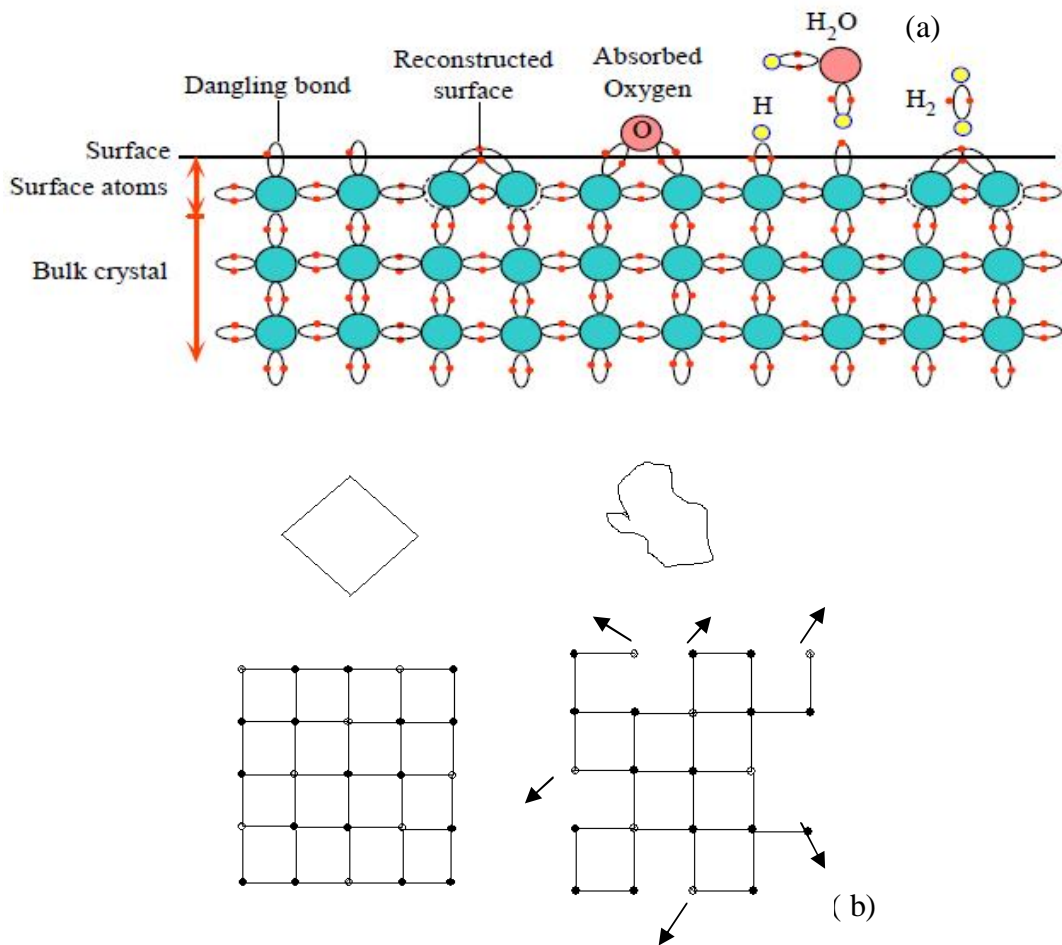


Figure 4.5. (a) Schematic illustration illustration of silicon dangling bond (Kasap 2001) and (b) euhedral and subhedral crystals arrows indicating dangling bonds

A hypothetical 2-D crystal (Figure 4.5a) has on its surface atoms that cannot fulfil their bonding requirements and therefore have broken or dangling bonds (Kasap 2001). These surface atoms can either bond with each other in the case of surface reconstruction or have physisorbed and chemisorbed atoms (Kasap 2001). The rough edges have a lot of ‘dangling’ bonds (Figure 4.5b), to which new atoms/molecules can easily bond to, as the crystal grows. The smooth planes have fewer dangling bonds, and new atoms cannot easily attach, so these planes grow outwards more slowly. This is corroborated by the findings of Schofield and Samson (1954). In their studies they found that the edges of kaolinite crystals with imperfections are a result of bond breakages and these sites carry positive charges. These broken bonds can therefore act as sites for further chemical reaction.

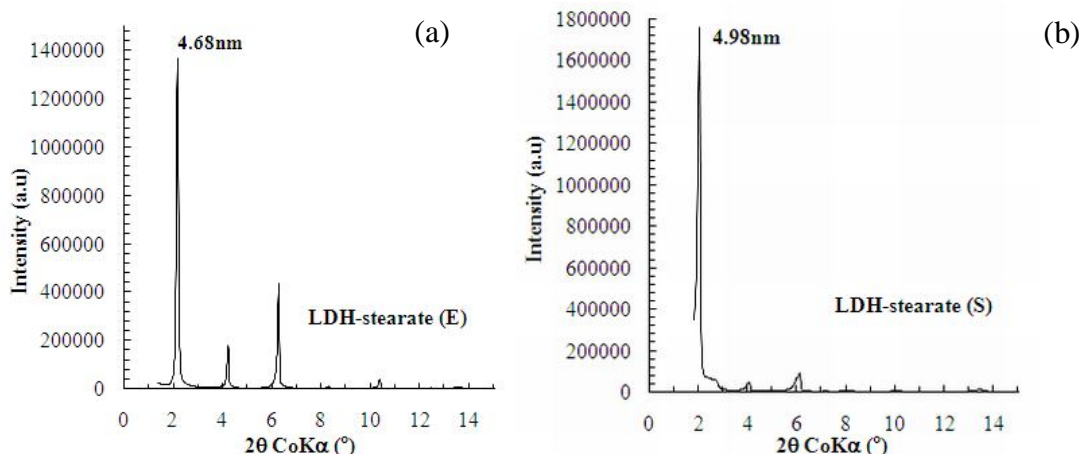


Figure 4.6. XRD diffractograms of: (a) LDH-St (E) and (b) LDH-St (S)

Figure 4.6 shows the diffractograms of each of the respective species of platelets. It is evident that the LDH-stearate (E) had a well-developed crystal form and good ordering, due to the symmetry of the reflections observed. On the other hand, the LDH-stearate (S) exhibited a strong primary basal reflection, although the other peaks are not symmetrical, this is an indication of crystal irregularities. These observations support the observed morphology of platelets.

The properties of the LDH used in the formulation with Jojoba oil are summarised in Table 4.2.

Table 4.2. Summary of XRD and TGA results for the LDH-CO₃, LDH-stearates (E and S), magnesium stearate and aluminium stearate samples

Sample	d-spacing (nm)	TG residue (wt.%)	Intercalation (multiples of AEC)
LDH-CO ₃	0.76	59.7	-
LDH-CO ₃ + Tween 60	0.76	58.4	-
LDH-stearate E	4.68	10.36	3.22
LDH-stearate S	4.88	9.73	3.48
Mg-St/Al-St	5.08	8.23	5.16
Magnesium stearate	4.94	7.30	(5.70)
Aluminium stearate	4.01	8.57	(5.11)

Figure 4.7. shows the FTIR spectrum of the LDH-stearate. The observed bands are consistent with those found in previous investigations (Nhlapo *et al.*, 2008; Focke *et al.*, 2010). Each respective assignment is found in the caption to the figure. Being a bilayer intercalated LDH-stearate, both derivatives (S) & (E) have very similar spectra.

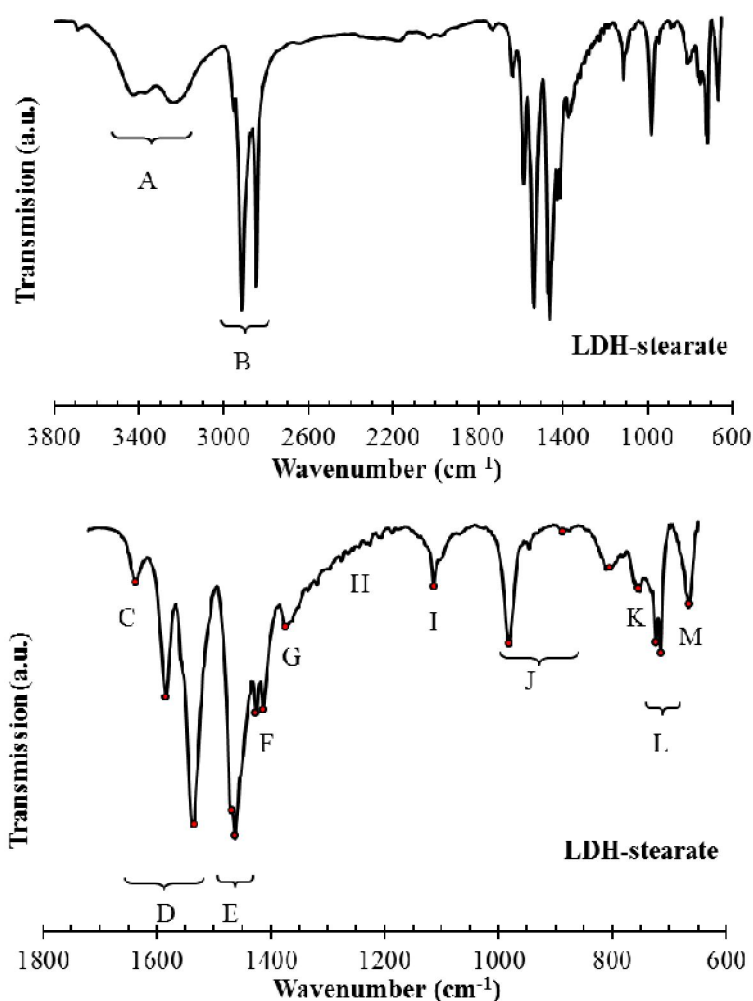


Figure 4.7. FTIR spectrum of the LDH-St

Legend: (A) broad O-H stretch, 3460 cm^{-1} ; (B) C-H stretch, $2954, 2917, 2870\text{ cm}^{-1}$; (C) H_2O bending modes, 1637 cm^{-1} ; (D) asymmetric carboxylic C=O stretch, $1588, 1554$ and 1540 cm^{-1} ; (E) C-H bend (scissoring), $1472, 1466\text{ cm}^{-1}$; (F) C-O-H bend (involving O-H interaction), 1415 cm^{-1} ; (G) CO_3^{2-} ν_3 antisymmetric vibration, $1367, 1363\text{ cm}^{-1}$; (H) $-\text{CH}_2-$ wagging bands; (I) ν_1 CO_3^{2-} , 1114 cm^{-1} ; (J) M-OH deformation modes, $984, 877\text{ cm}^{-1}$; (K) M-OH translation mode, 757 cm^{-1} ; (L) $-\text{CH}_2-$ in-phase rocking vibrations, $724, 716\text{ cm}^{-1}$; (M) ν_4 (in-plane bending) vibrations of CO_3^{2-} , 668 cm^{-1}

In all other characterisation techniques the two LDH-stearates showed similarities. However, the dispersion of LDHs resulted in different viscosity and flow behaviours as a function of temperature. The LDH-stearate (S) in Jojoba oil had a substantially higher viscosity and a

complex flow behaviour as temperature was increased. On the other hand, LDH-stearate (E) had a much lower viscosity and showed a slight bump in the very same area (see Figure 4.8). This anomaly is thought to be attributable to the shape and size of the LDH particles. The LDH-stearate (S) has a considerably smaller particle size, which leads to a greater area of contact and, in turn, a greater particle interaction. In addition, the unassociated atoms/ions shown in Figure 4.5 could potentially be ‘active sites’ for further chemical reactions. When a crystal grows, new atoms attach easily to the rougher and less stable parts of the surface, but less easily to the flat, stable surfaces. Therefore, the flat surfaces tend to grow larger and smoother, until the whole crystal surface consists of all plane surfaces.

It was therefore of interest to explore this anomaly, clearly seen with the LDH-stearate. However, from this point onwards the LDH-stearate referred to is the form that has subhedral platelets, unless stated otherwise.

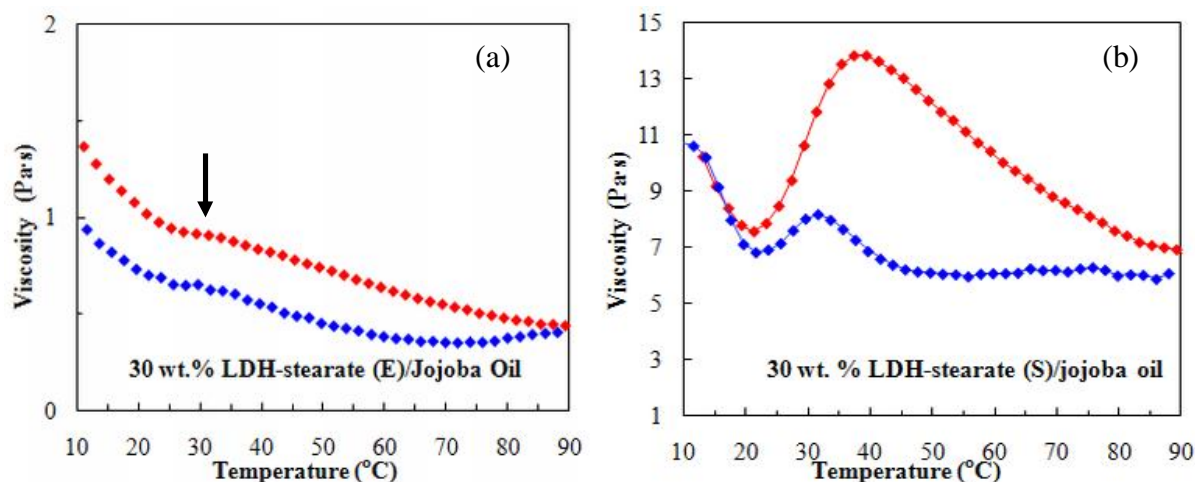


Figure 4.8. Viscosity curves as a function of temperature of: (a) 30 wt.% LDH-St (E) and (b) 30 wt.% LDH-St (S) (The heating run is shown in red and the cooling run in blue)

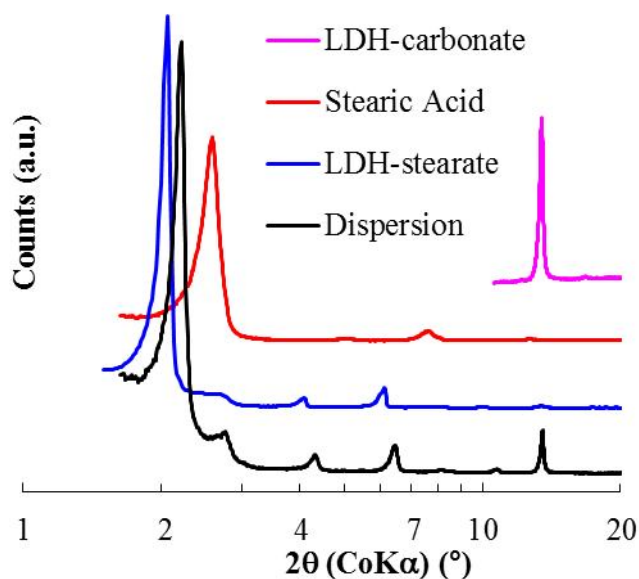


Figure 4.9. Arbitrarily scaled X-ray diffractograms for stearic acid, LDH-CO₃, LDH-stearate (S) and a 30 wt.% dispersion of LDH-stearate (S) in Jojoba oil prepared at a temperature of 80 °C

Figure 4.9 shows the X-ray diffractograms for stearic acid (99%), LDH-CO₃ and LDH-St prepared with Tween 60 as surfactant at an intercalation temperature of 80 °C. It also shows a diffractogram for the gelled Jojoba oil dispersion containing 30 wt.% LDH-St. The reflection at 0.76 nm ($2\theta = 13.49^\circ$) for LDH-CO₃ is present in the LDH-St and its Jojoba oil dispersion, confirming that the former is present as an impurity. The reflections at 4.98 nm ($2\theta = 2.06^\circ$), 2.51 nm ($2\theta = 4.08^\circ$) and 1.68 nm ($2\theta = 6.12^\circ$) are consistent with bilayer intercalated LDH-St. The d-spacing of the LDH-stearate decreased slightly to 4.65 nm in the 30 wt.% in the Jojoba oil dispersion.

4.6.2 Jojoba oil/LDH-derivative formulation

4.6.2.1 Viscosity of stearic acid suspensions

Figure 4.10 shows the effect of temperature on the apparent viscosity of selected stearic acid suspensions in Jojoba oil. The DSC traces are shown in Figures 4.11 and 4.12 show optical micrographs of the 20 wt.% stearic acid suspension, which is roughly the same amount contained in the LDH-stearate/Jojoba oil formulation. The observations with regard to Figures 4.10 to 4.12 can be summarised as follows. Figure 4.10 shows that the low-

temperature viscosity of the suspensions increases dramatically with stearic acid content (also shown in Appendix D). However, when the samples are heated, a rapid drop is observed to values comparable to or lower than the viscosity observed for the Jojoba oil at higher temperatures.

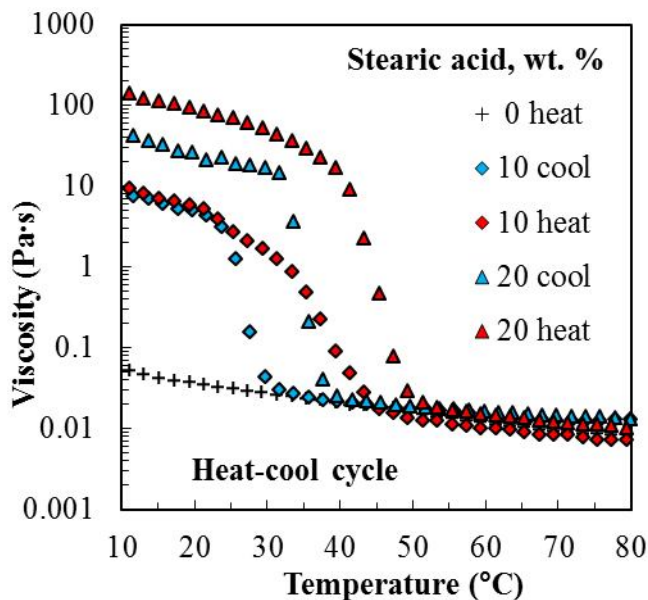


Figure 4.10. Viscosity-temperature curves of Jojoba oil/stearic acid suspensions heated at 5 °C/min from 10 to 90°C and cooled at the same rate back to 10 °C (The heating runs are shown in red and the cooling run in blue)

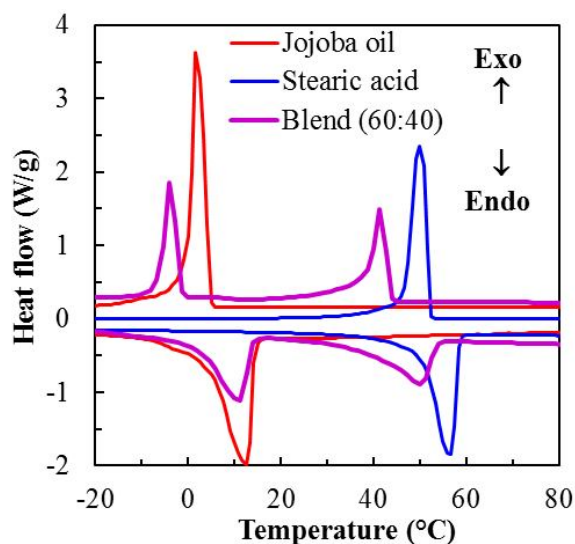
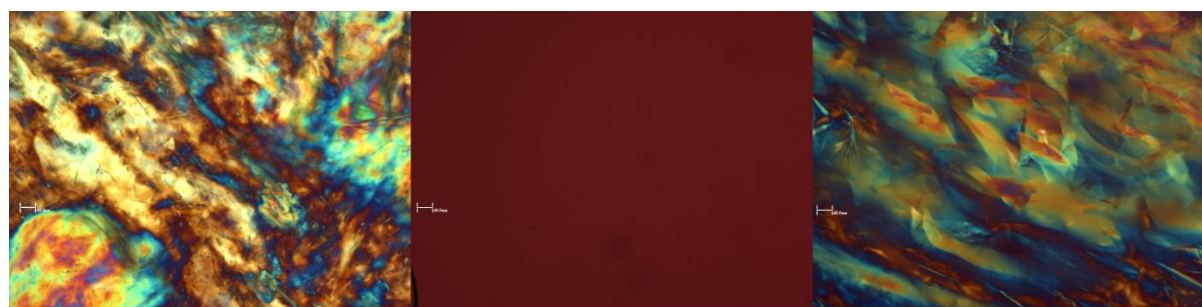


Figure 4.11. DSC traces for neat Jojoba oil and stearic acid as well as a 60:40 blend of the oil with the acid; samples were heated at 5 °C/min from -40 to 200 °C and cooled at the same rate back to -40 °C

Figures 4.11 and 4.12 confirm that this step change in the viscosity can be associated with the melting of the stearic acid. Figure 4.11 also shows that Jojoba oil and stearic acid are fully molten above 15 and 60 °C respectively. In the presence of Jojoba oil, the stearic acid melts at a lower temperature, but the converse does not hold.



A. Heating: 50°C

B. Heating: 60°C

C. Cooling: 49°C

Figure 4.12. Hot-stage optical microscopy of Jojoba oil suspension containing 20 wt.% stearic acid (magnification bar: 40µm)

The heats of melting and of crystallisation, for the suspended stearic acid, are nearly in proportion to the amount of acid present. This implies that the stearic acid is partially soluble in Jojoba oil at low temperatures. This is corroborated by the fact that even a 10 wt.% suspension increases the viscosity of the oil by two orders of magnitude. This observation can be explained by the formation of a space-filling network of fat crystal (Thareja *et al.*, 2010) (see also Figure 4.11). The network crystal interaction provides firmness or gel-like character. Note also that the crystallisation of both the stearic acid and the Jojoba oil is more sluggish in the blend. This implies that the presence of stearic acid in the Jojoba oil matrix retards the crystallisation of Jojoba oil chains.

From the above data it is clear that colligative properties exist between stearic acid and Jojoba oil. Figure 4.13 illustrates a phase diagram of a generalised temperature versus composition for the Jojoba oil-stearic acid formulations. The left side of the curve intersects the ordinate at the melting point of pure Jojoba oil; on the right it intersects the ordinate at the melting point of pure stearic acid. The minimum is the eutectic and a horizontal line is drawn along the eutectic temperature. The left side can be considered as the ‘freezing-point-depression’ curve for stearic acid dissolved in Jojoba oil, and the curve to the right Jojoba oil dissolved in stearic acid. This is typical of binary systems in which the liquids are completely

miscible and the solids completely insoluble in each other (clearly demonstrated in Figures 4.11 and 4.12).

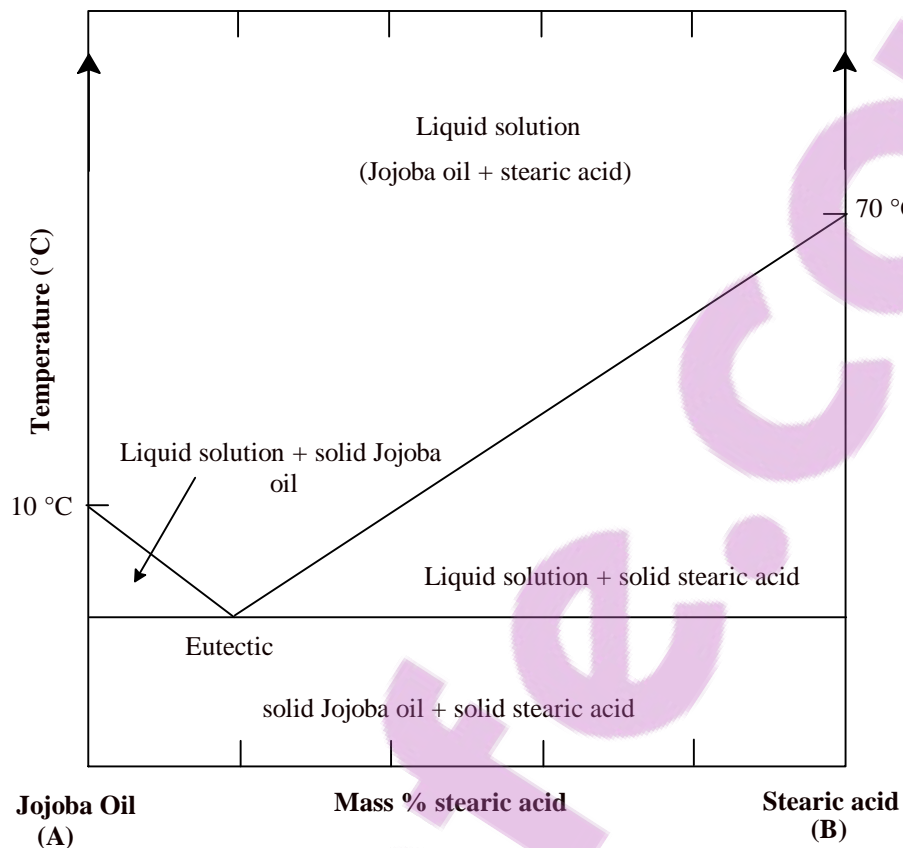


Figure 4.13. General illustration of a Jojoba oil-stearic acid phase diagram

4.6.2.2 Effect of concentration on viscosity of the Jojoba oil formulation

Figure 4.14 shows the relationship that exists between viscosity and increase in the LDH-stearate content in the Jojoba oil matrix. All samples continue to exhibit shear-thinning behaviour, which is an indication of the internal structure within the matrix. As the shear rate increases, the LDH particles will tend to align themselves to the direction of flow. Viscosity continues to increase with the increase in the amount of LDH-stearate used in the formulation. This is due to 'jamming up' of the suspension giving rise to a continuous three-dimensional contact through out the system, thus making flow restricted (Barnes *et al.*, 1986). Since the material under consideration also contained derivatives of magnesium and aluminium stearates, it was decided to study the effect that adding them would have on the viscosity of the Jojoba oil suspensions. Figure 4.15 shows the effect of Al-stearate, Mg-

stearate and LDH-stearate on the viscosity of Jojoba oil as the shear rate changes. The viscosity of Mg-stearate is much higher than that of both Al-stearate and LDH-stearate. Interestingly, the LDH-stearate depicts a viscosity that is in between that of Al-stearate and Mg-stearate.

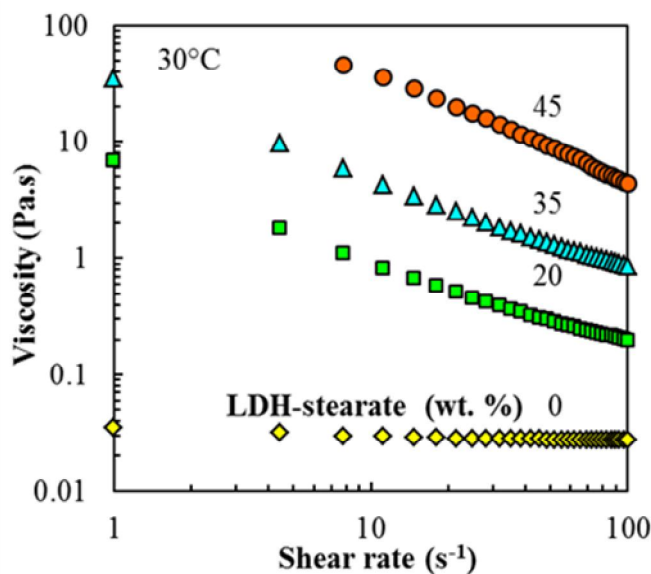


Figure 4.14. The effect of shear rate and LDH-St content on the viscosity of Jojoba oil suspensions (the temperature was kept constant at 30 °C)

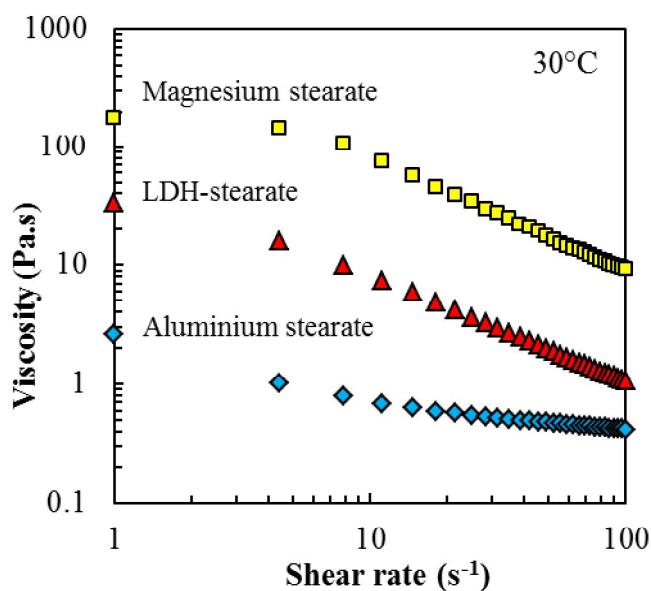


Figure 4.15. Comparison of the Jojoba oil thickening efficiency of 30 wt.% Mg-stearate, Al-stearate and LDH-St (the temperature was 30 °C)

It is usual to add small organic/polar molecules that act as activators in organoclay suspensions. The effect of addition of 5 wt.% of alcohol on the LDH-St/Jojoba oil formulation is shown in Figure 4.16. The apparent viscosity of the dispersion seemed to decrease with increase in chain length. This is an indication that the presence of alcohol helps in the dispersion of the organo-LDH in the Jojoba oil matrix. The LDH-St is partially covered with the stearate chains, meaning that there are areas with exposed OH groups that are able to interact with the alcohol hydroxyl groups. This enhances the wettability and dispersion of the LDH-St particles in the Jojoba oil. As the chain length increases, there is better compatibility of the alcohol hydrophobic tail with the matrix (which is typically composed of liquid wax esters of C₁₆–C₂₂). Better dispersion or solvation of fatty acid chains by the alcohol leads to lower apparent viscosity.

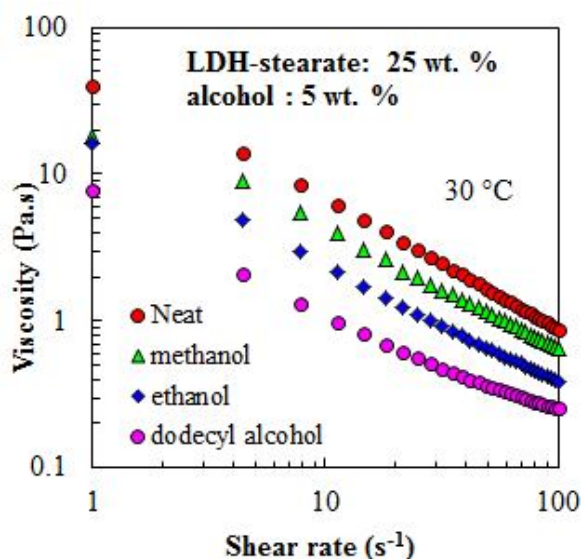


Figure 4.16. Effect of the presence of small amounts of alcohols (5 wt.%) to 25 wt.% LDH-St suspension in Jojoba oil on the suspension viscosity

4.6.2.3 Effect of temperature on viscosity of the Jojoba oil formulation

Generally, viscosity tends to decrease with increasing temperature. Surprisingly, when a 30 wt.% suspension of LDH-St in Jojoba oil was heated, it showed an increase in viscosity in a certain temperature region (Figure 4.17). When heated, the viscosity initially decreases with temperature, but then increases in the temperature range of 25 to 35°C before decreasing again. This is an indication of changes in flow behaviour, as well as of probable

microstructures forming during the rheological study at the given temperature ranges. An increase in temperature results in an increase in the molecular or particle movement.

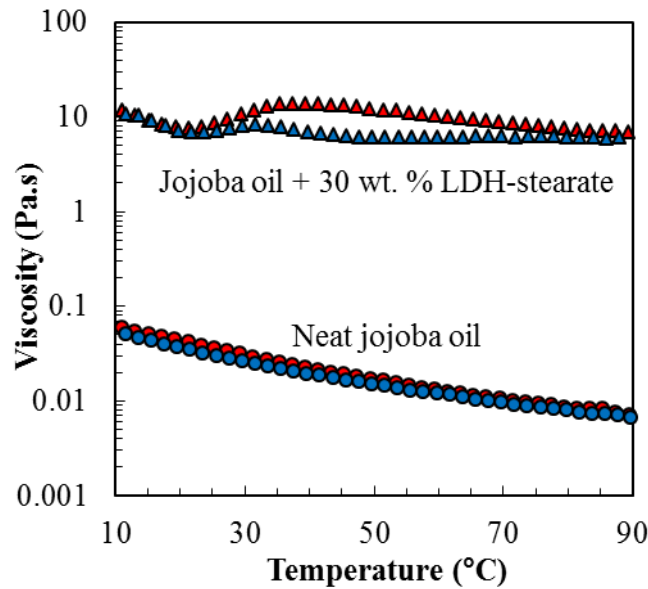


Figure 4.17. The effect of temperature on the viscosity of Jojoba oil and a 30 wt.% LDH-St suspensions subjected to a heating-cooling cycle (The shear rate was 30 s^{-1} ; the temperature was scanned at $5 \text{ }^\circ\text{C}/\text{min}$ from 10 to $90 \text{ }^\circ\text{C}$ and back. The heating run is shown in red and the cooling run in blue)

As demonstrated in previous sections, free stearic acid molecules are exuded into the Jojoba oil matrix as the temperature increases. Depending on the concentration of stearic acid in the Jojoba matrix, the acid begins to melt at as low as $20 \text{ }^\circ\text{C}$ (see Appendix D). This means that the matrix is composed three components, i.e. LDH-St particles, Jojoba oil chains and the expelled stearic acid. As molecular/particle mobility increases as a function of temperature, so do the chances of particle-particle, particle-molecule and molecule-molecule interactions taking place. Figure 4.18 shows the viscosity-temperature curve of 30 wt.% of the LDH-St/Jojoba formulation. The heating run that is divided into three sections according to the different flow behaviour. The stages have been assigned the following events:

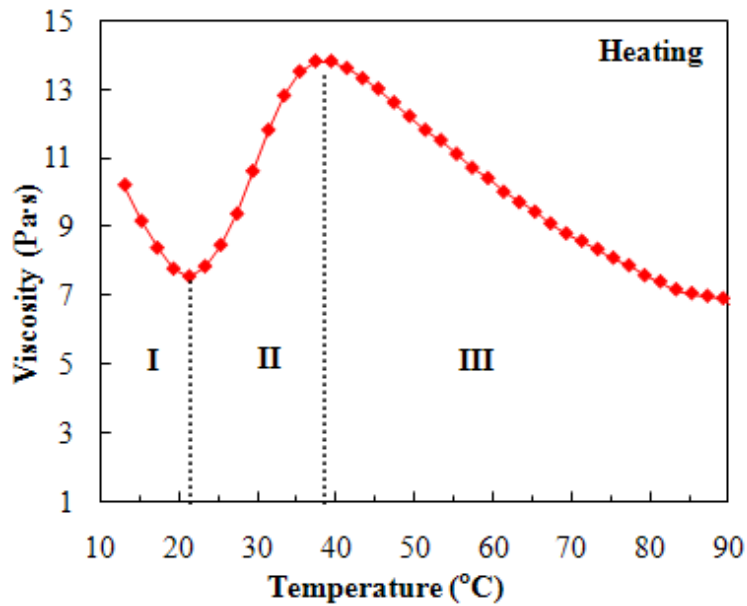


Figure 4.18. Viscosity-temperature heating run subdivided into three stages

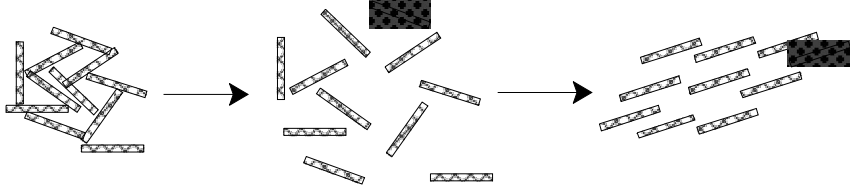
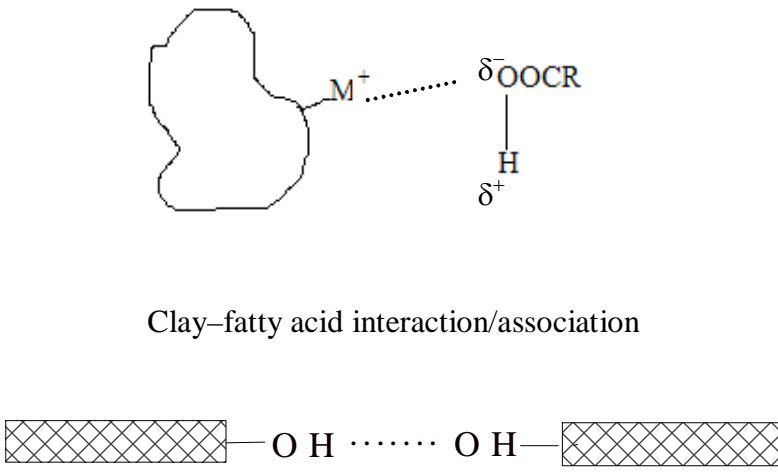
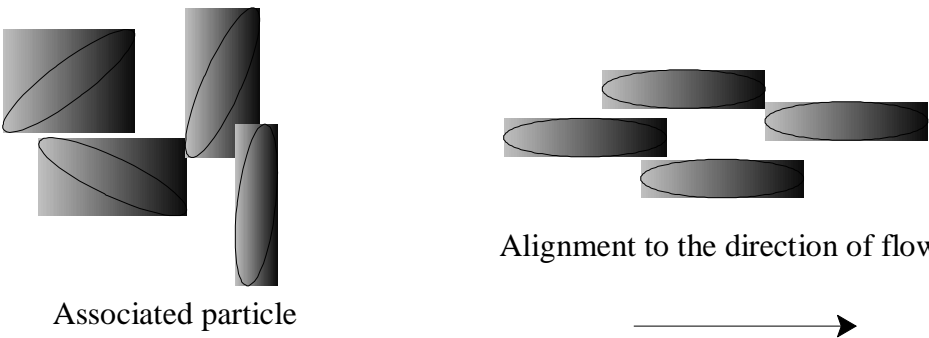
I – This stage is not unusual; the inverse relationship of decrease in viscosity as a function of temperature increases is strongly exhibited. As temperature increases, the Jojoba oil becomes less viscous and flows readily. Particles introduced into a liquid at rest usually assume a state of thermodynamic equilibrium forming aggregated microstructures (Barnes *et al.*, 1989). The microstructures breakdown from edge-to-face (house of cards) aggregation due to shear and align themselves to the direction of flow as shown in the Figure 4.18 and Table 4.3.

II – This stage exhibits an increase in viscosity as temperature increases. This begins at about 20 °C; at this temperature bilayer intercalated LDH begins to exude excess stearic acid into the Jojoba oil matrix. Addition of stearic acid into the Jojoba oil matrix would naturally increase the viscosity. The presence of ‘dangling bonds’ on the subhedral LDH-St particles previously mentioned can result in an inductive effect on the neighbouring acid group, as shown in Table 4.3. These associations could substantially increase the size of the LDH-St particle. This in turn will cause viscosity drag, resulting in a higher resistance to flow. On the other hand, the external hydroxyl groups of the LDH-St can also form hydrogen bonds. However, because of the presence of shear, the neighbouring platelets are envisaged to have edge-to-edge interaction, as shown in Table 4.3. These flocculated platelets also contribute to resistance to flow. Flocculated structures give rise to greater resistance to flow by enclosing and immobilising some of the continuous phase (Jojoba oil) hence increasing the apparent phase volume.

III – As temperature increases, the continuous phase (Jojoba oil) flows readily and the newly associated particles move as one mass and align to the direction of shear. Hence a steady

decrease in viscosity as a function of temperature is observed. Another plausible explanation is shearing of flocculated suspensions could possibly deform or even break them down at elevated temperatures.

Table 4.3. Illustration of the different stages associated with the heating run in the viscosity-temperature curve

Stage	Illustration
I	 <p>House of cards structure Deaggregation Orientation</p>
II	 <p>Clay-fatty acid interaction/association</p> <p>Clay-clay platelet interaction/association</p>
III	 <p>Associated particle</p> <p>Alignment to the direction of flow</p>

When cooled, the apparent viscosity decreases slightly (Stage I) (see Figure 4.19), and then starts to increase at 54 °C. This marks the beginning of Stage II when the free stearic acid in the matrix begins to crystallise out. The viscosity continues to increase as the stearic acid crystallises, forming a fatty acid crystal network. In stage III the viscosity decreases; this could be explained by the fact that the fatty acid crystal network has been broken down due to continued shear action. Thareja *et al.* (2011) also cite the breakdown of some of the fatty acid crystal network due to applied strain. Stage IV shows another increase in the viscosity. The temperature in this region is low, the mobility of the matrix is greatly reduced and resistance to flow increases. The excess stearic acid molecules that continue to crystallise out and form networks also add to the viscosity increase in this stage.

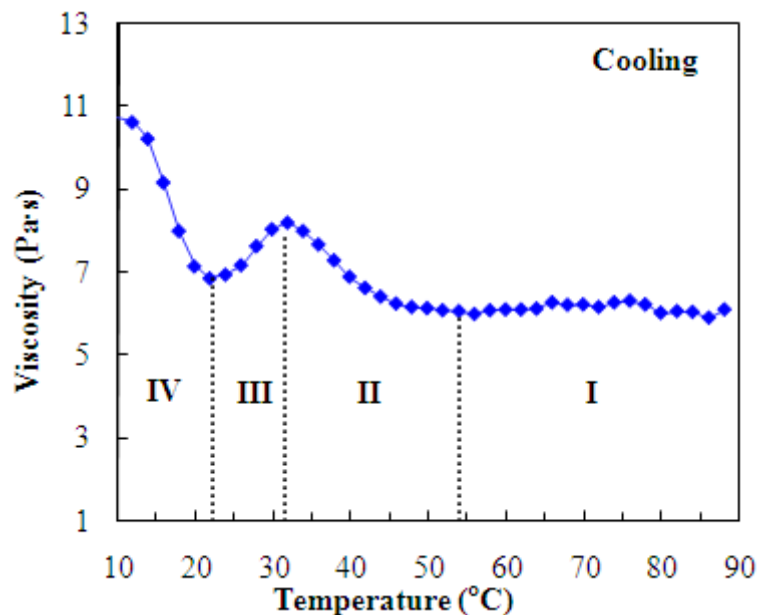


Figure 4.19. Viscosity-temperature cooling run subdivided into four stages

Figure 4.20 shows the viscosity-temperature behaviour of Mg-stearate, Al-stearate and LDH-stearate. The complex behaviour observed in the LDH-stearate is absent in both Al-stearate and Mg-stearate.

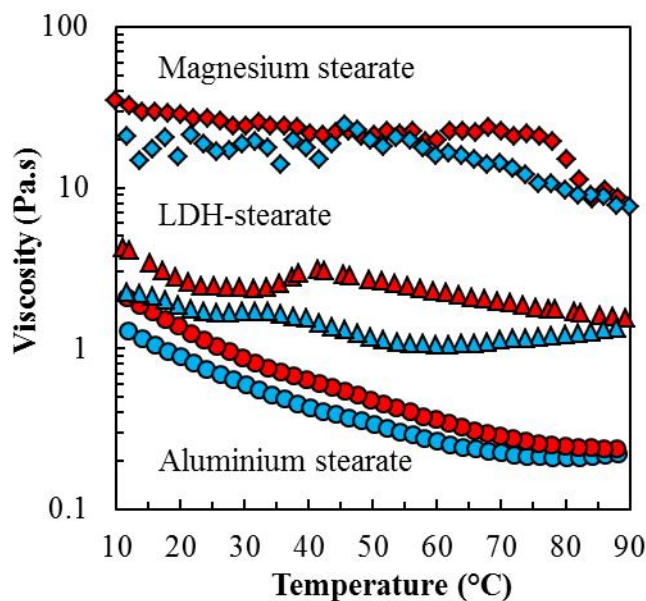


Figure 4.20. Comparison of the Jojoba oil thickening efficiency of Mg-St, Al-St and LDH-St, all at a loading of 30 wt.%. (The shear rate was 5 s^{-1} ; temperature was scanned at 5 °C/min from 10 to 90 °C and back. The heating runs are shown in red and the cooling runs in blue coloured symbols)

4.6.2.4 State of LDH-St in Jojoba oil matrix

Figure 4.21 shows the diffractograms of stearic acid, LDH-St and the LDH-St/Jojoba oil formulation. The d-spacing of the LDH-St used is 4.98 nm. Next to the primary basal reflection is a shoulder which could be an indication of unreacted stearic acid. The typical characteristics of stearate-intercalated LDH have been previously discussed in other sections. After the heating and cooling run on the rheometer of the 30 wt.% formulation, XRD analysis was carried out on the sample and showed a slight decrease in the d-spacing (4.86 nm). This reduction could be a result of the exudation of the excess stearic acid. The peaks appear broader, especially the primary peak, which indicates the presence of numerous phases, as well as poor ordering. Such observations point to the possibility of delamination occurring to a certain extent.

The temperature scan XRD showed very little change within the anomalous region of 30–45 °C (see Appendix D). The d-spacing remained effectively the same. However, the element of shear was absent in the test and hence the results cannot be accurately correlated.

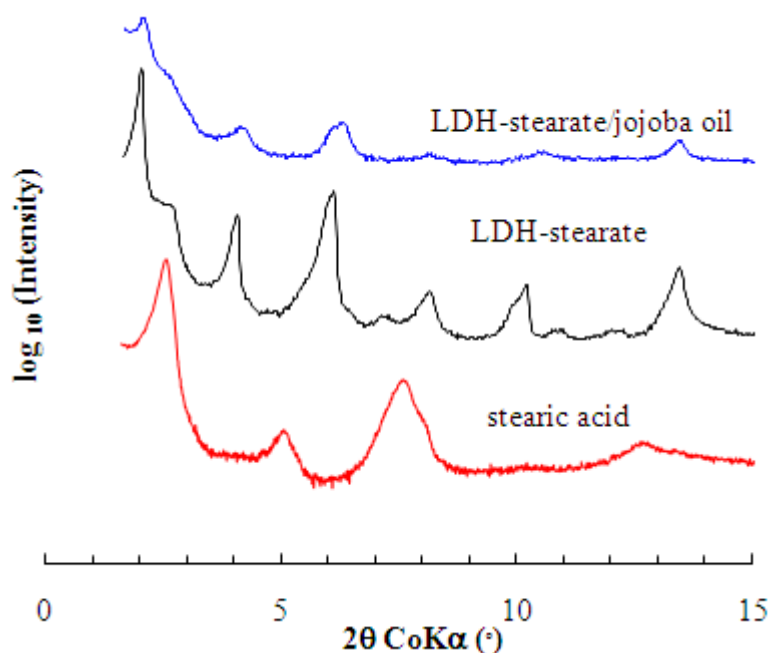


Figure 4.21. X-ray diffractograms of stearic acid, LDH-St and the LDH-St/Jojoba oil formulation

Figure 4.22 shows the FTIR spectra of the LDH-St/Jojoba oil formulation as temperature is increased. The spectra remained very similar to those of the bilayer intercalated LDH-St, which has previously been characterised to contain both un-ionised and ionised fatty acid species. A major change in the spectra was observed at 80 °C where the 1541 cm^{-1} peak, shoulder at 1643 cm^{-1} , disappears. Borja & Dutta (1992) assigned these peaks to unassociated carboxylic acid.

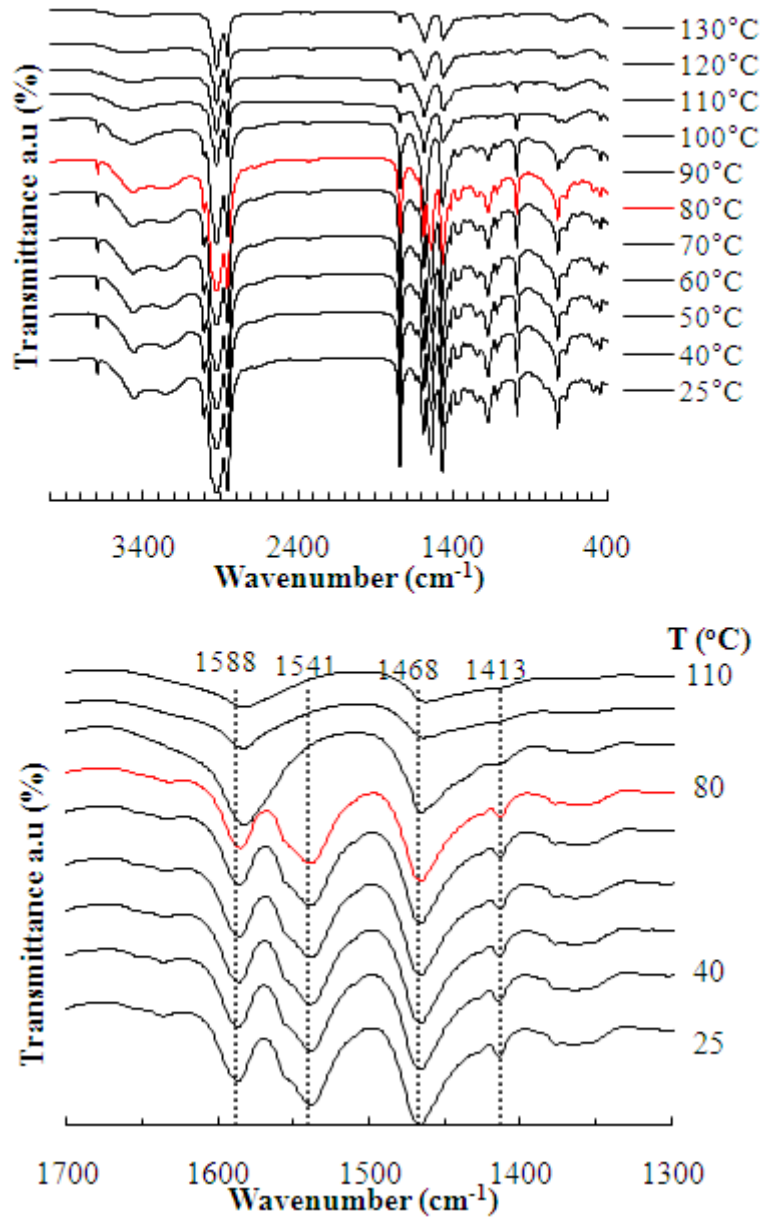


Figure 4.22. FTIR spectra of 30 wt.% LDH-St/Jojoba oil formulation obtained as temperature is increased

4.7 CONCLUSION

The viscosity of the 30 wt.% LDH-St formulation shows complex temperature behaviour at a constant shear of 30 s^{-1} . It was initially thought that the increase and decrease in the apparent viscosity on heating and cooling respectively, in the low-temperature range 20 to 35 °C, is caused by reversible delamination and reassembly to a partially intercalated form. However, experiments such as temperature-scanned IR, DSC and XRD conducted on the LDH-St Jojoba oil formulation did not correlate well with the proposed hypothesis. The XRD analysis of the gel exposed to a cycle of heating and cooling shows a reduction in the d-spacing which could be explained by the exudation of the excess stearic acid. On the other hand, the reduction in the d-spacing could also be explained by delamination. This is further supported by the lack of ordering shown by peak broadening and symmetry changes. However, there is no concrete evidence of restacking. A more plausible explanation is the formation of a fat crystal network formed from the anchoring of exuded stearic acid molecules to the subhedral LDH particles. The observed anomalous response appears to be strongly related to the crystal structure of the platelets used. Association between platelets and platelet-free fatty acid molecules results in flocculated structures and substantially larger particles respectively. These are envisaged to cause 'viscosity drag', hence increasing the apparent viscosity of the matrix.

4.8 REFERENCES

- Abend, S., Bonnke, N., Gutschner, U. & Lagaly, G. (1998). Stabilization of emulsions by heterocoagulation of clay minerals and layered double hydroxides. *Colloid Polym. Sci.*, 276: 730–737.
- Adachi-Pagano, M., Forano, C. & Besse, J-P. (2000). Delamination of layered double hydroxides by use of surfactants. *Chem. Commun.* : 91–92.
- Albiston, L. (1996). Rheology and microstructure of aqueous layered double hydroxide dispersions. *J. Mater. Chem.*, 6(5): 871.
- Barnes, H.A., Hutton, J.F. & Walters, K. (1989). An introduction to rheology. Elsevier Ltd, Oxford, UK. p. 199
- Borja, M. & Dutta, P. K. (1992). Fatty acids in layered metal hydroxides: Membrane-like structure and dynamics. *J. Phys. Chem.* 96: 5434–5444.
- Dèkány, I., Berger, F., Imrik, K. & Lagaly, G. (1997). Hydrophobic layered double hydroxides (LDHs): Selective adsorbents for liquid mixtures. *Colloid. Polym. Sci.*, 275: 681–688.
- Focke, W.W. (2012). Rheology- The science of flow (Course note). Department of Chemical Engineering, University of Pretoria
- Forano, C., Hibino, T., Leroux, F. & Taviot-Gueho, C. (2006). Layered double hydroxides. In. Bergaya, E., Theng, B. K. G. & Lagaly, G. (Eds.), *Handbook of Clay Science*, Amsterdam: Elsevier, pp 1021–1095.
- Hibino, T. (2004). Delamination of layered double hydroxides containing amino acids. *Chem. Mater.*, 16(24): 5482–5488.
- Hibino, T. (2010). New nanocomposite hydrogels containing layered double hydroxide. *Appl. Clay Sci.*, 50: 282–287.
- Hibino, T., & Jones, W. (2001). New approach to the delamination of layered double hydroxides. *J. Mater. Chem.*, 11(5): 1321–1323.
- Hibino, T., & Kobayashi, M. (2005). Delamination of layered double hydroxides in water. *J. Mater. Chem.*, 15(6): 653.

- Iyi, N. & Sasaki, T. (2008). Decarbonation of MgAl-LDHs (layered double hydroxides) using acetate-buffer/NaCl mixed solution. *J. Colloid Interface Sci.*, 322: 237–245.
- Iyi, N., Ebina, Y. & Sasaki, T. (2011). Synthesis and characterization of water-swelling LDH (layered double hydroxide) hybrids containing sulfonate-type intercalant. *J. Mater. Chem.*, 21(22): 80–85.
- Jobbágy, M. & Regazzoni, A. E. (2004). Delamination and restacking of hybrid layered double hydroxides assessed by in situ XRD. *J. Colloid Interface Sci.*, 275: 345–348.
- Jones, R. (1983). The properties and uses of clays which swell in organic solvents. *Clay Miner.*, 18(4): 399–410.
- Kasap, S. O. (2001) Principles of electronic materials and devices, 2nd Edition. McGraw-Hill. p.252
- King, H., Milner, S., Lin, M., Singh, J. & Mason, T. (2007). Structure and rheology of organoclay suspensions. *Phys. Rev. E: Stat. Phys., Plasmas, Fluids*, 75(2): 1–20.
- Lagaly, G. & Malberg, R. (1990). Disaggregation of alkylammonium montmorillonites in organic solvents. *Colloids Surf. Sci.*, 49: 11–27.
- Lagaly, G., Reese, M. & Abend, S. (1999) Smectites as colloidal stabilizers of emulsions I. Preparation and properties of emulsions with smectites and non-ionic surfactants. *Appl. Clay Sci.*, 14: 83–103.
- Le Dréau, Y., Dupuy, N., Gaydou, V., Joachim, J., & Kister, J. (2009). Study of jojoba oil aging by FT-IR. *Anal. Chim. Acta.*, 642(1-2): 163–70.
- Leroux, F., Adachi-Pagano, M., Intissar, M., Chauvière, S., Forano, C. & Besse, J-P. (2001). Delamination and restacking of layered double hydroxides. *J. Mater. Chem.*, 11: 105–112.
- Martin, R., Schanz, K. & Kaufmann, B. (1991) Gel composition and cosmetic/compositions containing the same. Giulini Chemie GmbH, United States Patent No. 5 073 573.
- Mezger, T.G. (2006). The rheology handbook. For users of rotational and oscillatory rheometers. 2nd Edition. Dobler-Druck, Alfeld (Leine)/Germany, Hannoprint, Isernhagen/Germany.
- Miwa, T. (1971). Jojoba oil wax esters and derived fatty acids and alcohols: Gas chromatographic analyses. *J. Am. Oil Chem. Soc.* : 2–7.

- Nhlapo, N., Motumi, T., Landman, E., Verryyn, S. M. C. & Focke, W. W. (2008). Hydrotalcite: Surfactant-assisted fatty acid intercalation of layered double hydroxides. *J. Mater. Sci.*, 43(3): 1033–1043.
- Rye, G. G., Litwinenko, J. W. & Marangoni, A. G. (2005) Fat crystal networks. In: Shahidi, F. (Ed.), *Bailey's Industrial Oil and Fat Products*, 6th edition, New York: Wiley.
- Sandha, G. K. & Swami, V. K. (2009). Jojoba oil as an organic, shelf-stable standard oil-phase base for cosmetic industry. *Rasayan J. Chem*, 2(2): 300–306.
- Schofield, R. K. & Samson, H. R. (1954) Flocculation of kaolinite due to attraction of oppositely charged crystal faces. *Disc. Farad. Soc.*, 18: 135–145.
- Shenoy, A. V. (1999). Rheology of filled polymer systems. Kluwer Academic Publishers. Dordrecht, Netherlands.
- Spencer, G. F., Plattner, R. D. & Miwa, T. (1976). Jojoba oil analysis by high pressure lipid chromatography/mass spectrometry. Paper delivered at the 2nd International Conference on Jojoba and its Uses, Ensanada, Mexico.
- Stokes, J. R. & Frith, W.J. (2008) Rheology of gelling and yielding soft matter systems, *Soft Matter*: 4: 1133–1140.
- Thareja, P., Street, C. B., Wagner, N. J., Vethamuthu, M. S., Hermanson, K. D. & Ananthapadmanabhan, K. P. (2011). Development of an in situ rheological method to characterize fatty acid crystallization in complex fluids. *Colloids Surf. A: Physicochem. Eng. Asp.*, 388(1–3): 12–20.
- Venugopal, B. R., Shivakumara, C. & Rajamathi, M. (2006). Effect of various factors influencing the delamination behavior of surfactant intercalated layered double hydroxides. *J. Colloid Interface Sci.*, 294(1): 234–239.
- Wang, L., Li, B., Chen, C. & Jia, L. (2010). Structural characterization and related properties of the stearate anions intercalated Ni–Al hydrotalcite-like compound prepared by the microwave crystallization. *J. Alloys Compd.*, 508(2): 426–432.
- Yan, Y., Pal, R. & Masliyah, J. (1991a). Rheology of oil-in-water emulsions with added kaolinite clay. *Ind. Eng. Chem. Res.*, 30(8): 1931–1936.
- Yan, Y., Pal, R. & Masliyah, J. (1991b). Rheology of oil-in-water emulsions with added solids. *Chem. Eng. Sci.*, 46(4): 985–994.

- Yang, F., Liu, S., Xu, J., Lan, Q., Wei, F. & Sun, D. (2006). Pickering emulsions solely by layered double hydroxides particles: The effect of salt on emulsion formation and stability. *J. Colloid Interface Sci.*, 302: 159–169.
- Yang, F., Niu, Q., Lan, Q. & Sun, D. (2007). Effect of dispersion pH on the formation and stability of Pickering emulsions stabilized by layered hydroxides particles. *J. Colloid Interface Sci.*, 306: 285–295.
- Yilmaz, H., Guler, S. & Guler, Ó. (1999). The rheological and dielectric properties of kaolinite suspensions in the presence of alcohols. *Phys. Scr.*, 59: 77–80.
- Yun, S .K. & Pinnavaia, T. J. (1995). Water content and particle texture of synthetic hydrotalcite-like layered double hydroxides. *Chem. Mater.*, 7(2): 348–354.

Chapter 5

Conclusion and Recommendations

The chapter presents the general conclusions and makes recommendations regarding the findings of the research. The more specific conclusions are found at the end of each chapter.

5. CONCLUSION AND RECOMMENDATIONS

The work described in the thesis is a further contribution to the Hydrotalcite Project at the Institute of Applied Materials, University of Pretoria. The one-pot fatty acid intercalation technique was developed by Landman *et al.*, 2005.¹ Different types of starting material were used, i.e. LDH-CO₃ and LDO. Nhlapo *et al.* (2008)² undertook a follow-up study using sodium dodecyl sulphate as a surfactant, and it was found that excess stearates were intercalated as their sodium salt. In this current study Tween 60 was employed, yielding sodium-free fatty acid-intercalated LDH. The carbonate form of layered double hydroxide (LDH-CO₃) was successfully intercalated with fatty acids (C₁₄–C₂₂) in a direct one-pot synthesis. The method yielded a product with minimal carbonate contamination. The highlights of this work with regard to the intercalation chemistry are:

- The different sizes and shapes of platelets formed during the modification process indicate that the intercalation entails dissolution and recrystallisation of the LDH-lattice.
- Intercalation can yield a mixed product, either aluminium-rich and/or magnesium-rich platelets or LDH platelets with the correct magnesium and aluminium ratio. Researchers have hardly probed the composition of the individual platelets, but from this study it would appear to be a worthwhile practice.
- High levels of intercalation are envisaged to be driven by the insertion of both ionised and un-ionised fatty acids.
- Changes occur in the interlayer structure as temperature is increased and the excess fatty acids are eventually exuded at elevated temperatures.

Polymer composites containing 5 and 10 wt.% LDH-St or LDH-CO₃ were prepared via melt-compounding. No marked difference in characteristics was observed and hence the 10 wt.% formulation formed the basis of the current study. The polymer matrices employed were EVA, LLDPE and EVAL. The LDH fillers appear to act as nucleating agents for EVA and LLDPE as the DSC crystallisation temperatures increased. However, in the EVAL

¹ Landman, E. P. (2005) Stearate intercalated layered double hydroxides: Methods and application. PhD thesis, Pretoria: University of Pretoria.

² Nhlapo, N., Motumi, T., Landman, E., Verryn, S. M. C. & Focke, W. W. (2008). Hydrotalcite: Surfactant-assisted fatty acid intercalation of layered double hydroxides. *J. Mater. Sci.*, 43(3): 1033–1043.

composites nucleation appeared to be retarded. A marked improvement in the Charpy notched impact strength was noted for the EVAL/LDH-St composite. The difference in the performance of the EVAL/LDH composites, compared with the less-polar polymers, is tentatively attributed to strong hydrogen bonding interaction between the -OH groups on the polymer backbone and those on the clay sheets. The melt-compounding process involved the removal of excess interlayer stearate anions, resulting in a monolayer arrangement. The exuded stearate ions were found to have lubricating and plasticising effects on the matrices. Although various improvements were obtained, it would be more beneficial to make composites from low-melting polymer matrices. In this instance the true nature of the organo-LDH is conserved.

In order to make a more detailed interpretation of the changes in mechanical properties presented earlier, an in-depth study of other factors, such as processing, thermomechanical history and structure development, is essential. Changes in molecular weight, orientation of polymer chains and filler, as well as crystallinity, all play a major role in the properties observed.

Although LDH-based composites appear to be attractive, their utilisation is hampered by their small aspect ratio (an aspect ratio of less than 80). Within a specific area ($A_{sp} < 100 \text{ m}^2/\text{g}$), the platelets are thin (about 0.5 to 0.8 nm) and fragile (as seen by the platelet size reduction after melt processing). These properties can be manipulated in the use of LDHs as rheological modifiers in cosmetic or personal care product formulation. This section of the Hydrotalcite Project demonstrated the effectiveness of LDH-St as a rheological modifier by increasing the viscosity of the Jojoba oil. When viscosities of organo-LDH/Jojoba oil formulations were studied as a function of temperature, gelling was observed. This has been attributed to the formation of a fatty acid crystal network from the exuded excess acid. However, the gels were observed to form preferentially from subhedral-shaped LDH particles. Further study is essential to ascertain the effect of platelet shape on the anomalous viscosity observation. Particles with a uniform size distribution should be employed in the study. Modified LDHs could also be used for emulsion stabilisation.

Appendix A: Publications and conference proceedings

Publications:

- Moyo L., Focke, W. W., Labuschagne, F. J., Heidenrich, D. & Radusch, H.-J. (2013). Properties of layered double hydroxide micro- and nanocomposites. *Materials Research Bulletin*. (48) 1218-1227.
- Moyo L., Focke, W. W., Labuschagne, F. J. & Verryn, S. (2012). Layered double hydroxide intercalated with sodium dodecyl sulphate *Mol. Cryst. Liq. Cryst.*, 555(1): 51–64.
- Focke, W.W., Nhlapo, N. S., Moyo, L. & Verryn, S. M. C. (2010). Thermal properties of lauric- and stearic acid-intercalated layered double hydroxides. *Mol. Cryst. Liq. Cryst.*, 521(1), 168–178.

Pending publications:

- Focke, W. W., Moyo L., Labuschagne, F. J. W. & Ramjee, S. Fatty acid intercalated hydrotalcite as a rheology modifier in Jojoba oil (November 2012).

Conference contributions:

- Moyo L, Heidenrich, D., Labuschagne, F. J., Radusch, H.-J. & Focke, W. W. (2011). Impact strength of LDH-St polymer composites. Poster presentation at the 15th International Conference on Polymeric Materials, Halle (Saale), Germany, September 2011.
- Moyo, L., Focke, W. W., Labuschagne F. J. & and Verryn, S. (2011). Layered double hydroxide intercalated with sodium dodecyl sulphate. Oral and poster presentation at the 11th International Conference on Frontiers of Polymers and Advanced Materials, Pretoria, South Africa, May 2011.
- Moyo, L, Heidenrich, D., Labuschagne, F. J., Androsch, R. & Focke, W. W. (2010). The effect of matrix polarity on the impact properties of LDH-stearate polymer composites. Poster presentation at the 14th International Conference on Polymeric Materials, Halle (Saale), Germany, September 2010.

Appendix B: Fatty acid-intercalated layered double hydroxides

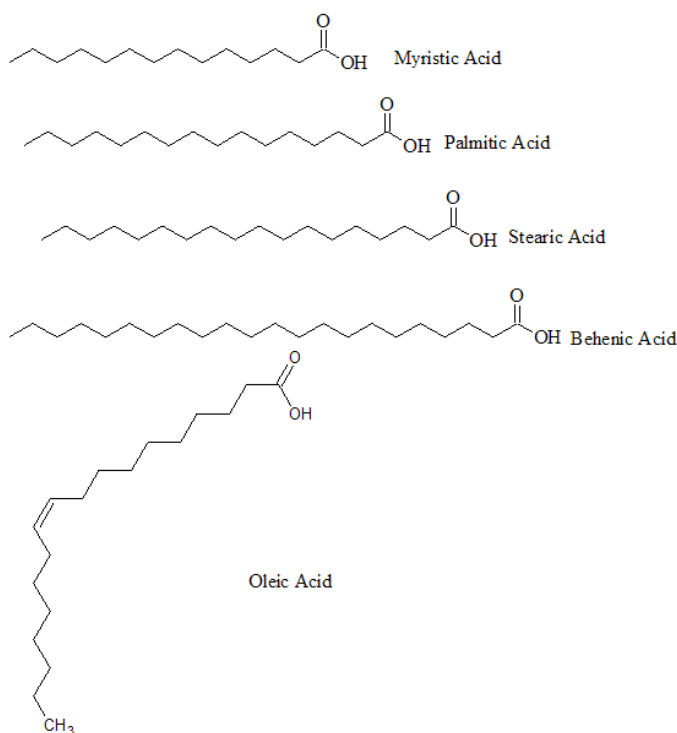


Figure B-1. Fatty/carboxylic acids used in the study

Figure B-1 shows the fatty acids used in the intercalation reaction. Oleic acid was also intercalated to demonstrate the close packing phenomenon. Due to the presence of the *cis*-double bond, the molecules pack with difficulty as this bond limits chain flexibility and decreases adhesion to adjacent chains. The limiting area of oleic acid is about 32 \AA^2 , which is much greater than that of saturated fatty acid chains, which is $\approx 21 \text{ \AA}^2$.

The basic method was adapted from Nhlapo et al. (2008) for the one-pot synthesis. The LDH-carbonate precursor was obtained from Chamotte Holdings and used as is.

Table B-1. Summary of intercalation experiments

Sample I.D	AEC (Acid)	Temperature (°C)	pH
<i>LDH- stearate A</i>	4	80	~9-10
<i>LDH- stearate B</i>	4	80	~9-10
<i>LDH- stearate C</i>	4.5	80	~9-10
<i>LDH-laurate/jojoba oil</i>	2 lauric + 1 jojoba oil	85	~9-10
<i>LDH-stearate/jojoba oil (1AEC)</i>	1 stearic + 2 jojoba oil	85	~9-10
<i>LDH-stearate/jojoba oil (2AEC)</i>	2 stearic + 1 jojoba oil	85	~9-10
<i>LDH-stearate/Jojoba oil (2AEC)</i>	2 stearic + 1 jojoba oil	85	~9-10
<i>LDHSt 1 AEC</i>	1	80	~9-10
<i>LDHSt 2AEC</i>	2	80	~9-10
<i>LDH-myristate 1</i>	4	70	~9-10
<i>LDH-myristate 2</i>	4	70	~9-10
<i>LDH-myristate 3</i>	3	70	~9-10
<i>LDH-myristate 4</i>	4	70	~9-10
<i>LDH- palmitate 1</i>	3	75	~9-10
<i>LDH-palmitate 2</i>	4.5	75	~9-10
<i>LDH- palmitate 3</i>	4.5	75	~9-10
<i>LDH- palmitate 4</i>	4	75	~9-10
<i>LDH-palmitate/stearate</i>	2 palmitic + 2 stearic	80	~9-10
<i>LDH-behenate 1</i>	4	90	~9-10
<i>LDH-behenate 2</i>	3.5	90	~9-10

X-Ray Diffraction

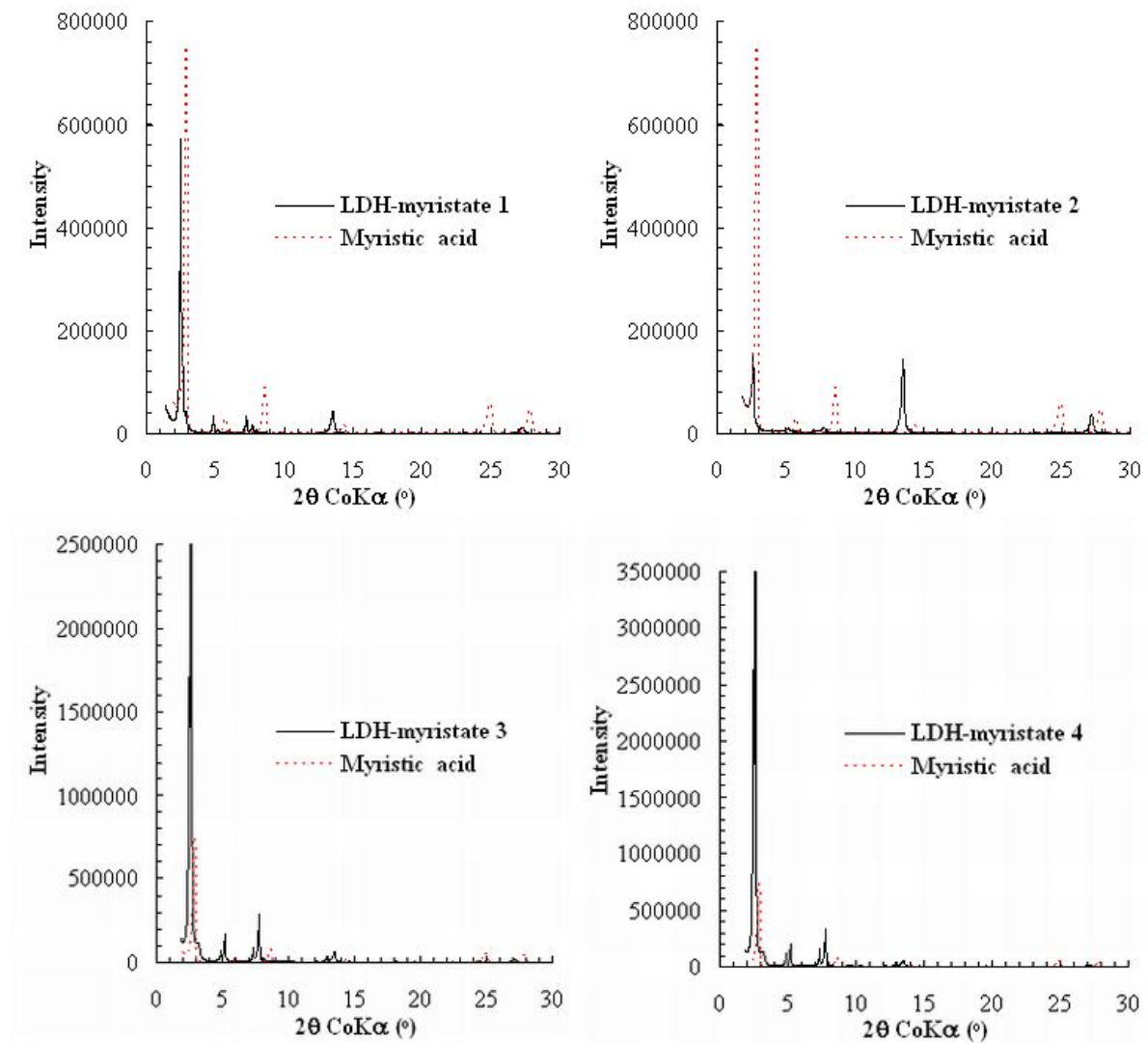


Figure B-2. XRD diffractograms for LDH-myristate

Table B-2. Observed 2θ reflections of XRD of neat myristic acid and LDH-myristate

Sample	Reflections					
	$2\theta(^{\circ})$	d_{003}	$2\theta(^{\circ})$	d_{006}	$2\theta(^{\circ})$	d_{009}
Myristic acid	2.94	3.50	5.77	1.78	8.63	1.19
LDH-myristate 1	2.48	4.14	4.86	2.11	7.26	1.41
LDH-myristate 2	2.30	4.46	4.58	2.24	6.84	1.50
LDH-myristate 3	2.26	4.55	4.41	2.32	6.57	1.56
LDH-myristate 4	2.18	4.71	4.34	2.37	6.50	1.58

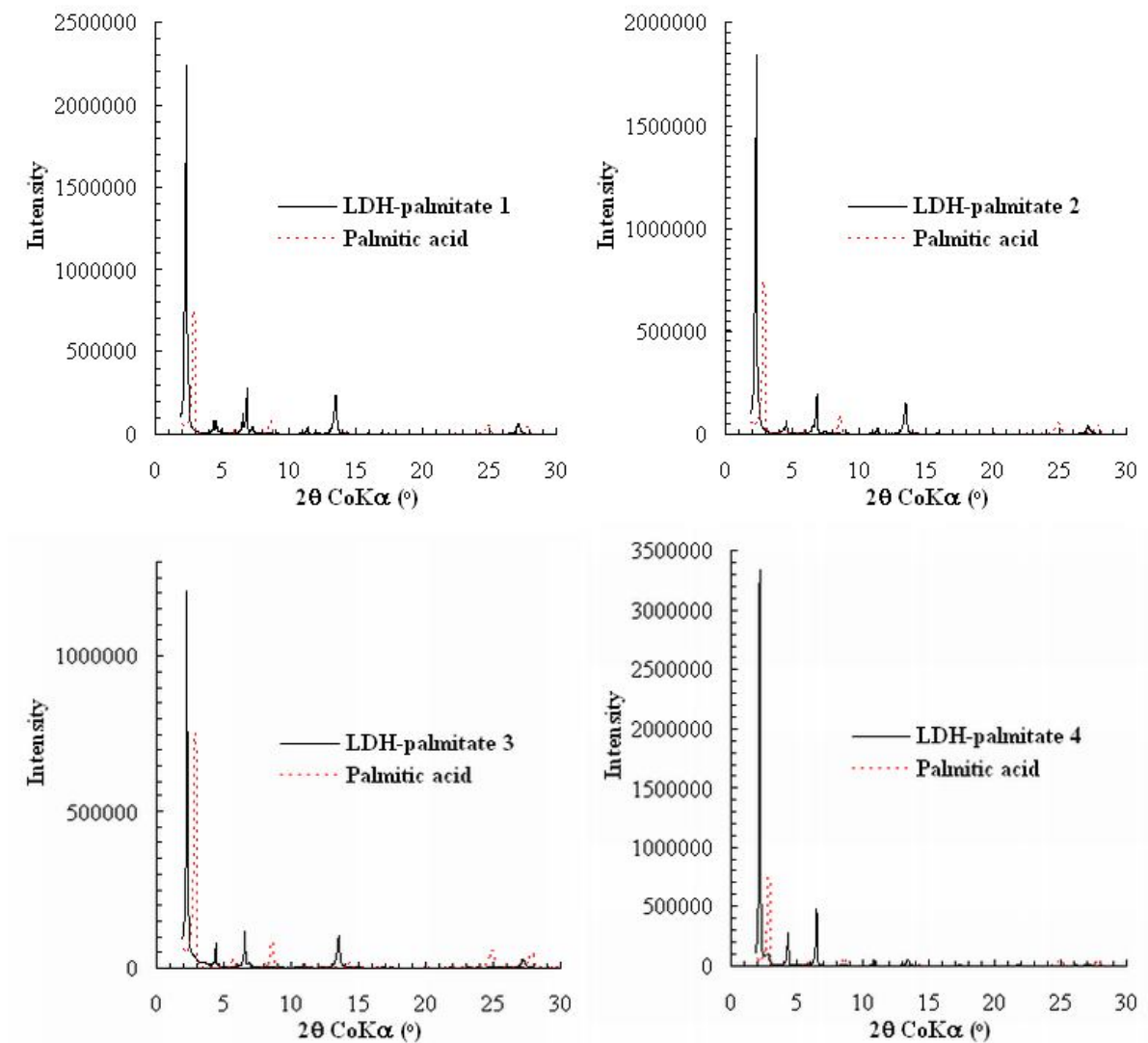


Figure B-3. XRD diffractograms for LDH-palmitate

Table B-3. Observed 2θ reflections of XRD of neat palmitic acid and LDH-palmitate

Sample	Reflections					
	$2\theta(^{\circ})$	$d_{003}(\text{nm})$	$2\theta(^{\circ})$	$d_{006}(\text{nm})$	$2\theta(^{\circ})$	$d_{009}(\text{nm})$
Palmitic acid	2.94	3.50	5.77	1.78	8.63	1.19
LDH-palmitate 1	2.32	4.43	4.60	2.23	6.86	1.50
LDH-palmitate 2	2.30	4.46	4.58	2.24	6.84	1.50
LDH-palmitate 3	2.26	4.55	4.41	2.32	6.57	1.56
LDH-palmitate 4	2.18	4.71	4.34	2.37	6.50	1.58

The average d-spacing observed for LDH-palmitate samples was 4.538 nm. However, it is clear that there are palmitic acid impurities in the case of LDH-palmitate 4. This further substantiates the observations by Kuehn and Poelmann (2010) that a second layer of undissociated acid will lead in greater d-spacings.

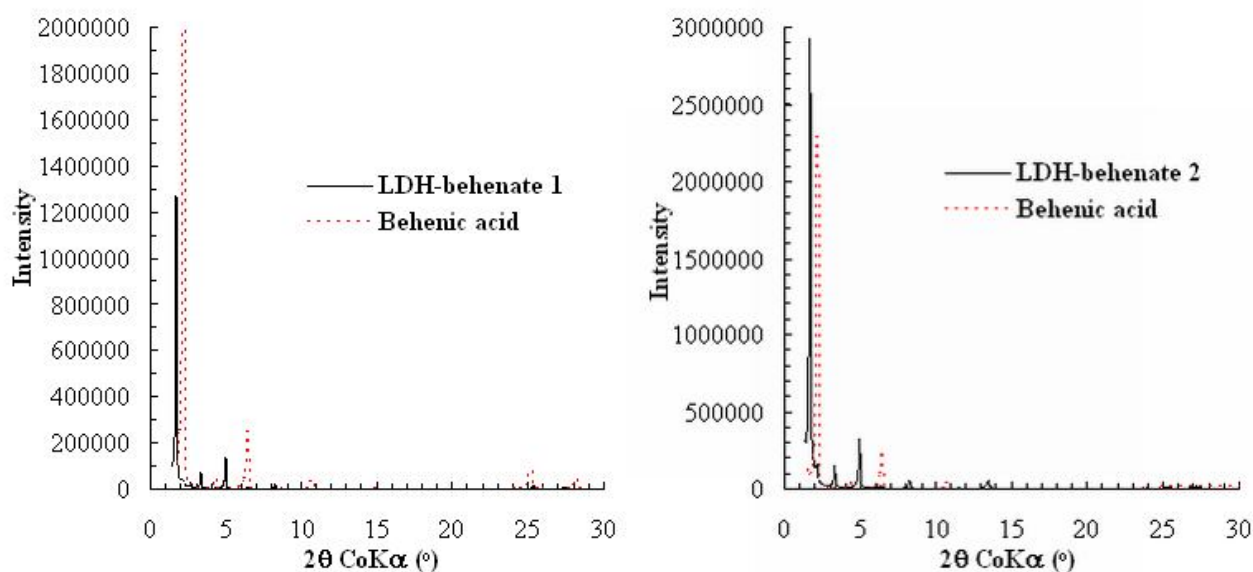


Figure B-4. XRD diffractograms for LDH-behenate

Table B-4. Observed 2θ reflections of XRD of neat behenic acid and LDH-behenate

Sample	Reflections					
	$2\theta(^{\circ})$	$d_{003}(\text{nm})$	$2\theta(^{\circ})$	$d_{006}(\text{nm})$	$2\theta(^{\circ})$	$d_{009}(\text{nm})$
Behenic acid	2.22	4.62	4.35	2.36	6.45	1.59
LDH-behenate 1	1.69	6.08	3.33	3.09	4.96	2.07
LDH-behenate 2	1.68	6.12	3.31	3.10	4.96	2.07

The average d-spacing observed for LDH-behenate samples was 6.097 nm.

Co-intercalation Trials

Two different fatty acids were used in the intercalation reaction, i.e. palmitic acid and stearic acid. The resultant intercalation product had a d-spacing of 4.56 nm (Figure B-5). This is substantially higher than what is normally obtained for bilayer LDH-palmitate (4.46 nm), yet it is lower than that of bilayer LDH-St (4.88 nm). This is an indication that the fatty acids will orient themselves in such a manner that they can accommodate each other, despite the difference in chain length.

In other scenarios, an attempt was made to co-intercalate Jojoba oil and stearic acid into LDH in a ratio of 2:1 and 1:2 respectively. However, co-intercalation was only observed in the later ratio of Jojoba oil to stearic acid (Figure B-5).

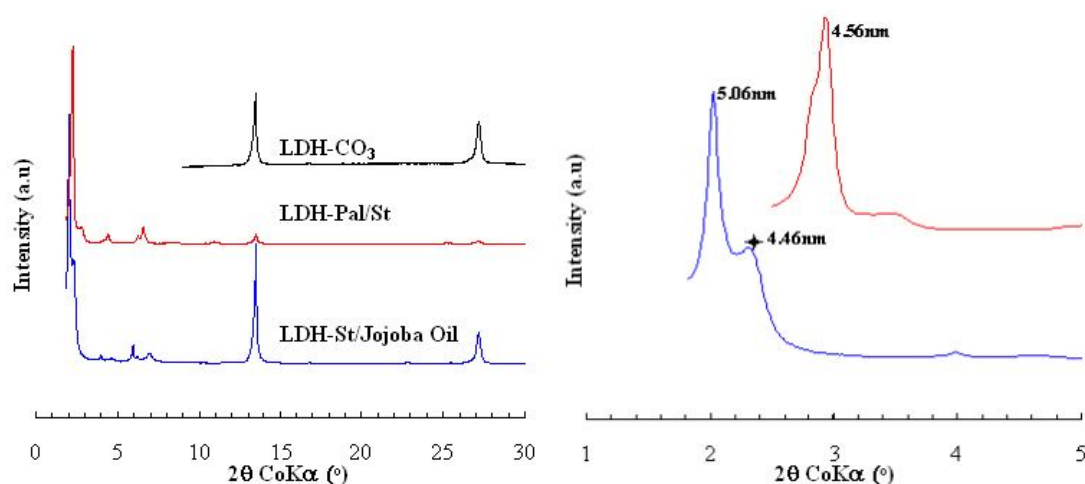


Figure B-5. XRD diffractogram of co-intercalated organo-LDH

Co-intercalation of stearate anion and Jojoba oil yielded a mixed-order product with crystallites with d-spacings of 5.06 and 4.46 nm. The latter is assumed to be a constituent of Jojoba oil; its phases are marked by means of asterisks in Figure B-5. This points to the possible exchange/incorporation of the Jojoba oil constituents with the LDH interlayer anions. The narrow symmetric peaks observed are indicative of a highly crystalline and well-ordered material. This is primarily explained by the fact that Jojoba oil wax esters have a chain length of C₃₄–C₅₀ with an alcohol/acid combination of C₁₆–C₂₆, and hence allow interaction with the interlayer anions. The fatty acid and alcohol component of the ester is usually unsaturated, both possessing a cis-ethylenic bond between the 9th and the 10th carbon, counting from either of the terminal methyl groups (Miwa, 1984³). The cis-geometry has bends at the position of the double bond. The ill-defined secondary peak is due to co-intercalation of a Jojoba oil constituent. However, as mentioned earlier, the fact that the Jojoba oil esters possess a double bond imposes some steric challenges. Hence, minimal intercalation is observed as well as poor ordering/absorption within the interlayer.

Table B-5 shows the elemental composition as determined by ICP-EOS.

Table B-5. Compositional data and formulae of co-intercalated organo-LDHs

Intercalated Anion	Aluminium mol		<i>x</i>
	ratio to		
	Mg	Na	
Carbonate	2.33	0.14	0.30
Pal/St	2.33	0.02	0.30
St/Jojoba oil	1.80	0.29	0.36

³ Miwa, T.K. (1984). Structural determination and uses of Jojoba Oil. *Journal of the American Oil Chemists' Society*. 61(2), 407E410.

Morphology

Figure B-6 shows the typical platelet morphology of the co-intercalated LDHs described above.

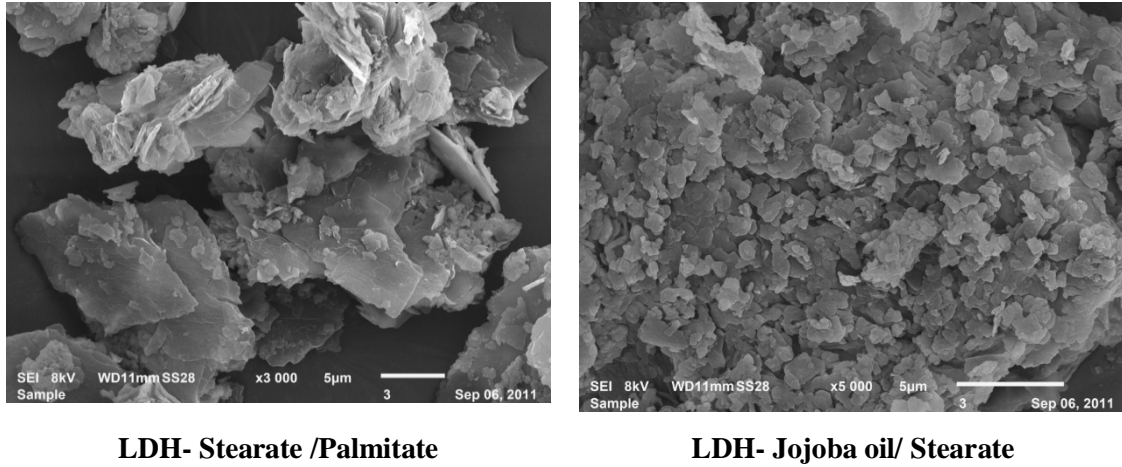


Figure B-6. SEM micrographs of co-intercalated LDHs

EDS Analysis of Clay Platelets

During the study some samples showed unusually high AEC levels or elevated levels of organic incorporation. For this reason the composition of the clay platelets was investigated.

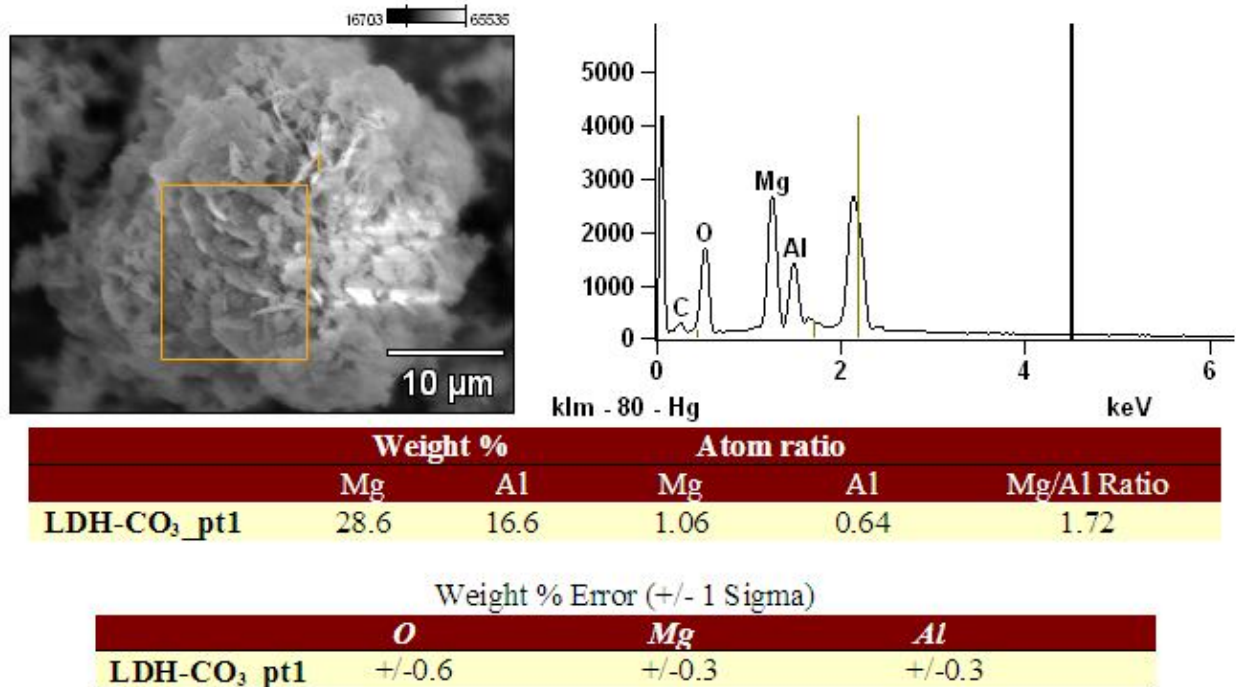


Figure B-7. LDH-CO₃ SEM micrograph, X-ray and composition of platelets

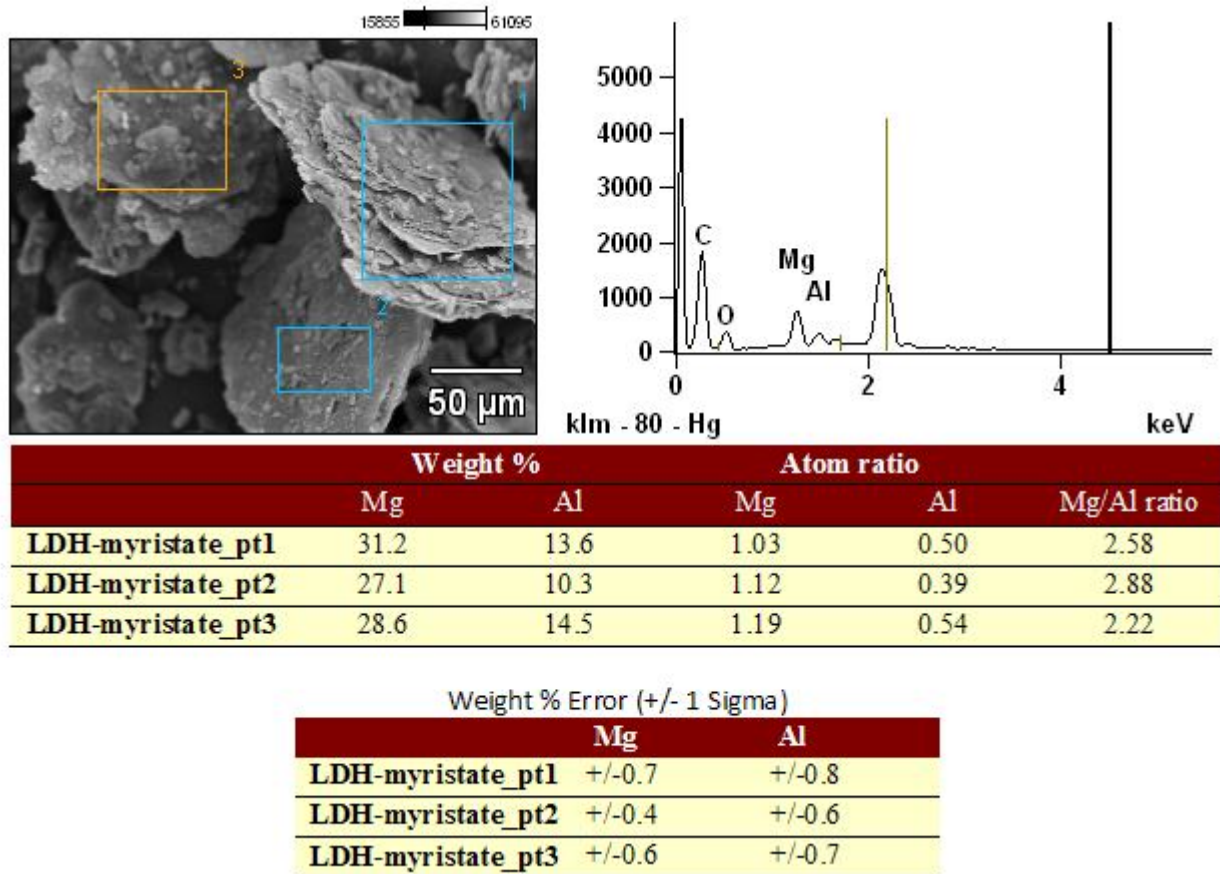


Figure B-8. LDH-myristate SEM micrograph, X-ray and composition of platelets

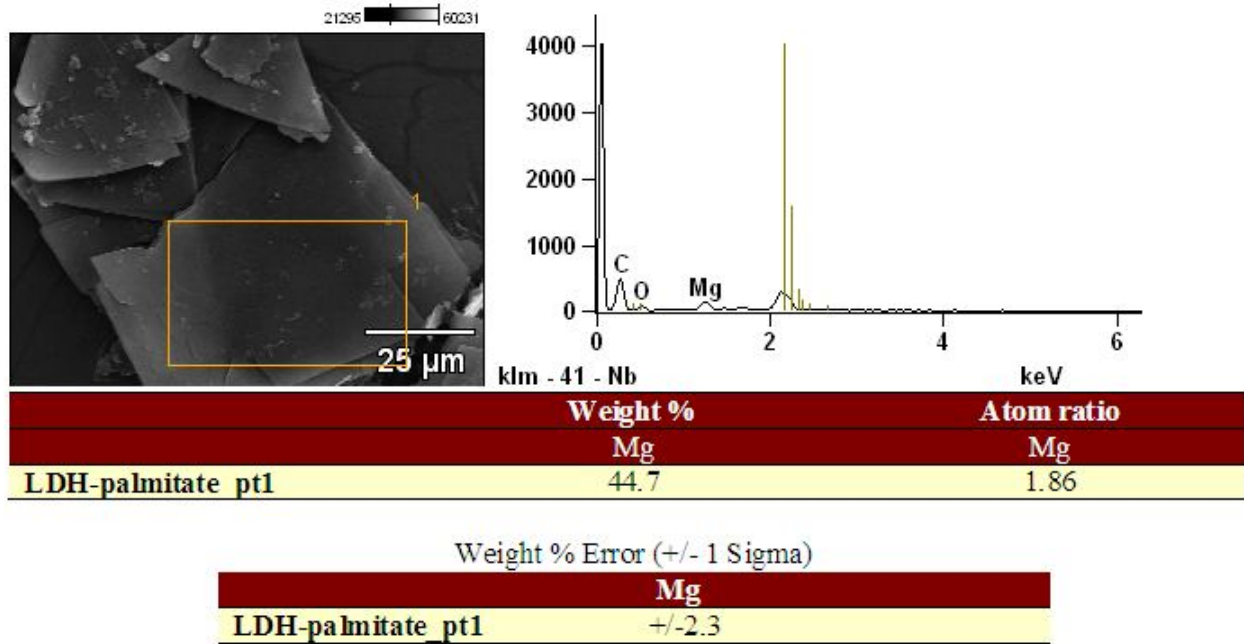


Figure B-9. LDH-palmitate SEM micrograph, X-ray and composition of platelets

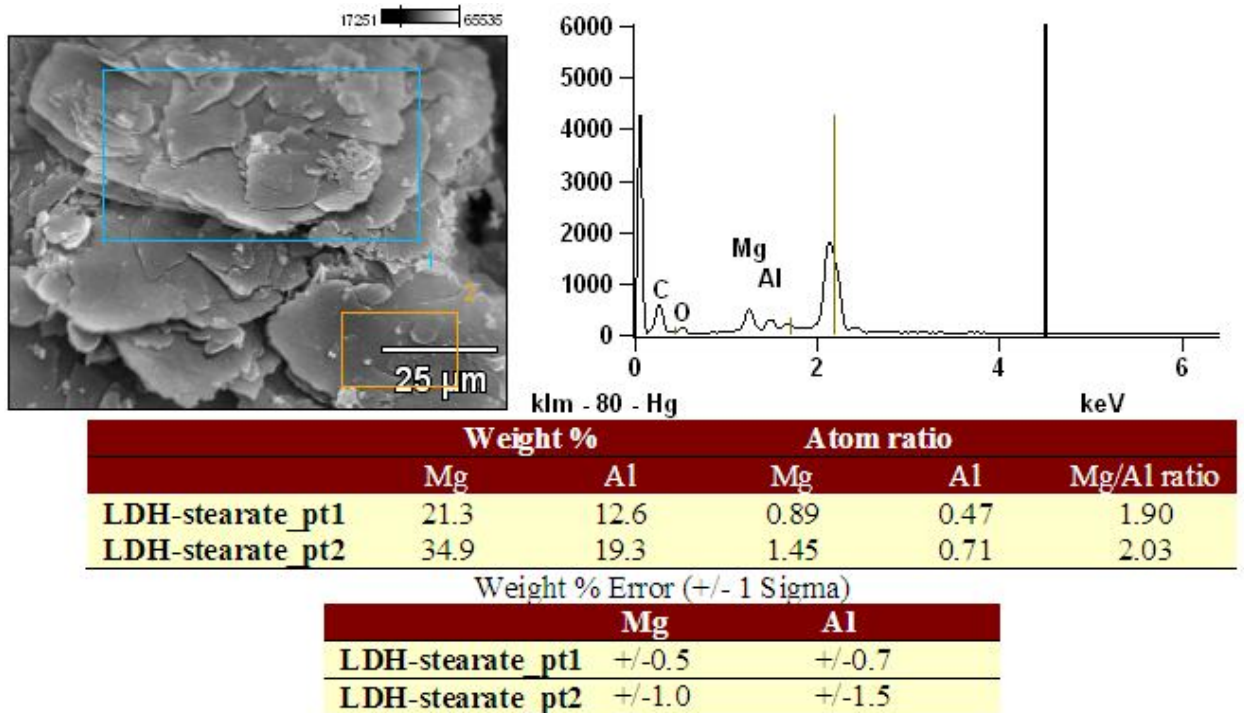


Figure B-10. LDH-St SEM micrograph, X-ray and composition of platelets

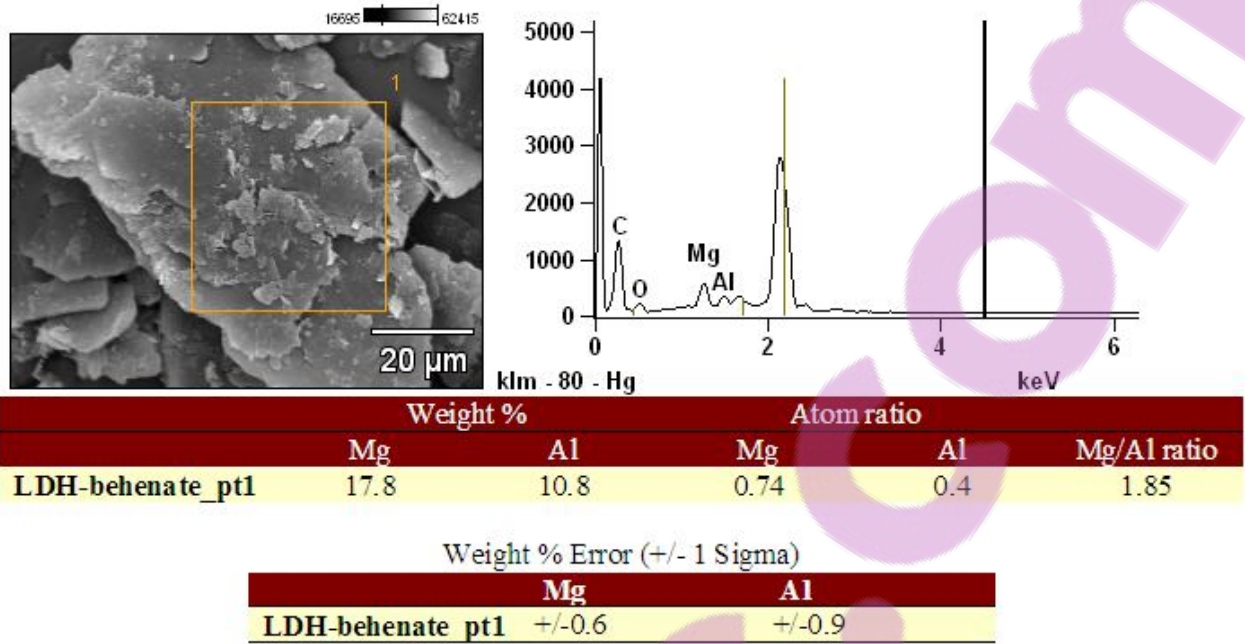


Figure B-11. LDH-behenate SEM micrograph, X-ray and composition of platelets

Thermogravimetric Analysis

The formulae used in the calculation of the clay content on a dry basis; actual clay and percentage organic content are:

$$\text{Clay content on a dry basis} = \frac{\% \text{ Residue at } 900 \text{ } ^\circ\text{C}}{\% \text{ Residue at } 150 \text{ } ^\circ\text{C}}$$

Actual clay content is obtained by multiplying the ratio of the clay content on a dry basis to that of 100% clay of the LDH precursor. For example, using LDH-CO₃,

$$\begin{aligned} \text{Clay content on a dry basis} &= 57.33/98.51 \\ &= 58.19\% \end{aligned}$$

$$\begin{aligned} \text{Ratio of clay on a dry basis to 100\%} &= 100/58.19 \\ &= \underline{1.718} \end{aligned}$$

$$\% \text{ Organic content} = 100 - \text{Actual \% clay}$$

Table B-6. Summary of thermogravimetric data and estimates for the degree of intercalation

Sample identity	Residual mass loss (wt.%) at		Carboxylate/Al mol ratio
	150 °C	900 °C	
LDH-CO ₃	98.10	57.68	-
LDH-myristate 1	92.90	23.63	1.19
LDH-myristate 2	96.88	14.61	2.64
LDH-myristate 3	97.77	48.59	0.17
LDH-myristate 4	96.83	13.65	2.88
LDH-palmitate 1	95.99	21.05	1.36
LDH-palmitate 2	96.23	20.54	1.42
LDH-palmitate 3	95.50	26.54	0.90
LDH-palmitate 4	95.73	14.92	2.24
LDH-stearate	95.40	13.11	2.39
LDH-behenate 1	96.45	8.71	3.36
LDH-behenate 2	96.04	10.72	2.60

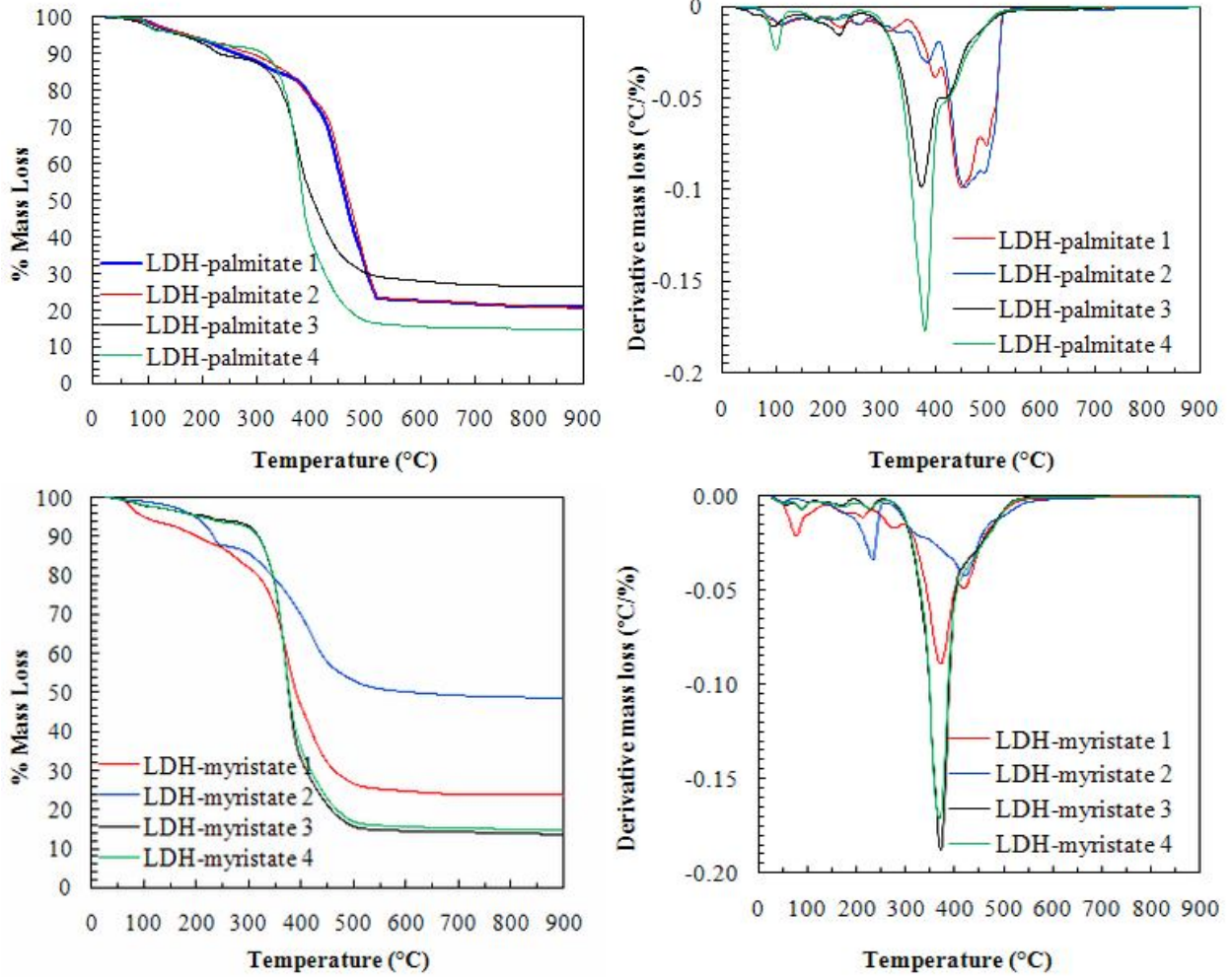


Figure B-12. LDH-palmitate and myristate TG profile

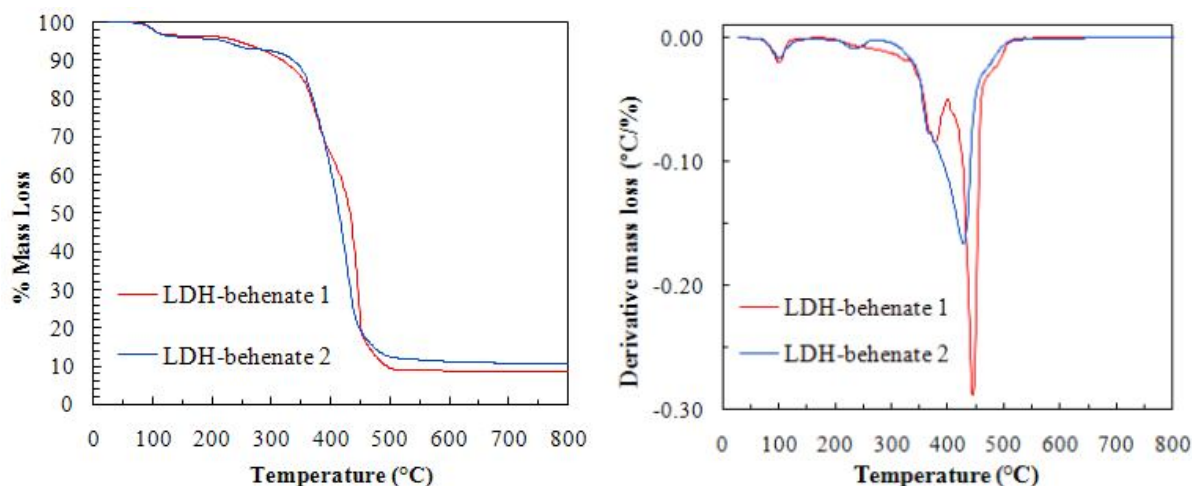


Figure B-13. LDH-behenate TG profile

Table B-7. Summary of thermogravimetric data, estimates for the degree of intercalation and d-spacing

Sample identity	Residual mass loss (wt.%) at		Carboxylate/Al mol ratio	d-spacing (nm)
	150 °C	900 °C		
LDH-CO ₃	98.10	57.68	-	0.76
LDH- stearate 1	95.15	15.05	1.98	5.06
LDH- stearate 2	95.10	13.30	2.34	4.93
LDH- stearate 3	94.29	13.66	2.23	4.94
LDH- stearate 4	94.75	11.80	2.72	5.04
LDH- stearate 5	95.40	13.11	2.39	4.98
LDH- stearate 6	95.28	13.55	2.29	4.95
LDH- stearate 7	95.18	14.92	2.01	4.93
LDH- stearate 8	95.44	13.78	2.24	4.89
LDH- stearate 9	95.57	11.62	2.80	4.95
LDH- stearate 10	94.71	11.17	2.91	5.00
LDH- stearate 11	94.94	11.29	2.88	5.06
LDH- stearate 12	94.99	10.84	3.03	5.02
LDH- stearate 13	94.68	10.29	3.22	4.68
Average	95.04	12.64	2.54	4.96
Standard deviation	0.36	1.56	0.40	0.10
LDH- stearate 14	95.27	9.29	3.67	4.98
LDH- stearate 15	95.27	9.62	3.52	4.94
LDH- stearate 16	95.52	9.73	3.48	4.98
Average	95.35	9.55	3.56	4.97
Standard deviation	0.14	0.23	0.10	0.02

The division indicates samples prepared by two different individuals. The bottom three exhibit exceptionally high carboxylate/Al mol ratios. Discrepancies could have arisen from the pH regulation during synthesis, as well as the washing procedure used for the sample.

Appendix C: LDH-based polymer composites

Injection Moulding Comments

Table C-1. Injection moulding comments on EVA and derivative composites

Mould:	ASTM T.S	
	Set point	Indicated
Temperatures:	(°C)	(°C)
Barrel 1	170	170
Barrel 2	175	176
Barrel 3	180	182
Melt	180	182
Mould	-	RT
Injection time	12 s	
Injection speed	8 mm/s	
Injection pressure	180 bar	
Hold on pressure	85 bar	
Back pressure	10 bar	
Screw speed	50 %	
Cooling time	25 s	
Stroke	22 mm(g)	
Clamping force	350 kN	
Remarks:	Fed with difficulty Moulded with ease Mouldings very rubbery Moulded all samples under the same moulding conditions Short cycle times	

Table C-2: Injection moulding comments on EVAL and derivative composites

Mould:	ASTM T.S	
	Set point	Indicated
Temperatures:	(°C)	(°C)
Barrel 1	190	189
Barrel 2	195	195
Barrel 3	200	200
Melt	200	200
Mould	-	RT
Injection time	15 s	
Injection speed	15 mm/s	
Injection pressure	180 bar	
Hold on pressure	85 bar	
Back pressure	10 bar	
Screw speed	50 %	
Cooling time	25 s	
Stroke	22 mm(g)	
Clamping force	350 kN	
Remarks:	<p>Fed with ease Moulded with ease but stuck to the stationary half of the mould Mouldings very hard Moulded all samples under the same moulding conditions Mouldings hammered out after each shot; long cycle time</p>	

Table C-3. Injection moulding comments on LLDPE and derivative composites

Mould:	ASTM T.S	
	Set point	Indicated
Temperatures:	(°C)	(°C)
Barrel 1	220	219
Barrel 2	210	210
Barrel 3	200	200
Melt	191	190
Mould	-	RT
Injection time	10 s	
Injection speed	10 mm/s	
Injection pressure	180 bar	
Hold on pressure	75 bar	
Back pressure	10 bar	
Screw speed	50 %	
Cooling Time	25 s	
Stroke	22 mm(g)	
Clamping force	350 kN	
Remarks:	Fed with ease Moulded with ease Mouldings tended to shrink Moulded all samples under the same moulding conditions	

Polymer resin product sheets



Polymer-E 百利滿-E
Ethylene-Vinyl Acetate Copolymer Resin
乙 烯 醋 酸 乙 烯 酯 樹 脂

物性 Physical Properties	產品 Products	單 位 Unit	檢驗方法 Test Method (ASTM)	發泡及鑄膜級 Foaming & Casting Grades		
				EV101	EV102	EV103
主要用途 Application				鞋材 運動器材 發泡 流延膜 Shoe Soles Sport Goods Foaming Extrusion Casting	鞋材 運動器材 發泡 流延膜 Shoe Soles Sport Goods Foaming Extrusion Casting	鞋材 運動器材 發泡 流延膜 Shoe Soles Sport Goods Foaming Extrusion Casting
特 性 Characteristics				優異的發泡加工性 優異的成品物性 Good Processability Good Physical Properties	優異的發泡加工性 優異的成品物性 Good Processability Good Physical Properties	優異的發泡加工性 優異的成品物性 Good Processability Good Physical Properties
熔融指數 / Melt Index		公克/10分鐘 g/10min	D1238	1.8	1.5	1.5
密度 / Density		公克立方公分 g/cm ³	D1505	0.941	0.938	0.943
混濁度 / Haze		%	D1003	-	-	-
光澤度 (60°) / Gloss (60°)		%	D523	-	-	-
抗衝擊強度 / Impact Strength		公克, 50% F g/50% Failure	D1709	-	-	-
摩擦係數 / Coefficient of Friction		-	D1894	-	-	-
斷裂點抗張強度 (薄膜) Ultimate Tensile Strength (Film)	MD	公斤/平方公分	D882	-	-	-
	TD	Kg/cm ²		-	-	-
(模壓) / (Molded)	MD	公斤/平方公分	D638	210	200	220
	TD	Kg/cm ²				
1%伸長彈性係數 (薄膜) 1% Secant Modulus (Film)	MD	公斤/平方公分	D882	-	-	-
	TD	Kg/cm ²		-	-	-
伸長率 (薄膜) Elongation (Film)	MD	%	D882	-	-	-
	TD	%		-	-	-
(模壓) / (Molded)	MD	%	D638	730	700	750
	TD	%				
抗撕裂強度 (薄膜) Tear Strength (Film)	MD	公斤/公分	D1922	-	-	-
	TD	Kg/cm		-	-	-
低溫脆裂溫度 Low Temperature Brittleness		°C	D746	< -70	< -70	< -70
韋氏軟化點 Vicat Softening Point		°C	D1525	65	73	63
硬度 Hardness		蕭氏 D Shore D	D2240	35	38	33
熱變形溫度 (66 psi) Heat Deflection Temp. (66 psi)		°C	D648	40	42	38
熔點 / Melting Point		°C	APC Method	82	86	79
醋酸乙烯含量 / VA Content		%	APC Method	18	14	21

Notes : (1) For general purpose and thin gauge film applications, film properties are based on thickness of 1.25 mil (32 micron) extruded on a blown film line at 330°F(165°C) and 2.1 BUR. For Heavy Duty films, properties are based on thickness of 7mil(180micron) and blown at 420°F (215°C) and blow-up ratio 1.8:1.

(2) The data reported are typical properties for reference only and are not to be construed as specification.

說明：(1) 上述之抗張強度、光學性、抗衝擊強度等各項物性是以 50 m/m, L/D 26:1 之擠壓機，吹袋比 2.1:1 和1.8:1 條件，製出厚度為 32 micron/180 micron薄膜樣品之測試結果。

(2) 上述資料均經本公司細心編撰，惟因使用情況之變化，非受本公司控制，恕不負責保證之責。



LLDPE - Product Data Sheet

HR 411

LLDPE

sasol
reaching new frontiers



Date of Issue: February 2002

Print Date: July 2002

Information
Polymer technology centre
P O Box 72
Modderfontein 1645
South Africa

Tel: +27 (0) 11 458 0700
Fax: +27 (0) 11 458 0734

Polyethylene sales
Sasol Polymers
Johannesburg
Tel: +27 (0) 11 790 1250
Cape Town
Tel: +27 (0) 21 686 7740
Durban
Tel: +27 (0) 31 267 0777

www.sasol.com/polymers

Sasol Polymers
Polythene Business

Rotational moulding/injection moulding

Melt index: 3.5 Density: 0.939

Features	Additives	Applications
<ul style="list-style-type: none"> High rigidity Excellent impact strength Excellent chemical resistance Good ESCR Tough and abrasion resistant Colourable Hexene copolymer 	<ul style="list-style-type: none"> Antioxidant 	<ul style="list-style-type: none"> Large mouldings Thick walled containers Articles for indoor use

Performance properties - HR 411

Test	Value	Unit	Test method
MFI (190°C/2.16kg)	3.5	g/10min	ASTM D1238
Nominal density	0.939	g/cm ³	ASTM D1505
Tensile strength at yield	19	MPa	ASTM D638 ¹⁾
Tensile strength at break	24	MPa	ASTM D638 ¹⁾
Elongation at break	820	%	ASTM D638 ¹⁾
Flexural modulus	846	MPa	ASTM D790
ESCR F ₅₀	>500	hr	ASTM D1693 ²⁾
Impact energy at -40°C	35	J/mm	ASTM D3029 ³⁾
Vicat softening temperature	121	°C	ASTM D1525
Shore D hardness	61	Shore D	ASTM D2240

¹⁾ Crosshead speed 50mm/min

²⁾ 100% Igepal C0630

³⁾ Tested on rotomoulded product





LLDPE - Product Data Sheet

sasol
reaching new frontiers



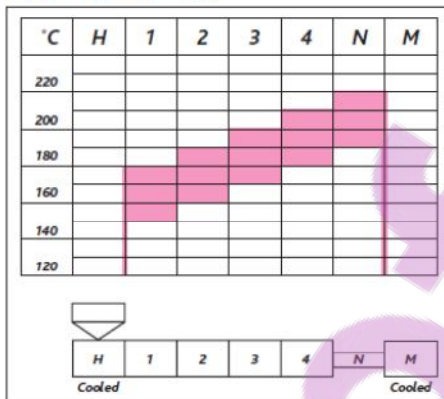
Processing (Rotomoulding)

An air temperature of 270°C to 300°C is recommended for processing of HR 411. Temperatures above 300°C should be avoided as this would narrow the processing window considerably and could result in poor physical properties.

Processing (Injection moulding)

HR 411 has a medium melt viscosity making it unsuitable for moulds with long flow paths. Typical melt temperatures would be 200°C - 280°C. Parts can be demoulded at relatively high temperatures due to the material's high melting point and rigidity.

Typical temperature profile (Injection moulding)



Presentation

Supplied in pellet form packed in 25kg bags. Grinding of pellets is required to make it suitable for rotomoulding.

Handling

Workers should be protected from the possibility of skin or eye contact with molten polymer. Safety glasses are suggested as a minimal precaution to prevent possible mechanical or thermal injury to the eyes. Fabrication areas should be ventilated to carry away fumes or vapours.

Combustibility

Polyethylene resins will burn when supplied with adequate heat and oxygen. They should be handled and stored away from contact with direct flames and/or other ignition sources. In burning, polyethylene resins contribute high heat and may generate a dense black smoke. Fires can be extinguished by conventional means, with water and water mist preferred. In enclosed areas, fire fighters should be provided with self-contained breathing apparatus.

Pigmentation (Rotomoulding)

For colouring purposes inorganic pigments should be added at the lowest possible concentration and mixed in using a high speed mixer or a tumble blender, prior to moulding. Pigment preparations should contain only minimal amounts of dispersants.

Food Packaging

This material complies with F&DA regulation 177.1520 when used unmodified and according to good manufacturing practices for food contact applications. Accordingly, this material may be used in all food contact applications (except holding food during cooking).

Conveying

Conveying equipment should be designed to prevent accumulation of fines and dust particles that are contained in all polyethylene resins. These fines and dust particles can, under certain conditions, pose an explosion hazard. We recommend the conveying system used:

1. be equipped with adequate filters;
2. is operated and maintained in such a manner to ensure no leaks develop;
3. that adequate grounding exists at all times.

We further recommend good housekeeping be practised throughout the facility.

Storage

As ultraviolet light may cause a change in the material, all resins should be protected from direct sunlight during storage.

This information is based on our current knowledge and experience. In view of many factors that may affect processing and application, this data does not relieve processors from the responsibility of carrying out their own tests and experiments, neither does it imply any legally binding assurance of certain properties or of suitability for a specific purpose. It is the responsibility of those to whom we supply our products to ensure that any proprietary rights and existing laws and legislation are observed.



 Building better barriers					
Datasheet Typical Properties of EVAL™ Resin					
EVAL™ T101B					
	Test method		Unit	Value	
Ethylene Content	Kuraray Method		mol %	32	
Oxygen Transmission Rate	ISO 14663-2 annexC	20°C 0%RH	cm³.20µm/m².day.atm	0.23	
	ISO 14663-2 annexC	20°C 35%RH	cm³.20µm/m².day.atm		
	ISO 14663-2 annexC	20°C 50%RH	cm³.20µm/m².day.atm		
	ISO 14663-2 annexC	20°C 65%RH	cm³.20µm/m².day.atm		0.5
	ISO 14663-2 annexC	20°C 85%RH	cm³.20µm/m².day.atm		
	ISO 14663-2 annexC	20°C 90%RH	cm³.20µm/m².day.atm		1.8
ISO 14663-2 annexC	20°C 100%RH	cm³.20µm/m².day.atm			
Water Vapour Transmission Rate	ASTM E96-E		g.30µm/m².day.	37	
Density	ISO 1183		kg/m³	1.17	
Yield Stress	ISO 527		MPa		
Stress at Break	ISO 527		MPa		
Yield Strain	ISO 527		%		
Strain at Break	ISO 527		%		
Young's Modulus	ISO 527		MPa		
Flexural Modulus	ISO 178		MPa		
Izod Impact Strength	ISO 180		kJ/m²		
Izod at -40°C	ISO 180				
Charpy Impact Strength	ISO 179-1		kJ/m²		
Charpy at -40°C	ISO 179-1		kJ/m²		
Rockwell Hardness	ISO 2039-2		M		
Melting Temperature	ISO 11357		°C	183	
Crystallisation Temperature	ISO 11357		°C	161	
Glass Transition Point	ISO 11357		°C	69	
Vicat Softening Point	ISO 306		°C		
Melt Mass-Flow Rate	ISO1133	190°C	g/10min	1.7	
	ISO1133	210°C	g/10min	4.3	
	ISO1133	230°C	g/10min		
	ISO1133	250°C	g/10min		
Contact:	EVAL Europe nv Haven 1053 - Nieuwe Weg 1, bus 10 2070 Zwijndrecht (Antwerp), Belgium Tel +32 3 250 9733 Fax +32 3 250 9745				
Data updated on:	18-nov-04				
Layout updated on:	11-dec-06				
Note: The information and data contained in this document are believed to be correct and are given in good faith. However, no liability, warranty or guarantee of final product performance is created by this document. No freedom from any patent is granted or to be inferred. This document does not constitute a sales specification and the EVAL Europe nv Sales Contract General Terms and Conditions continue to apply.					
		EVAL Europe nv Haven 1053 Nieuwe Weg 1 - Bus 10 B-2070 Zwijndrecht (Antwerp) Belgium Telephone +32 3 250 97 33 Fax +32 3 250 97 04 www.eval.be VAT BE 0461.831.747 RPR Antwerpen			

FT-IR of Composites

Figure C-1 shows the FTIR results of the LDH-stearate and each of the 10 wt% composites prepared. The LDH-CO₃ exhibits a broad band at 3455 cm⁻¹, which is characteristic of the hydroxyl stretching vibration of free hydrogen, hydrogen bonded to the octahedral layer and water molecules. The LDH-CO₃ has a peak at 1360 cm⁻¹, which is attributed to carbonate anions. For the LDH-St there is minimal carbonate contamination as the peak within the specified area is weak or in some cases absent. The OH stretching vibrations are also observed, as well as a shoulder between 3247 and 3225 cm⁻¹, which is attributed to the water molecules bonded to the interlayer anion by hydrogen bonding. The peaks between 2940 and 2847 cm⁻¹ are assigned to -CH₂ asymmetric and symmetric vibrations of aliphatic groups, while the peaks at 1630 and 1462 cm⁻¹ are due to O-H deformation of entrapped water molecules and CH₂ deformation respectively. The CH₂ wagging modes are also observed in the 1300–1250 cm⁻¹ range. The 1534 cm⁻¹ peak is due to the symmetric stretching mode of the ionised -C-O group. The M-O in-plane stretching and deformation of the LDH metal lattice is observed between 1000 and 719 cm⁻¹. Generally, all these peaks are preserved in the composite materials. However, a few peaks from the polymer overlap with those in the LDH stearate, e.g. the OH band overlaps with that of the LDH-St and EVAL due to the existence of OH groups in the polymer itself. However, the -OH band in the EVAL/LDH-St composite broadens and its intensity is reduced. This could be attributed to the interaction of the -OH groups of the metal hydroxide with that of the polymer. This band is retained in the EVA and LLDPE composites, pointing to no interaction of the aforementioned functional groups. The peaks at 1735 and 1235 cm⁻¹ in the EVA samples are a result of O-C=O carbonyl stretching vibrations of the ester and asymmetric vibration of the C-O-C bond respectively.

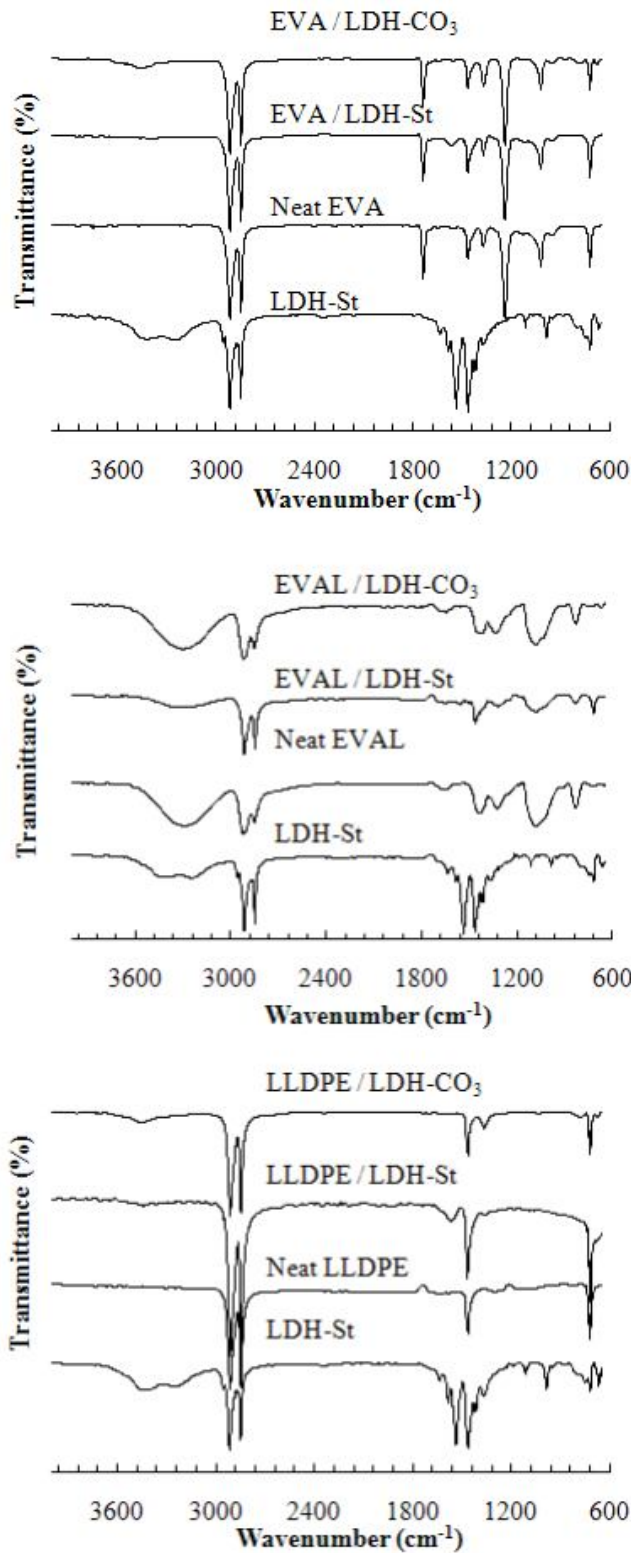


Figure C-1. FTIR of the neat and composite derivatives

Low magnification

High magnification

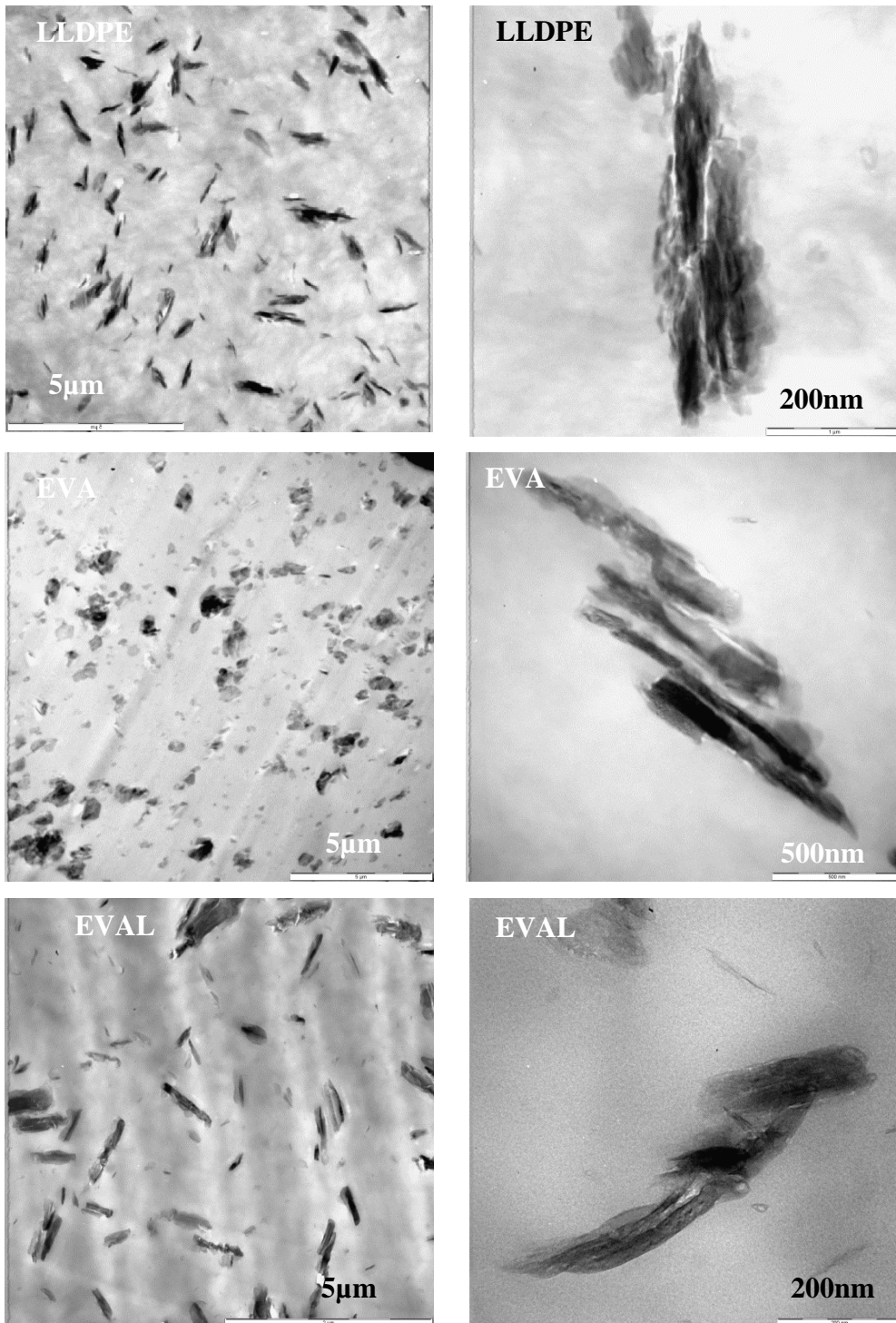


Figure C-2. TEM micrographs of the 5 wt.% LDH-carbonate polymer composites

Low magnification

High magnification

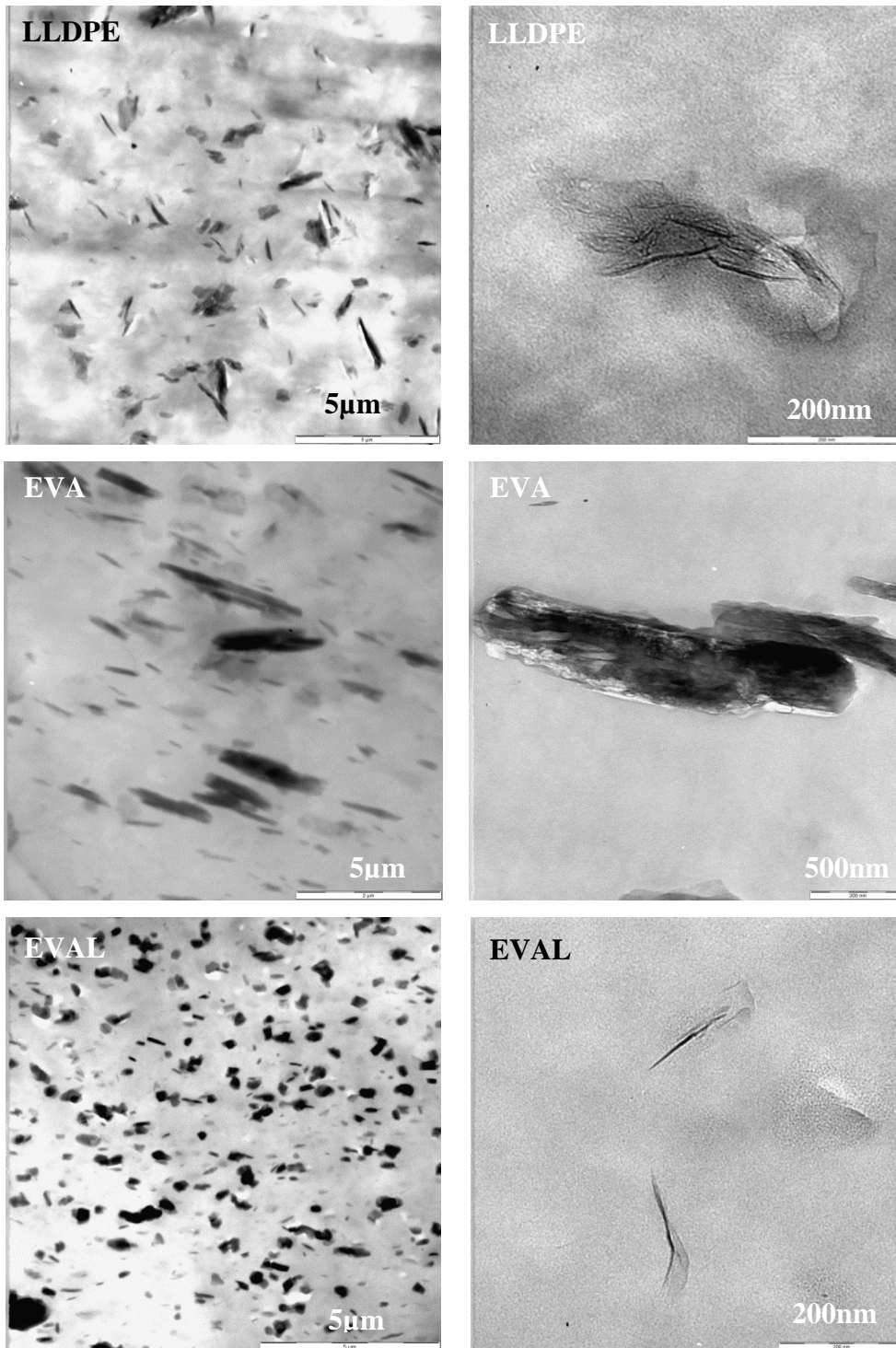


Figure C-3. TEM micrographs of the 5 wt.% LDH-stearate polymer composites

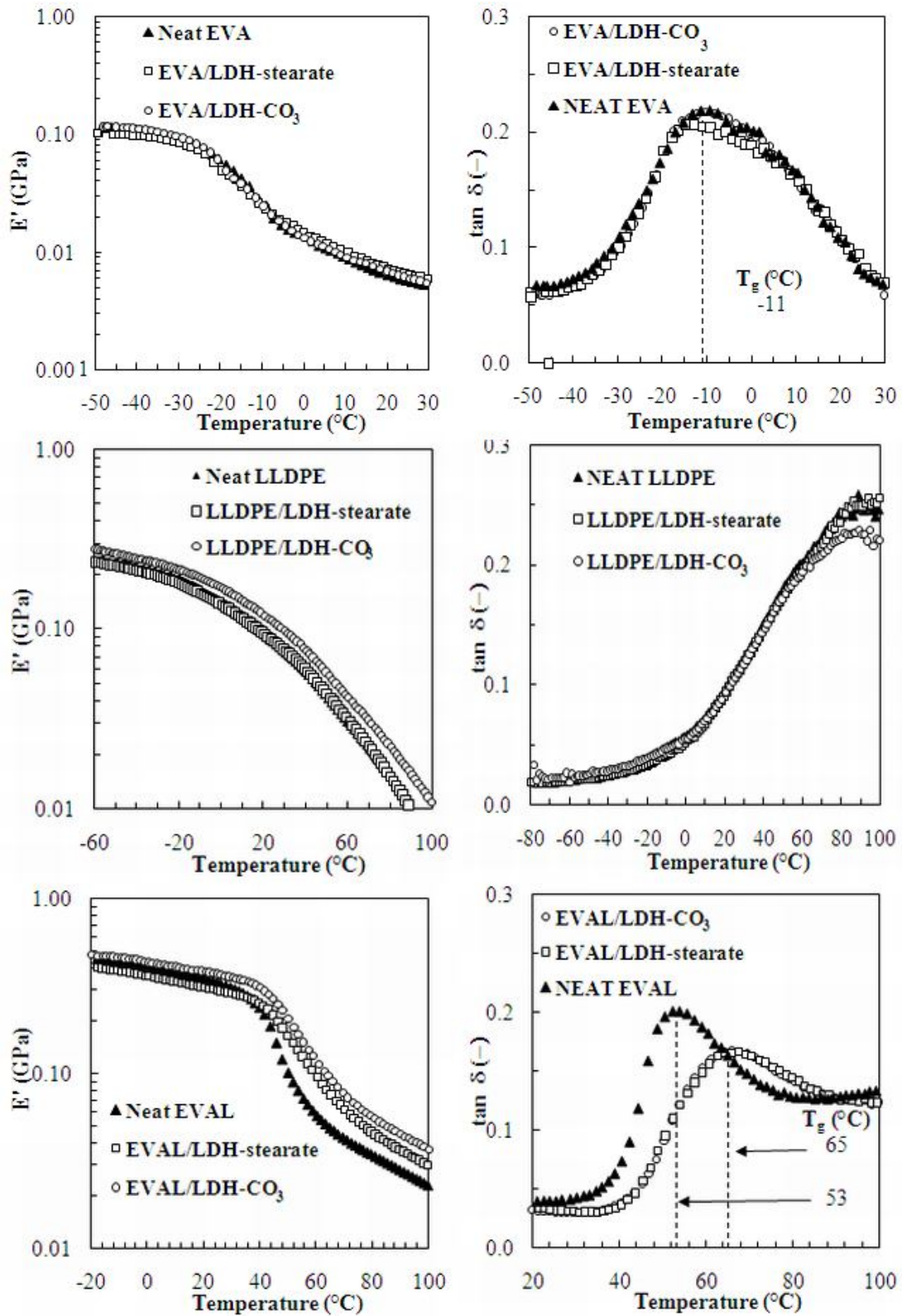


Figure C-4. Dynamic mechanical properties of 5% filler formulations

Mechanical Properties

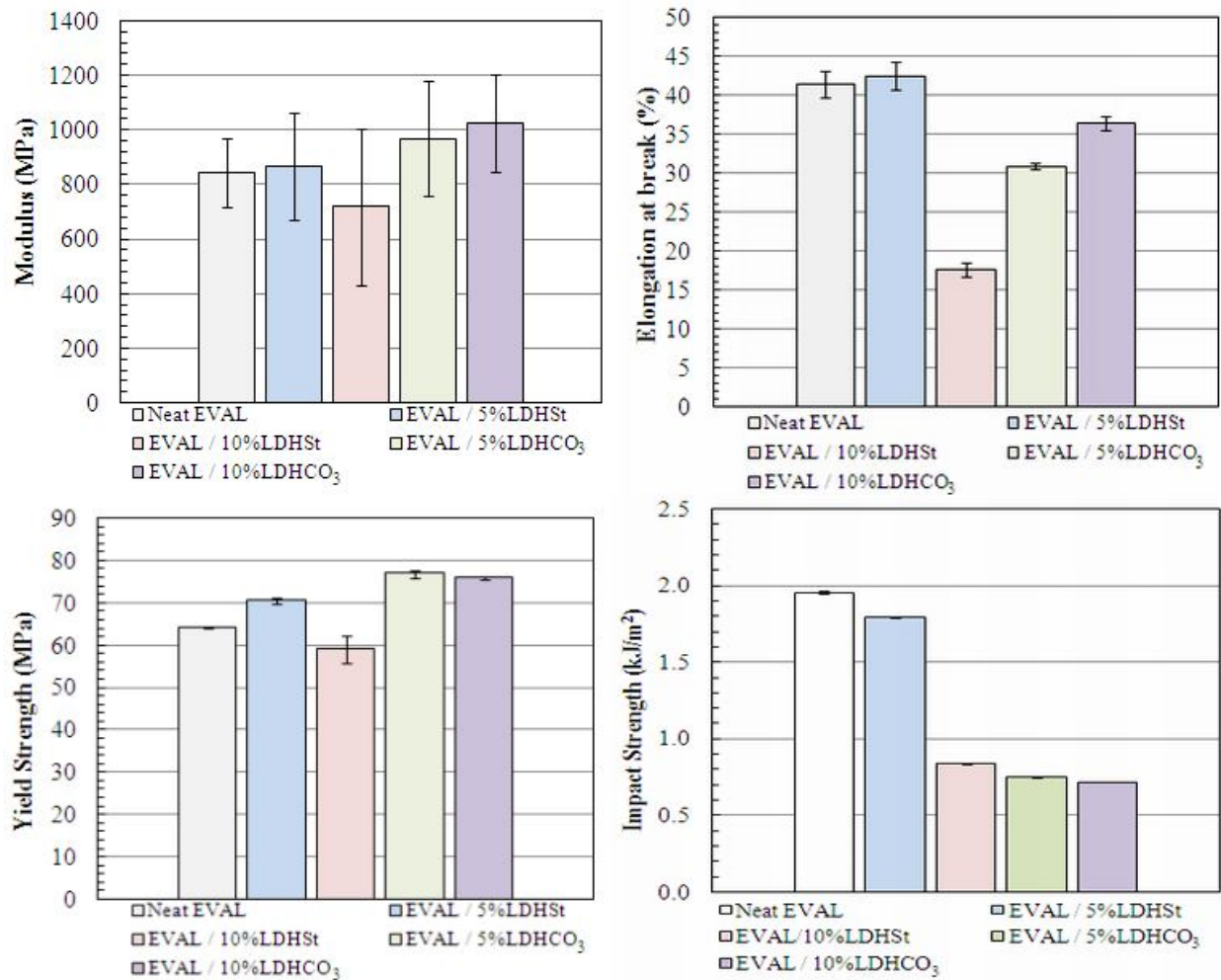


Figure C-5. Tensile strength and tensile impact test summary of neat EVAL and derivative composites

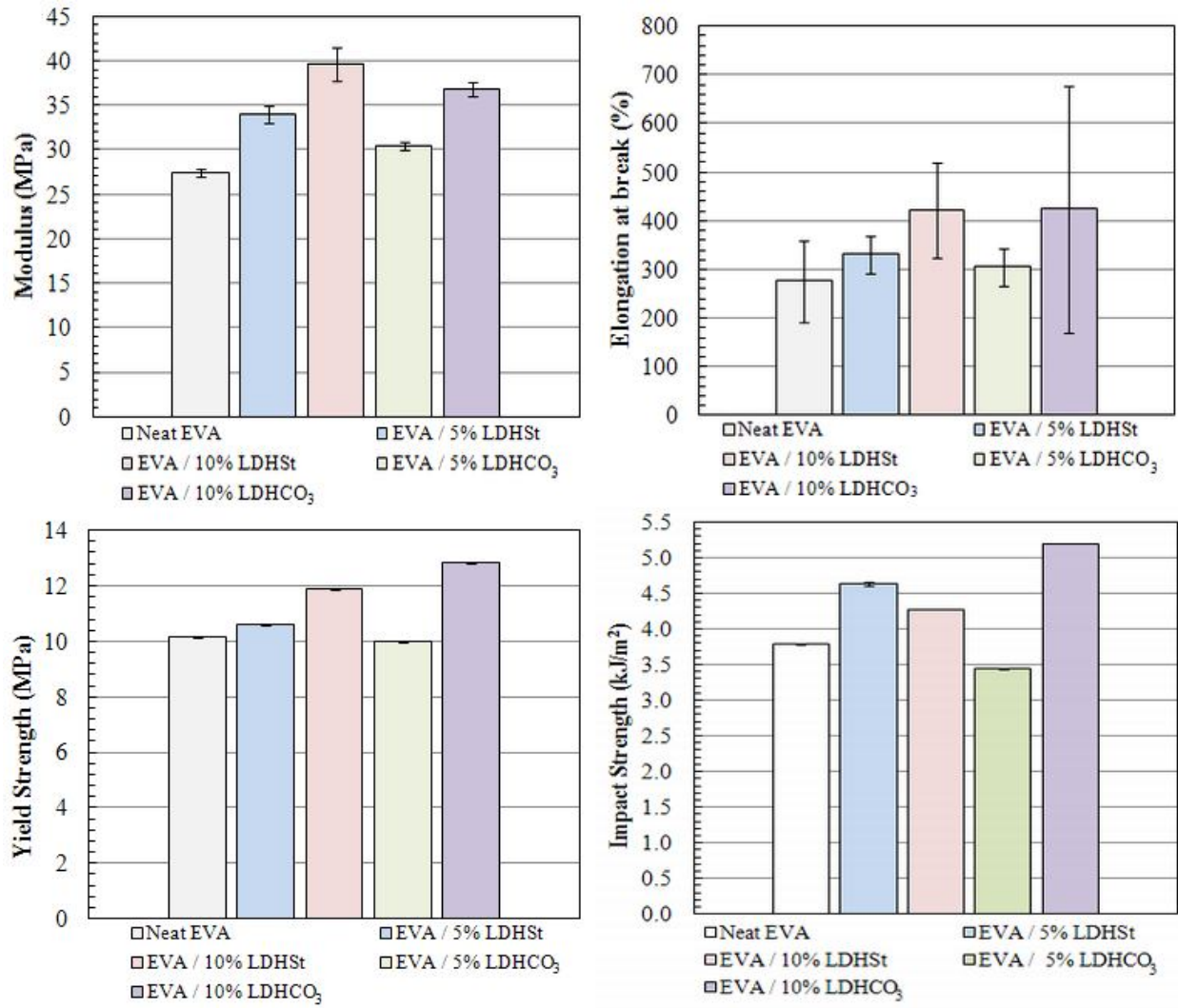


Figure C-6. Tensile strength and tensile impact test summary of neat EVA and derivative composites

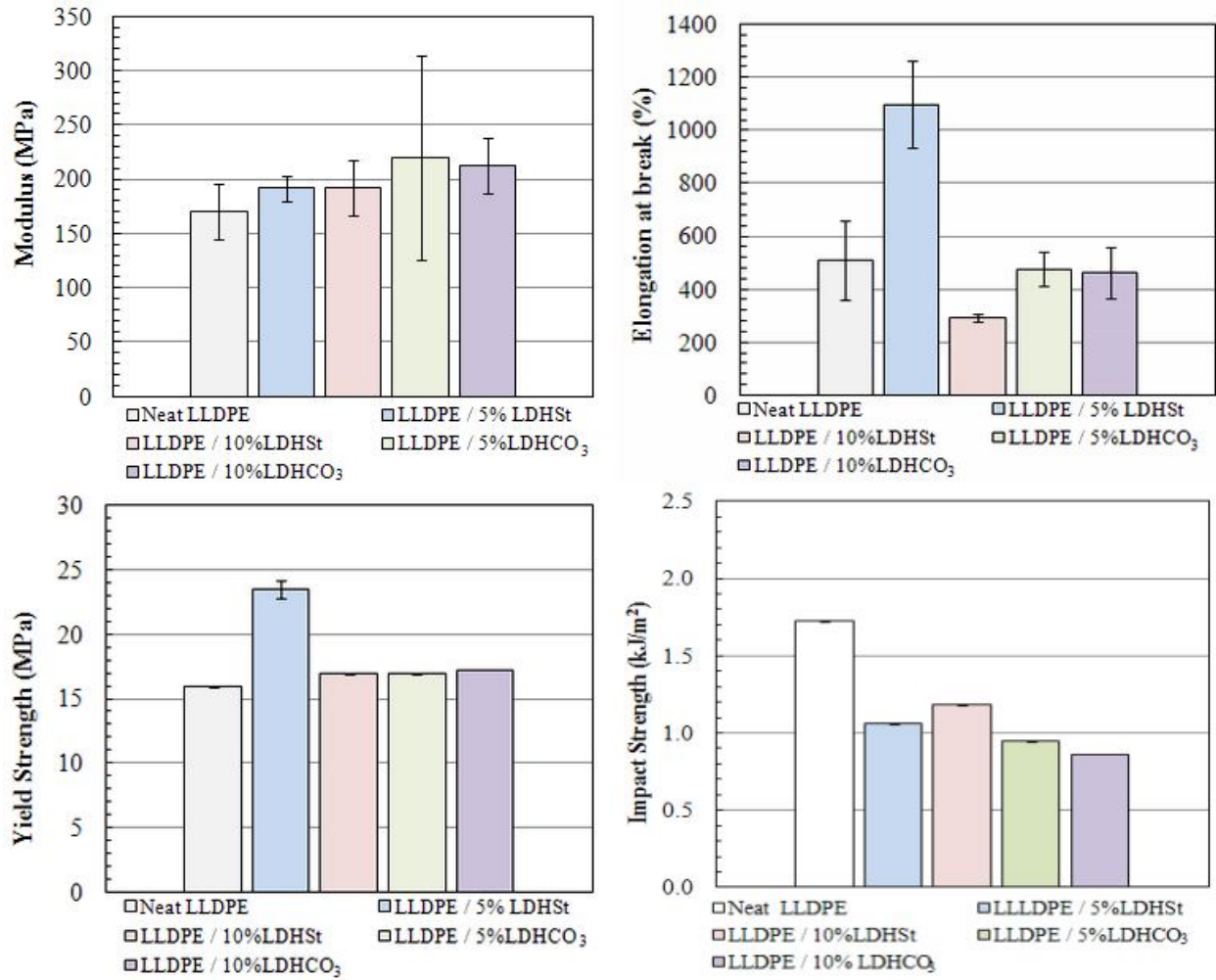


Figure C-7. Tensile strength and tensile impact test summary of neat LLDPE and derivative composites

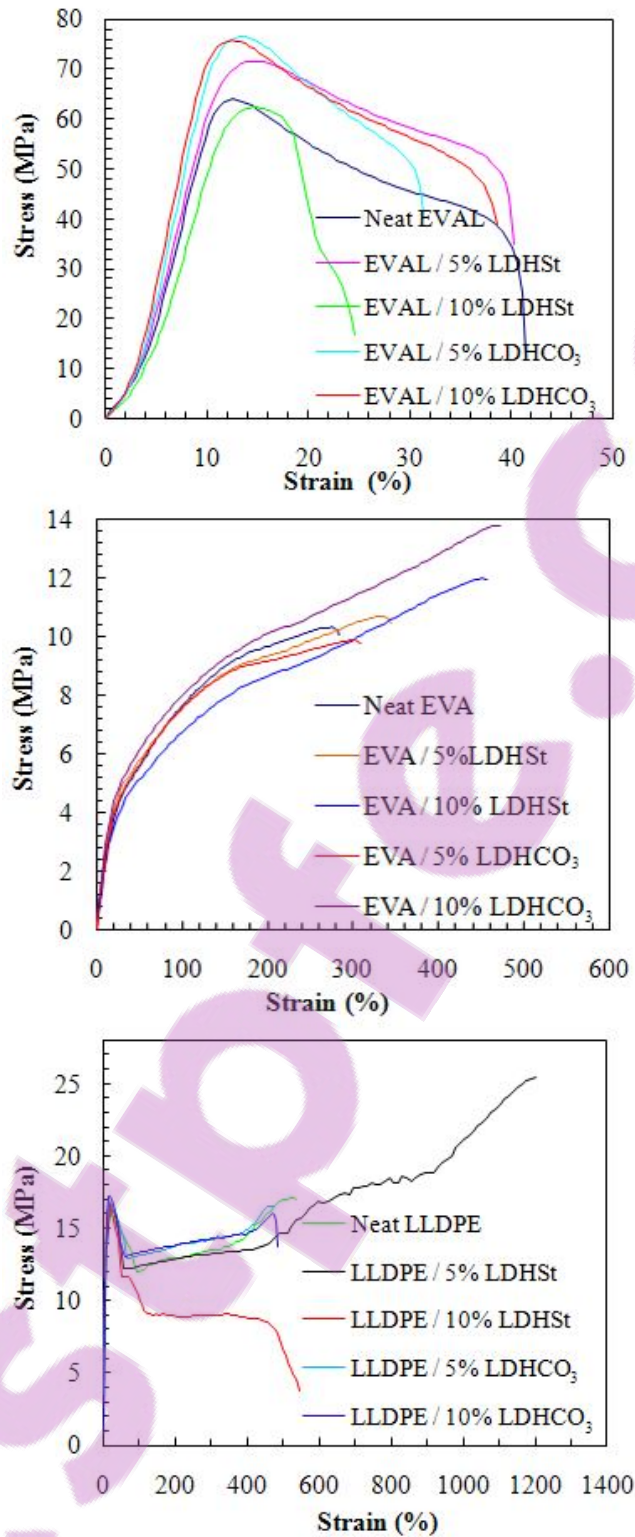


Figure C-8. Tensile test results

Fracture Behaviour

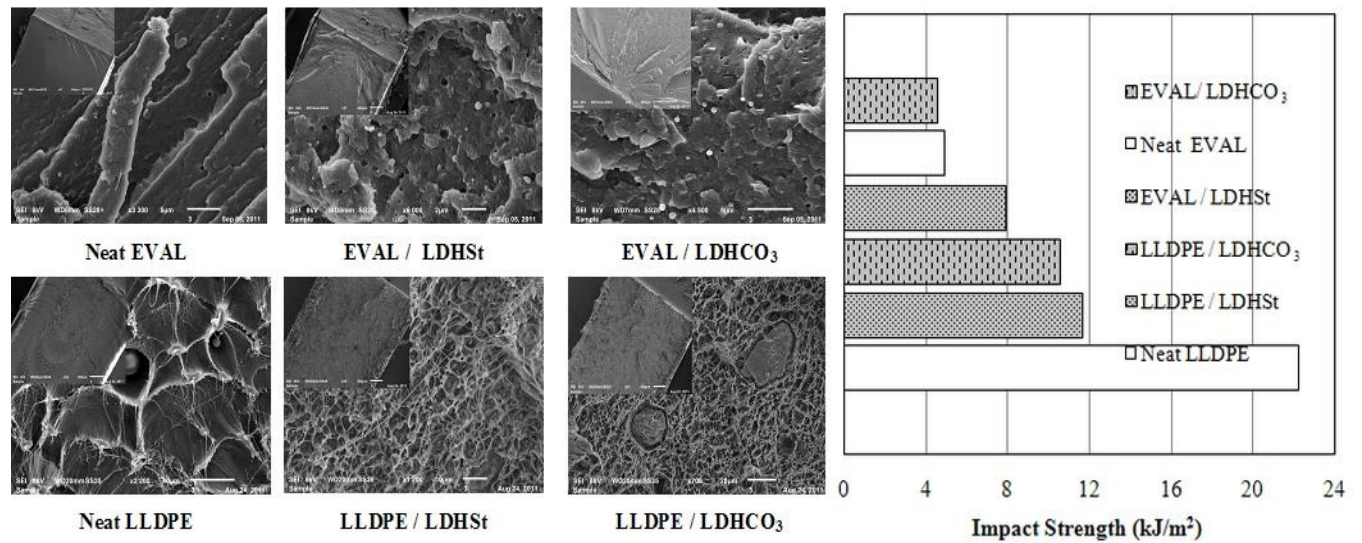


Figure C-9. SEM micrographs of fractured surfaces from the Charpy impact test and corresponding data (composites of 10 wt.% LDH)

Figure C-9 shows SEM micrographs of the Charpy impact specimens of the LDH/polymer composite samples. As mentioned earlier, breaks were observed in the EVAL and LLDPE samples. The two matrix systems show two different types of break, i.e. a brittle and a ductile break for the EVAL and LLDPE composites respectively. The EVAL specimens show a classic brittle break, with a mirror region extending radially outward from the initial flaw, forming a hackled region. Normally, fracture is perpendicular to polymer fibres, but angular cracks and breaks are observed in the composite samples. A closer look at the inserts of EVAL composites shows a granular fracture, implying that the addition of the LDH induces strong association within the polymer matrix. It is clear that the adhesion between the EVAL and the LDH is good as there is no clear distinction between the platelets and the polymer. The polymer continued to cover the LDH particles at the time of fracture.

DSC Data

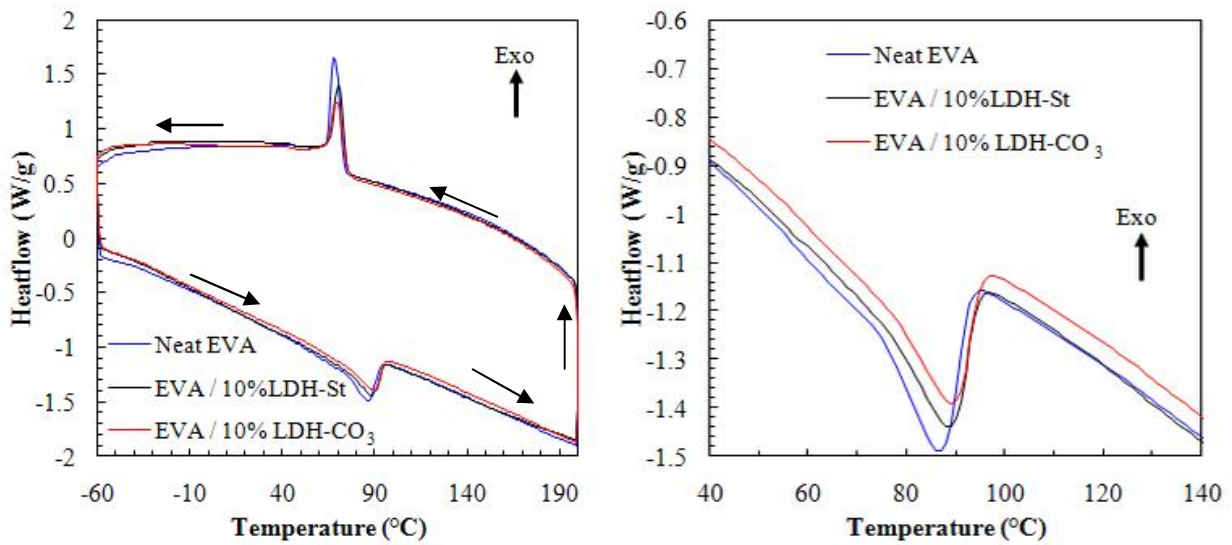


Figure C-10. DSC scans of EVA and derivative composites

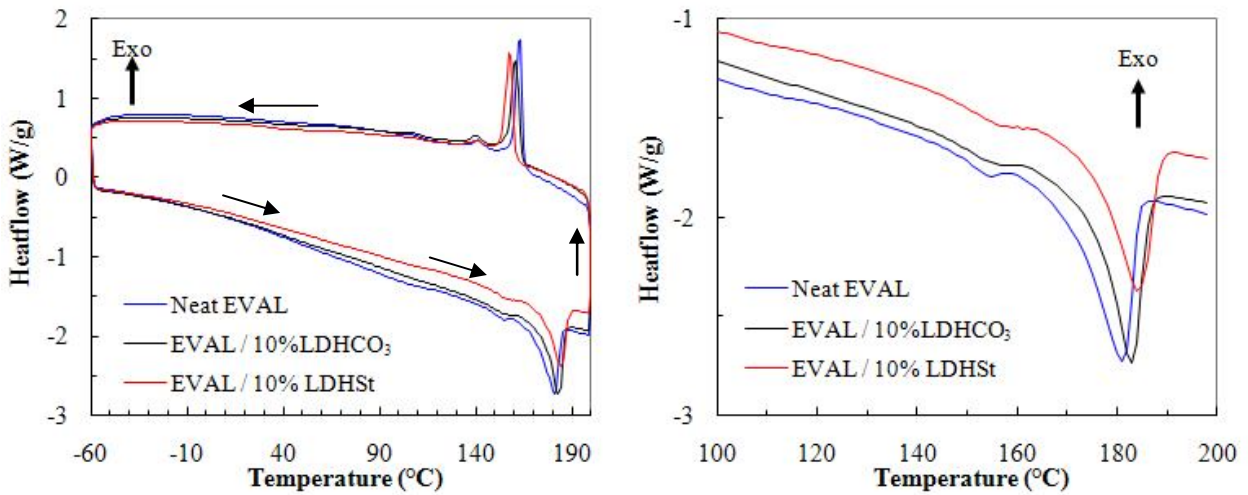


Figure C-11. DSC scans of EVAL and derivative composites

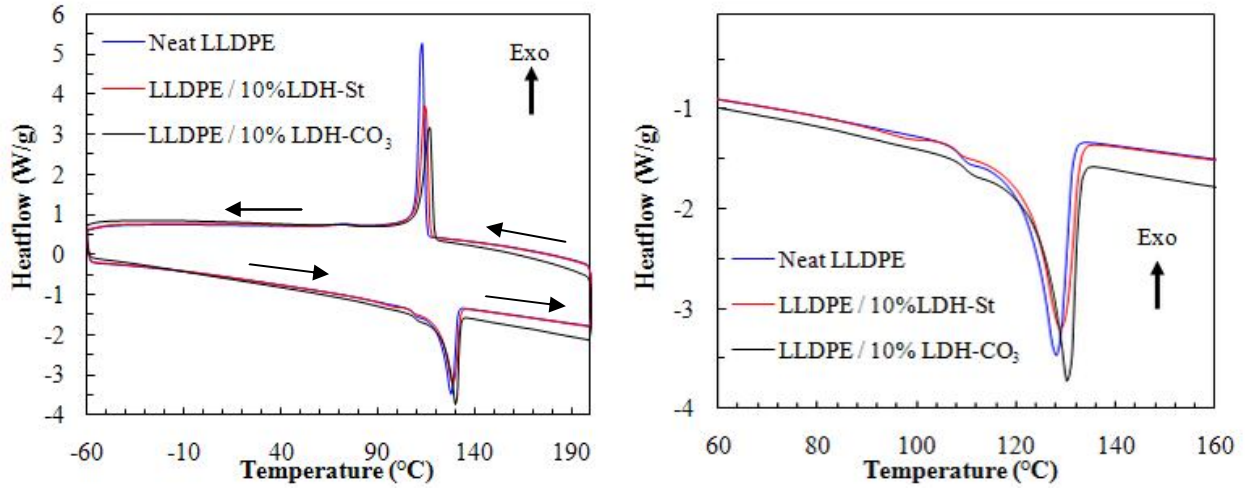


Figure C-12. DSC scans of LLDPE and derivative composites

The figures below are DSC scans of the 5% LDH loading. A slight change is observed in the melting and crystallisation temperatures of each of the filled systems.

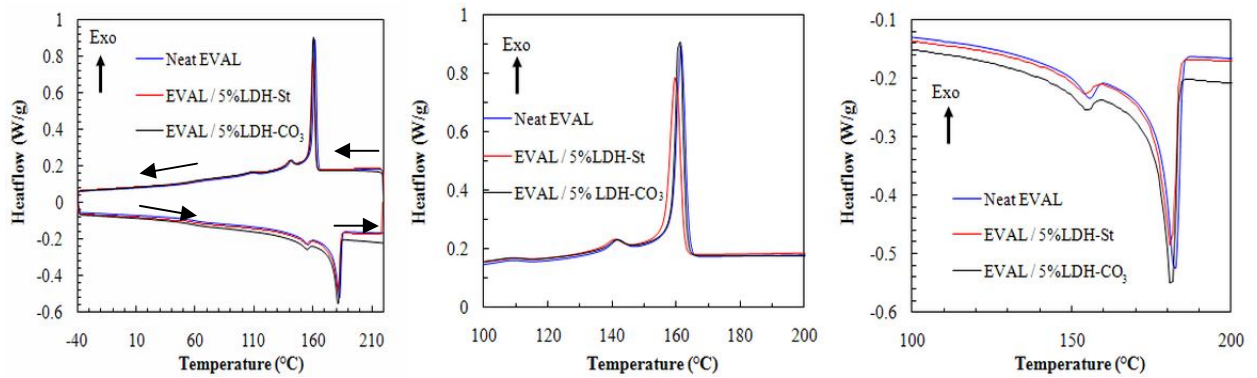


Figure C-13. DSC scans of EVAL and derivative composites

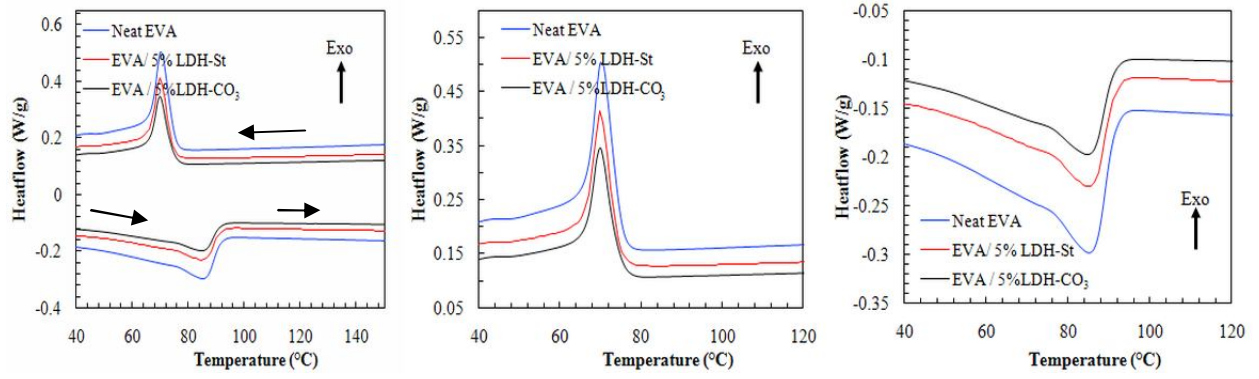


Figure C-14. DSC scans of EVA and derivative composites

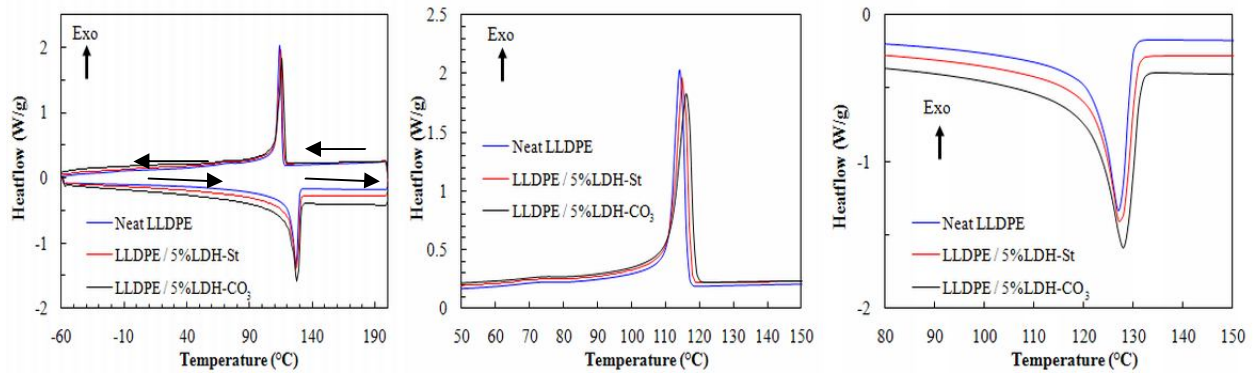


Figure C-15. DSC scans of LLDPE and derivative composites

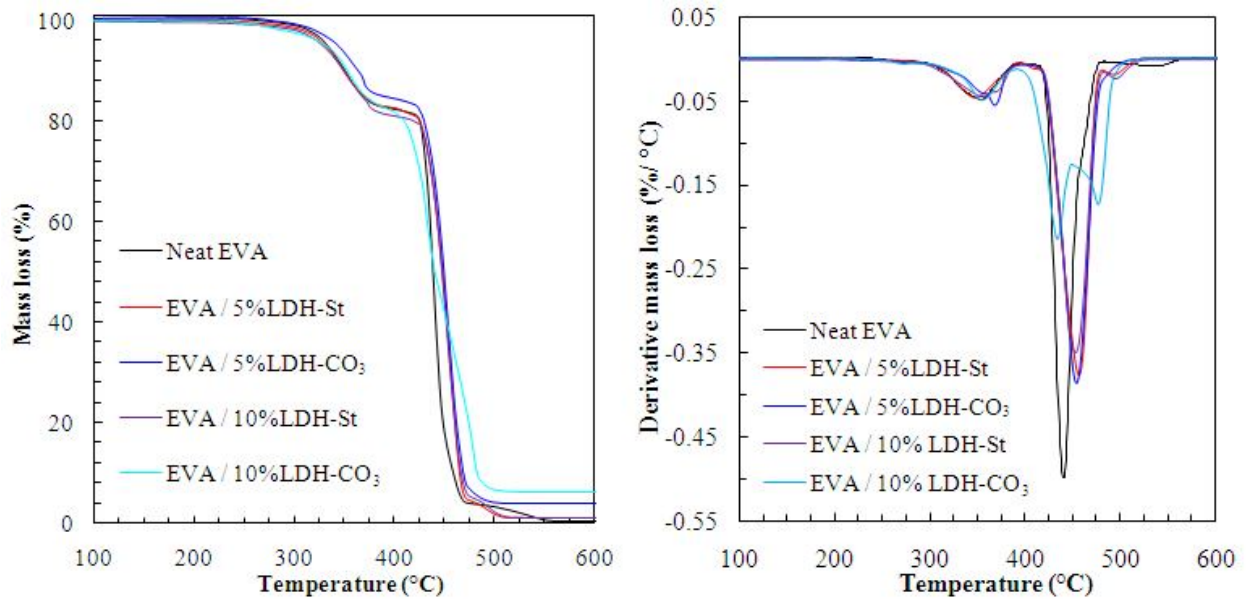


Figure C-16. TG data of EVA and derivative composites

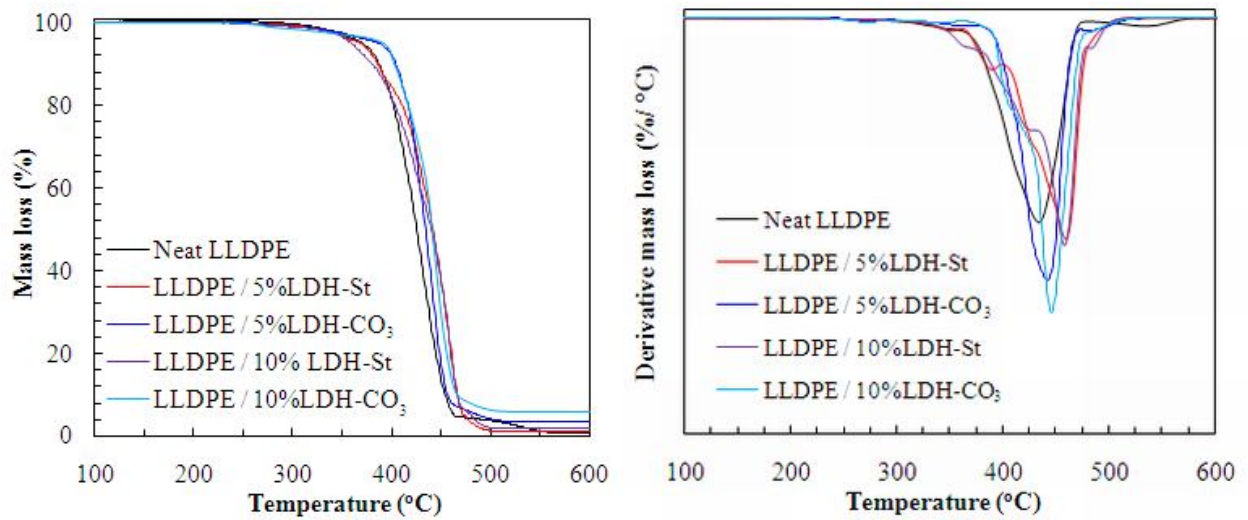


Figure C-17. TG data of LLDPE and derivative composites

Evolved Gas Analysis

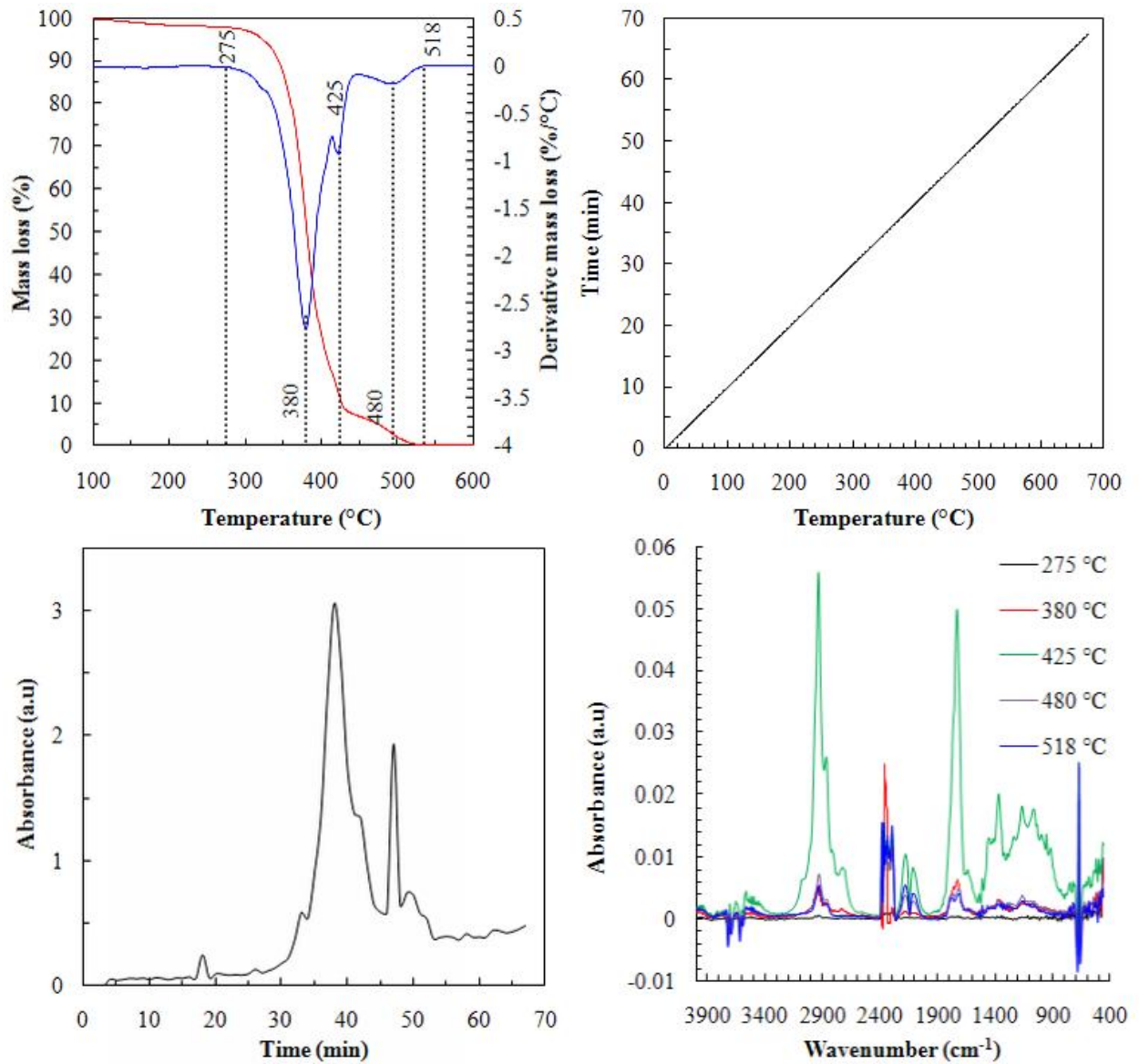


Figure C-18. Evolved gas analysis of neat EVAL by TG-FTIR

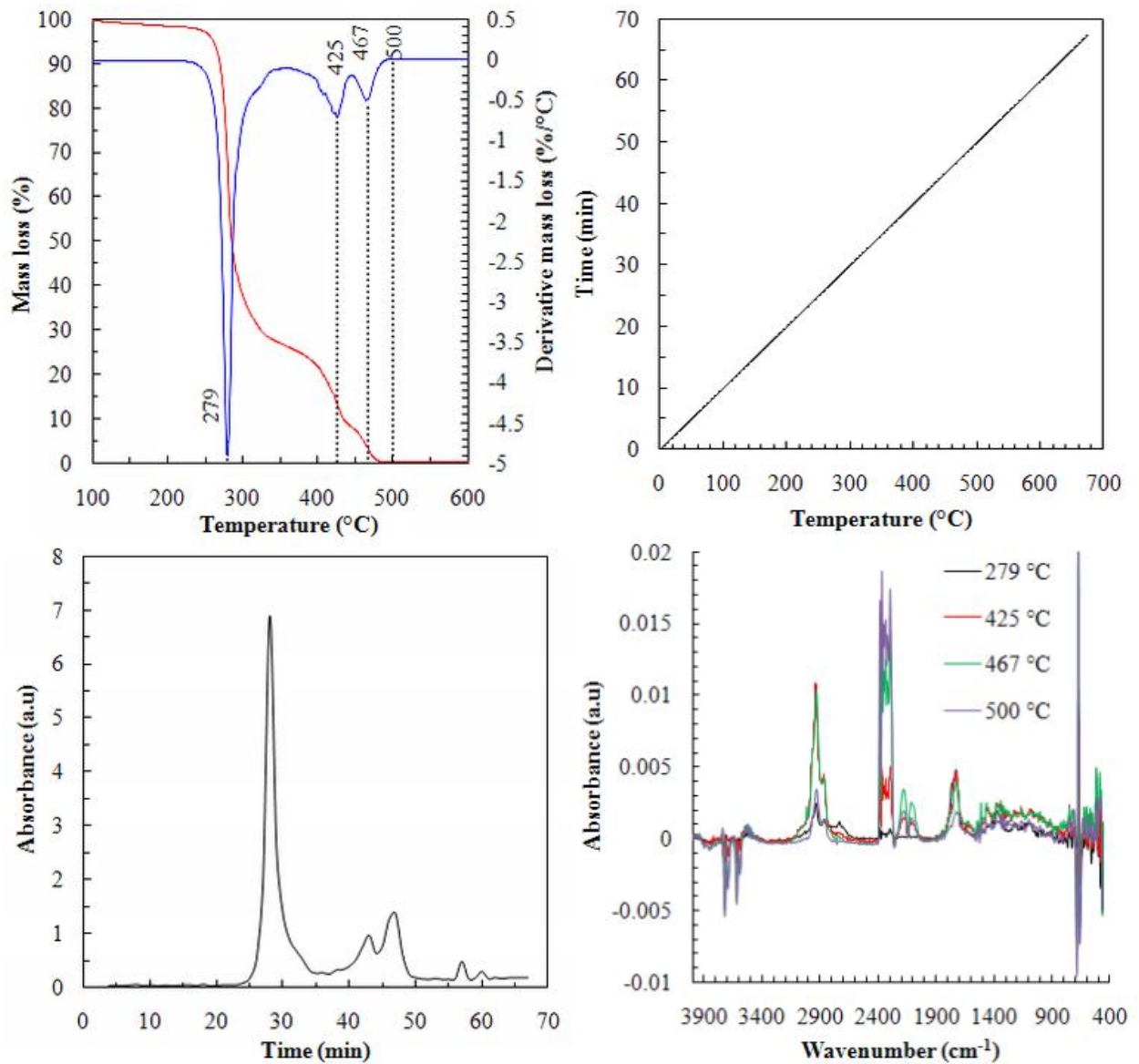


Figure C-19. Evolved gas analysis of EVAL/5% LDH-St by TG-FTIR

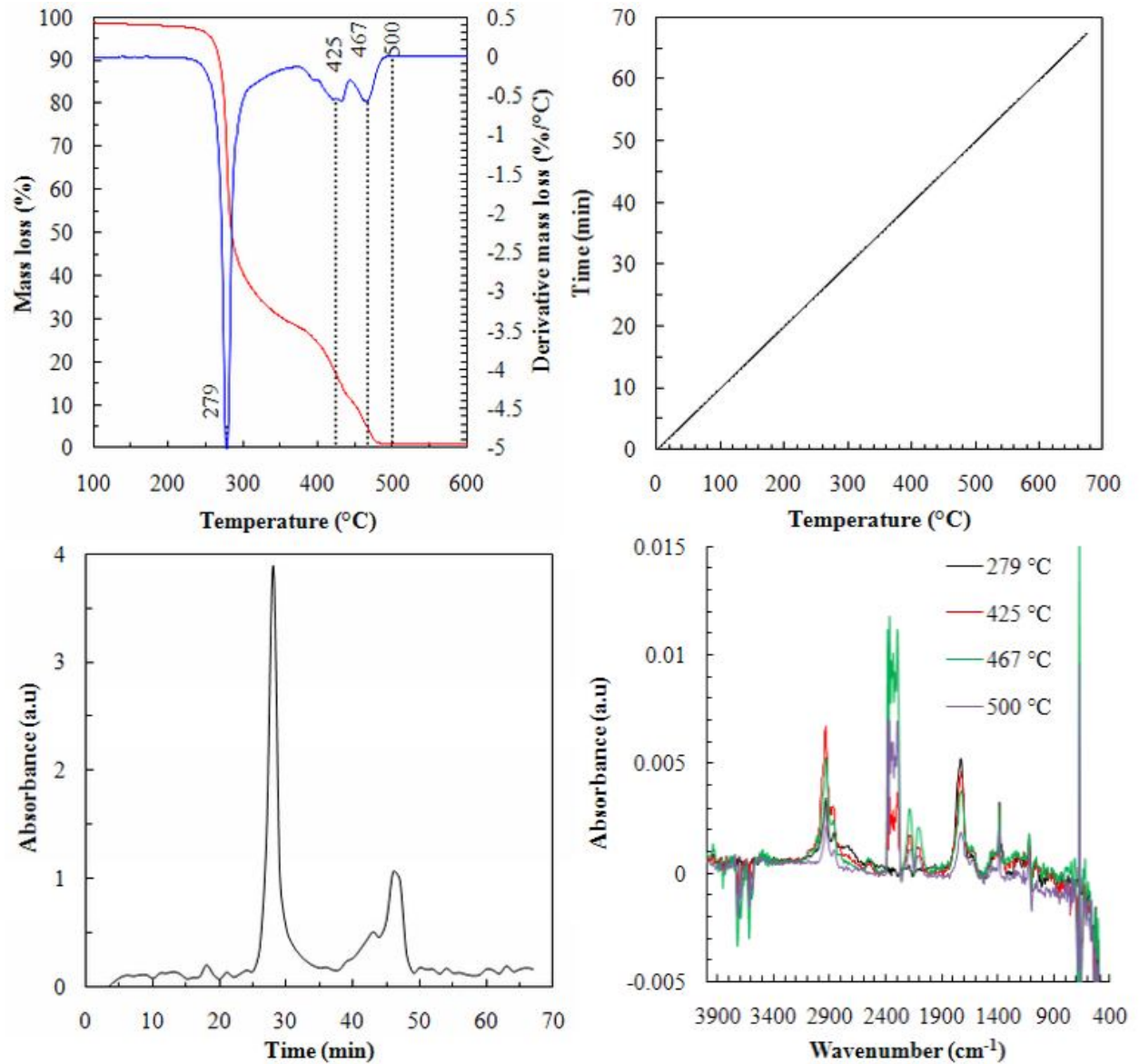


Figure C-20. Evolved gas analysis of EVAL/10% LDH-St by TG-FTIR

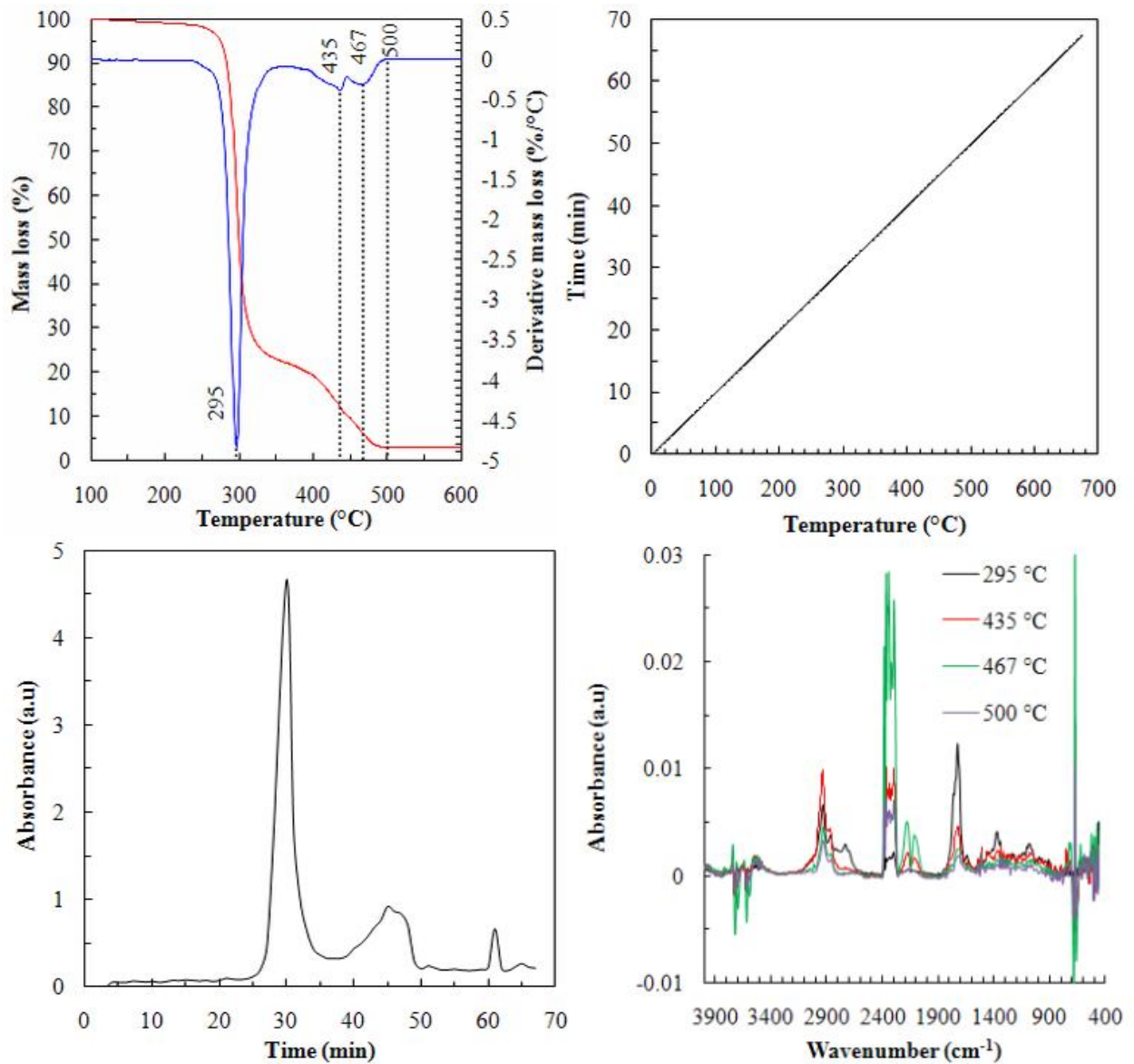


Figure C-21. Evolved gas analysis of EVAL/5% LDH-CO₃ by TG-FTIR

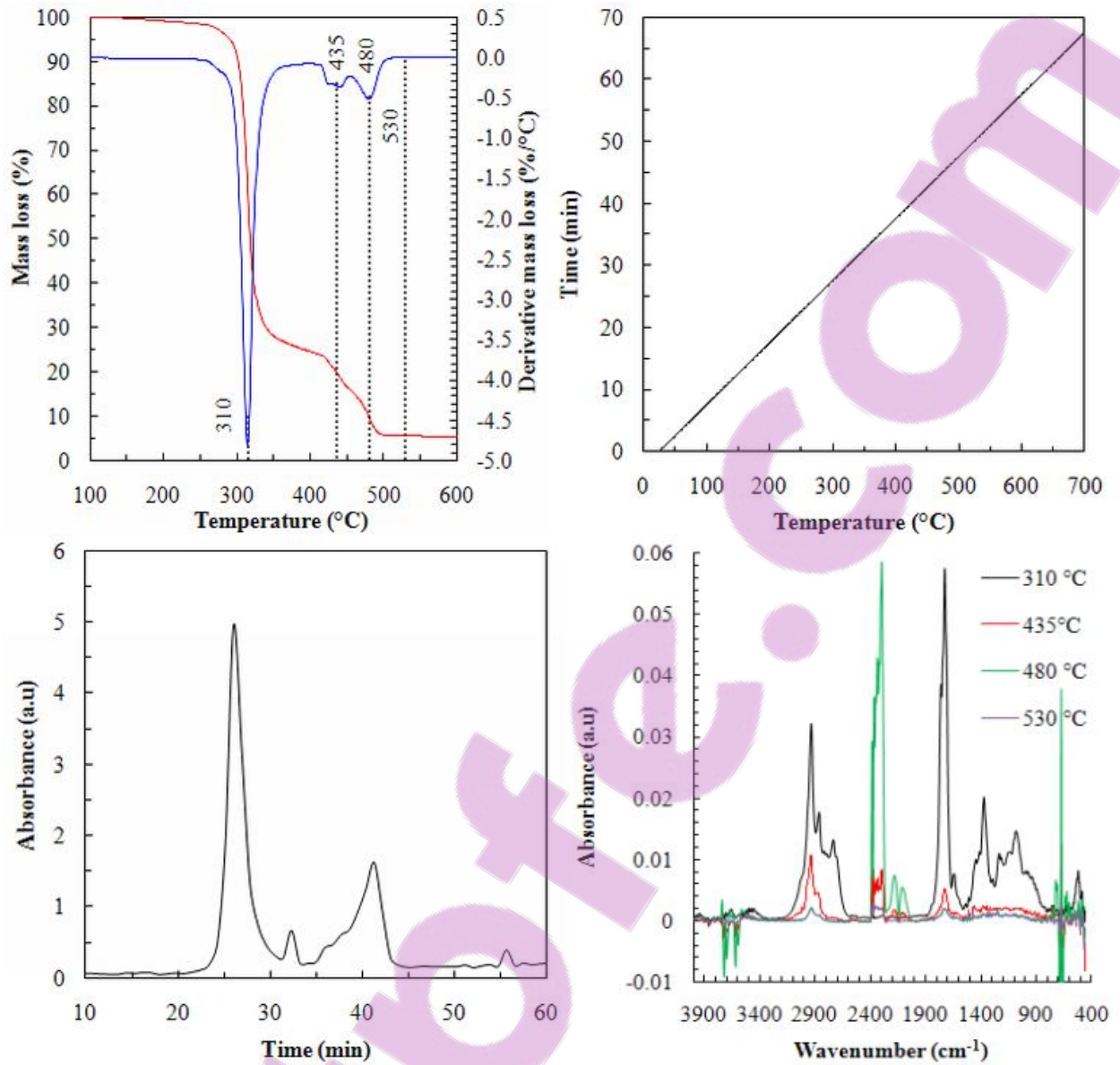


Figure C-22. Evolved gas analysis of EVAL/10% LDH-CO₃ by TG-FTIR

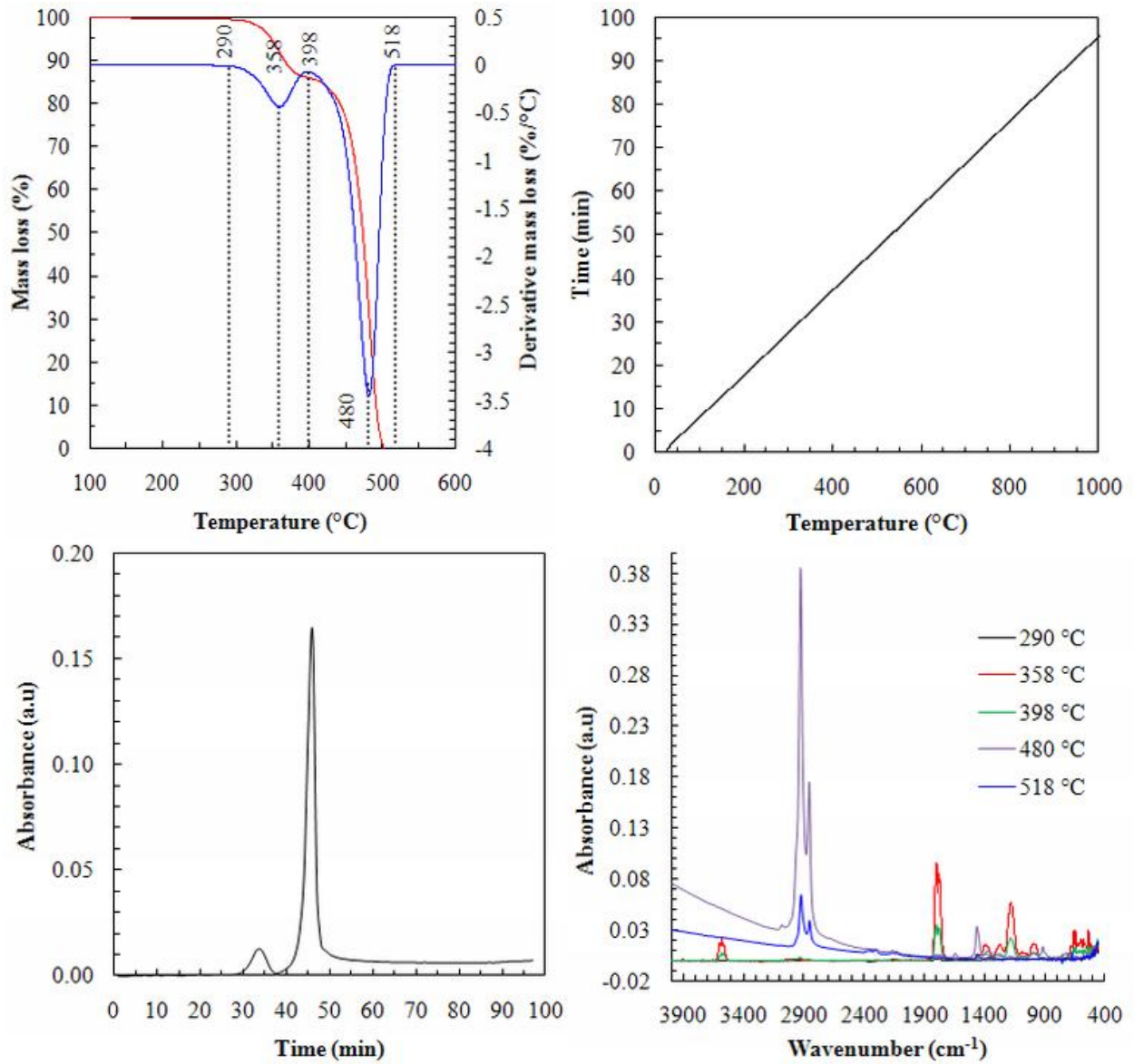


Figure C-23. Evolved gas analysis of neat EVA by TG-FTIR

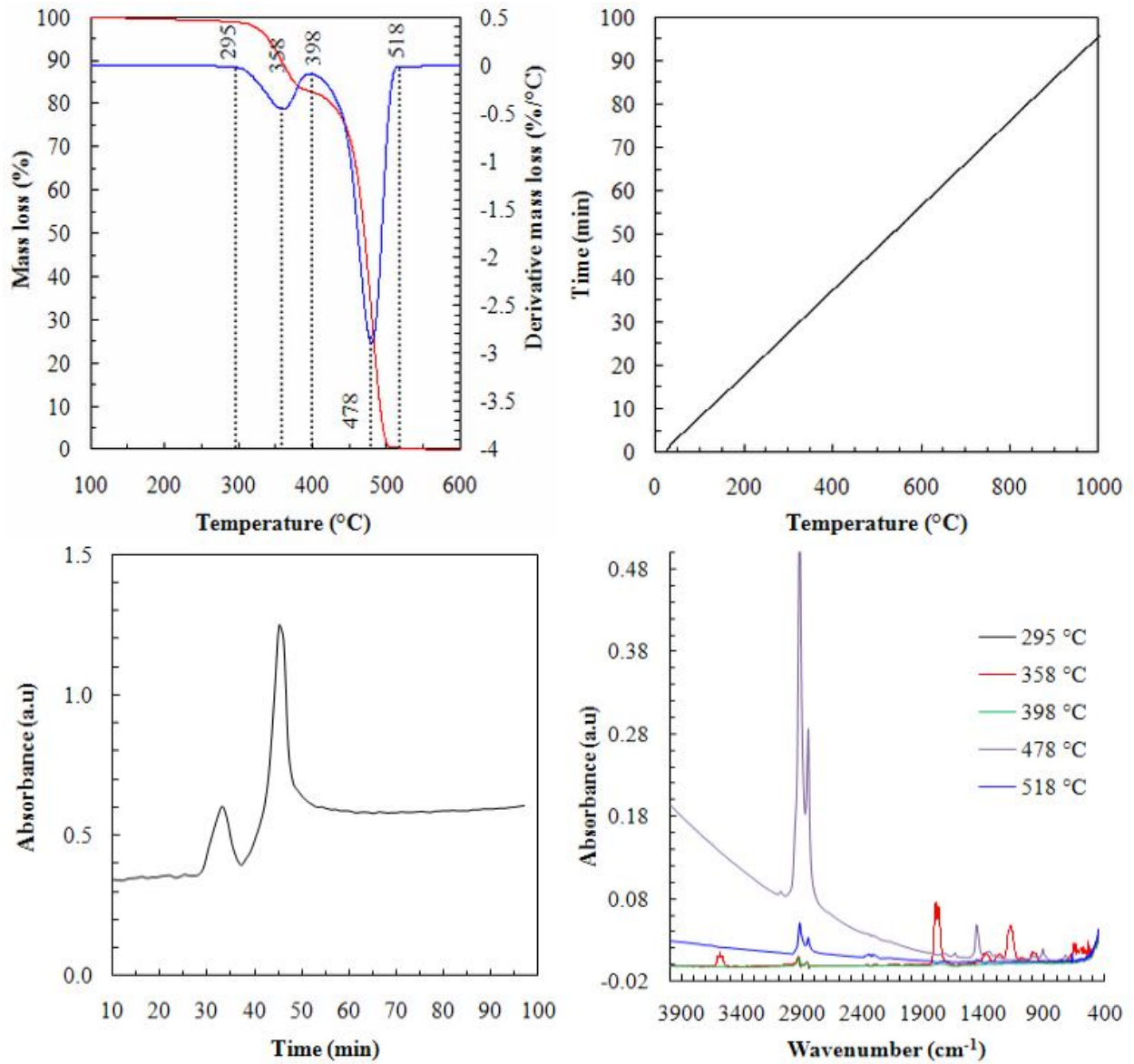


Figure C-24. Evolved gas analysis of EVA/5% LDH-St by TG-FTIR

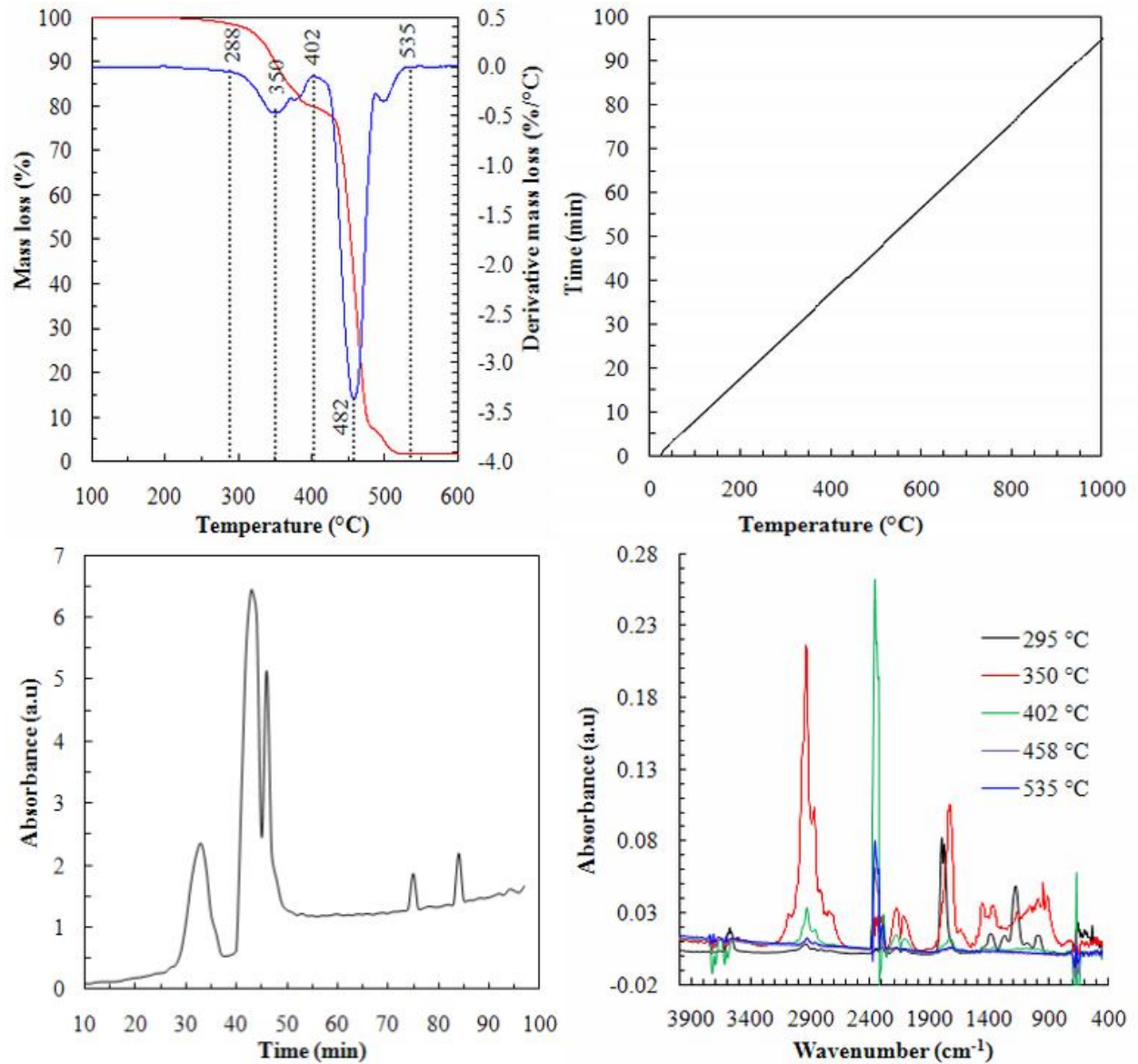


Figure C-25. Evolved gas analysis of EVA/10% LDH-St by TG-FTIR

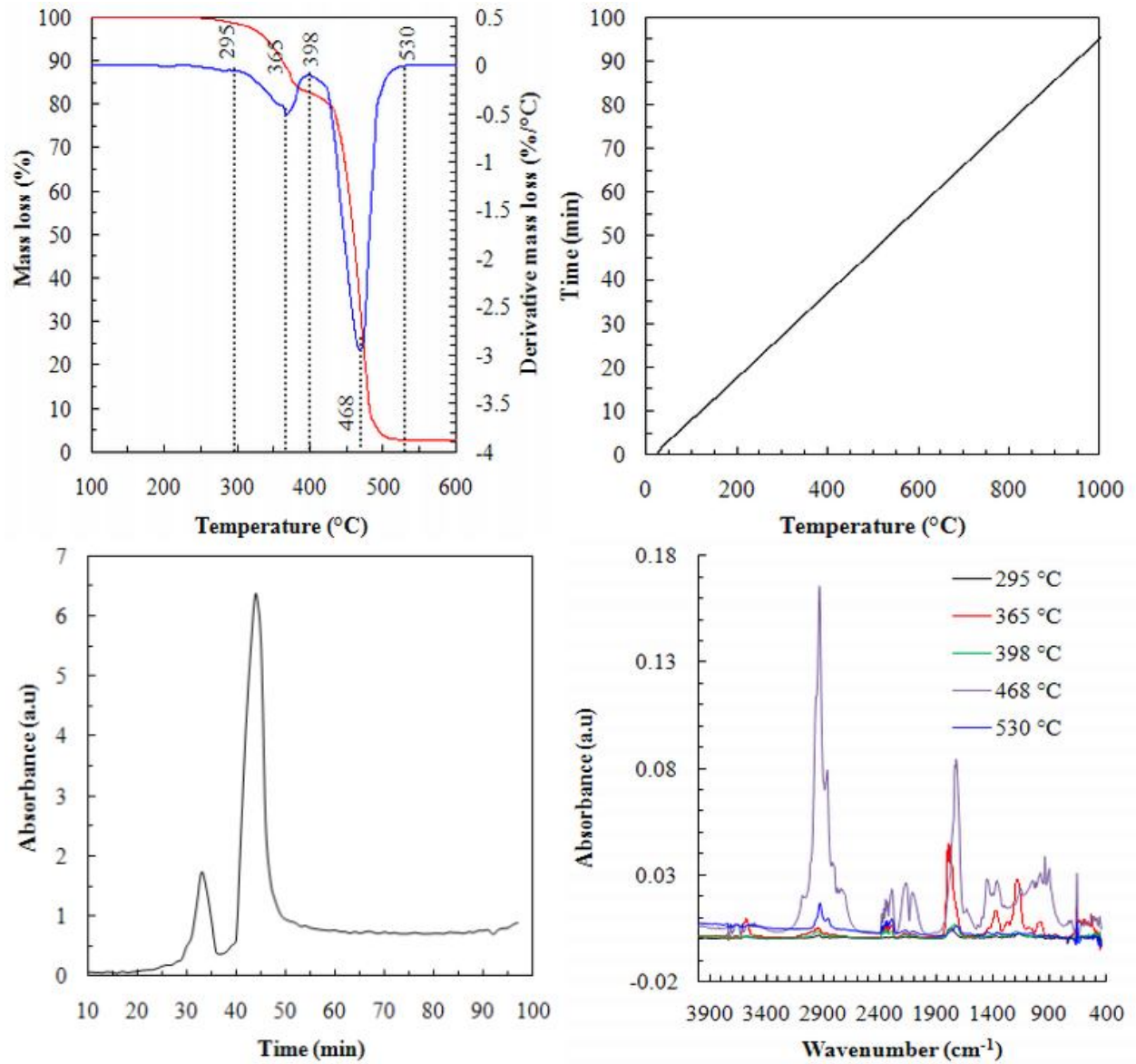


Figure C-26. Evolved gas analysis of EVA/5% LDH-CO₃ by TG-FTIR

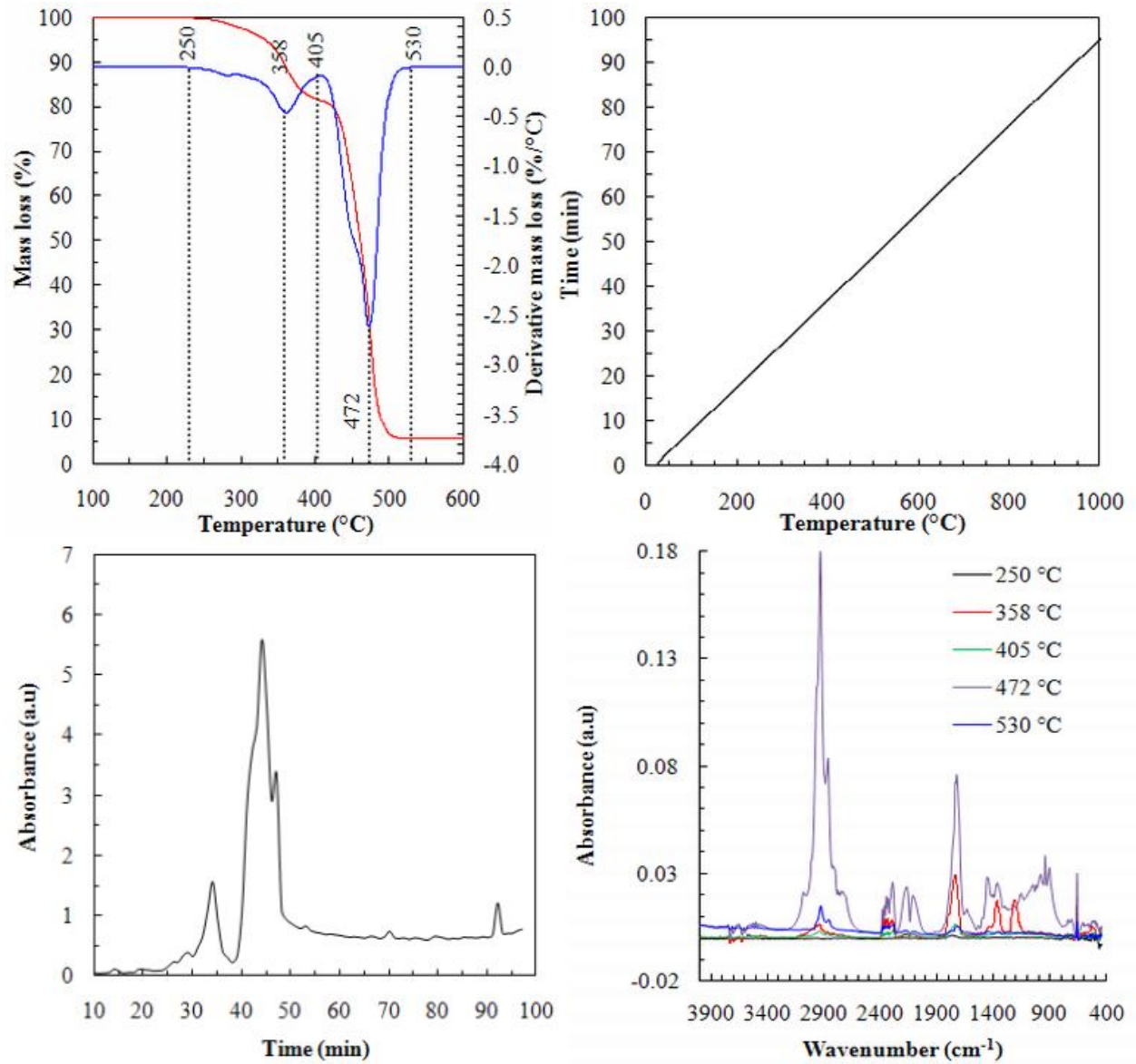


Figure C-27. Evolved gas analysis of EVA/10% LDH-CO₃ by TG-FTIR

Appendix D: Organo-LDH / Jojoba oil suspension

Fatty Acid-Jojoba Oil Formulation

Table D-1. Stearic acid in Jojoba oil formulation (J stands for Jojoba oil and S for stearic acid and their respective compositions)

Sample ID Formulation ratio	Weight of acid (g)	Weight of Jojoba oil (g)
J-S 95-5	0.5001	9.5028
J-S 90-10	1.004	9.0151
J-S 80-20	2.003	8.0044
J-S 70-30	3.007	7.0023

Table D-2. Palmitic acid in Jojoba oil formulation (J stands for Jojoba oil and P for palmitic acid and their respective compositions)

Sample ID Formulation ratio	Weight of acid (g)	Weight of Jojoba oil (g)
J-P 95-5	0.5003	9.5011
J-P 90-10	1.001	9.0034
J-P 80-20	2.009	8.0166
J-P 70-30	3.000	7.023

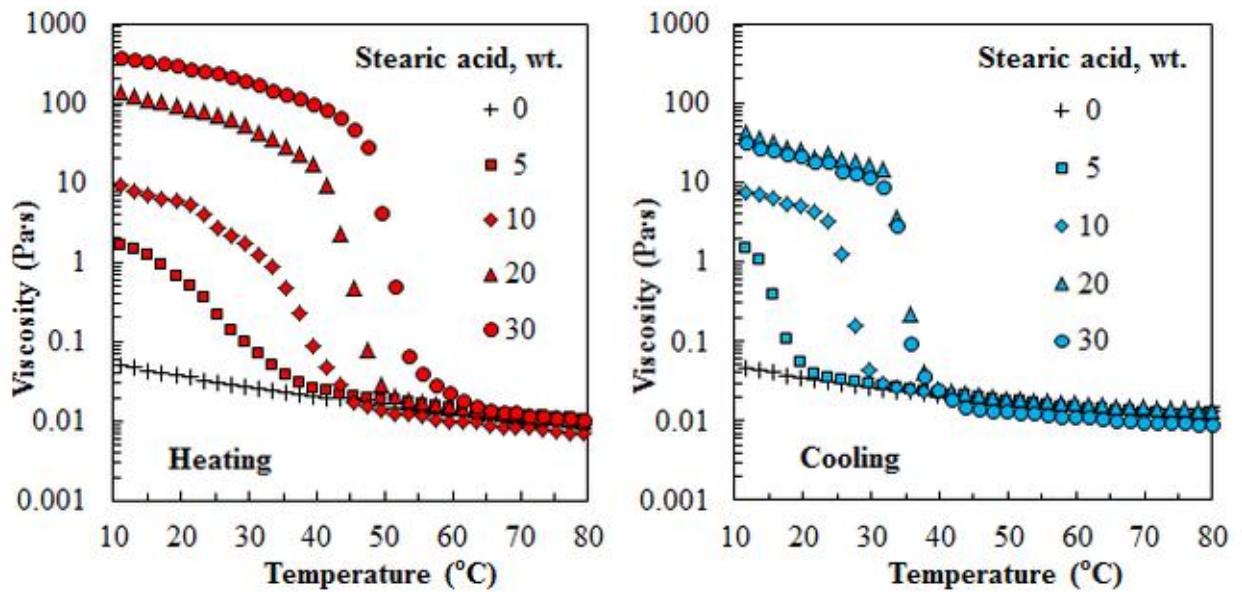


Figure D-1. Viscosity-temperature curve of different stearic acid compositions in Jojoba oil

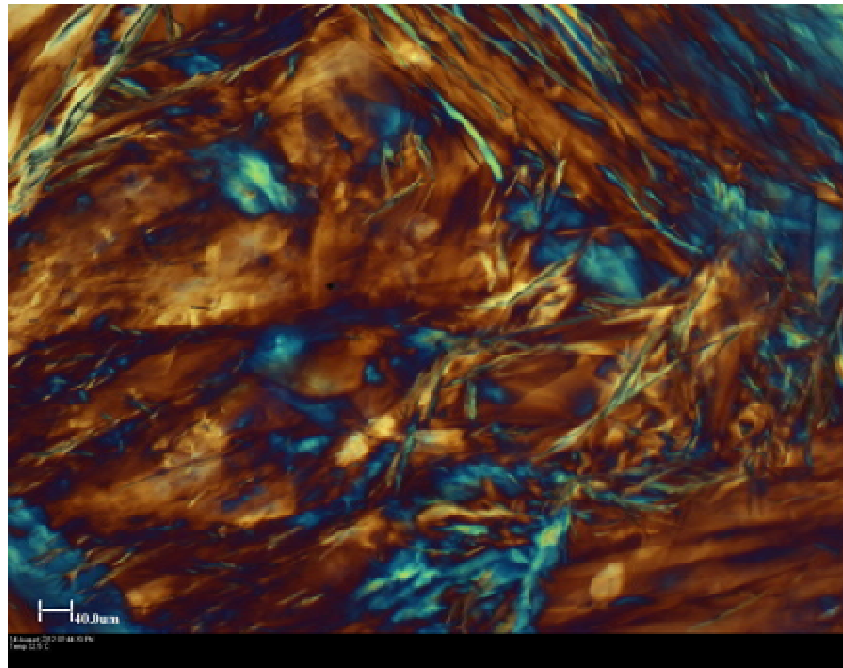


Figure D-2. 20 wt.% of stearic acid in Jojoba oil heated and cooled to 24 °C (measurement bar is 40 μm)

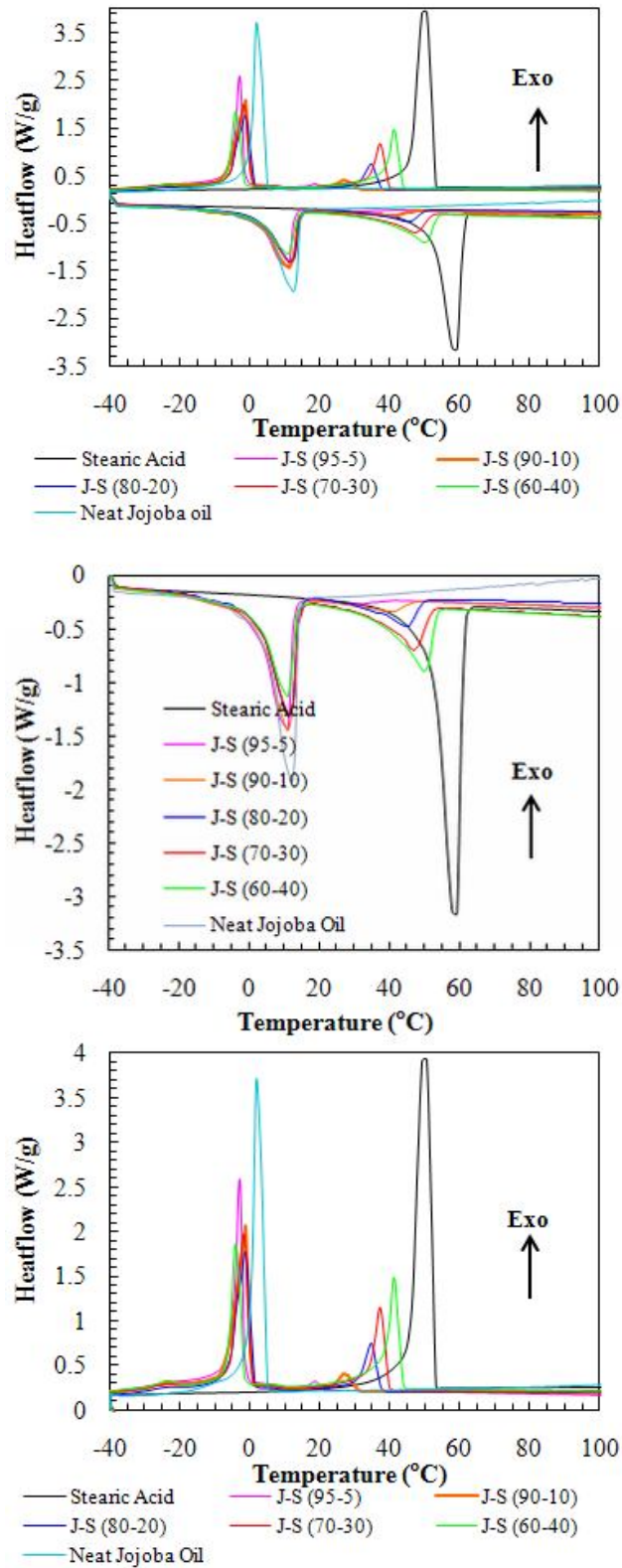


Figure D-3. DSC curves of different stearic acid compositions in Jojoba oil

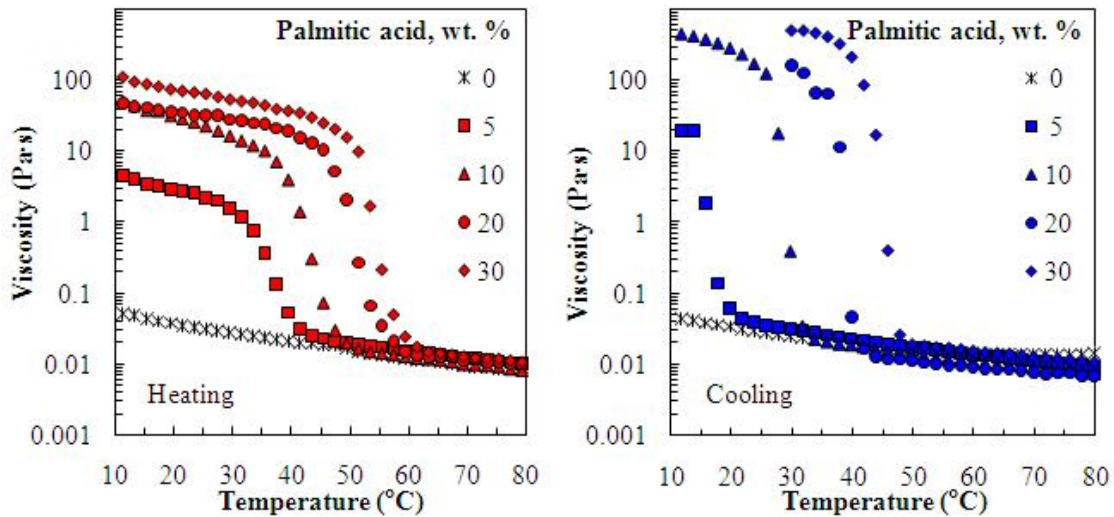


Figure D-4. Viscosity-temperature curve of different palmitic acid compositions in Jojoba oil

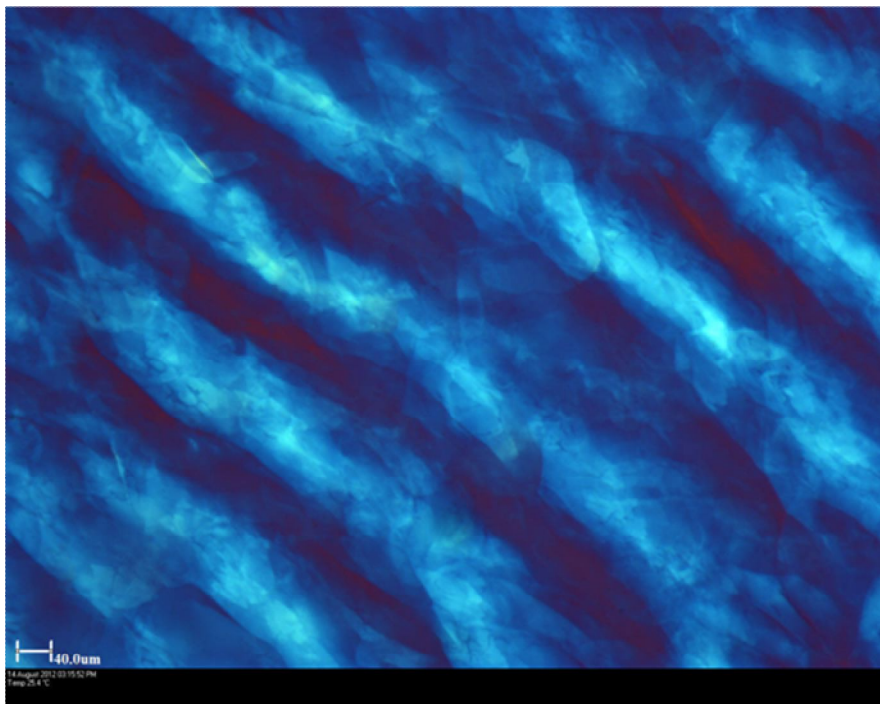


Figure D-5. 20 wt.% palmitic acid in Jojoba oil heated and cooled to 25 °C (measurement bar is 40 μm)

It is interesting to note that fatty acid crystallisation behaviour in Jojoba oil differs for stearic and palmitic acid. This could also explain the different gels obtained from the LDH-stearate and from the LDH-palmitate. Crystal shape, size and density were found to affect the physical properties of the final solid fat matrix (Rye *et al.*, 2005)

FT-IR Spectra

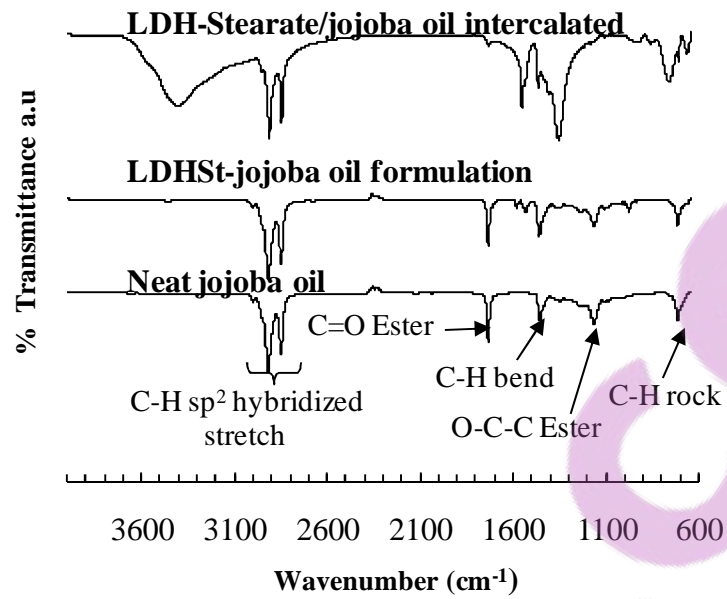


Figure D-6. FTIR spectra of neat Jojoba oil, 30 wt.% LDH-stearate/Jojoba oil formulation and stearate

The Jojoba oil peaks are the same as those observed in Le Dreau *et al.*, 2008.

Rheology of Fatty Acid-Intercalated LDH/Jojoba Oil Formulation

Table D-3. Visual observation of different 30 wt% of intercalated LDHs

Sample ID	Carbon chain number	Orientation of intercalated anion	Appearance: unheated treated formulation	Appearance: heated treated formulation
LDH-myristate	C ₁₄	Bilayer	Runny	Thickens slightly on standing
LDH-palmitate	C ₁₆	Bilayer	Slightly runny	Thickens slightly on standing
LDH-stearate	C ₁₈	Bilayer	Dropping consistency	Thickens slightly on standing
LDH-oleate	C ₁₈	Bilayer	Runny	No change
LDH-behenate	C ₂₂	Bilayer	Soft dropping consistency	Thickens slightly on standing

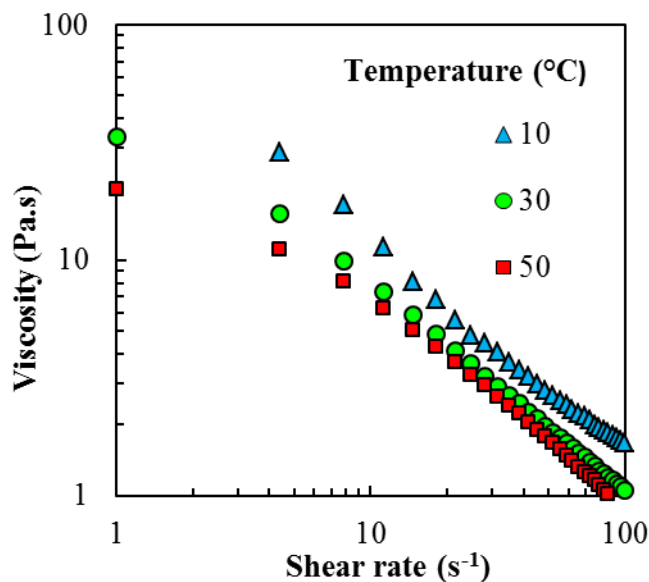


Figure D-7. The effect of shear rate and temperature on the viscosity of Jojoba oil suspensions (the LDH-stearate content was 30 wt.% and the shear rate was kept constant at 5 s^{-1})

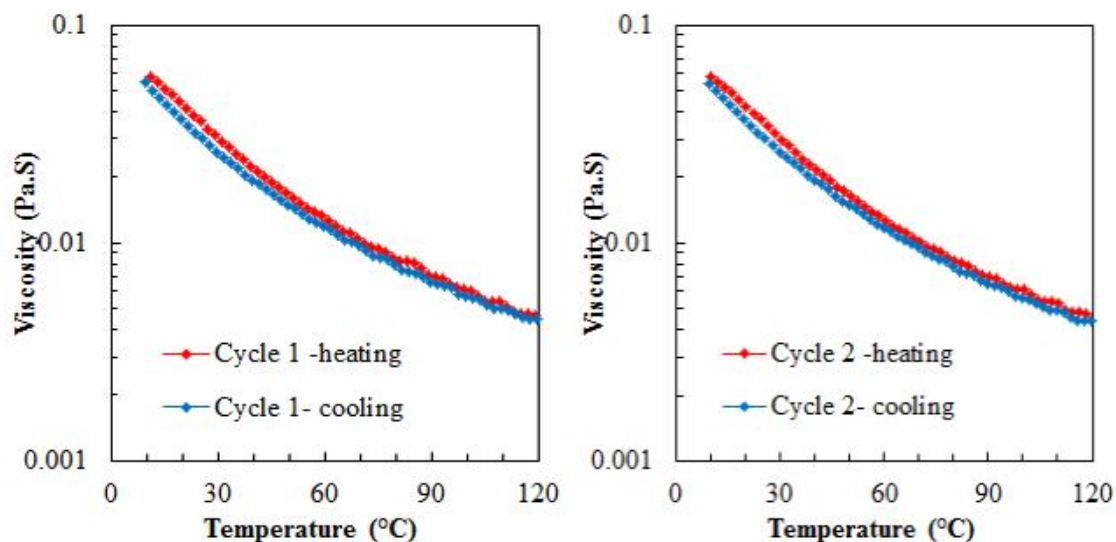


Figure D-8. Viscosity as a function of temperature of the neat Jojoba oil

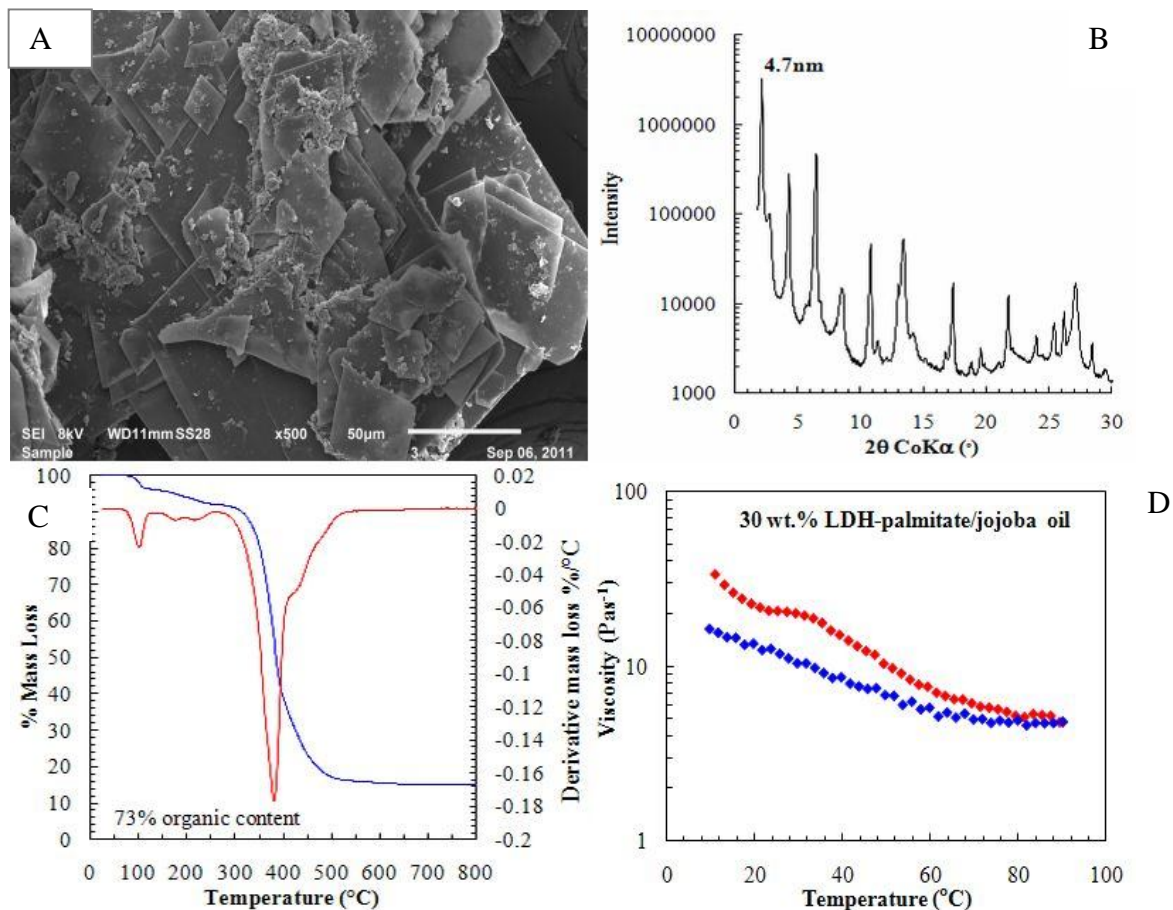


Figure D-9. Summary of rhombohedral-shaped LDH-palmitate: A – SEM image of morphology of particles; B – XRD diffractograms with a d-spacing of 4.7 nm; C – TGA data indicating organic content; D – viscosity curve as a function of temperature of the derivative 30 wt.% formulation

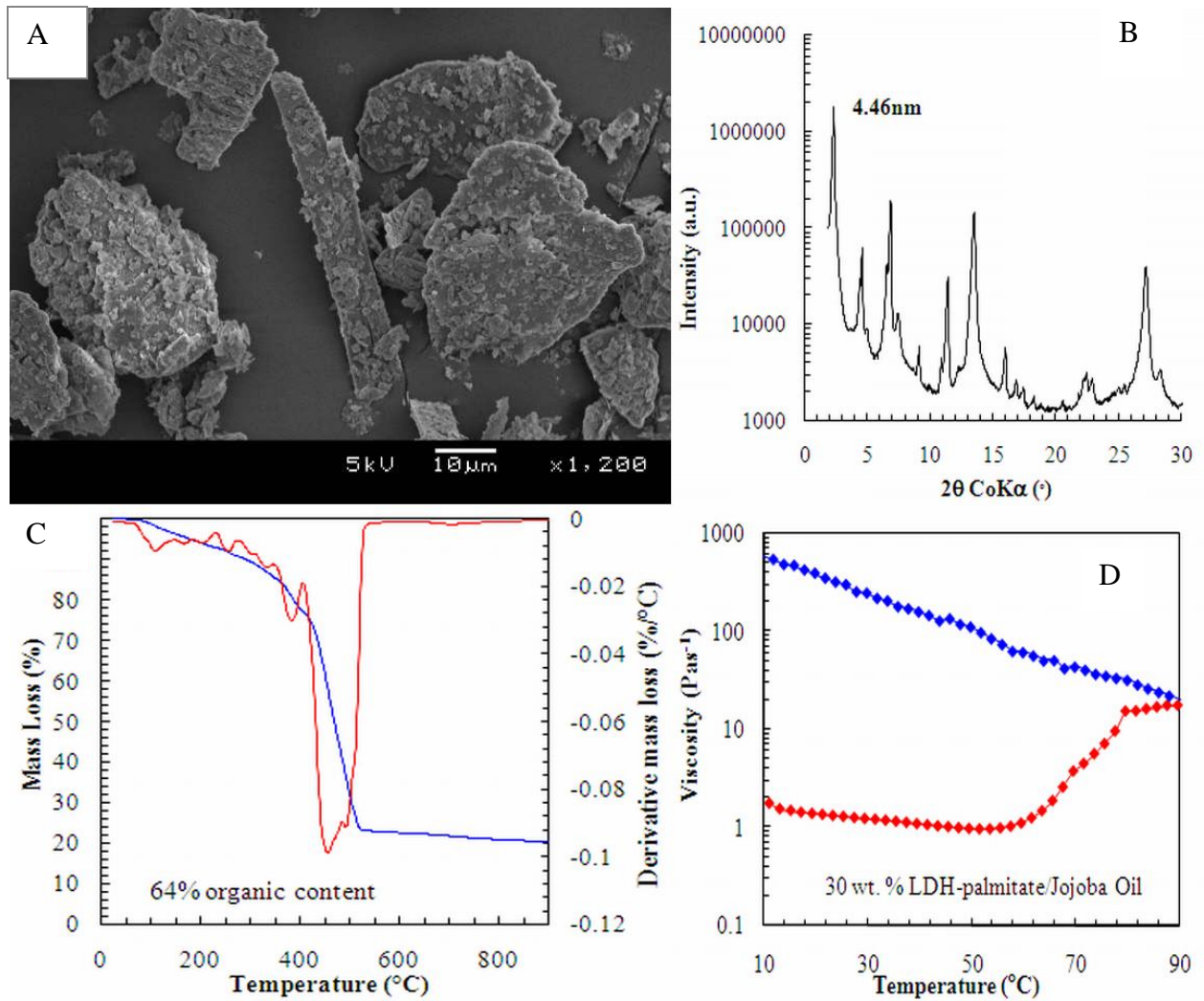


Figure D-10. Summary of subhedral-shaped LDH-palmitate: A – SEM image of morphology of particles; B – XRD diffractograms with a d-spacing of 4.46 nm; C – TGA data indicating organic content; D – viscosity curve as a function of temperature of the derivative 30 wt.% formulation

Complex viscosity behaviour was observed for the C₁₆–C₂₂ intercalated LDHs.

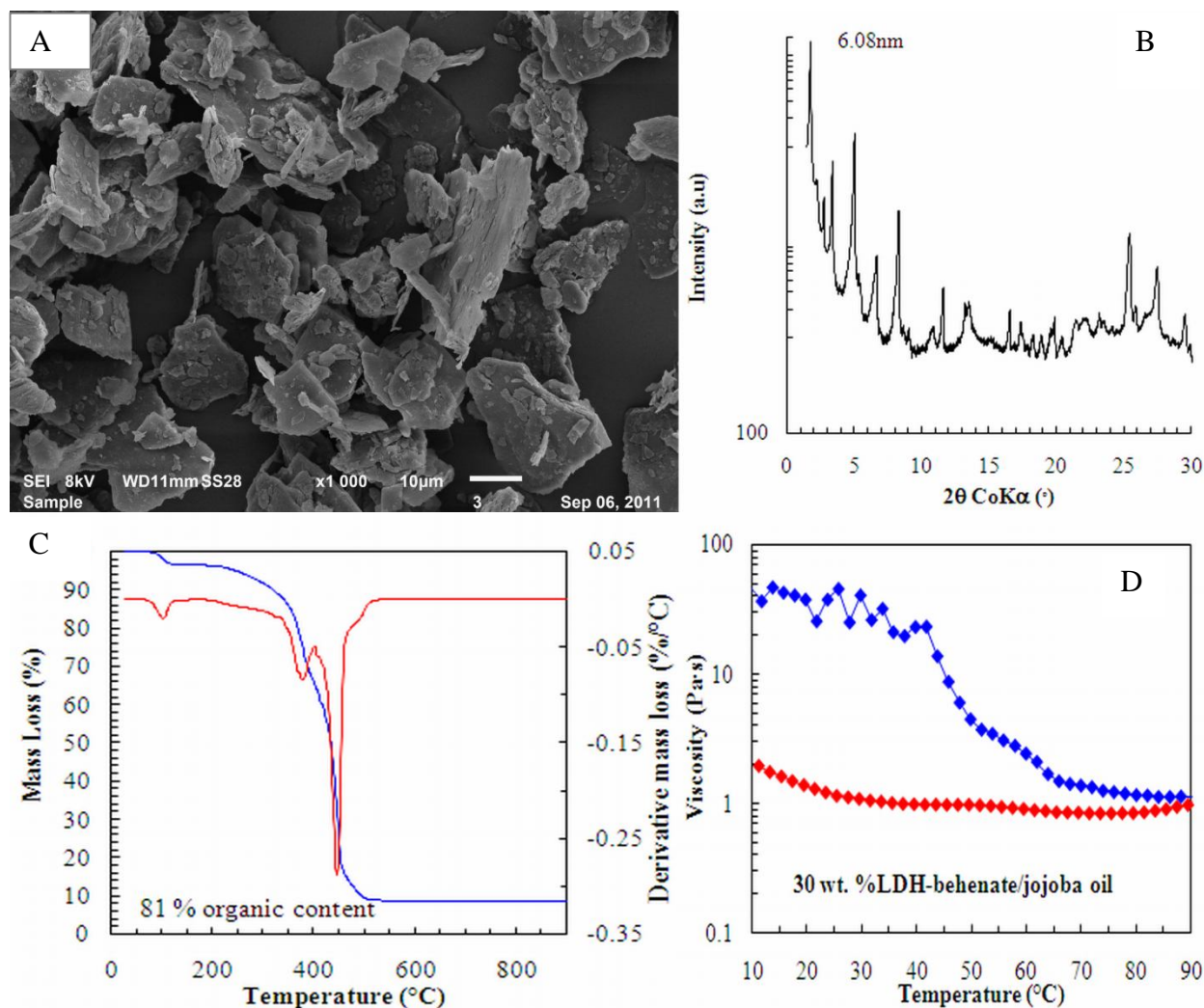


Figure D-11. Summary of subhedral-shaped LDH-behenate: A – SEM image of morphology of particles; B – XRD diffractograms with a d-spacing of 6.08 nm; C – TGA data indicating organic content; D – viscosity curve as a function of temperature of the derivative 30 wt.% formulation

Other formulations were attempted with LDH-palmitate and behenate/Jojoba oil systems, and similar results were obtained. However, the products were found to have a higher viscosity than the LDH-stearate derivatives and became grease-like. This could be explained by the fatty acid-platelet association, which results in the release of a hydrogen ion (H⁺). The hydrogen attacks the unsaturated bonds of the Jojoba oil. Hydrogenation of these bonds

results in the change of properties from oil (liquid) to wax (solid-like). Hence, fatty acid-intercalated LDHs may potentially be used as rheological modifiers. As a result it is recommended that further analysis and experimentation be conducted to determine the effect that LDH-fatty acid has on the rheological behaviour of Jojoba oil.

The co-intercalated samples also showed this complex viscosity, i.e. for the palmitic and stearic acid co-intercalated LDH (LDH-Pal-St), and for the Jojoba oil and stearic acid-intercalated LDH (LDH-Jojoba/stearate).

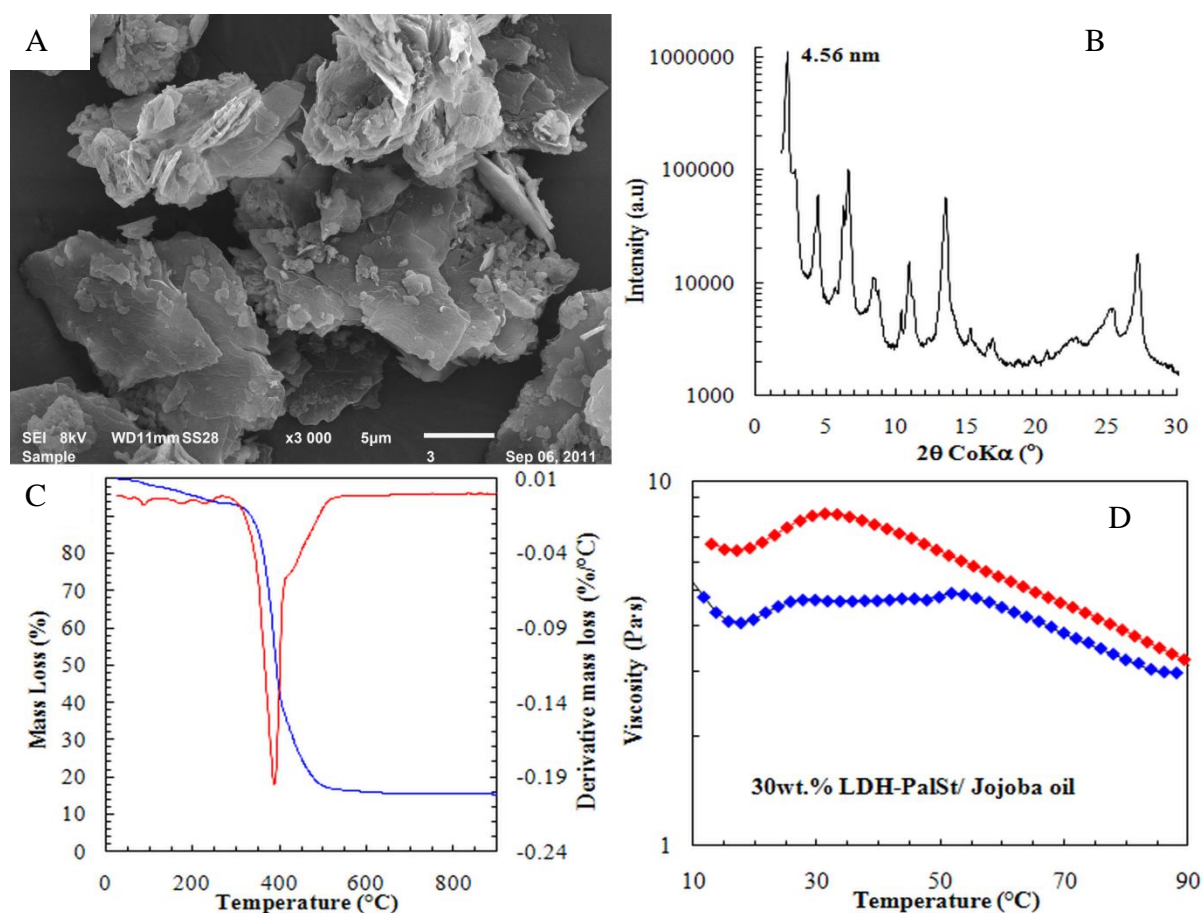


Figure D-12. Summary of subhedral-shaped LDH-Pal-St: A – SEM image of morphology of particles; B – XRD diffractograms with a d-spacing of 4.56 nm; C – TGA data indicating organic content; D – viscosity curve as a function of temperature of the derivative 30 wt.% formulation

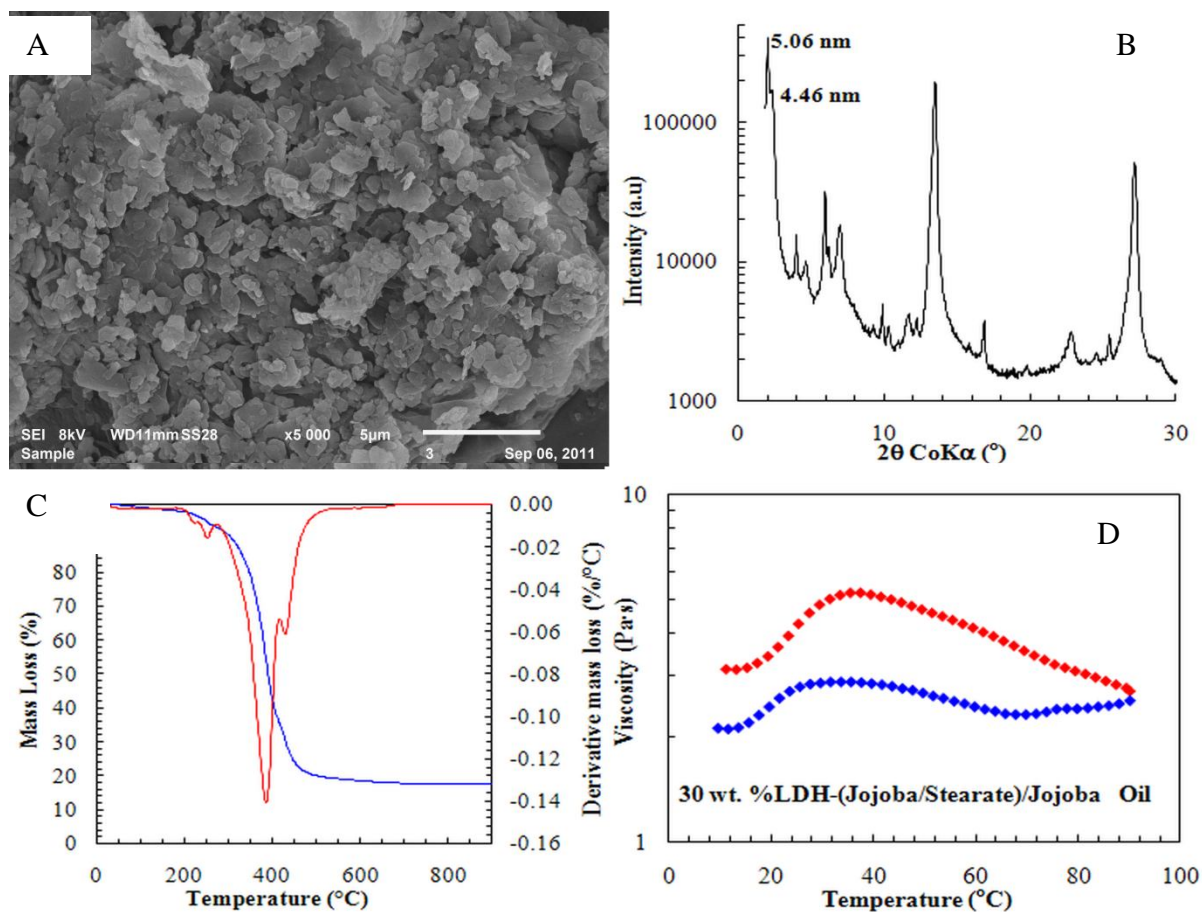


Figure D-13. Summary of subhedral-shaped LDH-(Jojoba/stearate): A – SEM image of morphology of particles; B – XRD diffractograms with d-spacings of 5.06 and 4.46 nm; C – TGA data indicating organic content; D – viscosity curve as a function of temperature of the derivative 30 wt.% formulation